Investigating the role of the protein tyrosine phosphatase non-receptor type 22 (PTPN22) in Fc receptor signalling in myeloid cells

Clarke, Fiona

Awarding institution:
King's College London

Investigating the role of the protein tyrosine phosphatase non-receptor type 22 (PTPN22) in Fcγ receptor signalling in myeloid cells

Fiona Clarke

Faculty of Life Science and Medicine

School of Immunology and Microbial Sciences

King's College London

Thesis submitted for the degree of Doctor of Philosophy

2019

Table of Contents

a. Abstract

The C1858T single nucleotide polymorphism in the human protein tyrosine phosphatase non-receptor type 22 (*PTPN22*) gene encodes an R620W missense mutation in PTPN22 ($PTPN22^{R620W}$) and is associated with an increased susceptibility to multiple autoimmune diseases including rheumatoid arthritis, systemic lupus erythematosus and type 1 diabetes. PTPN22 is expressed in all immune cells and is a negative regulator of Src and spleen tyrosine kinase (Syk) family kinases downstream of multiple immunoreceptors including the T cell receptor, the B cell receptor, the αLβ2 integrin LFA-1, Toll-like receptors and dectin-1.

As many of the autoimmune diseases associated with the polymorphism in *PTPN22* have an autoantibody component to their pathology, the aim of this thesis was to identify whether PTPN22 regulates signalling downstream of Fc receptors. Fcγ receptors (FcγRs) recognise the Fc region of IgG autoantibodies when they bind to autoantigens and form immune complexes. After immune complex binding and receptor crosslinking, FcγRs signal via Src and Syk family kinases, known targets of PTPN22, leading to effector functions including antigen uptake, antigen presentation and cytokine secretion. Bone marrow derived dendritic cells (BMDCs) from wild type (WT) and $Ptpn22^{-/-}$ mice were pulsed with ovalbumin:anti-ovalbumin immune complexes (ova ICs). Co-culture with WT ova specific $CD4^+$ T cells revealed that ova IC pulsed $Ptpn22^{-/-}$ BMDCs have an enhanced capability to induce T cell proliferation. PTPN22 was found to be dispensable for ova IC binding, internalisation and processing, but the enhanced T cell proliferation was associated with an increased capability of $Ptpn22^{-/-}$ BMDCs to present immune complex derived antigens and to form ova IC dependent BMDC-T cell conjugates. These findings highlight PTPN22 as a negative regulator of FcγR mediated responses and provide a link between the association of $PTPN22^{R620W}$ with autoantibody associated autoimmune diseases. Despite the requirement for PTPN22 in regulating T cell responses after ova IC stimulation, PTPN22 was not required for T cell responses after BMDCs were pulsed with $OVA_{323-339}$ peptide or ova protein.

To investigate the role of PTPN22 in autoimmunity in more detail, a mouse model of rheumatoid arthritis was utilised. $Ptpn22^{-/-}$ mice were found to develop more severe disease using the K/BxN serum transfer model. Despite this, WT and $Ptpn22^{-/-}$ arthritic mice displayed similar joint erosion and immune cell infiltration. In addition, PTPN22 was found to be dispensable for the *in vitro* differentiation and function of osteoclasts, the cells which are responsible for the bone erosion observed in arthritis.

b. Acknowledgements

I would like to thank Professor Andrew Cope and Dr Pierre Guermonprez for their supervision and guidance. In addition, I would like to thank all members of the Cope laboratory, especially Dr Harriet Purvis, for their support and friendship. Finally, I would like to thank my husband and family for their continued love and confidence in me.

c. List of Figures

d. List of Tables

e. List of Abbreviations

ABCs	age dependent B cells
ACPA	anti-citrullinated protein antibody
ADCC	antibody dependent cell mediated cytotoxicity
Anti-ova	rabbit anti-chicken egg albumin
APC	antigen presenting cell
Bcl-2	B cell lymphoma-2
BCR	B cell receptor
BiP	binding immunoglobulin protein
BLC	B lymphocyte chemoattractant
Blk	B cell lymphocyte kinase
BMDC	bone marrow derived dendritic cell
BMDM	bone marrow derived macrophages
C	constant domain
CAIA	collagen antibody-induced arthritis
cDC	conventional dendritic cell
CDP	common dendritic cell progenitor
CFA	complete Freud's Adjuvant
c-Fms	colony-stimulating factor-1 receptor
CIA	collagen-induced arthritis
CLIP	class II-associated invariant chain peptide
CLR	c-type lectin receptor
cMoP	common monocyte progenitor
CMP	common myeloid progenitor
CpG	unmethylated CG dinucleotides
Csk	c-terminal Src kinase
CT	computed tomography
CTFR	CellTrace Far Red
CTV	CellTrace Violet
DAG	diacylglycerol
DAMP	damage-associated molecular pattern
DAS28	disease activity score 28
DC	dendritic cell
DHR123	dihydrorhodamine 123
E. coli	*Escherichia coli*
EGTA	ethylene glycol-bis(2-aminoethylether)-*N,N,N',*N'-tetraacetic acid
ELISA	enzyme-linked immunosorbent assay
ER	endoplasmic reticulum
ERK	extracellular signal regulated kinase
FBS	fetal bovine serum
FcR	fragment crystalline receptor
FcγR	Fc gamma receptor
Fgr	gardner-rasheed feline sarcoma viral oncogene homologue
Flt3	fms-like tyrosine kinases 3
Flt3L	fms-like tyrosine kinases 3 ligand
fMLP	*N*-Formyl-Methionyl-Leucyl-Phenylalanine
Frk	Fyn related kinase
GlcNAc	*N*-acetylglucosamine
GM-CSF	granulocyte macrophage-colony stimulating factor
GMFI	geometric mean fluorescent intensity
GPI	glucose-6-phosphate isomerase

Grb2	growth factor receptor bound protein 2
GWAS	genome wide association studies
H	heavy chain
H+E	hematoxylin and eosin
HA	heat aggregated
Hck	hematopoietic cell kinase
HKCA	heat killed *Candida albicans*
HKLM	heat killed *Listeria monocytogenes*
HLA	human leukocyte antigen
HSC	hematopoietic stem cell
IC	immune complex
ICAM-1	intercellular adhesion molecule 1
IFNα	interferon α
IFNαR	interferon α receptor
IFNβ	interferon β
IFNγ	interferon γ
Ig	immunoglobulin
IgG	immunoglobulin G
IKKε	inhibitor of nuclear factor kappa epsilon
IL-10	interleukin-10
IL-12	interleukin-12
IL-12/23p40	interleukin-12/23p40
IL-12p40	interleukin-12p40
IL-17A	interleukin-17A
IL-1α	interleukin-1α
IL-1β	interleukin-1β
IL-2	interleukin-2
IL-21	interleukin-21
IL-23	interleukin-23
IL-32	interleukin-32
IL-4	interleukin-4
IL-6	interleukin-6
IL-8	interleukin-8
IP_3	inositol-(1,4,5)-trisphosphate
IRF	interferon regulatory factor
ITAM	immunoreceptor tyrosine-based activation motif
ITAMi	inhibitory ITAM signalling
ITIM	immunoreceptor tyrosine-based inhibition motif
JAK2	janus kinase 2
JIA	juvenile idiopathic arthritis
JNK	c-Jun N-terminal kinase
KC	keratinocyte chemoattractant
L	light chain
LAMP-1	lysosomal associated membrane protein-1
Lck	lymphocyte specific protein tyrosine kinase
LCMV	lymphocytic choriomeningitis virus
LFA-1	lymphocyte function associated antigen 1
Li	invariant chain
LIX	liposaccharide induced CXC chemokine
LN	lymph node
LPS	lipopolysaccharide
LY	lucifer yellow
MAPK	mitogen activated protein kinase

mBSA	methylated bovine serum albumin
MCP-1	monocyte chemoattractant protein-1
MDP	monocyte and dendritic cell progenitor
MHCI	major histocompatibility complex class I
MHCII	major histocompatibility complex class II
micro-CT	Micro-computed tomography
MIP-1α	macrophage inflammatory protein-1α
MIP-1β	macrophage inflammatory protein-1β
MIP-2	macrophage inflammatory protein 2
MMP9	matrix metalloprotease 9
NET	neutrophil extracellular trap
NK cell	natural killer cell
NLR	nucleotide oligomerisation domain-like receptor
NOD mice	non-obese diabetic mice
NP-KLH	NP-Keyhole Limpet Hemocyanin
NSF	*N*-ethylmaleimide-sensitive fusion factor
NSG mice	NOD *scid* gamma mice
OPG	osteoprotegerin
Ova	ovalbumin
Ova IC	ovalbumin:anti-ovalbumin immune complex
PAD	peptidylarginine deiminase
PAMP	pathogen-associated molecular pattern
PBMC	peripheral blood mononuclear cell
PCR	polymerase chain reaction
pDC	plasmacytoid dendritic cell
PEST	proline-, glutamic acid-, serine- and threonine-rich
PET	positron emission tomography
PET/CT	positron emission tomography/computed tomography
PFA	paraformaldehyde
PI3K	phosphoinositide 3 kinase
PKC	protein kinase C
PLCγ	phospholipase C-γ
PMA	phorbol 12-myristate 13-acetate
poly(I:C)	polyinosine-polycytidylic acid
polyU	poly-uridine
PRR	pattern recognition receptor
PSTPIP	F-BAR-Proline-Serine-Threonine Phosphatase Interacting Protein
PTEN	phosphatase and tensin homologue
PTPN22	protein tyrosine phosphatase non-receptor type 22
RA	rheumatoid arthritis
Rag1	recombination activating gene 1
RANK	receptor activator of nuclear factor kappa-B
RANK-L	receptor activator of nuclear factor kappa-B ligand
RANTES (CCL5)	regulated on activation, normal T cell expressed and secreted
RGD peptide	arginine-glycine-aspartic acid peptide
RLR	retinoic acid-inducible gene I-like receptor
ROS	reactive oxygen species
SCID	severe combined immunodeficient
SH2	src homology 2
SH3	src homology 3
SHIP-1	SH2-domain-containing inositol polyphosphate 5' phosphatase 1
SHIP-2	SH2-containing inositol 5’-phosphatase 2
SHP-1	src homology region 2 domain containing phosphatase-1

SLE	systemic lupus erythematosus
SNP	single nucleotide polymorphism
SPECT	single-photon emission computed tomography
Syk	spleen tyrosine kinase
T1D	type 1 diabetes
TBK1	TANK-binding kinase 1
TCR	T cell receptor
T_{fh} cell	T follicular helper cell
T_{fr} cell	T follicular regulatory cell
Th1	type 1 helper T cells
Th2	type 2 helper T cells
Th17	type 17 helper T cells
TIR	toll/interleukin-1 receptor
TLR	toll-like receptor
TNFα	tumour necrosis factor α
TNP-Ficoll	trinitrophenol-Ficoll
TNP-ova	trinitrophenyl-ovalbumin
TRAF3	TNF receptor associated factor 3
TRAP	tartrate-resistant acid phosphatase
T_{regs} cells	regulatory T cells
TRIM21	tripartite motif containing protein 21
TrkA	tropomyosin receptor kinase A
UC	ulcerative colitis
V	variable domain
WT	wild type
ZAP-70	zeta chain associated protein kinase, 70 KDa

1. Introduction

1.1 PTPN22

1.1.1 Phosphatases and kinases

Protein tyrosine phosphatases dephosphorylate target proteins by removing phosphate groups from tyrosine residues. In this way, they oppose the actions of tyrosine kinases, which catalyse the addition of phosphate groups to tyrosine residues. Together, protein kinases and phosphatases regulate a vast array of signalling pathways, including those involved in cell differentiation, activation, migration and apoptosis. The importance of phosphatases in regulating signalling is exemplified by mice which express a loss-of-function mutation in *Ptpn6* (which encodes the hematopoietic phosphatase Src homology region 2 domain containing phosphatase-1, SHP-1), and display the *motheaten* phenotype, characterised by chronic skin inflammation and systemic autoimmunity[1,2]. In addition, a loss of balance between protein kinases and phosphatases is involved in the pathogenesis of human diseases including cancer[3].

1.1.2 The structure and function of PTPN22

PTPN22 is located on human chromosome 1p13 and *Ptpn22* is located on mouse chromosome 3. These encode the protein tyrosine phosphatase non-receptor type 22 (PTPN22), a cytoplasmic tyrosine phosphatase belonging to the proline-, glutamic acid-, serine- and threonine-rich (PEST) family of phosphatases. PTPN22 is expressed in all hematopoietic cells, but different immune cell subsets express varying levels of the phosphatase, with natural killer (NK) cells and neutrophils expressing the most in mice[4]. The mouse protein was identified in 1992[5] and the human protein was identified a few years later in 1999[6]. There are three splice isoforms of the human protein, the most abundant of which is isoform 1, which is the full length 807 amino acid protein. Isoforms 2 and 3 are shorter variants and have unknown functions[6,7]. The mouse and human proteins share 89% sequence homology in their catalytic domains, but are only 61% identical in the rest of the protein. This indicates that extrapolations between results found in human and mouse experiments should be carried out with caution.

PTPN22 is composed of an N-terminal catalytic domain, an interdomain and a C-terminal PEST domain containing four proline-rich regions, named P1-4 (Figure 1-1). These proline-rich regions can interact with Src homology 3 (SH3) containing proteins. A single nucleotide polymorphism (SNP) in the human gene (C1858T) causes an arginine to a tryptophan substitution at amino acid 620 of the human protein (R620W), located in the P1 PEST domain of PTPN22. This prevents PTPN22 from interacting with the negative regulatory C-terminal Src kinase (Csk)[8]. Csk usually works in concert with PTPN22 to negatively regulate T cell receptor (TCR) signalling. Other known interactors of PTPN22 include lymphocyte specific protein tyrosine kinase (Lck)[9], zeta chain associated protein kinase, 70 KDa (ZAP-70)[9], the TCRζ chain[9], tumour necrosis factor (TNF) receptor associated factor 3 (TRAF3)[10], the adaptor molecule Growth factor receptor bound protein 2 (Grb2)[11] and the E3 ubiquitin ligase c-Cbl[6].

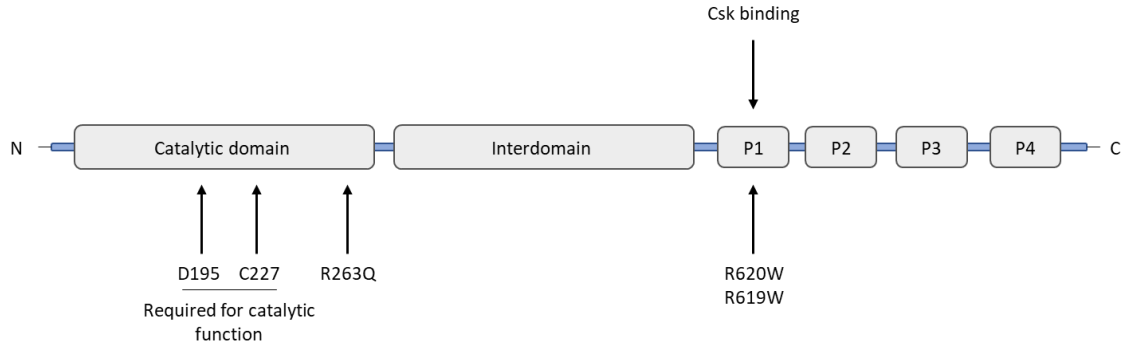

Figure 1-1: The structure of PTPN22.

PTPN22 is composed of an N-terminal catalytic domain, an-interdomain and a C-terminal binding domain, which contains 4 polyproline rich motifs (P1-4). Mouse PTPN22 is 802 amino acids in length and human PTPN22 is 807 amino acids in length. Diagram has been adapted from Stanford SM and Bottini N, Nature Reviews Rheumatology, 2014.

One report indicated that although mRNA levels of *Ptpn22* were similar in lymphoid organs from WT and *Ptpn22*^{R619W} mice (which express the orthologue of the human autoimmune associated variant), the PTPN22^{R619W} protein was more sensitive to calpain mediated degradation than the WT protein. This was shown by reduced expression of PTPN22 in thymocytes from *Ptpn22*^{R619W} mice compared with PTPN22 expression in thymocytes from WT mice[12]. However, a subsequent report did not corroborate this finding[13].

1.1.3 PTPN22 and autoimmunity

The C1858T (rs2476601) SNP in human *PTPN22* (which encodes PTPN22^{R620W}, with PTPN22^{R619W} being the mouse orthologue) is associated with an increased susceptibility to multiple

autoimmune diseases including type 1 diabetes (T1D)[14–21], rheumatoid arthritis (RA)[14,22–27], systemic lupus erythematosus (SLE)[28,29], Graves' disease[17,30–32] and Addison's disease[33,34]. The first association between the SNP and autoimmune disease was discovered by Bottini and colleagues, in which they found, in two independent cohorts, that T1D patients were more likely to express the SNP than healthy controls[8]. Despite these associations, the C1858T SNP in *PTPN22* is not associated with an increased susceptibility to all autoimmune diseases. For example, there is no association or a negative association between the SNP and multiple sclerosis[35,36], ulcerative colitis (UC)[37] and Crohn's disease[37]. Furthermore, carriers of PTPN22 C1858T are protected from tuberculosis[38,39] but are more susceptible to other infections including invasive pneumococcal infections[40]. However, the SNP has no effect on susceptibility to hepatitis C infections[41].

Although the C1858T SNP in *PTPN22* is the most commonly found variant, other SNPs exist in *PTPN22* which have also been linked with autoimmunity. These include PTPN22 C1123G (rs2488457), which is located in the promoter region of the gene, and has been linked with an increased susceptibility to UC[42]. It has also been linked with a modestly increased risk of T1D[43,44], juvenile idiopathic arthritis (JIA)[45] and RA[46,47], but not all of these associations have been confirmed in independent cohorts[48,49]. The PTPN22 C1123G and PTPN22 C1858T polymorphisms have also been shown to cause reduced mRNA expression of PTPN22 in RA patients compared to healthy controls not carrying the polymorphisms[50]. In addition, PTPN22 G788A (rs33996649), which encodes PTPN22^{R263Q}, is located in the catalytic domain of the protein and confers reduced enzymatic activity[51], has been associated with a slight protection against SLE[51,52], RA[53] and UC[54].

1.2 The role of PTPN22 and PTPN22^{R619W} in murine immune cells in the steady state

Despite the strong association between PTPN22 polymorphisms and autoimmune disease susceptibility, mice in which PTPN22 is absent do not develop spontaneous autoimmunity on a C57Bl/6 genetic background. PTPN22 is expressed in all hematopoietic cells and the role of PTPN22 has been investigated in a variety of immune cells, with its role in T cells receiving the most attention. How the mouse orthologue of the autoimmune associated variant (PTPN22^{R619W}) affects the functions of immune cell subsets is complex, as depending on the cellular context and signalling pathway under investigation, both gain- and loss-of-phosphatase function effects have been reported.

1.2.1 The role of PTPN22 in murine T cells

In *Ptpn22*$^{-/-}$ mice, T cell development and TCR signalling in naïve T cells is grossly normal, although TCR signalling is enhanced in *Ptpn22*^{R619W} naïve and memory T cells[13]. With age, both *Ptpn22*$^{-/-}$ and *Ptpn22*^{R619W} mice develop larger lymph nodes (LNs) and spleens or LNs, thymus and spleens, respectively, with increased cellularity[12,55]. This may be partly due to the fact that *Ptpn22*$^{-/-}$ mice have increased numbers of CD44^{+} CD62L^{lo} effector/memory CD4^{+} and CD8^{+} T cells that are hyper-responsive to TCR engagement[55]. This is due to a role of PTPN22 in dephosphorylating Src and Syk family kinases, namely Lck, Fyn and ZAP-70, downstream of the TCR, in addition to dephosphorylating the immunoreceptor tyrosine-based activation motifs (ITAMs) in the CD3ζ chain[56]. *Ptpn22*^{R619W} mice also show an expansion in the effector/memory T cell compartment in lymphoid organs[12].

In addition to an expansion of effector/memory T cells, *Ptpn22*$^{-/-}$ mice also have increased numbers of CD25^{+} Foxp3^{+} regulatory T cells (T_{regs}) in the thymus[57], lymph nodes[58] and spleens[57,58]. Peripheral *Ptpn22*$^{-/-}$ T_{regs} were found to express augmented levels of CD25 than WT T_{regs}, and this correlated with enhanced phosphorylation of STAT5 after interleukin-2 (IL-2) stimulation of *Ptpn22*$^{-/-}$ splenic T_{regs}[57]. Although this enhanced STAT5 phosphorylation was not found in *Ptpn22*$^{-/-}$ T_{regs} after IL-2 stimulation in a separate report[58]. WT and *Ptpn22*$^{-/-}$ T_{regs} showed equal phosphorylation of signalling intermediates including Src, ZAP-70 and extracellular signal regulated kinase (ERK), and calcium flux after anti-CD3 crosslinking. *In vitro*, splenic *Ptpn22*$^{-/-}$ T_{regs} were found to be equally suppressive of effector T cell proliferation as WT T_{regs}[57]. However, *in vivo*, *Ptpn22*$^{-/-}$ T_{regs} were found to be more suppressive than their WT counterparts, in this way reducing *Ptpn22*$^{-/-}$ effector T cell induced colitis[58]. This outgrowth of both effector/memory T cells and T_{regs} over time may provide one explanation why *Ptpn22*$^{-/-}$ mice do not develop spontaneous autoimmunity. *Ptpn22*^{R619W} mice do not show any differences in T_{reg} numbers or their suppressive capacity[13].

Alongside the expansion of effector/memory T cells and T_{regs} in *Ptpn22*$^{-/-}$ mice, they also have an increased number of T follicular helper (T_{fh}, CD4^{+} CD44^{hi} CXCR5^{+} PD-1^{+}) cells in the draining LNs 7 days after immunisation with NP-Keyhole Limpet Hemocyanin (NP-KLH) in Complete Freud's Adjuvant (CFA). The expansion of T_{fh} cells in *Ptpn22*$^{-/-}$ mice was not accompanied by an expansion of follicular regulatory T (T_{fr}) cells, indicating that these cells were not capable of regulating the proliferation of the T_{fh} cells, leading to an increase in B cell numbers and antibody production in the absence of PTPN22. The expansion of T_{fh} cells in *Ptpn22*$^{-/-}$ mice was shown to be due to the cells being more proliferative than WT T_{fh} cells, and because they expressed higher mRNA

expression of the apoptosis regulator, and master regulator of T_{fh} cell differentiation, *Bcl2*, suggestive of a survival advantage. Finally, *Ptpn22*$^{-/-}$ T_{fh} cells expressed higher *Il21* and *Il4* mRNA and interleukin-21 (IL-21) protein than WT T_{fh} cells. Interleukin-4 (IL-4) provides B cell help[59].

Data from our own laboratory has demonstrated that PTPN22 also regulates signalling downstream of the integrin lymphocyte function associated antigen-1 (LFA-1) in T cells. Both *Ptpn22*$^{-/-}$ and *Ptpn22*^{R619W} effector T cells adhered more and migrated faster on intercellular adhesion molecule-1 (ICAM-1) coated glass. In addition, *Ptpn22*$^{-/-}$ effector T cells were found to have enhanced ERK phosphorylation after a 20 minute stimulation with ICAM-1, indicating that PTPN22 negatively regulates signalling downstream of LFA-1 in T cells[60]. In a separate report, *Ptpn22*$^{-/-}$ T_{regs} were found to express more LFA-1 and make larger contact areas with ICAM-1 coated surfaces than WT T_{regs}[58].

With age, both *Ptpn22*$^{-/-}$ and *Ptpn22*^{R619W} mice show an expanded $CD4^+$ $IFN\gamma^+$ T cell population in lymph nodes and spleen. Our laboratory described a phenotype that was also apparent in *Ptpn22*$^{-/-}$ mice 96 days after the induction of collagen-induced arthritis. *Ptpn22*$^{-/-}$ $CD4^+$ T cells secreted enhanced IFNγ after stimulation with anti-CD3 and ICAM-1. This was not the case using anti-CD3/anti-CD28 stimulation, again demonstrating that PTPN22 regulates signalling downstream of LFA-1 in T cells. In addition, *Ptpn22*$^{-/-}$ $CD4^+$ T cells plated on anti-CD3 and ICAM-1 showed an enhanced ICAM-1 density at the immune synapse compared to WT $CD4^+$ T cells, and were capable of forming more conjugates with WT BMDCs[61]. This indicates that in the absence of PTPN22, $CD4^+$ T cells have an enhanced LFA-1 responsiveness, potentially resulting in the observed expansion of $CD4^+$ $IFN\gamma^+$ T cells.

1.2.2 The role of PTPN22 in murine B cells

B cell development and B cell receptor (BCR) signalling are largely normal in the absence of PTPN22, however, *Ptpn22*$^{-/-}$ and *Ptpn22*^{R619W} mice have increased numbers of germinal centres[12,59]. In addition, *Ptpn22*$^{-/-}$ mice have increased splenic follicular B cells[59]. The increase in germinal centres has been attributed to increased T_{fh} cell proliferation, survival and IL-21 secretion in *Ptpn22*$^{-/-}$ mice (as discussed above)[59], and not due to a B cell specific role for PTPN22. In *Ptpn22*$^{-/-}$ mice, this increase in germinal centres is accompanied by enhanced serum levels of IgG1, IgG2a and IgE[55], however in *Ptpn22*^{R619W} mice, serum levels of IgM, IgG3 and IgA were similar to WT mice[12]. Despite this, after immunisation with trinitrophenol-Ficoll (TNP-Ficoll), *Ptpn22*^{R619W} mice showed enhanced serum IgG3 and IgM anti-TNPs[12].

Some PTPN22 dependent differences in B cells were observed when *Ptpn22*^{R619W} mice were on a mixed background or with increased age. These included enhanced levels of autoantibodies, autoreactive B cells, splenic T1 B cells and age dependent B cells (ABCs), and enhanced BCR signalling[13]. A separate report also demonstrated enhanced anti-IgM stimulated BCR signalling using splenic CD19^{+} B cells from *Ptpn22*^{R619W} mice.

To further identify a role of PTPN22 in B cell tolerance, non-obese diabetic (NOD) severe combined immunodeficient (SCID) gamma (NSG) mice were engrafted with CD34^{+} hematopoietic stem cells (HSCs) from human foetuses expressing the PTPN22 C1858T allele. Once engrafted, the expression of the variant led to an abnormal central B cell tolerance checkpoint. This resulted in an increase in autoreactive new emigrant B cells. PTPN22^{R620W} expression therefore prevents the normal removal of autoreactive B cells, thus affecting B cell tolerance. Using the inhibitor LTV-1 (which inhibits the phosphatase activity of human PTPN22), or by using shRNA directed against *PTPN22*, the authors were able to show that this reduced the frequency of autoreactive new emigrant B cells in mice transplanted with PTPN22^{R620W} expressing HSCs[62]. This data indicates that it is the enzymatic activity of PTPN22 which is regulating B cell tolerance.

1.2.3 The role of PTPN22 in murine neutrophils

Although PTPN22 is highly expressed in neutrophils, to date there has only been one study which has investigated its function in this cell type in mice. PTPN22 was found to play an important role in positively regulating immune complex induced effector functions, such that *Ptpn22*$^{-/-}$ neutrophils displayed reduced adhesion, reactive oxygen species (ROS) production and degranulation in response to immune complex stimulation. However, PTPN22 was found to be dispensable for neutrophil chemotaxis to macrophage inflammatory protein 2 (MIP2) and neutrophil diapedesis through an endothelial cell layer. *Ptpn22*$^{-/-}$ mice were protected from development of arthritis using the K/BxN serum transfer model, which was attributed to a lack of neutrophil infiltration into the joints[63].

1.2.4 The role of PTPN22 in murine myeloid cells

PTPN22 is also highly expressed in myeloid cells and has been found to regulate signalling downstream of a variety of pattern recognition receptors[10,12,64]. For example, PTPN22 promotes

type I interferon production after Toll-like receptor (TLR) engagement in dendritic cells (DCs) and macrophages[10]. *Ptpn22*$^{-/-}$ BMDCs and bone marrow derived macrophages (BMDMs), in addition to WT RAW 264.7 macrophages subjected to suppression of PTPN22 expression, were stimulated with TLR3, 4, 7 or 9 ligands, using polyinosine-polycytidylic acid (poly(I:C)), lipopolysaccharide (LPS), poly-uridine (polyU) and unmethylated CG dinucleotides (CpG) respectively. Reduced expression of TLR induced anti-inflammatory type I interferons was detected, however no differences in the production of LPS induced pro-inflammatory cytokines by WT and *Ptpn22*$^{-/-}$ BMDCs and BMDMs were observed. *Ptpn22*$^{-/-}$ BMDMs also displayed reduced upregulation of CD86 after 16 hours of stimulation with LPS or poly(I:C). Reduced interferon β (IFNβ) was also detected in the serum of *Ptpn22*$^{-/-}$ mice 4 hours after LPS injection, although TNFα and interleukin-6 (IL-6) levels were normal. As type I interferons are vital for anti-viral responses, WT and *Ptpn22*$^{-/-}$ mice were infected with lymphocytic choriomeningitis virus (LCMV). 24 hours after infection, serum IFNβ was reduced in *Ptpn22*$^{-/-}$ mice, upregulation of CD40 and CD86 on splenic DCs was reduced, and LCMV specific $CD8^+$ T cells in the spleen 7 days after infection were also reduced. The proposed mechanism was that after TLR stimulation, PTPN22 associates with TNF receptor associated factor 3 (TRAF3) and promotes TRAF3 ubiquitination. This in turn leads to the activation of the serine/threonine kinases TANK-binding kinase 1 (TBK1) and inhibitor of nuclear factor kappa epsilon (IKKε), which then phosphorylate interferon regulatory factors 3 and 7 (IRF3 and IRF7), which can then translocate to the nucleus and induce expression of type I interferons. As a result of PTPN22 promoting the expression of TLR induced type 1 interferons, *Ptpn22*$^{-/-}$ mice failed to suppress inflammatory arthritis after poly(I:C) treatment using the K/BxN model[10]. Reduced levels of type I interferons were also observed in a separate study, where *Ptpn22*^{R619W} mice were injected with the TLR7/8 agonist R848 and serum levels of cytokines were measured after 1 hour[64].

Ptpn22$^{-/-}$ hematopoietic progenitor cells show augmented IFNα receptor (IFNαR) signalling, indicating that PTPN22 negatively regulates IFNαR signalling[65]. This was shown by enhanced STAT1 phosphorylation in *Ptpn22*$^{-/-}$ hematopoietic progenitor cells after stimulation with IFNα. Expression of IFN-inducible genes, such as *Irf8*, were found to be increased in *Ptpn22*$^{-/-}$ BMDMs after 4 hours of IFNα stimulation. Using an IFNα-induced mouse model of lupus, *Ptpn22*$^{-/-}$ mice were found to be more prone to disease, showing more anti-nuclear antibodies and increased mortality[65]. As both IFNα and PTPN22 have been previously linked to SLE in humans, this paper demonstrated a potential mechanism whereby expression of PTPN22^{R619W} may be linked to an enhanced susceptibility to lupus development.

The C-type lectin receptor dectin-1 recognises fungal β-glucans. Dectin-1 signals via Syk so the role of PTPN22 in regulating signalling downstream of this receptor in BMDCs was investigated

by our laboratory. *Ptpn22*$^{-/-}$ BMDCs pulsed with $OVA_{323-339}$ peptide and the dectin-1 agonist curdlan caused enhanced interleukin-17A (IL-17A) secretion from WT $CD4^+$ OT-II T cells, both *in vitro* and *in vivo*. This was found to be due to enhanced interleukin-1β (IL-1β) secretion from curdlan stimulated *Ptpn22*$^{-/-}$ BMDCs. Enhanced ERK and Syk phosphorylation was also observed in *Ptpn22*$^{-/-}$ BMDCs stimulated with the dectin-1 agonist heat killed *Candida albicans* (HKCA). Similar results were found using *Ptpn22*^{R619W} BMDCs. This indicates that in the absence of PTPN22, or in the presence of the autoimmune associated variant of PTPN22, BMDCs show enhanced signalling downstream of dectin-1, thus demonstrating that PTPN22 negatively regulates dectin-1 signalling[66].

A recent study reported that ovalbumin (ova) pulsed *Ptpn22*^{R619W} macrophages induced augmented WT $CD4^+$ OT-II T cell activation and proliferation, demonstrated by enhanced CD69 expression after 18 hours of co-culture and enhanced CFSE dilution after 5 days of co-culture. The authors suggested that this was caused by an enhanced phagocytic capability of *Ptpn22*^{R619W} macrophages, by measuring uptake of fluorescent *Escherichia coli* (*E. coli*), and an increased expression of CD80, CD86 and major histocompatibility complex class II (MHCII)[67]. A further report showed that LPS matured *Ptpn22*^{R619W} BMDCs or splenic DCs also induced enhanced WT $CD4^+$ OT-II T cell proliferation when pulsed with ova or $OVA_{323-339}$ peptide. This was attributed to increased co-stimulation rather than alterations in phagocytosis, through LPS induced upregulation of CD40 and CD86 and enhanced secretion of interleukin-12 (IL-12)[12]. This data, however, is in contrast with other reports using *Ptpn22*$^{-/-}$ mice, which showed that *Ptpn22*$^{-/-}$ BMDMs displayed reduced upregulation of CD86 after LPS stimulation[10], or no difference in LPS induced WT and *Ptpn22*$^{-/-}$ BMDC co-stimulatory molecule expression or cytokine secretion[61]. This shows that myeloid cells respond differently either in the absence of PTPN22, or in the presence of $PTPN22^{R619W}$.

In addition to the role of PTPN22 in regulating LFA-1 signalling in T cells, PTPN22 has also been shown to induce reduced IFNγ expression by WT and *Ptpn22*$^{-/-}$ $CD4^+$ OT-II T cells after 6 days of co-culture with LPS matured, $OVA_{323-339}$ peptide pulsed BMDCs, followed by restimulation with freshly pulsed BMDCs for 2 days. This was not due to differences in LPS induced WT and *Ptpn22*$^{-/-}$ BMDC cytokine secretion, expression of co-stimulatory molecules, or due to the release of a soluble factor. Instead, it was found to be as a result of an LFA-1 dependent mechanism, as blocking LFA-1 during the co-cultures led to loss of the *Ptpn22*$^{-/-}$ BMDC induced IFNγ response[61].

1.3 Phenotype of *Ptpn22*$^{-/-}$ and *Ptpn22*^{R619W} mice using models of autoimmunity

As discussed above, *Ptpn22*$^{-/-}$ mice do not develop spontaneous autoimmunity. Despite this, when they are crossed with mice that express a mutated form of the phosphatase CD45, they do develop a lupus like disease[68]. In addition, when *Ptpn22*$^{-/-}$ mice are crossed onto a more susceptible genetic background (129/Sv), spontaneous autoimmunity does develop[13]. Induced models of autoimmunity have also been used to investigate the role of PTPN22 and these are summarised in Table 1-1 below.

Mouse genotype	Autoimmune disease model	Genotype effect on disease	Mechanism	Reference
Ptpn22$^{-/-}$ (C57Bl/6)	Experimental autoimmune encephalomyelitis	Reduced	Increased number of T_{regs} inhibits disease. T_{reg} depletion increases disease severity in *Ptpn22*$^{-/-}$ mice	Maine CJ, JI, 2012[57]
Ptpn22$^{-/-}$ (C57Bl/6)	Colitis	Enhanced	Increased T_{regs}, which are more suppressive, secrete more IL-10 and are more adhesive via LFA-1 than WT T_{regs}.	Brownlie RJ, Science Signaling, 2012[58]
Ptpn22$^{-/-}$ (C57Bl/6)	DSS induced colitis	Enhanced	Lack of TRAF3 ubiquitination leads to reduced production of Type 1 IFNs (which would normally suppress inflammation in colitis)	Wang Y, Immunity, 2013[10]
Ptpn22$^{-/-}$ and CD45 E613R (C57Bl/6)	Lupus like disease	Enhanced	Loss of tolerance due to an outgrowth of PTPN22 dependent hyperresponsive memory/effector T cells, giving rise to PTPN22 independent hyperresponsive B cells.	Zikherman J, JI, 2009[68]
PTPN22 knock down (NOD)	Diabetes	Reduced	Potentially due to more T_{regs} and reduced survival of B cells (which are required for full penetrance of diabetes in NOD mice).	Zheng P, Diabetes, 2013[69]
PTPN22 overexpression in T cells (NOD)	Diabetes	Reduced	More T_{regs} and reduced TCR dependent effector T cell proliferation and Th1 differentiation.	Yeh LT, JI, 2013[70]

Ptpn22^{R619W} knock in (NOD)	Diabetes	Enhanced	Early loss of tolerance to insulin, causing the production of insulin autoantibodies.	Lin X, Diabetes, 2016[71]
Ptpn22$^{-/-}$ (C57Bl/6)	Virus induced diabetes (RIP-LCMV-GP)	Enhanced	Increases antiviral effector T cell responses.	Fousteri G, Clinical Immunology, 2015[72]
Ptpn22^{R619W} (C57Bl/6 x 129/Sv)	Systemic autoimmunity (including STZ-induced diabetes)	Enhanced	Altered T and B cell homeostasis, including enhanced TCR and BCR signalling, leading to a loss of tolerance.	Dai X, Journal of Clinical Investigation, 2013[13]
Ptpn22$^{-/-}$ (SKG)	SKG arthritis (T cell mediated)	Reduced	More T cell skewing to Th1/T_{reg}, and reduced skewing to Th17 (which are pathogenic in this model).	Sood S, JI, 2016[73]
Human PTPN22^{R620W} knock in (SKG)	SKG arthritis (T cell mediated)	No effect	Overexpression may have been too low, or other phosphatases may play redundant roles.	Wu DJ, PLoS ONE, 2014[74]
Ptpn22$^{-/-}$ (C57Bl/6)	K/BxN arthritis	Enhanced	Increased frequency of T_{fh} cells and a lower T_{fr}/T_{fh} ratio.	Maine CJ, JI, 2014[59]
Ptpn22$^{-/-}$ (C57Bl/6)	K/BxN serum transfer model of arthritis	No effect	PTPN22 is not required after the production of autoantibodies.	Maine CJ, JI, 2014[59]
Ptpn22$^{-/-}$ (C57Bl/6)	K/BxN serum transfer model of arthritis	Reduced	Lack of neutrophil recruitment to joints.	Vermeren S, JI, 2016[63]
Ptpn22$^{-/-}$ (C57Bl/6)	K/BxN serum transfer model of arthritis	No effect	PTPN22 is not required after the transfer of arthritogenic serum.	Wang Y, Immunity, 2013[10]
Ptpn22^{R619W} (C57Bl/6)	K/BxN serum transfer model of arthritis	No effect	PTPN22 is not required after the transfer of arthritogenic serum.	Wang Y, Immunity, 2013[10]

Table 1-1: Models of autoimmunity used with PTPN22 variant mice.

Table shows the outcomes of each model and the potential mechanisms. Mouse backgrounds are shown in brackets in the first column.

1.4 Phenotype of *Ptpn22*$^{-/-}$ and *Ptpn22*^{R619W} mice using viral infection models

Due to the high prevalence of *PTPN22* variants in the population, and their association with autoimmunity, it has been speculated that the variants should also provide an immunological advantage. To date, a small number of studies have been published investigating whether PTPN22 is involved in defending against viral infections in mice.

As mentioned previously, PTPN22 is required for type I interferon production after TLR stimulation in myeloid cells. As part of this study, the response of WT and *Ptpn22*$^{-/-}$ mice to an acute infection with LCMV Armstrong was tested. PTPN22 was found to promote anti-viral responses as LCMV infected *Ptpn22*$^{-/-}$ mice were more susceptible to infection. This was due to a reduction in serum type I interferons one day after infection and a reduced activation of splenic CD8α^{+} DCs and plasmacytoid DCs. *Ptpn22*$^{-/-}$ mice also showed an impaired expansion of LCMV-specific CD8^{+} T cells[10]. A separate report also showed that *Ptpn22*$^{-/-}$ LCMV-specific CD8^{+} T cells failed to accumulate in WT hosts after acute infection with LCMV. This was accompanied by reduced pSTAT-1 in these T cells after stimulation with IFNα. However, in the same report, *Ptpn22*$^{-/-}$ CD8^{+} T cells showed enhanced expansion in a lymphopenic host[75].

A contrasting result was found using a different strain of LCMV which causes a chronic infection (clone 13). In this case, *Ptpn22*$^{-/-}$ mice were shown to be more capable of controlling the infection than WT mice, as shown by a lack of weight loss and reduced viral titres in the spleens over the course of the infection. This was accompanied by an increase in the number of LCMV-specific CD8^{+} T cells, which did not display an exhausted phenotype. In addition to enhanced *Ptpn22*$^{-/-}$ CD8^{+} T cell anti-viral responses, *Ptpn22*$^{-/-}$ CD4^{+} T cells also showed enhanced IFNγ and TNFα production after infection with LCMV clone 13[76]. A separate report also showed that *Ptpn22*$^{-/-}$ mice were able to resist a chronic viral infection with LCMV clone 13. After 28 and 39 days of infection, serum viral titres in *Ptpn22*$^{-/-}$ mice were substantially lower than those found in WT mice, and were also lower in the spleen, lung, liver and kidneys 14 days after infection. Viral clearance was found to be dependent on CD4^{+} T cells, as when they were depleted from *Ptpn22*$^{-/-}$ mice, the mice were no longer able to control the infection. 1 day post infection, *Ptpn22*$^{-/-}$ mice had a reduced frequency of IFNα and IFNβ producing splenic plasmacytoid DCs, which was accompanied by a subtle reduction in CD86 expression on splenic conventional DCs and plasmacytoid DCs[77].

Taken together, this data indicates that in the context of an acute viral infection, PTPN22 is needed for the production of anti-viral type I interferons by myeloid cells, which are required to induce an efficient T cell dependent adaptive response. However, PTPN22 also inhibits CD8^{+} T cell homeostatic proliferation during lymphopenia. In the case of a chronic viral infection, PTPN22 inhibits the differentiation of LCMV-specific CD8^{+} T cells, thereby promoting viral persistence.

1.5 The role of PTPN22 and PTPN22^{R620W} in human immune cells

The role of PTPN22 has also been studied in humans. However, due to the unavailability of tissue samples, most of the experiments have focussed on immune cell populations within the peripheral blood.

1.5.1 The role of PTPN22 in human T cells

Naïve CD4$^+$ T cells from the peripheral blood of healthy donors expressing *PTPN22^{R620}* or the disease associated *PTPN22^{R620W}* proliferate similarly after anti-CD3/anti-CD28 stimulation. Despite this, bulk CD4$^+$ T cells from healthy donors expressing *PTPN22^{R620W}* (homozygous) produce more IFNγ, TNFα and IL-2 and less IL-17A than WT CD4$^+$ T cells after 20 hours of TCR stimulation. However, suppression of IFNγ production by *PTPN22^{R620W}* CD4$^+$ T cells was impaired using T_{regs} from the same donor, indicating that *PTPN22^{R620W}* T_{regs} are less capable of suppression[78].

Enhanced TCR induced IL-2 secretion was not found in a separate study. In this case, CD4$^+$ T cells from children with type 1 diabetes expressing *PTPN22^{R620W}* (heterozygous) secreted reduced levels of IL-2 after anti-CD3/anti-CD28 stimulation, compared to those patients not expressing the variant[79]. This data indicates that the variant acts as a gain-of-function mutation with respect to TCR signalling. This finding was confirmed by another study which showed reduced IL-2 production, proliferation and activation of peripheral blood *PTPN22^{R620W}* CD4$^+$ T cells after TCR stimulation, and reduced calcium flux after PHA stimulation[80]. Reduced response to TCR stimulation by PTPN22^{R620W} expressing human T cells was also found in a separate report. Anti-CD3 stimulation of PTPN22^{R620W} T cells showed reduced calcium mobilisation compared to WT T cells from age and disease status matched controls. In addition, PTPN22^{R620W} (heterozygous) expressing T cells stimulated with irradiated antigen presenting cells (APCs) or with anti-CD3/anti-CD28 for 3 days showed reduced upregulation of the activation marker CD25 in comparison to WT T cells. This was accompanied by a reduction in interleukin-10 (IL-10) secretion after 24 hours of anti-CD3/anti-CD28 stimulation. Phenotyping of T cells from PTPN22^{R620} and PTPN22^{R620W} carriers showed that a higher proportion of peripheral blood CD4$^+$ T cells in individuals expressing PTPN22^{R620W} (heterozygous) were memory T cells (identified by their expression of CD45RO)[81].

The kinases Lck and ZAP-70 are phosphorylated after LFA-1 engagement, and as these are substrates of PTPN22, the role of PTPN22 in regulating LFA-1 signalling in human T cells was investigated. To begin, the localisation of PTPN22 in migrating primary T cell blasts was assessed. PTPN22 was found to co-localise with phosphorylated Src, ZAP-70 and Vav at the leading edge. siRNA suppression of PTPN22 in human T cell blasts led to an increased migration velocity on ICAM-1 coated surfaces. In addition, human T cell blasts from healthy donors expressing $PTPN22^{R620W}$ showed increased phosphorylation of ERK after stimulation with ICAM-1. In WT human T cells plated on ICAM-1 coated surfaces, PTPN22 clustered at the plasma membrane, close to LFA-1, where it could inhibit LFA-1 signalling, however T cells expressing $PTPN22^{R620W}$ did not form clusters of PTPN22 at the plasma membrane after ICAM-1/LFA-1 engagement, thus preventing the regulation of LFA-1 signalling[60].

Taken together, this indicates that in the context of TCR signalling, $PTPN22^{R620W}$ is generally acting as a loss-of-function mutation, such that it negatively regulates signalling downstream of TCR engagement, similarly to what has been demonstrated using PTPN22 deficient mice.

1.5.2 The role of PTPN22 in human B cells

Humans expressing $PTPN22^{R620W}$ (heterozygous) have a reduced frequency of peripheral blood $CD19^{+}$ $CD27^{+}$ memory B cells. In addition, memory B cells from these subjects demonstrated a lower level of calcium flux after anti-IgM stimulation[81]. A separate report showed that healthy humans expressing $PTPN22^{R620W}$ (heterozygous) had increased frequencies of peripheral blood transitional $CD19^{+}$ B cells ($CD19^{+}$ $CD27^{neg}$ $CD10^{+}$ $CD24^{+}$ $CD38^{hi}$) and anergic B cells ($CD19^{+}$ $CD27^{neg}$ IgD^{+} IgM^{neg})[82]. In addition, healthy individuals carrying the *PTPN22*^{R620W} risk allele were found to have more autoreactive B cells, with a 3-fold increase in the proportion of polyreactive B cells seen (that reacted to ssRNA, dsDNA, insulin and LPS)[83]. However, in a separate study, healthy subjects carrying the risk variant were found to have fewer autoreactive VH4-34^{+} transitional B cells, compared to healthy subjects not carrying the risk allele[84]. Both naïve and transitional B cells from $PTPN22^{R620W}$ (heterozygous) carriers display reduced apoptosis[82]. B cells from healthy $PTPN22^{R620W}$ (heterozygous) carriers also showed increased expression of genes involved in B cell activation, proliferation and survival, including *CD40, SLAMF6, BCL2 and ICOSL*. The increased *CD40* gene expression resulted in increased CD40 expression on the surface of naïve B cells from people harbouring the *PTPN22*^{R620W} risk allele, and these cells were more responsive to CD40 ligand stimulation, as judged by increased expression of CD25 and CD69 after 2 days[83]. Taken together, this data indicates that $PTPN22^{R620W}$ alters B cell homeostasis, potentially by

altering BCR signalling and resistance to BCR mediated apoptosis. This may lead to a loss of B cell tolerance in humans expressing the autoimmune associated variant of PTPN22.

1.5.3 The role of PTPN22 in human neutrophils

Neutrophils from PTPN22^{R620W} (heterozygous) expressing RA patients or healthy donors were found to have enhanced effector functions compared to PTPN22^{R620} expressing individuals. Healthy human neutrophils expressing PTPN22^{R620W} (heterozygous) transmigrated through an activated endothelial layer more effectively than WT neutrophils. These neutrophils also released more ROS after TNFα and *N*-Formyl-Methionyl-Leucyl-Phenylalanine (fMLP) stimulation. In addition, neutrophils heterozygous for PTPN22^{R620W} from both healthy individuals and RA patients released more calcium after stimulation with fMLP[85]. These observations are important as neutrophils are the major immune cell infiltrate in arthritic joints, so in patients harbouring the R620W variant, disease may be exacerbated by the presence of overactive neutrophils.

1.5.4 The role of PTPN22 in human natural killer cells

A potential role of PTPN22 in human natural killer (NK) cells has been investigated in one report. Peripheral blood mononuclear cells (PBMCs) from healthy donors expressing PTPN22^{R620W} (heterozygous) or PTPN22^{R620} were cultured *in vitro* in the presence of IL-2 and anti-CD3 after density gradient centrifugation. The proportion of $CD3^-$ $CD56^+$ NK cells was monitored over 21 days, and it was found that PTPN22^{R620W} (heterozygous) cultures had a reduced proportion of NK cells compared to PTPN22^{R620} cultures. However, this may be due to a preferential expansion of $CD3^+$ T cells in the PTPN22^{R620W} (heterozygous) cultures[86].

1.6 Is PTPN22^{R620W} a gain- or loss-of function mutant?

As both gain- and loss-of-phosphatase function roles have been attributed to PTPN22^{R620W}, depending on the cell type and the signalling pathway being investigated, this variant has recently been described as a switch-of-function polymorphism. In this case, the function of PTPN22^{R620W} could be influenced both by its catalytic activity, but also by its cellular location,

giving rise to different functions depending on the signalling pathway under investigation[87]. The apparently contradicting results which have been found in different cell types and downstream of different immunoreceptors, highlights the utility of investigating the role of PTPN22 using *Ptpn22*$^{-/-}$ mice. In this case, the complete absence of the protein allows for the identification of its fundamental role in cells, after which the effect of the variant can be investigated.

1.7 DCs

1.7.1 DC development and differentiation in mice

DCs were first described by Ralph Steinman and Zanvil Cohn in 1973[88]. Their name refers to the presence of dendritic like protrusions, which they visualised on a phagocytic cell type in mouse spleens. DCs, although of myeloid lineage and closely related to macrophages and monocytes, develop from a DC specific committed progenitor in the bone marrow.

DCs are a heterogenous population and can be broadly divided into two subsets, namely plasmacytoid DCs (pDCs) and conventional CD11c^{+} DCs (cDCs) (Figure 1-2). pDCs recognise bacterial and viral pathogens via TLR9 and TLR7 respectively, and respond to infection by releasing type I interferons (mainly IFNα and IFNβ), IL-6 and TNFα. Type I interferon secretion is dependent on expression of the transcription factor IRF7, and induces an anti-viral response in addition to NK cell activation. pDCs are also capable of initiating adaptive immune responses by presenting antigens to CD4^{+} and CD8^{+} T cells and by expressing chemokines which lead to the recruitment of immune cells[89]. pDCs differentiate from common DC progenitors (CDPs) as a result of fms-like tyrosine kinases 3/fms-like tyrosine kinases 3 ligand (Flt3/Flt3L) engagement and downstream STAT3 signalling. This in turn enhances E2-2 expression, which is the major transcription factor involved in the development of pDCs[90], and suppresses the expression of ID2, a transcription factor required for cDC development[91]. Conversely, GM-CSF and STAT5 signalling induces the expression of ID2, which inhibits pDC development by antagonising E2-2. pDCs mainly reside in the lymph nodes and spleen under non-inflammatory conditions, and utilise endothelial venules to enter lymph nodes, aided by the expression of L-selectin on the high endothelial venules and CCL19 and CCL21 expression in the lymph node.

cDCs are superior to pDCs at internalising and presenting antigens to T cells, due to their enhanced endocytic capacity, higher MHCII and co-stimulatory molecule expression and

cathepsin S and D expression; enzymes which are required for antigen processing. As with pDCs, cDCs also depend on Flt3/Flt3L signalling for their development[92] and all express the transcription factor ZBTB46. cDCs can be further subdivided into cDC1s and cDC2s. cDC1s express the chemokine receptor XCR1 and are further distinguished by their expression of CD8α in lymphoid organs and CD103 in non-lymphoid organs. Their main role is cross-presentation of exogenous antigens on MHCI to $CD8^+$ T cells. There are multiple transcription factors that have been linked with the development of cDC1s, including ID2, BATF3, NFIL3 and IRF8. For example, *Batf3*$^{-/-}$ mice specifically lack $XCR1^+$ DCs, including splenic $CD8\alpha^+$ cDCs, and lung, dermal and intestinal $CD103^+$ cDCs[93]. Mouse cDC1s correspond to human $CD141^+$ DCs[94].

cDC2s are defined by their expression of the integrin CD11b or SIRPα, and form the most abundant cDC population found in lymphoid organs. They present antigens in MHCII, for the activation of $CD4^+$ T cells. cDC2s can be divided further into $ESAM^{hi}$ and $ESAM^{lo}$ populations, with $ESAM^{hi}$ being the major subtype. Transcription factors RelB, NOTCH2, IRF2, IRF4 and RBP-J have been shown to be involved in cDC2 development. For example, deletion of NOTCH2 or RBP-J in $CD11c^+$ cells caused a lack of cDC2s in the spleen[95,96], and this led to a reduced activation of $CD4^+$ T cells[96]. After TLR stimulation, cDC2s produce pro-inflammatory cytokines IL-6 and interleukin-23 (IL-23), with $ESAM^{lo}$ cells being the best producers. Mouse cDC2s correspond to human $CD1c^+$ DCs[94].

In addition to cDCs and pDCs, there are also a subset of non-classical DCs, which include monocyte-derived DCs (also known as inflammatory DCs). These differentiate in both lymphoid and non-lymphoid organs from monocytes in the presence of inflammation or infection. Monocyte-derived DCs, as opposed to cDCs or pDCs, are thought to be somewhat similar to GM-CSF induced BMDCs[97], which have commonly been used to study DCs *in vitro*.

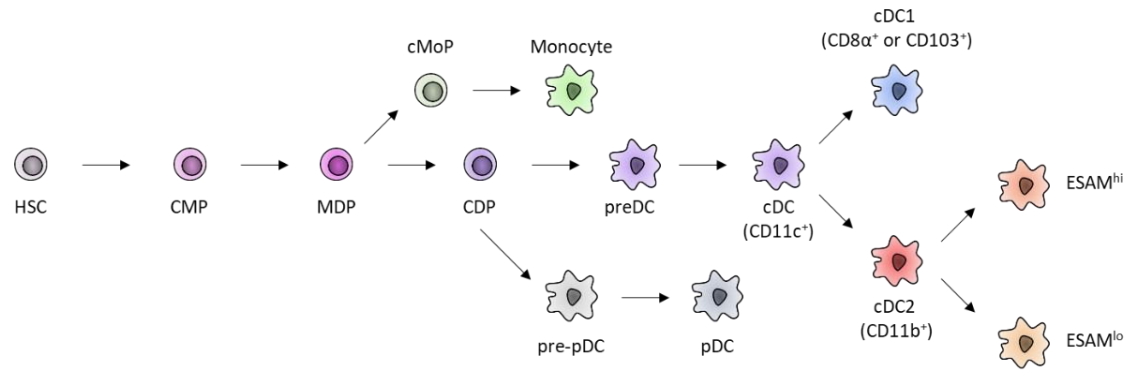

Figure 1-2: DC development in mice.

Hematopoietic stem cells (HSC) differentiate into a variety of progenitor cells, including common myeloid progenitors (CMP). These in turn differentiate into monocyte and DCl progenitors (MDP). MDPs lack the potential to differentiate into lymphoid, megakaryocyte and granulocyte cells, but can give rise to both monocytes (and their progenitors), plasmacytoid DCs (pDCs) and conventional DCs (cDCs). MDPs can differentiate into common monocyte progenitors (cMoPs), which lack Flt3 expression and therefore can not produce DCs, but instead produce monocytes. Alternatively, MDPs differentiate into common DC progenitors (CDP), which express Flt3 and M-CSFR, but have lost monocyte potential, so give rise to preDCs and pre-pDCs. preDCs become cDCs, which can be further divided into cDC1s (CD8α⁺ or CD103⁺) and cDC2s (CD11b⁺). cDCs can be further subdivided into ESAM^{hi} and ESAM^{lo} subsets. Diagram has been adapted from Merad M et al., Annual Review of Immunology, 2013 and Mildner A and Jung S, Immunity, 2014.

1.7.2 General functions of DCs

DCs are professional APCs which are critical for pathogen sensing, antigen uptake and presentation. Although macrophages and B cells are also capable of presenting antigen, they are more specialised for phagocytosis and antibody production respectively. Immature DCs are found in peripheral tissues (although lymphoid resident DCs also exist), where they display high levels of endocytosis, required for sampling antigens. Once DCs have internalised an antigen, they migrate to draining lymph nodes via the afferent lymph, a process which can take between 1-3 days and is dependent on CCR7 expression[98]. During this period, DCs also undergo a process termed maturation. DC maturation involves increased expression of MHCII and co-stimulatory molecules, production of cytokines and chemokines, and an enhanced migratory capacity due to the upregulation of chemokine receptors. Once in the lymph node, the DCs present antigens to T and B cells, to either promote tolerance (if the antigen was internalised in the absence of an inflammatory signal) or to initiate an adaptive immune response. DCs are the only APC which can activate naïve T cells and are therefore vital in initiating an adaptive immune response. DCs then receive feedback from the adaptive immune cells, including via the secretion of cytokines and antibodies, which further shape the immune response.

To understand the role of DCs in immunity, mice have been engineered that lack DCs. This was achieved by crossing CD11c-Cre mice with mice expressing diptheria toxin under the control of a loxP flanked neomycin resistance (neo^R) cassette from the ROSA26 locus. In the absence of DCs (cDCs, plasmacytoid DCs and Langerhans cells), these mice had reduced body weight, developed spontaneous autoimmunity, had enlarged spleens and lymph nodes (mainly as a result of increased neutrophil frequencies), had more activated $CD4^+$ T cells in the spleens, lymph nodes and peripheral organs, and displayed enhanced serum autoantibody production[99]. In addition, 40% of mice lacking DCs died within 8 weeks of age. This demonstrates that DCs are required to promote immune tolerance and to therefore prevent the development of autoimmunity under non-inflammatory conditions.

1.7.3 Antigen uptake by DCs

Although lymphoid resident DCs are able to present lymph and blood derived antigens which drain through lymphatic vessels from the periphery to the lymph nodes and spleen, this is only efficient if the antigen is present at a high concentration. Alternatively, DCs present in the peripheral tissues can take up soluble and particulate matter from extracellular fluid using a process known as endocytosis, which includes both phagocytosis and macropinocytosis. As discussed above, these tissue resident DCs can then migrate to draining lymph nodes and present antigens to T and B cells.

Receptor mediated endocytosis is aided by the presence of numerous cell surface receptors, referred to as pattern recognition receptors (PRRs). These include Toll-like receptors (TLRs), C-type lectin receptors (CLRs), nucleotide oligomerisation domain (NOD)-like receptors (NLRs) and retinoic acid-inducible gene I (RIG-I)-like receptors (RLRs). Together these receptors recognise a wide variety of pathogen-associated molecular patterns (PAMPs) and damage-associated molecular patterns (DAMPs). After recognition of PAMPs and DAMPs by receptors present on DCs, signalling downstream of the receptor leads to its internalisation, often via the recruitment of clathrin, leading to the formation of clathrin coated endocytic vesicles. For larger, particulate antigens, receptor mediated phagocytosis is utilised, which generally uses the same receptors as receptor mediated endocytosis. Phagocytosis requires the actin cytoskeleton and leads to the formation of large intracellular vacuoles.

Although PRRs can bind and recognise a vast array of PAMPs and DAMPs, DCs also require an alternative mechanism to internalise antigens. For this, they use macropinocytosis to internalise

large amounts of soluble antigens from their environment. Macropinocytosis is an actin dependent process, as preventing actin polymerisation blocks macropinocytosis in BMDMs[100], but it does not require the presence of cell surface receptors. Macropinocytosis requires phosphoinositide 3 (PI3)-kinase activity, as inhibition using wortmannin or LY294002 prevented closure of macropinosomes in mouse BMDMs[101]. GTPases have also been shown to be involved in macropinocytosis, for example, splenic DCs expressing a dominant negative form of Rac are unable to form macropinosomes[102].

Extracellular material internalised via macropinocytosis enters macropinosomes, which can be up to 5 µm in diameter, and form as a result of membrane ruffling. Depending on the type of APC, macropinosomes enter different intracellular processing pathways. In human DCs, antigens internalised by macropinocytosis enter compartments which contain MHCII, cathepsin D and lysosomal associated membrane protein-1 (LAMP-1), indicating that they enter late endosomes/lysosomes to be degraded[103], and do not enter early endosomes[104]. In addition, antigen which has been internalised via macropinocytosis can be released into the cytoplasm where they can be processed and cross-presented via MHCI[105]. As a result of PRR stimulation, DCs mature, and this is accompanied by a decreased capacity to internalise material via macropinocytosis *in vitro*. Despite this, mature DCs still endocytose and phagocytose, but their function shifts towards presentation of previously internalised antigens. The fact that mature DCs are still capable of endocytosis is exemplified by the fact that splenic DCs matured using LPS or CpG and pulsed with ova *in vivo* are still capable of internalising ova, as they cause similar ova specific $CD4^+$ and $CD8^+$ T cell proliferation as immature splenic DCs, after being co-cultured *in vitro* for 60 hours[106].

1.7.4 Antigen processing and presentation by DCs

The delivery of internalised antigens into the appropriate antigen processing pathways is essential so that DCs can process antigens into peptides which can be presented to T cells. Generally, the proteasome, a multi-subunit protease, is responsible for the degradation of intracellular antigens found in the cytosol[107], whereas lysosomal proteolysis is used to degrade internalised antigens[108]. Presentation of peptides in MHCI leads to the activation of $CD8^+$ T cells, mainly for the elimination of infected cells and tumour cells. However, this also requires the activation of $CD4^+$ T cells via peptides expressed in MHCII. MHCI is expressed on nearly all cell types, and non-immune cell expression of peptides in MHCI are derived from cytosolic proteins which have been processed by the ubiquitin/proteasome system. Cytosolic peptides, usually 8-

10 amino acids in length, are loaded onto MHCI in the endoplasmic reticulum (ER) and then transported to the plasma membrane via the Golgi apparatus[107]. If the DC is immature, in the case of presentation of self-peptides, then this should promote tolerance. However, if the DC is mature, then $CD8^+$ T cells should be activated to recognise and kill infected cells. In addition to presenting endogenous antigens on MHCI, DCs can also present exogenous antigens on MHCI, by a process known as cross-presentation.

Instead of being processed by the proteasome, exogenous, internalised antigens enter endolysosomal compartments. These consist of early endosomes, late endosomes and lysosomes, which in turn are more acidic and proteolytically active. For example, lysosomes have a pH of 4-4.5 and contain cathepsin proteases which lead to the degradation of the internalised pathogens, allowing for the loading of peptides onto MHCII molecules, and subsequent presentation to $CD4^+$ T cells.

MHCII is assembled in the ER and relocates to endosomal compartments bound to the invariant chain (Ii, CD74). The invariant chain is also synthesised in the ER, where it forms trimers. Three MHCII αβ heterodimers associate with one Ii trimer, and this MHCII-Ii complex facilitates MHCII stabilisation, as in the absence of Ii, an accumulation of misfolded MHCII molecules are found in the ER[109,110]. The invariant chain also targets MHCII to endosomal compartments, via the Golgi and *trans*-Golgi network, and requires the presence of a conserved di-leucine motif in its N-terminal cytoplasmic domain[111]. These leucine residues can associate with the adaptor molecules AP1 and AP2[112], and are responsible for endocytosis of MHCII-Ii found on the plasma membrane. The invariant chain prevents peptide binding and is released from MHCII via progressive proteolysis in endosomes, until only the class II-associated invariant chain peptide (CLIP) remains in the binding grove of MHCII. In late endosomes, the non-classical MHC glycoprotein HLA-DM (H2-M in mice) then aids the release of CLIP from MHCII by inducing a conformation change. HLA-DM also stabilises empty MHCII molecules, thus preventing their aggregation. Once CLIP is released, antigenic peptides can be loaded onto MHCII in the late endosomal compartment. The MHCII groove, formed by the alpha and beta chain can accommodate peptides of 13-25 amino acids in length[108]. HLA-DM can also remove low affinity peptides from MHCII[113]. In mature DCs, peptide-MHCII complexes then traffic to the plasma membrane via endolysosomal tubules[114], which are positive for LAMP-1, CD63 and CD82. Endolysosomal tubules colocalise with microtubules and do not form when LPS matured DCs are treated with nocodazole, which destabilises microtubules, indicating that microtubules act as scaffolds for endolysosomal tubules. Cytochalasin D, on the other hand, had no effect on the presence of endolysosomal tubules, indicating that the actin cytoskeleton is not required[114] (Figure 1-3).

If peptide-MHCII complexes presented on the cell surface of APCs are not recognised by T cells, they are targeted for degradation by ubiquitination. This allows APCs to present a wider variety of antigens to T and B cells. In human DCs, peptide-MHCII complexes are internalised by clathrin-independent endocytosis after ubiquitination by March-1, an E3 ubiquitin ligase[115,116]. After DC maturation, peptide-MHCII complexes are maintained on the cell surface for longer, partly due to an overall reduction in endocytosis, but also by the fact that peptide-MHCII complexes are no longer ubiquitinated by March-1[116].

In comparison to macrophages, DCs have higher endosomal pH and lower protease contents, which causes less antigen degradation, and therefore favours antigen presentation. The low antigen degradation in DCs may favour the production of longer antigenic peptides which can be presented in MHCII and may contribute to their ability to cross-present exogenous antigens on MHCI, potentially explaining why DCs are more effective APCs than macrophages[117].

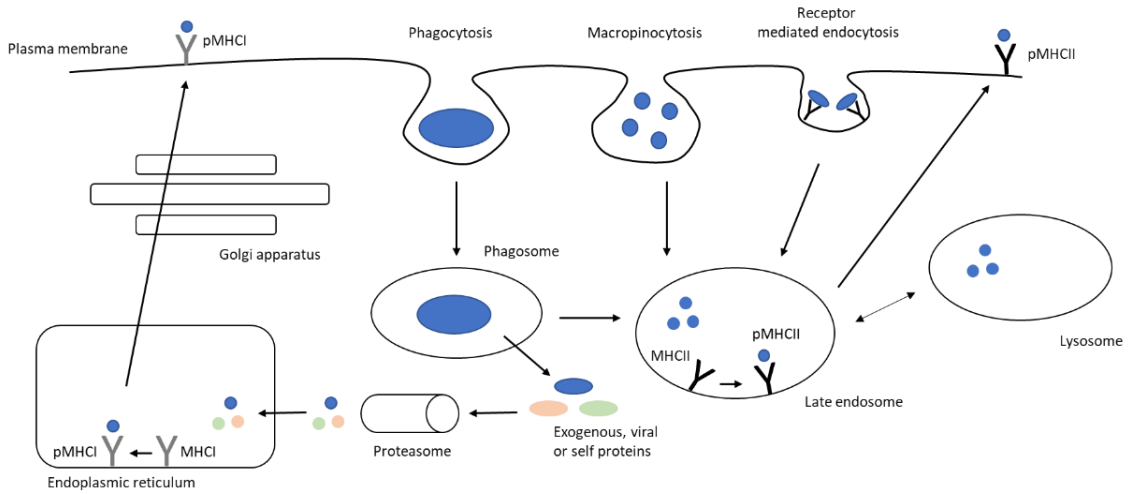

Figure 1-3: Routes of antigen uptake, processing and presentation by DCs.

Antigens can be internalised via phagocytosis, macropinocytosis or receptor mediated endocytosis. Once internalised, they enter early endosomes, late endosomes and lysosomes, which are progressively more acidic, leading to antigen degradation. Peptides can then be loaded onto MHCII molecules and transported to the plasma membrane, for presentation to $CD4^+$ T cells. Alternatively, internalised antigens, along with self-proteins and viral proteins can be degraded by the proteasome and be loaded onto MHCI, for presentation to $CD8^+$ T cells. Diagram has been adapted from Liu Z and Roche PA, Frontiers in Physiology, 2015 and Blum JS et al., Annual Review of Immunology, 2013.

1.7.5 The role of Src and Syk family kinases in regulating antigen uptake, processing and presentation

Protein kinases and phosphatases are essential for regulating numerous receptor signalling pathways present in DCs. Src and Syk family kinases are expressed in innate cells and play a fundamental role in initiating and regulating signalling for receptors that utilise ITAMs, including C-type lectin receptors and immunoreceptors[118]. The Src family of tyrosine kinases consists of Src, Yes, Fyn, Gardner-Rasheed feline sarcoma viral oncogene homologue (Fgr), Lck, hematopoietic cell kinase (Hck), B cell lymphocyte kinase (Blk), Lyn and Fyn related kinase (Frk), while innate cells predominantly express Hck, Fgr, Lyn and Src[118]. The Syk family of tyrosine kinases includes Syk and ZAP-70, but only Syk is expressed in innate cells[118].

The role of Syk in the presentation of immune complex derived antigens has been investigated using selective inhibitors. Syk inhibition in mouse BMDCs inhibited immune complex internalisation and led to the subsequent reduction in immune complex induced BMDC cytokine secretion[119] and presentation of antigens to T cells[120]. In addition, Syk deficient BMDMs are defective in FcγR dependent phagocytosis of IgG opsonised sheep red blood cells[121]. In the same study and in a subsequent one, the role of Src family kinases was also tested, and BMDMs deficient for Hck, Fgr and Lyn were capable of phagocytosing opsonised red blood cells, albeit at a reduced rate compared to WT BMDMs[121,122]. BMDMs lacking either Syk or Src family kinases were capable of internalising latex beads and *E. coli*, indicating that these kinases are not required for general phagocytosis by all cell surface receptors.

1.8 FcγRs

1.8.1 FcγR expression and function

Autoantibodies have long been implicated in the aetiology of autoimmune diseases including RA, T1D, Graves' disease and SLE, diseases for which *PTPN22*^{R620W} is also a susceptibility risk allele[123]. Autoantibodies are produced by B cells and bind to self-antigens forming immune complexes (ICs) which are recognised by fragment crystalline (Fc) receptors (FcRs), thus inducing FcR mediated antigen uptake and cell activation.

FcRs are found on most innate immune cells, including DCs, and are part of the immunoglobulin superfamily. FcRs recognise the Fc region of immunoglobulins (Igs) and can be categorised depending on which class of Ig they recognise. FcγRs recognise the Fc regions of IgGs, FcεRI recognises IgE, FcαRs recognise IgA, FCMRs recognise IgM and FcδRs recognise IgD. IgG is the most abundant immunoglobulin class found in mice and humans[124]. IgG can be further divided into subclasses, namely IgG1, IgG2, IgG3 and IgG4 in humans, and IgG1, IgG2a, IgG2b and IgG3 in mice[125]. These are detected by FcγRs as either monomeric, as part of an aggregate, an IC or opsonised particle. There are four cell surface FcγRs expressed in mice, FcγRI, IIb, III and IV, and six expressed in humans, FcγRI, FcγRIIA, FcγRIIB, FcγRIIC, FcγRIIIA and FcγRIIIB (see Tables 1-2 and 1-3). The FcγRs have different affinities for IgG subclasses. For example, mouse FcγRIV is a high affinity receptor for IgG2b[126], but does not bind to IgG1 or IgG3. Mouse FcγRI is a high affinity receptor for IgG2a and a low affinity receptor for IgG2b and IgG3. FcγRIIb and FcγRIII are low affinity receptors for mouse IgG1, IgG2a and IgG2b. FcγRIIb, III and IV can also bind to IgE with low affinity, making FcγRI the only specific IgG receptor expressed in mice[126]. There are also two cytoplasmic FcγRs which recognise internalised IgGs, tripartite motif containing protein 21 (TRIM21) and neonatal FcR (FcRn). FcγRI, III and IV are classed as activating receptors, whereas FcγRIIb is the only inhibitory receptor expressed in mice. Most innate immune cells express both activating and inhibitory FcγRs, allowing for the modulation of downstream signalling. However, there are exceptions, as NK cells only express FcγRIII and B cells only express FcγRIIb, which allows them to regulate signalling via the BCR[125].

FcγR	Cell location	Activating or inhibitory	IgG subclass affinity
FcγRI	Plasma membrane	Activating	High affinity for IgG1, IgG3 and IgG4
FcγRIIA	Plasma membrane	Activating	Low affinity for IgG1, IgG2, IgG3 and IgG4
FcγRIIB	Plasma membrane	Inhibitory	Low affinity for IgG1, IgG3 and IgG4
FcγRIIC	Plasma membrane	Activating	Low affinity for IgG1, IgG3 and IgG4
FcγRIIIA	Plasma membrane	Activating	Low affinity for IgG1, IgG3 and IgG4
FcγRIIIB	Plasma membrane	Activating	Low affinity for IgG1, IgG3 and IgG4
FcRn	Intracellular	IgG recycling and transport	High affinity for IgG1, IgG2, IgG3 and IgG4
TRIM21	Intracellular	Activating and proteasome targeting	High affinity for IgG1, IgG2, IgG3 and IgG4

Table 1-2: IgG recognising FcR expression in humans and their IgG binding affinities.

FcγR	Cell location	Activating or inhibitory	IgG subclass affinity
FcγRI	Plasma membrane	Activating	High affinity for IgG2a, low affinity for IgG2b. No binding to IgG1
FcγRIIb	Plasma membrane	Inhibitory	Low affinity to IgG1, IgG2a and IgG2b. No binding to IgG3
FcγRIII	Plasma membrane	Activating	Low affinity to IgG1, IgG2a and IgG2b. No binding to IgG3
FcγRIV	Plasma membrane	Activating	High affinity for IgG2a and IgG2b. No binding to IgG1 and IgG3
FcRn	Intracellular	IgG recycling and transport	High affinity for IgG1, IgG2a, IgG2b and IgG3
TRIM21	Intracellular	Activation and proteasome targeting	Binds to IgG2a, IgG2b and IgG3 with unknown affinity

Table 1-3: IgG recognising FcR expression in mice and their IgG binding affinities.

IgG immunoglobulins are composed of two heavy (H) chains and two light (L) chains, linked by disulphide bonds. The heavy chains contain an N-terminal variable domain (V_H) and three constant domains (C_H1, C_H2 and C_H3). The light chain consists of an N-terminal variable domain (V_L) and a constant region (C_L). The Fc region, which is recognised by FcγRs, is composed of the lower hinge region between C_H1 and C_H2, in addition to the C_H2 and C_H3 domains. Although the subclasses of IgG show high homology, there is variation in the Fc regions, and this affects IgG binding to FcγRs. A conserved N-linked glycosylation site between C_H2 and C_H3 in the heavy chain (N297) affects binding to FcγRs by modulating the quaternary structure of the Fc region of the IgG[127]. The presence of a glycan at this position acts to stabilise the Fc region and leads to a more open IgG conformation, thus enhancing FcγR binding. The glycan is composed of a core structure of *N*-acetylglucosamine (GlcNAc) and mannose groups, which can be extended by the presence of galactose, sialic acid, fucose and bisecting GlcNAc, the combination of which affects FcγR binding. The glycan is also able to directly bind to the FcγR, through glycan protein binding. The glycosylation state of N297 has been adapted to modulate and improve FcγR binding of therapeutic monoclonal antibodies. For example, the lack of fucose enhances IgG binding to human FcγRIII[126,128].

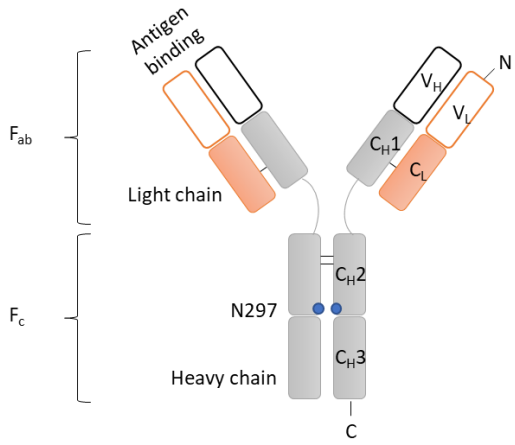

Figure 1-4: The structure of IgG.

IgGs are formed of two heavy (H, grey) and two light (L, orange) polypeptide chains, linked by disulphide bonds (black lines). These contain both constant (C, filled) and variable (V, open) regions. The F_{ab} region is composed of the light chains and the V_H and C_H1 domains of the heavy chains. The F_c region is composed of the lower hinge region between C_H1 and C_H2, as well as the C_H2 and C_H3 domains of the heavy chains. An N-linked glycosylation site is located within the heavy chain (N297, blue circles). Diagram has been adapted from Shade K et al., Antibodies, 2013.

When the Fc region of an IgG is recognised by an activating FcγR, this leads to receptor crosslinking and induces Src family kinase activation, which in turn phosphorylates two tyrosine residues in the ITAM, located in the associated common γ chain. Syk is then recruited via its tandem SH2 domains to the phosphorylated tyrosines. After Syk recruitment, downstream targets are phosphorylated, including LAT. Phosphorylated LAT then recruits phospholipase Cγ (PLCγ) which hydrolyses phosphatidyl inositol 4,5-bisphosphate to soluble inositol 1,4,5-triphosphate (IP_3) and membrane bound diacylglycerol (DAG). This results in enhanced intracellular calcium, leading to further downstream signalling involving ERK, p38 and c-Jun N-terminal kinase (JNK). This signalling ultimately leads to a range of cellular processes including DC maturation, cytoskeletal rearrangement, oxidative burst, antibody dependent cell mediated cytotoxicity (ADCC) and chemokine/cytokine production[125] (Figure 1-5a). The presence of Src and Syk family kinases downstream of FcγRs raises the possibility that PTPN22 may be involved in regulating signalling via its ability to dephosphorylate these kinases.

Alternatively, if the Fc region of an IgG is recognised by the inhibitory receptor FcγRIIb, phosphatases such as SH2-domain-containing protein tyrosine phosphatase 1 (SHP-1) and SH2-domain-containing inositol polyphosphate 5' phosphatase 1 (SHIP-1) are recruited to the phosphorylated tyrosines in the immunoreceptor tyrosine-based inhibition motif (ITIM), located in the cytoplasmic tail of the receptor. Co-ligation of an activating FcγR with the inhibitory FcγRIIb reduces activating signalling by dephosphorylation of signalling intermediates. To reduce signalling downstream of an activating receptor, FcγRIIb needs to be co-ligated with the same

immune complex[129] (Figure 1-5b). Therefore, the cellular response depends on a balance between the positive and negative signals. Ideally, foreign antigens will promote positive signals, giving rise to a pro-inflammatory response, whereas in the case of self-antigens, an anti-inflammatory response will be mounted. If this balance is not regulated appropriately, then pathogens may not be eliminated, or autoimmunity may ensue.

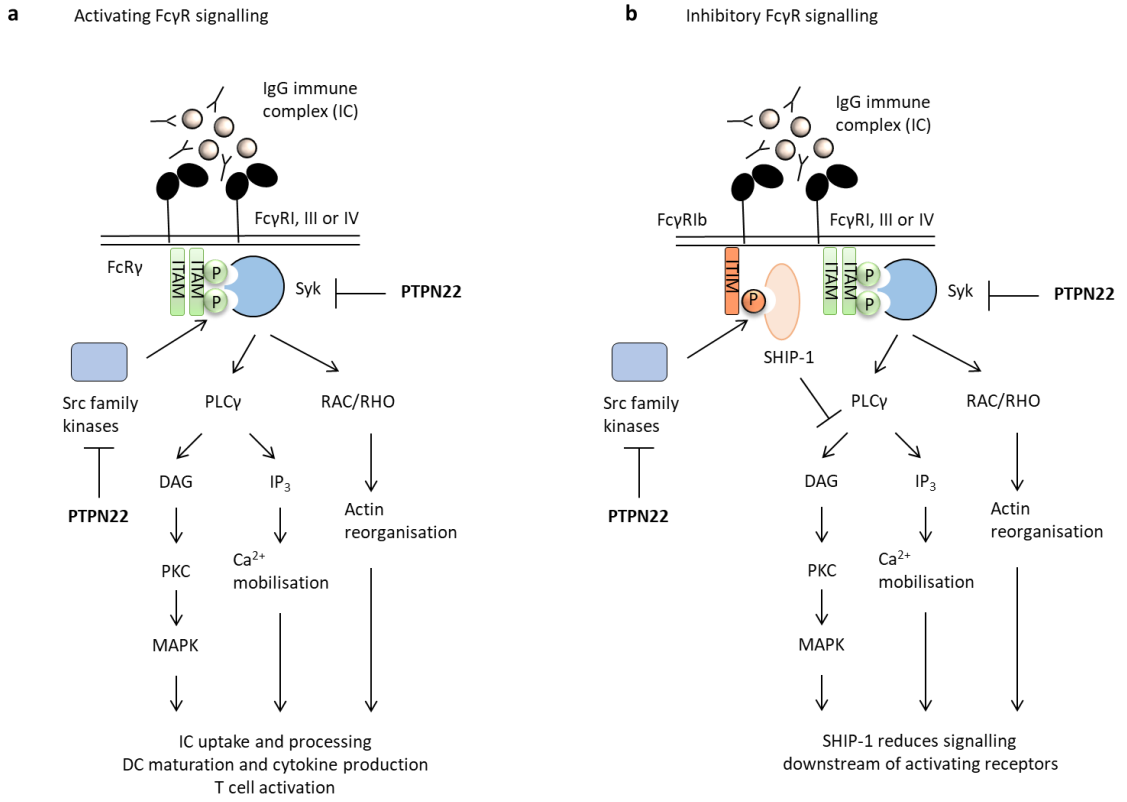

Figure 1-5: Schematic showing activating and inhibitory FcγR signalling.

(a) Activating FcγR signalling is initiated by the Fc regions of IgGs in immune complexes being recognised by FcγRs. This causes receptor crosslinking, which leads to Src family kinase dependent phosphorylation of the tyrosines in the ITAM of the associated common gamma chain (FcRγ). Syk binds to the phosphorylated tyrosines via its SH2 domains and leads to downstream signalling resulting in cellular processes including immune complex uptake, processing and presentation, cell maturation, cytokine production, and T cell activation. (b) Inhibitory FcγR signalling occurs when an immune complex is bound by both an activating FcγR and the inhibitory receptor FcγRIIb. Src family kinases phosphorylate a tyrosine in the ITIM, located in the cytoplasmic tail of FcγRIIb, leading to SHIP-1 recruitment. SHIP-1 then negatively regulates signalling downstream of the activating receptor, leading to increased hydrolysis of PIP_3 and ERK inhibition. Diagrams have been adapted from Takai T, Nature Reviews Immunology, 2002, Schmidt RE et al, Immunology Letters, 2005 and Ivashkiv LB, Immunology, 2011.

In myeloid cells, both the activating and inhibitory FcγRs internalise IgG-containing particles after they are recognised. Internalisation of ICs via activating FcγRs is dependent on the presence of the two tyrosines in the ITAM[130]. However, the di-leucine motif in the intracellular domain of FcγRIIb is required for uptake via this receptor[131]. There are three isoforms of FcγRIIb in mice,

FcγRIIb1, FcγRIIb1' and FcγRIIb2[132]. FcγRIIb1 contains an insertion of 47 amino acids in its cytoplasmic domain and is incapable of endocytosis, whereas this insertion is lacking in FcγRIIb2, and it is this isoform that mediates endocytosis and clearance of immune complexes[131]. FcγRIIb2 is predominantly expressed in myeloid cells, whereas FcγRIIb1 is expressed by lymphoid cells. ICs taken up by activating FcγRs are thought to enter a degradative pathway, to allow for the production of peptides which can be presented to both $CD4^+$ and $CD8^+$ T cells. Uptake via the inhibitory FcγR is thought to cause retention of the IgG-containing particle, potentially for presentation of intact antigen to B cells[133]. The intracellular IgG receptors, TRIM21 and neonatal FcR are thought to play an important role in routing FcγR-IgG complexes to specific endosomes for either degradation or recycling[134–137]. TRIM21 is especially important in orchestrating the degradation of antibody bound viruses, by routing these to the proteasome via its E3 ubiquitin ligase activity[137].

The requirement for intact ITAM signalling downstream of FcγRs in BMDCs has been investigated and found to be required for optimal T cell responses. This was demonstrated using NOTAM BMDCs, which are unable to signal through ITAMs, but have normal FcγR cell surface expression[138]. NOTAM BMDCs show normal ova IC binding, but reduced uptake and degradation. As a result, NOTAM BMDCs are unable to present ova IC derived antigens on MHCI and MHCII (despite being capable of stimulating T cells when pulsed with $OVA_{323-339}$ peptide or ova protein)[139]. ITAM signalling was also demonstrated to be important using DAP12 and FcRγ doubly deficient mice, as BMDCs from these mice were pulsed with ova coated beads and were unable to cause ova specific $CD4^+$ T cell proliferation[140].

1.8.2 Regulation of FcγR signalling

Polymorphisms have been detected in human *FCGR* genes and shown to be associated with autoimmune diseases such as SLE, RA and multiple sclerosis[141], which demonstrates the requirement for effective regulation of FcγR signalling. The major mechanism used to regulate signalling downstream of activating FcγRs is the presence of the inhibitory receptor. As discussed above, if the inhibitory receptor is crosslinked by the same immune complex as an activating receptor, then the inhibitory receptor negatively regulates signalling downstream of the activating receptors. This is due to the recruitment of phosphatases including SHP-1, SHP-2 and SHIP-1 to the phosphorylated tyrosines in the ITIM in the intracellular domain of the receptor. SHIP-1 is thought to be the major phosphatase involved in FcγRIIb signalling and subsequent

inhibition of activating FcγR effector responses in mast cells and B cells[142–144]. SHIP dephosphorylates phosphatidylinositol-3,4,5-triphosphate, thus preventing the production of IP_3 and DAG[145]. FcγRIII and FcγRIIb bind to IgG containing immune complexes with similar affinity and specificity, indicating that if FcγRIIb is present on the same cell as FcγRIII then it is likely that it will reduce activating FcγRIII signalling. In the steady state, the ratio of activating FcγR to FcγRIIb expression is low, preventing undesirable responses to immune complexes. However, this ratio increases during inflammation. Expression of these opposing receptors can be modulated *in vitro* using a variety of pro and anti-inflammatory cytokines. For example, IFNγ can enhance FcγRI and FcγRIII expression, while also reducing FcγRIIb expression on the cell surface of kidney mesangial cells[146]. Alternatively, anti-inflammatory cytokines IL-4 and TGFβ have been shown to increase the expression of FcγRIIb on THP-1 cells[147]. This demonstrates that during a type 2 helper T cell (Th2) mediated immune response, IL-4 enhances FcγRIIb signalling, preventing excessive IgG dependent inflammatory responses. Whereas, during a type 1 helper T cell (Th1) mediated response, IFNγ favours activating FcγR signalling.

An additional level of modulation is provided by inhibitory ITAM signalling (ITAMi), where monomeric antibodies (in the absence of antigen) cause recruitment of the phosphatase SHP-1 to the ITAM, thus suppressing cell activation downstream of other activating receptors[148]. Inhibitory signalling may be due to only one ITAM tyrosine residue being phosphorylated after IgG engagement with the receptor[149] (Figure 1-6). This mechanism may continuously reduce immune cell activation and therefore contribute to maintaining immune homeostasis[148]. This can also occur as a result of chronic activating receptor stimulation.

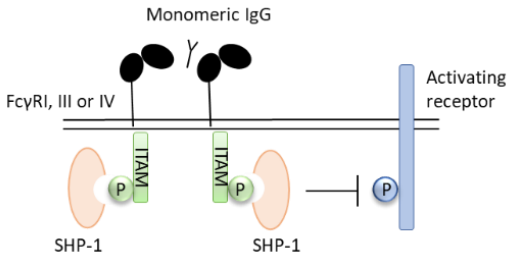

Figure 1-6: Schematic showing inhibitory ITAM FcγR signalling.

Inhibitory ITAM signalling (ITAMi) occurs after low avidity engagement of an activating FcγR, for example, with monomeric IgG, which causes mono-phosphorylation of a tyrosine in the ITAM. Instead of leading to the recruitment of Syk (which requires that both tyrosines are phosphorylated), this leads to SHP-1 recruitment, which in turn inhibits signalling from activating receptors. Diagrams have been adapted from Takai T, Nature Reviews Immunology, 2002, Schmidt RE et al, Immunology Letters, 2005 and Ivashkiv LB, Immunology, 2011.

Ubiquitination also provides a mechanism for negative regulation of FcγR signalling. Ubiquitination can lead to internalisation and/or delivery of antibody or immune complex bound

FcγRs to lysosomes or proteasomes for degradation. Ubiquitin is added to lysine residues in the target proteins, either via monoubiquitination (a single ubiquitin being added to one lysine residue), multiunbiquitination (ubiquitin molecules being added to multiple lysine residues), or polyubiquitination. Ubiquitin tagged proteins mainly become internalised via clathrin dependent endocytosis[150].

The complement component C5a, which forms during immune complex induced cell activation regulates the expression of the activating and inhibitory FcγRs. For example, binding of C5a to its receptor C5aR on alveolar macrophages has been shown to increase transcription of *Fcgr3* and reduce expression of FcγRIIb[151,152]. Regulation also occurs in the other direction, in that C5a production can be induced after immune complex binding to activating FcγRs in macrophages[151]. Co-stimulation of immune complexes with C5a results in enhanced FcγRIII dependent cell activation[152].

1.8.3 Association of SNPs in *FCGR* genes with autoimmunity

Polymorphisms are present in human *FCGR* genes which are linked to the development of autoimmune diseases including SLE, RA, multiple sclerosis, Wegener's granulomatosis and Guillain-Barre syndrome. For example, the V158F (rs396991) variant of FcγRIIIA was found to be expressed at a higher frequency in SLE patients compared to healthy controls[153]. This variant was also found at higher frequencies in RA patients compared to healthy controls[154,155]. A T695C polymorphism in *FCGR2B* leads to an isoleucine to a threonine amino acid change at position 232 of the protein, and has been associated with an enhanced susceptibility to SLE[156]. Conversely, a T559G base pair change in *FCGR3A*, which leads to F176V substitution in FcγRIIIA is associated with a reduced risk of SLE, as fewer SLE patients were found to carry the variant[157].

1.8.4 Phenotypes of mice lacking FcγR expression

Mice that lack expression of the activating FcγRs (*FcRγ*$^{-/-}$), and therefore only express the inhibitory receptor FcγRIIb, are resistant to a variety of models of autoimmune diseases such as immune complex-induced alveolitis[158], antibody-induced vasculitis[159] and collagen-induced arthritis (CIA) (on the DBA/1 susceptible background)[160], but are susceptible to infections including *Mycobacterium tuberculosis*[161]. Mice lacking the inhibitory receptor FcγRIIb, and

therefore only expressing the activating receptors, have enhanced levels of autoantibodies which lead to IC-induced autoimmune diseases such as methylated bovine serum albumin (mBSA)-induced arthritis[162]. They are also more susceptible to CIA (on the DBA/1 background), which is accompanied by enhanced anti-collagen II IgG[160]. *FcγRIIb* deletion renders arthritis resistant 129/SvJ and C57Bl/6 mice sensitive to disease using the CIA model[163]. *FcγRIIb*$^{-/-}$ mice are also more susceptible to immune complex-induced alveolitis[158], and on a C57Bl/6 background develop a spontaneous autoimmune phenotype which resembles SLE, including glomerulonephritis, anti-nuclear antibodies and proteinuria[164]. However, *FcγRIIb*$^{-/-}$ mice are more resistant to infections with *Streptococcus pneumoniae* as their macrophages are more effective at clearing the bacteria[165].

Microarrays carried out on immune complex stimulated WT, *FcγRIIb*$^{-/-}$ and *FcRγ*$^{-/-}$ mouse BMDCs showed that FcγRIIb regulates gene expression. The authors reported a 75% increase in differentially expressed genes between *FcγRIIb*$^{-/-}$ and WT immune complex stimulated BMDCs, indicating that FcγRIIb normally acts to limit FcγR dependent cell activation. In addition, gene expression profiles associated with T cell activation were seen in WT and *FcγRIIb*$^{-/-}$ BMDCs, but not in *FcRγ*$^{-/-}$ BMDCs. In order to activate T cells, BMDCs need to mature after immune complex stimulation. This includes upregulation of MHCII and co-stimulatory molecules, cytokine secretion and an increased migratory capacity. mRNA and protein expression of CD40 and CD86 were all enhanced after IC stimulation in WT and *FcγRIIb*$^{-/-}$ BMDCs, but not in *FcRγ*$^{-/-}$ BMDCs. Immune complex induced cytokine secretion was found to be lowest by *FcRγ*$^{-/-}$ BMDCs and highest by *FcγRIIb*$^{-/-}$ BMDCs, both in comparison to WT BMDCs. This indicates that cytokine secretion is mainly due to activating FcγR signalling and that it is regulated by FcγRIIb. Immune complex stimulation also leads to the production of chemokines and growth factors. Genes for these were more highly upregulated in stimulated WT and *FcγRIIb*$^{-/-}$ BMDCs compared to *FcRγ*$^{-/-}$ BMDCs. This all resulted in an enhanced capacity of IC pulsed *FcγRIIb*$^{-/-}$ BMDCs to cause ova specific $CD8^+$ T cell proliferation[166].

1.9 Rheumatoid Arthritis

Rheumatoid arthritis (RA) is an autoimmune chronic disease, which, if left untreated, causes synovial inflammation and loss of normal joint architecture due to bone and cartilage destruction. It also includes extra-articular features including those associated with the cardiovascular and pulmonary systems. The joint infiltrating leukocytes activate synovial fibroblasts and macrophages. This leads to the production of a variety of pro-inflammatory

cytokines and soluble mediators, which lead to angiogenesis, cartilage destruction and bone erosion. Unlike other autoimmune diseases such as T1D, the autoantigen response of patients with RA is not joint specific, since autoantibodies are directed against ubiquitous antigens found throughout the body. Autoantibodies include those against citrullinated proteins (ACPAs), rheumatoid factor (directed against the Fc region of IgG), collagen II, glucose-6-phosphate isomerase (GPI) and binding immunoglobulin protein (BiP). These can often be detected years before development of synovial inflammation, in the pre-clinical phase of the disease[167]. As autoantibodies are often detected in the blood long before the onset of clinical disease, this suggests that disease initiation may occur at non-articular sites. The exact mechanism behind the transition from the pre-clinical to the clinical phase of disease is not known, however, it involves the presentation of self-peptide in MHCII to autoreactive T cells.

Both genetic and environmental factors are thought to play a role in the aetiology of the disease. Genome wide association studies (GWAS) have found links between RA and more than 100 loci, the most highly associated polymorphisms are found within the human leukocyte antigen (HLA) region, especially the HLA-DRB1 locus. This allele of HLA-DRB1 has a higher affinity for citrullinated peptides[168], indicating that this may favour the presentation of modified self-peptides, potentially leading to a breach of tolerance. In addition, there is an increased concordance rate in monozygotic compared to dizygotic twins (15-30% and 5% respectively); thus demonstrating the presence of genetic risk factors[169]. There is also an environmental influence to the disease, with smoking being the strongest environmental risk factor[170]. It has been suggested that smoking may affect the expression, particularly in the lung, of peptidylarginine deiminases (PADs), the enzymes responsible for citruillinating proteins[171]. In addition, infectious agents including *E. coli* and Epstein-Barr virus[172] and the oral and gut microbiota[173] have been linked with RA.

1.10 Mouse models of rheumatoid arthritis

Mouse models of rheumatoid arthritis have been instrumental in increasing our understanding of the mechanistic basis behind the human disease. Although they each have their limitations, they have underpinned the testing and advancing of a wide range of therapies and facilitated investigation of the pre-clinical phase and initial onset of disease, which is often not possible in humans. In addition, these models allow for the study of clinically relevant tissues including lymph nodes and joints, which are not so readily available from patients. Mouse models which

have been commonly used include collagen-induced arthritis (CIA), collagen antibody-induced arthritis (CAIA), zymosan-induced arthritis, K/BxN serum transfer model and the methylated BSA model. In addition, there are spontaneous models which include the K/BxN model, the TNFα transgenic mouse and the SKG mouse.

1.10.1 Collagen-induced arthritis

Collagen-induced arthritis (CIA) was first reported in 1977, where human, chicken or rat type II collagen in the presence of complete or incomplete Freund's adjuvant caused inflammatory arthritis in 40% of rats after intradermal injection[174]. Mouse strains that express MHCII I-A^q, such as DBA/1 mice, are particularly susceptible to this model. The model shares several hallmarks of the human disease, including a breach of tolerance, the generation of autoantibodies against type II collagen, and, less commonly, the presence of rheumatoid factor or antibodies against citrullinated peptides. Signs of disease are visible between 21-25 days post injection and peak at approximately 35 days, after which mice enter a phase of remission. Both T and B cells are required for the initiation of CIA, resulting in the presence of collagen specific T cells and collagen type II antibodies, which are generally IgG2a or IgG2b. Although C57Bl/6 mice do not express MHCII I-A^q, and are considered to be resistant to CIA, arthritis can be induced, albeit a milder more chronic disease, with a lower penetrance. The role of PTPN22 has been investigated using this model of arthritis, where it was found to be dispensable, although *Ptpn22*$^{-/-}$ mice did develop a more severe disease, which did not reach statistical significance[61].

1.10.2 Collagen antibody-induced arthritis

The collagen antibody-induced arthritis (CAIA) model is initiated by the transfer of arthritogenic antibodies against type II collagen from mice subjected to the CIA model[175], human RA patients or commercially available antibody cocktails[176] into recipient mice. As autoantibodies are being transferred, T and B cells are not required for initiation of disease, so this model does not completely recapitulate the complexities of the human disease. The clinical features of this model are similar to those found using CIA, including immune cell infiltration of the synovium, pannus formation, bone remodelling and cartilage damage. The CAIA model can be used in mouse strains which are resistant to CIA, and signs of disease are present after 8 days and mice enter remission within 1 month.

1.10.3 Zymosan-induced arthritis

The zymosan-induced arthritis model is more transient than both CIA and CAIA, where signs of inflammatory arthritis can be seen 3 days after intraarticular injection with zymosan. Clinical signs include immune cell infiltration into the synovium, pannus formation and synovial hypertrophy[177]. However, one drawback of this model is that disease is only seen in the joints that have received the zymosan.

1.10.4 K/BxN and K/BxN serum transfer model of arthritis

The K/BxN model of rheumatoid arthritis was developed in the lab of Benoist and Mathis in the 1990s[178]. By crossing KRN TCR transgenic mice with NOD mice, the offspring (referred to a K/BxN mice) developed a joint disease similar to RA after approximately 4 weeks of age. NOD mice express the MHCII allele I-A^{g7}, and this was the only requirement from the NOD mouse needed to cause spontaneous disease, as when they crossed KRN mice with a C57Bl/6 line expressing the NOD I-A^{g7}, the offspring also developed disease. The KRN T cell receptor recognises the bovine ribonuclease$_{43\text{-}56}$ peptide presented in the context of I-A^{k}. Disease arises from the activation of T cells which express the KRN TCR, which also recognises a self-peptide of glucose-6-phosphate isomerase (GPI) when presented in the NOD I-A^{g7}. The activated T cells then provide help to B cells which leads to the production of IgG1 GPI autoantibodies. GPI catalyses the conversion of glucose-6-phosphate to fructose-6-phosphate during glycolysis. Being a glycolytic enzyme, GPI does not show joint specific expression, but is ubiquitously expressed. Despite this, clinical signs of disease are mostly detected in the joints. This may be due to the presence of GPI, in close proximity to IgG and complement component C3 on the cartilage surface, along the thickened synovium and the pannus of arthritic mice. In healthy mice, the GPI on the cartilage surface was not localised with IgG[179].

Arthritis developing in K/BxN mice has some similarities to human RA, characterised by joint swelling and redness, leading to joint deformities and eventually causing reduced mobility. Histology showed leukocyte infiltration, synovial inflammation, pannus formation, cartilage and bone destruction, and fibrosis; all reminiscent of the human disease. The bones and joints that are affected include the metatarsal, tarsal, ankle and knee joints, but not the hips or the spine. In the initial study by Benoist and Mathis, they did not detect circulating autoantibodies such as those against dsDNA or rheumatoid factor. Although they did detect IgG deposits on sections of

many organs. T cells are required for disease initiation as by treating K/BxN mice with a non-depleting CD4 monoclonal antibody for 1 week, they were able to prevent disease initiation. B cells are also required for disease development, as when they used μMT mice to create K/BxN mice that lacked B cells, no signs of disease were visible[178].

By harvesting serum or purified autoantibodies from arthritic K/BxN mice, disease can be transferred to recipient mice. This is called the K/BxN serum transfer model of arthritis and has the benefit that arthritis can be investigated in any mouse strain and with established gene deficient mouse lines. The disease observed using this model is transient, but can be maintained by repeated injections of GPI autoantibodies. Autoantibodies to GPI have been detected in RA patients[180], thus demonstrating the utility of these models to investigate the human disease. As autoantibodies are being transferred, the serum transfer model focusses on the effector phase of the disease, and as such T and B cells are not required for disease initiation. Using a variety of gene deficient mice, it has been shown that neutrophils[181] and macrophages[182,183] are required for disease development. Mast cells were initially thought to be required for disease, as mast cell deficient *Kit$^{W/W-v}$* mice and mast cell deficient Kit-ligand (Kitl)-mutated *Kitl$^{Sl/Sl-d}$* mice were found to be resistant[184]. However, more recent evidence has shown that mast cell deficient mice are able to develop disease[185]. Other vital factors for disease initiation include the complement component C5[186], FcγRIII[187], IL-1[188] and LFA-1[189,190]. In addition, Syk dependent signalling has been found to be required, as mice lacking Syk expression in neutrophils are resistant[185]. *Syk$^{-/-}$* neutrophils were recruited normally to the joints, but once there, produced reduced levels of TNFα and were more sensitive to apoptosis. Src family kinases were also found to be required for disease development, as mice lacking Hck, Fgr and Lyn were protected[191]. This was not due to a cell intrinsic role in leukocyte migration, but a role in establishing an inflammatory microenvironment, potentially due to the impact of Src family kinases in regulating immune complex induced neutrophil and macrophage activation. Despite the abundance of TNFα and IL-6 in the joints of RA patients and in mouse models of arthritis, these cytokines were not required for disease initiation using the serum transfer model, although some TNFα$^{-/-}$ mice were protected[188].

The role of PTPN22 in the K/BxN serum transfer model of arthritis has been previously examined, however the results are contradictory. PTPN22 has either been found to augment[63] or not affect[10,59] disease severity. This indicates that other factors may be involved including the titre of the arthritogenic serum administered, and the microbiota of the recipient mice.

1.10.5 Methylated bovine serum albumin (mBSA)-induced arthritis

Methylated bovine serum albumin (mBSA) in complete Freund's adjuvant, when given systemically, followed by intraarticular injections of mBSA into the knee joint causes antigen-induced arthritis[192]. The model represents lots of the clinical features of RA, including synovitis, mononuclear cell infiltration of the synovium, and bone and cartilage erosion, and has been used in a range of animals to induce prolonged inflammation.

1.10.6 Spontaneous TNFα transgenic mouse model of arthritis

In 1991, a transgenic mouse line was created in which the human TNFα (hTNFtg) was dysregulated through mutation of the 3' untranslated region of the gene[193]. These mice develop spontaneous chronic inflammatory arthritis, which affects all joints and can be prevented using anti-TNFα treatment[194]. The disease closely mirrors RA in humans, and includes immune cell infiltration, pannus formation, cartilage damage and bone erosion, although rheumatoid factor is not detected in the serum of these mice. Depending on the level of TNFα overexpression, signs of disease are visible from 4-5 weeks of age. hTNFtg mice, when crossed onto *Recombination activating gene (Rag1)*$^{-/-}$ mice also develop arthritis, indicating that T and B cells are not required for disease initiation in these mice[195].

This model also demonstrated the important role of TNFα in RA. TNFα is highly expressed in the inflamed synovium of RA patients, where it can induce cartilage damage via collagenase, cause proliferation of fibroblast-like synoviocytes, and promote osteoclastogenesis. In addition, anti-TNFα inhibits the production of other pro-inflammatory cytokines, and has been used as a successful treatment in RA for over 20 years[196].

1.10.7 Spontaneous arthritis using SKG mice

The SKG mouse strain was established in 2003[197]. SKG mice develop a spontaneous T cell mediated chronic inflammatory arthritis. Clinical signs of disease are visible from 2 months of age and result in the formation of a pannus, immune cell joint infiltration, cartilage and bone erosion and the presence of autoantibodies including rheumatoid factor; many of which are also found in RA patients. SKG mice carry a mutation in the gene for the kinase *Zap70*, which leads

to a tryptophan to a cysteine substitution at position 163, located in the SH2 domain of the protein. This leads to a dramatic reduction in ZAP-70 protein expression, and impaired binding of the mutant kinase to the invariant CD3ζ chain subunit, and is accompanied by profound reductions in signalling via the TCR. This in turn reduces the threshold for thymic selection, leading to the positive selection of a repertoire of autoreactive T cells[198].

1.11 Imaging of arthritic mice

Positron emission tomography (PET) in combination with computed tomography (CT) is a technique which can be used to image mice and humans, in a non-invasive manner. One of the benefits of this technique is that it can be used to monitor disease progression or the efficacy of therapy in a longitudinal manner. Galium-68 is a radioactive isotope with a half-life of 68 minutes. By chelating gallium-68 to a trimeric arginine-glycine-aspartic acid (RGD) peptide, it can be used to visualise areas of inflammation. RGD is found in extracellular matrix proteins such as fibrinogen, vitronectin, von Willibrand's factor and osteopontin. RGD binds with high affinity to the integrin αvβ3. αvβ3 is expressed at low levels in the steady state, but is upregulated as a result of inflammation. Radiolabelled RGD peptides have been used extensively in the field of oncology[199] because tumour cells and the associated endothelial cells express αvβ3 during angiogenesis. New blood vessel formation is also a feature of the inflamed synovial tissue in RA joints. In addition, αvβ3 is highly expressed on the surface of osteoclasts, activated macrophages and activated endothelial cells, all of which are present in the RA joint[200]. Imaging of arthritis has been previously achieved using an indium-111 radiolabelled dimeric RGD peptide and single-photon emission computed tomography (SPECT) imaging, using the CIA model[201].

1.12 The human skeleton and osteoclasts

1.12.1 The skeleton and bone remodelling

The human skeleton is composed of bone and cartilage. The skeleton provides a structural role, in which it protects internal organs and is used for locomotion, via attachment to muscle. In addition, the skeleton provides a calcium and phosphate source, which is required for maintaining serum homeostasis. There are two types of bone present in the skeleton: cortical

and trabecular. Cortical bone forms the outer part of the skeleton and is dense and compact, thus providing mechanical strength and protection. Trabecular bone is less dense, contains the bone marrow, and has a higher turnover rate than cortical bone[202]. Both cortical and trabecular bone are eroded during RA[203].

The skeleton is continuously remodelled to remove old bone, to adjust to mechanical needs and to repair microfractures. Bone remodelling is achieved in stages referred to as resorption, reversal and formation. This occurs because of the combined effort of osteoclasts and osteoblasts, which together form basic multicellular units (or bone remodelling units). After bone resorption by osteoclasts, the reversal stage sees the appearance of mononuclear cells on the bone, followed by new bone formation by osteoblasts. The new bone is finally covered in a layer of lining cells[202]. Therefore, the actions of osteoblasts and osteoclasts need to be finely balanced to prevent an overall change in bone mass (Figure 1-7).

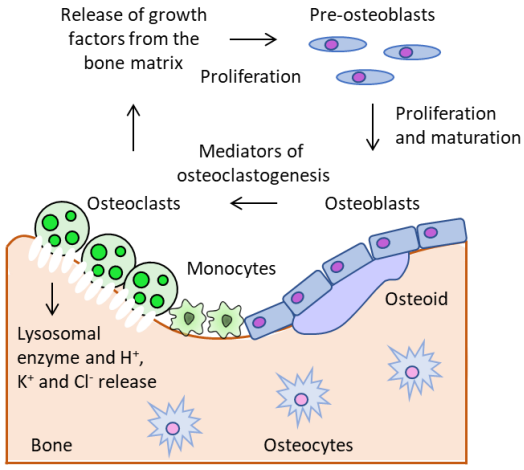

Figure 1-7: Schematic showing normal bone remodelling by osteoclasts and osteoblasts.

Bone remodelling is a vital process in order to maintain the structural integrity of the skeleton and to maintain mineral homeostasis. Remodelling begins with a resorption phase in which osteoclasts degrade the bone matrix and solubilise the bone mineral, due to their ability to release enzymes and to create an acidic environment. The reversal phase involves removal of debris by macrophages and monocytes. Bone formation occurs as osteoblasts produce osteoid matrix, which becomes mineralised. Diagram has been adapted from Lian JB et al., Nature Reviews Endocrinology, 2012.

Osteoclasts are the only cell type capable of resorbing bone and are therefore responsible for removing mineralised bone. As established RA is characterised by the presence of bone erosions, this demonstrates the essential nature of this cell type in disease. In addition, the requirement for osteoclasts in bone erosion is demonstrated by the fact that mice lacking osteoclasts do not develop bone erosions during mouse models of arthritis[204,205]. The importance of osteoclasts in RA is also exemplified by the number of anti-rheumatic drugs that have been developed that

target factors involved in osteoclastogenesis or osteoclast function. These include inhibitors of TNFα, IL-1 and IL-6R, including Tocilizumab, Adalimumab and Anakira respectively[203].

Osteoblasts counteract the role of osteoclasts by being responsible for the formation of new bone matrix. Osteoblasts originate from mesenchymal cells and are found on the bone surface, where they produce the bone matrix constituents. Osteoblasts also become incorporated into the new bone matrix where they regulate mineral metabolism as osteocytes. During homeostasis, levels of bone resorption and formation are equal, but in RA (and in other skeletal diseases such as osteoporosis), excessive bone loss is caused by a loss of equilibrium between osteoclast and osteoblast function[203].

1.12.2 Osteoclast differentiation and function

Osteoclasts are giant, multi-nucleated cells derived from the monocyte lineage. Hematopoietic stem cells differentiate into monocytes in the bone marrow. Monocytes further differentiate into osteoclast precursors as a result of receptor activator of nuclear factor kappa-B ligand (RANK-L) ligation with its receptor RANK on the precursors. RANK is a member of the TNF receptor superfamily. RANK-L is expressed on multiple cell types including osteoblasts, stromal cells and activated T cells. Both RANK and RANK-L are upregulated as a result of pro-inflammatory cytokines such as IL-1, IL-17A and TNFα, which are found in the inflamed joint[203]. RANK-RANK-L engagement leads to NFkB and NFAT-2 activation and signalling through colony-stimulating factor-1 receptor (c-Fms), the receptor for M-CSF. This causes osteoclast precursors to differentiate and fuse to become multinucleated osteoclasts[203]. Finally, the integrin αvβ3 is required for osteoclasts to adhere to bone and c-Src signalling allows them to become polarised, both of which cause the cells to become fully differentiated, active osteoclasts, complete with a ruffled border (Figure 1-8). αvβ3 is present within actin structures called podosomes. These are dynamic structures which continually dissolve and reform, allowing the osteoclast to move over the bone surface. A sealing zone is formed by podosomes, inside which is the resorption pit. Protons are released into the pit, creating an acidic environment, and enabling calcium to be solubilised. Surrounding the sealing zone are ruffled borders, through which enzymes such as matrix metalloprotease 9 (MMP9), tartrate-resistant acid phosphatase type 5 (TRAP) and cathepsin K are released, thereby degrading the bone[206].

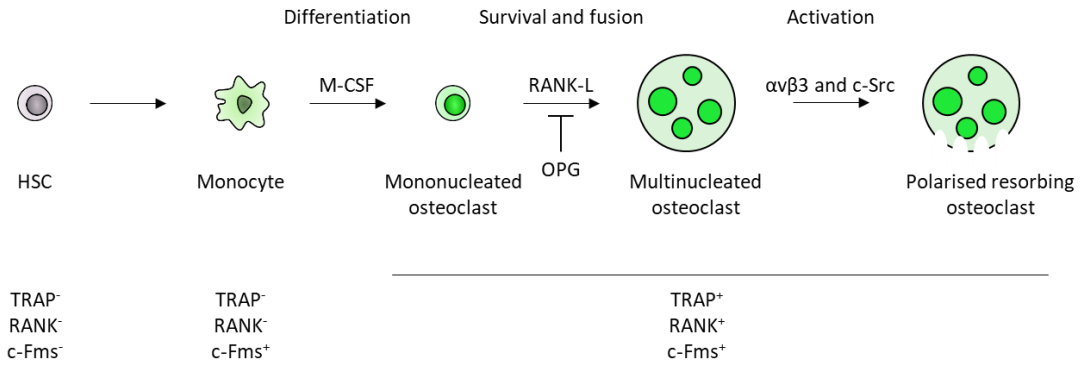

Figure 1-8: Schematic showing osteoclastogenesis.

Hematopoietic stem cells (HSCs) differentiate into monocytes. In the presence of M-CSF, these cells further differentiate into mononucleated osteoclasts. RANK-L engagement with its receptor RANK on the surface of mononucleated osteoclasts causes cell fusion, resulting in multinucleated osteoclasts. These use the integrin αvβ3 to adhere to the bone surface and use c-Src signalling to become polarised, thus creating fully differentiated, active osteoclasts which can resorb the underlying bone. Adapted from Lian JB et al., Nature Reviews Endocrinology, 2012.

The requirement for M-CSF and RANK-L for osteoclast survival and differentiation has been demonstrated using mice that lack these cytokines. *op/op* mice display osteopetrosis as they lack functional M-CSF[207]. Mice lacking expression of RANK-L also show osteopetrosis[208]. In both cases, the dense bone phenotype was attributed to the lack of osteoclasts. The opposite phenotype is apparent in mice that lack expression of osteoprotegerin (OPG), which is an inhibitor of osteoclast differentiation, and therefore in its absence, mice suffer from osteoporosis[209]. OPG is a receptor which also recognises RANK-L, therefore it acts as a decoy receptor.

In addition to M-CSF/RANK-L dependent osteoclast differentiation, osteoclastogenesis can also be stimulated by the presence of ACPAs. These autoantibodies are recognised by Fc receptors expressed on osteoclast precursors. It has been shown that FcγRs play an important role in osteoclast differentiation, such that FcγRIII-deficient mice show an osteoporotic phenotype, which is associated with an increased number of osteoclasts[210]. This suggest that FcγRIII has an inhibitory effect on osteoclastogenesis under homeostatic conditions.

1.12.2.1 Regulation of osteoclast function

As mentioned above, OPG binds to RANK-L, thus preventing RANK-L from binding to RANK. OPG is expressed by osteoblastic cells and B cells[211], and its expression is induced by cytokines, hormones and drugs, including IL-1 and TNFα; cytokines which also induce RANK-L expression[212].

OPG inhibits osteoclast differentiation and thus regulates bone resorption, in addition to inducing apoptosis of osteoclasts. This means that bone mass is affected by the RANK-L/OPG ratio.

Osteoclasts and osteoclast precursors also regulate their own differentiation. RANK-L activation of c-Fos leads to NFATc1 activation, a transcription factor required for osteoclast differentiation, RANK-L activation also causes secretion of IFNβ from osteoclast precursors. IFNβ binding to its receptor leads to degradation of TRAF6, which normally mediates the activation of a variety of signalling pathways downstream of RANK. In addition, TRAF6 is an E3 ubiquitin ligase and causes its own degradation, again regulating osteoclast differentiation[213].

Multiple cytokines regulate osteoclast differentiation. These can be either pro-osteoclastogenic, such as TNFα, IL-1, IL-6, IL-17A and IL-23, or anti-osteoclastogenic such as IFNα, IFNβ, IL-4 and IL-10[214]. The balance of these cytokines needs to be tightly regulated in order to maintain a normal bone mass.

TNFα leads to bone resorption by causing an increase in the ratio of RANK-L to OPG in stromal cells and osteoblasts and by increasing M-CSF expression on stromal cells, osteoblasts and activated T cells. TNFα also causes enhanced RANK expression on osteoclast precursors. In addition, it has been shown that TNFα works in synergy with RANK-L to promote osteoclast differentiation. A RANK-L independent role for TNFα in macrophage differentiation into osteoclasts has also been reported[215]. IL-6 stimulates osteoclastogenesis by causing enhanced RANK-L and IL-1 expression by osteoblasts, and enhanced RANK-L expression by stromal cells. Inhibiting IL-6 receptor signalling has been shown to prevent osteoclast formation *in vitro* and *in vivo*[216]. The pro-inflammatory cytokine IL-1β directly affects the resorptive ability of osteoclasts, by regulating cytoskeletal dynamics via Src/TRAF6[217]. It also causes bone resorption by inducing expression of RANK-L. Targeting IL-1 using IL-1 receptor antagonists has been successfully used in RA patients[218]. IL-17A causes the expression of TNFα, IL-1, IL-6 and interleukin-8 (IL-8), all of which are pro-osteoclastogenic cytokines[219,220]. In mouse models of RA, IL-17A has been shown to induce RANK-L expression, ultimately leading to osteoclast differentiation and bone erosion[221]. In synovial joints of RA patients, IL-17A and interleukin-32 (IL-32) work synergistically to cause expression of osteoclast specific genes encoding TRAP, MMP9 and cathepsin K, thus inducing osteoclast differentiation[222].

Both type I interferons, IFNα and IFNβ, inhibit RANK-L induced osteoclastogenesis[223]. IFNγ has also been shown to inhibit RANK-L and TNFα induced osteoclastogenesis, and IFNγ receptor deficient mice show an increased number of osteoclasts and a concomitant reduction in bone

mass[224]. This indicates that both type I and type II interferons act as inhibitors of osteoclast differentiation.

1.12.2.2 The role of kinases and phosphatases in osteoclast function

Protein kinases and phosphatases are known to play vital roles in osteoclast function. Protein tyrosine phosphatase activity inhibitors have been shown to prevent *in vitro* differentiation of osteoclasts and osteoclast-mediated bone resorption[225]. Phosphorylation also regulates signalling downstream of RANK and c-Fms (the receptors for RANK-L and M-CSF respectively), both of which are essential for osteoclast differentiation[226]. Mice with inactive SHP-1 have reduced bone mass and increased numbers and activity of osteoclasts, as SHP-1 is a negative regulator of signalling downstream of RANK in osteoclasts[227]. Osteoclasts from mice lacking c-Src are unable to form ruffled borders, have reduced cell migration and are unable to resorb bone[228]. Mice lacking the Src family kinase Hck have an osteopetrotic phenotype shown by decreased bone degradation[229]. Fyn deficiency also causes reduced osteoclast differentiation *in vitro*, indicating that Fyn positively regulates osteoclast differentiation[230]. In contrast, the Src family kinase Lyn is a negative regulator of osteoclast formation, such that *Lyn*$^{-/-}$ mice show enhanced bone loss due to increased osteoclastogenesis[231]. Finally, the phosphatase PTPN12 has been shown to be required for RANK-L-dependent fusion of macrophages into osteoclasts[232].

1.13 Hypothesis

As PTPN22 regulates signalling downstream of a variety of immunoreceptors, its targets Src and Syk family kinases are downstream of FcRs, and autoantibodies are a hallmark of many of the PTPN22^{R620W} associated diseases, I hypothesise that PTPN22 regulates immune complex stimulated FcR responses in DCs. Therefore, in its absence, FcR signalling will be enhanced, leading to augmented immune complex induced effector functions. If the autoimmune associated variant of PTPN22 acts as a loss-of-function variant in the context of FcR signalling, then expression of the variant could cause dysregulated responses to immune complexes during disease.

1.14 Aims

1. To investigate if PTPN22 regulates FcyR dependent effector functions in DCs.
2. To investigate the role of PTPN22 in DC antigen uptake, processing and presentation.
3. To investigate whether PTPN22 plays a role in the K/BxN serum transfer model of rheumatoid arthritis and in osteoclast function.

2. Materials and Methods

2.1 Materials

2.1.1 Reagents

Reagent	Catalogue number	Source
Ammonium acetate, 7.5M	A2706	Sigma Aldrich
β-mercaptoethanol	21985-023	Invitrogen
Bovine serum albumin (BSA)	A7906	Sigma Aldrich
CellTrace Violet (CTV) cell proliferation kit	C34557	Invitrogen
CellTrace Far Red (CTFR) cell proliferation kit	C34564	Invitrogen
Chloroform	404635000	Acros Organics
DELFIA europium-N1 streptavidin	1244-360	Perkin Elmer
DELFIA enhancement solution	4001-0010	Perkin Elmer
DHR123	D1054	Sigma Aldrich
Dibutyl phthalate	524980	Sigma Aldrich
DNase free water	10977-035	Invitrogen
DNase I	10104159001	Roche
EDTA, 0.5M	V4233	Promega
EGTA	E0396	Sigma Aldrich
EndoGrade ovalbumin (ova)	321000	Hyglos GmbH
Ethanol	1.08543.0250	Merck
FBS	F7524	Sigma Aldrich
FITC	F1300	Invitrogen
Fixable viability dye eFluor 506	65-0866-14	eBioscience
Gelatin	G2500	Sigma Aldrich
GelRed nucleic acid gel stain	41003	Biotium
Glycoblue	10301575	Invitrogen
GM-CSF	-	From B78H1/GM-CSF.1 cell line, from Professor Janis Burkhardt (University of Pennsylvania)
Heat killed *Candida albicans*	tlrl-hkca	InvivoGen
Heat killed *Listeria monocytogenes*	tlrl-hklm	InvivoGen
HEPES	15630-080	Invitrogen
hFlt3L	550606	BioLegend
Hygromycin B	SC-29067	Santa Cruz
Indo-1	I1203	Invitrogen
Ionomycin	I0634	Sigma Aldrich
Isopropanol	67-63-0	Acros Organics
Liberase TL	54010200001	Roche
LPS-EK	tlrl-eklps	InvivoGen
Lucifer yellow CH, lithium salt	L453	Invitrogen
Monensin	420701	BioLegend
OneComp eBeads	01-1111	eBioscience

$OVA_{323-339}$ peptide	SP1050B	Abgent
Ovalbumin-AF488	O34781	Invitrogen
Ovalbumin-AF594	O34783	Invitrogen
Ovalbumin-AF647	O34784	Invitrogen
Paraformaldehyde, 32%	15714-S	Electron Microscopy Services
PBS (magnesium and calcium free)	21-031-CVR	Corning
PCRBIO Taq Mix Red, 2x	PB10.13	PCR Biosystems
Penicillin/streptomycin	P4333	Sigma Aldrich
Phorbol 12-myristate 13-acetate (PMA)	P8139	Sigma Aldrich
Polybead microspheres, 3 µm	17134-15	Polysciences GmbH
Polymyxin B	P4932	Sigma Aldrich
Proteinase K	3115879001	Roche
QIAzol	79306	Qiagen
Rabbit anti-chicken egg albumin (anti-ova)	C6534	Sigma Aldrich
Rabbit IgG	I5006	Sigma Aldrich
Rainbow fluorescent particles (counting beads)	422907	BioLegend
Recombinant human Flt3L	550604	BioLegend
Recombinant human glucose-6-phosphate isomerase (GPI)	228-10568-1	RayBiotech
Recombinant mouse M-CSF	576404	BioLegend
Recombinant mouse RANK-L	577102	BioLegend
Red blood cell lysis buffer, 10x	420301	BioLegend
RPMI-1640 containing L-glutamine	R8758	Sigma Aldrich
Nuclease free water	20-9000-01	Severn Biotech Ltd
Sodium azide, 1%	40-2000-01	Severn Biotech Ltd
Src inhibitor-1	S2075	Sigma Aldrich
Streptavidin	405229	BioLegend
Syk inhibitor II	574712	Calbiochem
2,4,6-Trinitrophenyl ovalbumin (TNP-ova)	SC-396493	Santa Cruz Biotechnology
Trypan blue	T8154	Sigma Aldrich
Trypsin-EDTA	T3924	Sigma Aldrich
Tween 20	P1379	Sigma Aldrich
UltraPure agarose	16500500	Thermo Fisher Scientific
Zombie fixable viability dye	423107	BioLegend

Table 2-1: Source and catalogue numbers of reagents used.

2.1.2 Antibodies

Antigen	Clone	Source	Dilution
CD3	145-2C11	BioLegend	1:300
CD4	RM4-5	BioLegend	1:200
CD8	53-6.7	BioLegend	1:200
CD11b	M1/70	BioLegend	1:500
CD11c	N418	BioLegend	1:500
CD19	6D5	BioLegend	1:300
CD24	30-F1	BioLegend	1:200
CD25	3C7	BioLegend	1:400
CD40	3/23	BioLegend	1:100

CD45.1	A20	BioLegend	1:200
CD45.2	104	BioLegend	1:200
CD54	YN1/1.7.4	BioLegend	1:500
CD69	H1.2F3	BioLegend	1:100
CD80	16-10A1	BioLegend	1:100
CD86	GL-1	BioLegend	1:200
CD115	AF598	BioLegend	1:500
CD117	2B8	BioLegend	1:100
CD135	A2F10	BioLegend	1:200
B220	RA3-6B2	BioLegend	1:300
Dectin-1 (neutralising)	R1-8g7	InvivoGen	1:100
F(ab')2 goat anti-rabbit IgG	-	Invitrogen	1:500
F(ab')2 goat anti-mouse IgG-alkaline phosphatase	-	Jackson ImmunoResearch	1:2000
FcγRI	X545/7.1	BioLegend	1:100
FcγRIIb	K9.361 cl5	Professor Jeffrey Ravetch (Rockefeller University)	10 µg/ml
FcγRII/III	2.4G2	BioLegend	1:500
FcγRIV	MB 1 9E9 cl27	Professor Jeffrey Ravetch (Rockefeller University)	10 µg/ml
FcγRII/III	2.4G2	BioLegend	1:500
Goat anti-mouse IgG	-	Invitrogen	1:100
Goat anti-hamster IgG	-	AbD Serotec	1:100
IFNγ	XMG1.2	BioLegend	1:100
IgG1 anti-TNP	-	Dr Michael Robson (King's College London)	10 µg/ml
IgG1 anti-TNP glycoforms	-	Dr Gestur Vidarsson, (University of Amsterdam)	10 µg/ml
IL-17A	TC11-18H10.1	BioLegend	1:100
Ly6C	HK1.4	BioLegend	1:300
Ly6G	1A8	BioLegend	1:100
MHCII I-A^b	AF6-120.1	BioLegend	1:200
NK1.1	PK136	BioLegend	1:300
SIRPα	P84	BioLegend	1:500
TCR Vα2	B20.1	BioLegend	1:400
TCR Vβ5.1, 5.2	MR9-4	BioLegend	1:200
Ter119	TER-119	BioLegend	1:300
TNFα	MP6-XT22	BioLegend	1:400

Table 2-2: Source, catalogue numbers and clone numbers of antibodies used.

2.1.3 Solutions

Solution	Components	Storage
Calcium flux assay buffer	0.5% BSA in HBSS containing calcium and magnesium.	Stored at 4°C.
BMDC wash media	RPMI-1640 with L-glutamine supplemented with 1% heat-inactivated Fetal Bovine Serum (FBS) and	Sterile and stored at 4°C.

	penicillin/streptomycin (100 µg/ml).	
BMDC culture media (GM-CSF)	RPMI-1640 with L-glutamine supplemented with 10% heat-inactivated FBS, penicillin/streptomycin (100 µg/ml), β-mercaptoethanol (50 µM) and 1% murine GM-CSF.	Sterile and stored at 4°C.
BMDC culture media (Flt3L)	RPMI-1640 with L-glutamine supplemented with 10% heat-inactivated FBS, penicillin/streptomycin (100 µg/ml), β-mercaptoethanol (50 µM), HEPES (10 mM) and human Flt3L (0.2 µg/ml).	Sterile and stored at 4°C.
Cell line culture media (B78H1-GM-CSF)	RPMI-1640 with L-glutamine supplemented with 10% heat-inactivated FBS, penicillin/streptomycin (100 µg/ml) and ± hygromycin B (1.2 mg/ml).	Sterile and stored at 4°C.
Cell lysis buffer (for degradation assay)	0.5% NP-40, 50mM Tris, 150 mM NaCl in water.	Made fresh and stored on ice.
ELISA wash buffer (for anti-GPI)	0.05% Tween in PBS.	Made fresh and stored at room temperature.
FACS buffer	5% FBS, 1 mM EDTA, 0.01% sodium azide in PBS.	Stored at 4°C.
Freezing media	90% FBS and 10% DMSO.	Filter sterilised and stored at -20°C.
Immunoassay block buffer	2% BSA in PBS.	Stored at 4°C.
Immunoassay wash buffer	0.5% Tween in PBS.	Made fresh and stored at room temperature.
MACS buffer	0.5% BSA, 2mM EDTA in PBS.	Filter sterilised and stored at 4°C.
Mouse tail/ear lysis buffer	50mM Tris (pH 8), 25mM EDTA (pH 8), 100mM NaCl, 1% SDS and 0.4mg/ml Proteinase K.	Stored at room temperature.
Neutrophil ROS buffer	0.1% gelatin in PBS.	Incubated at 37°C to dissolve the gelatin. Stored at 4°C and warmed to room temperature before use.
Osteoclast culture media	RPMI-1640 with L-glutamine supplemented with 10% heat-inactivated FBS, penicillin/streptomycin (100 µg/ml), β-mercaptoethanol (50 µM, M-CSF (50 ng/ml) and RANK-L (50 ng/ml).	Sterile and stored at 4°C.
10 x PBS (magnesium and calcium free)	137mM NaCl, 2.7mM KCl, 8.1mM Na_2HPO_4, 1.5mM KH_2PO_4 (pH 7.4).	Stored at room temperature.

Table 2-3: Recipes for solutions used.

2.1.4 Commercial kits

Item	Catalogue number	Source
Acid phosphatase (TRAP) kit	387A-1KT	Sigma Aldrich
BCA protein assay kit	10678484	Thermo Fisher Scientific
Bio-Plex Pro mouse cytokine 23-plex assay	M60009RDPD	Bio-Rad
$CD4^+$ T cell isolation kit, mouse	130-104-454	Miltenyi Biotec
First strand cDNA synthesis kit	K1612	Thermo Fisher Scientific
Foxp3/transcription factor staining buffer set	11500597	eBioscience
IFNγ ELISA standard set	430804	BioLegend
IL-2 ELISA standard set	431001	BioLegend
IL-6 ELISA standard set	431301	BioLegend
IL-12/23p40 ELISA standard set	431604	BioLegend
IL-17A ELISA standard set	432504	BioLegend
LEGENDplex mouse inflammation panel	740446	BioLegend
LEGENDplex mouse proinflammatory chemokine panel	740451	BioLegend
OsteoLyse assay kit	PA-1500	Lonza
PowerUp SYBR green mastermix	A25741	Applied Biosystems
qPCRBIO cDNA synthesis kit	PB30.11	PCR Biosystems
TNFα ELISA standard set	430904	BioLegend

Table 2-4: Source and catalogue numbers for commercial kits.

2.1.5 Plastics

Item	Catalogue number	Source
6 well flat bottom tissue culture plate	140675	Thermo Fisher Scientific
24 well flat bottom tissue culture plate	142475	Thermo Fisher Scientific
96 well flat bottom tissue culture plate	167008	Thermo Fisher Scientific
96 well round bottom tissue culture plate	163320	Thermo Fisher Scientific
T25 tissue culture flask	430639	Corning
T175 tissue culture flask	431080	Corning
Non-TC treated 96 well plate (for dilutions)	650101	Greiner Bio-One Ltd
96 well flat bottom ELISA plate	442404	Thermo Fisher Scientific
96 well flat bottom assay black plate	3603	Corning
384 well plate (for qPCR)	AB-1384	Thermo Fisher Scientific
8 strip PCR tubes	732-0545	VWR
Cell strainers, 70 µm	542070	Greiner Bio-One Ltd
Cryovial	430487	Corning
LS positive selection columns	130-042-401	Miltenyi Biotec
Petri dishes	101R20	Thermo Fisher Scientific
Polystyrene 5ml tubes (FACS tubes)	352052	BD Falcon

Table 2-5: Source and catalogue numbers for plastics used.

2.2 Methods

2.2.1 Animals

2.2.1.1 Ethics Statement

All animal work has been conducted according to The Animals (Scientific Procedures) Act 1986 under Home Office License 70/8792. The King's College London Animal Welfare and Ethical Review Body (AWERB) approved the research. Animals were sacrificed using a rising concentration of carbon dioxide, and death was confirmed by cervical dislocation.

2.2.1.2 Mice

Wild type (WT) C57Bl/6, *Ptpn22*$^{-/-}$, *Ptpn22*^{R619}, *Ptpn22*^{R619W} (WT), OT-II, and OT-II x CD45.1 mice were housed under specific pathogen free conditions. *Ptpn22*$^{-/-}$ mice and *Ptpn22*^{R619W} mutant mice were backcrossed for more than 10 generations to the C57Bl/6 strain. WT and *Ptpn22*$^{-/-}$ mice were rederived from Professor Rose Zamoyska (University of Edinburgh). *Ptpn22*^{R619} and *Ptpn22*^{R619W} mice were rederived from Professor David Rawlings (University of Washington School of Medicine), and were bred as a separate colony from the WT and *Ptpn22*$^{-/-}$ mice. Mice used in experiments were age and gender-matched.

2.2.1.3 Mouse genotyping

Mouse tail tips or ear clips were digested overnight at 56°C in 375 µl tail lysis buffer (50 mM Tris (pH 8), 25 mM EDTA (pH 8), 100 mM NaCl, 1% SDS and 0.4 mg/ml Proteinase K (Roche)). The following day, 125 µl 5M NaCl was added per sample, vortexed and centrifuged for 5 minutes at 4°C and 13,500 rpm. The supernatants were transferred to new tubes and 250 µl isopropanol was added per sample, vortexed and centrifuged for 15 minutes at 4°C and 13,500 rpm. The supernatants were discarded and the DNA was washed with 500 µl 70% ethanol, before being centrifuged for 5 minutes at 4°C and 13,500 rpm. DNA was left to air dry for at least 30 minutes at room temperature, before being resuspended in 50 µl DNase free water.

All polymerase chain reactions (PCRs) were undertaken in a total volume of 25 µl, composed of 0.5 µl forward primer (see Table 2-6 for sequences, all from Sigma Aldrich), 0.5 µl reverse primer (see Table 2-6 for sequences, all from Sigma Aldrich), 12.5 µl 2 x PCRBIO Taq Mix Red (PCR Biosystems), 9 µl DNase free water and 2.5 µl DNA. Positive (previous DNA samples of known genotype) and negative (no DNA) PCRs were always run alongside the samples of unknown genotype.

Primer pairs	Primer sequence	PCR cycle	Expected products (bp)
PTPN22	Forward: 5' AGC CAA GTT TCT TTG TTG AGA A 3' Reverse: 5' CAG ACA CAA CAA AGC CCA GA 3'	94°C for 1 min 29 x 94°C for 15s 55°C for 15s 72°C for 12s 72°C for 10 mins 4°C hold	WT = 498 *Ptpn22*$^{-/-}$ = 221
R619W	Forward: 5' GAT AAG GTC TTA CTA CCC ATG CTG GC 3' Reverse: 5' GGA AGT GA A CTA GAG CGC TAG GA C 3'	94°C for 1 min 25 x 94°C for 15s 62°C for 15s 72°C for 12s 72°C for 10 mins 4°C hold	WT (*Ptpn22*^{R619}) = 482 *Ptpn22*^{R619W} = 640
TCRβ	Forward: 5' GGG CAA AAA CTG ACC TTG AA 3' Reverse: 5' GAG CCT GGT TGT TTG TGG 3'	95°C for 5 mins 30 x 95°C for 1 min 60°C for 1 min 72°C for 1 min 72°C for 5 mins 4°C hold	WT = no product KRN^{+} = 227

Table 2-6: PCR primer sequences, cycles and expected product sizes for mouse genotyping.

PCR products were run on a 1% agarose gel containing 1 x GelRed nucleic acid gel stain (Biotium) at approximately 100V for 30 minutes and bands were visualised using a Gel Doc EZ Gel Documentation System (Bio-Rad) (Figure 2-1). When bone marrow derived DCs (BMDCs) were genotyped, cells were harvested, pelleted and lysed in tail lysis buffer for 1 hour at 56°C. DNA was extracted and a PCR was carried out as per mouse tail tips/ear clips.

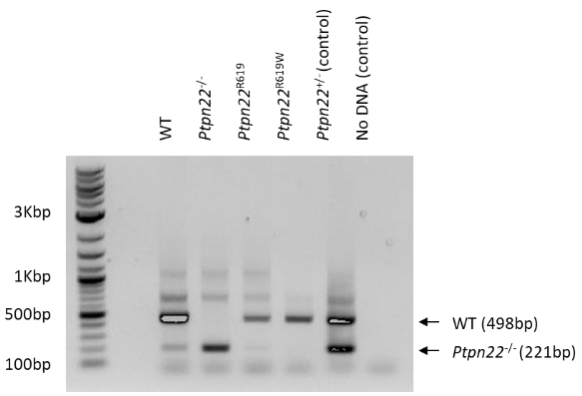

Figure 2-1: Representative DNA gel showing PCR products for mouse genotyping.

Ear clips from WT, Ptpn22$^{-/-}$, Ptpn22^{R619} (WT) and Ptpn22^{R619W} mice were digested and DNA was extracted. A PCR was run using PTPN22 specific primers. The PCR products were run on a 1% agarose gel and visualised using GelRed. The WT PCR product is 498bp in length and the Ptpn22$^{-/-}$ PCR product is 221bp in length. A DNA ladder is shown in the first lane, to aid with identifying the correct sized bands. A positive control (Ptpn22$^{+/-}$) and a negative control (no DNA) were also run. PCR and agarose gel was carried out by Wing Han Wu (Cope laboratory, King's College London).

To screen OT-II and OT-II x CD45.1 mice by flow cytometry, blood was harvested from tail veins and placed into tubes containing 200 µl 50 mM EDTA in PBS, to prevent coagulation. Samples were centrifuged for 5 minutes at 4°C and 1600 rpm before removing the supernatant. Cell pellets were lysed twice using 500 µl red blood cell lysis buffer (BioLegend) for 5 minutes at room temperature, washed with PBS and centrifuged for 5 minutes at 4°C and 1600 rpm before removing the supernatant. Cells were then stained for 30 minutes at 4°C with antibodies against CD4 (BioLegend), TCR Vα2 (BioLegend), TCR Vβ5 (BioLegend), CD45.1 (BioLegend) CD45.2 (BioLegend) and a fixable viability dye (eBioscience). Samples were washed with FACS buffer (5% FBS, 1 mM EDTA, 0.01% sodium azide in PBS) and fixed using 1% paraformaldehyde (PFA, Electron Microscopy Sciences) in PBS. Samples were analysed by flow cytometry, with OT-II^{+} T cells being identified as live, CD4^{+}, TCR Vα2^{+}, TCR Vβ5^{+} singlets. CD45.1 expression was then determined on these cells (Figure 2-2).

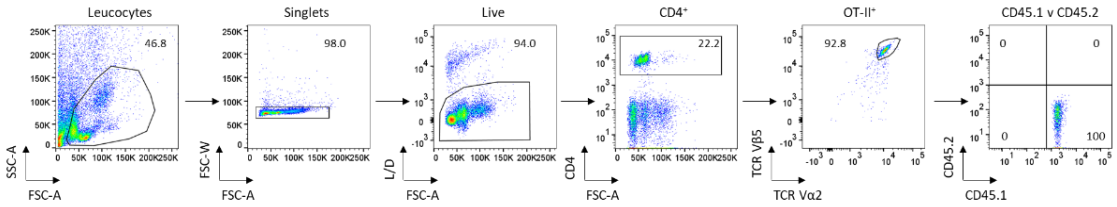

Figure 2-2: Representative flow cytometry plots from genotyping OT-II and OT-II x CD45.1 mice.

Blood from OT-II and OT-II x CD45.1 mice were collected and red blood cells were lysed. The remaining cells were stained with CD4, TCR Vα2, TCR Vβ5, CD45.1 and CD45.2 antibodies, in addition to a viability dye. Cells were analysed by flow cytometry and OT-II (TCR Vα2^{+} TCR Vβ5^{+}) and CD45.1 expression was determined by gating on live, CD4^{+} singlets.

2.2.2 Cell culture and cell isolation

2.2.2.1 Production of granulocyte macrophage-colony stimulating factor (GM-CSF)

A vial of B78H1-GM-CSF cells (Professor Janis Burkhardt, University of Pennsylvania) was thawed rapidly in a 37°C water bath, before being slowly transferred to a cooled 15 ml conical tube containing ice cold culture media (RPMI-1640 with L-glutamine (Sigma Aldrich) supplemented with 10% heat-inactivated Fetal Bovine Serum (FBS, Sigma Aldrich) and penicillin/streptomycin (100 µg/ml)). Cells were centrifuged for 5 minutes at room temperature and 1000 rpm before being resuspended in fresh culture media, and transferred into a T25 tissue culture flask. The following day, the media was replaced with culture media containing hygromycin B (1.2 mg/ml, Santa Cruz), to remove any dead or non-adherent cells and to continue to select for GM-CSF expressing B78H1 cells. Cells were propagated by removing the media, washing with PBS and incubating with Trypsin-EDTA (Sigma Aldrich) to remove the adherent cells from the flask. Cells were expanded in the presence of hygromycin B for 1 week. Cells were washed with culture media lacking hygromycin B three times and five T175 flasks were seeded with cells each containing 100 ml culture media lacking hygromycin B (so that hygromycin B was not present in the harvested GM-CSF containing media) and the cells were cultured for up to a week, until they began to die. The media was then harvested (which contained the GM-CSF), combined and centrifuged for 15 minutes at 4°C and 2000 rpm, to remove any dead cells and debris. The GM-CSF containing media was then aliquoted and stored at -80°C.

To determine at what concentration to use the GM-CSF containing supernatant in bone marrow derived DCs (BMDC) cultures, the supernatant was tested at 0.1, 0.3, 1, 3 and 10% in culture media (see Section 2.2.2.2 for BMDC culture details). DC differentiation and response to 100 ng/ml lipopolysaccharide (LPS, InvivoGen) was measured by blocking cells with a non-fluorescent FcγRII/III antibody (Biolegend) and staining with anti-CD11c (BioLegend), a fixable viability dye (BioLegend), and antibodies against CD54, CD80, CD86 and MHCII I-A^b (all from BioLegend) by flow cytometry. The optimal concentration for BMDC differentiation and maturation in response to LPS was determined to be 1%. Once thawed, GM-CSF aliquots were kept at 4°C and used within a week.

To store the B78H1-GM-CSF cells for future GM-CSF production, cells were collected using Trypsin-EDTA and centrifuged for 5 minutes at 4°C and 1600 rpm. Cells were resuspended in 0.5 ml ice cold culture media and quickly mixed with 0.5 ml freezing media (90% FBS and 10%

DMSO). Cells were then transferred to cooled, labelled Cryovials and stored at -80°C in a CoolCell, before being transferred to liquid nitrogen for long term storage.

2.2.2.2 Bone marrow derived DC (BMDC) culture using GM-CSF

BMDCs were produced using a protocol adapted from Inaba, K. *et al*[233]. Bone marrow was flushed from femurs and tibias of WT, *Ptpn22*$^{-/-}$, *Ptpn22*^{R619} or *Ptpn22*^{R619W} mice with wash media (RPMI-1640 with L-glutamine supplemented with 1% heat-inactivated FBS and penicillin/streptomycin (100 µg/ml)) using a 23G needle and a 10ml syringe. Cells were pelleted for 5 minutes at 4°C and 1600 rpm, then resuspended in culture media (RPMI-1640 with glutamine supplemented with 10% heat-inactivated FBS, penicillin/streptomycin (100 µg/ml) and β-Mercaptoethanol (50 µM). A single cell suspension was achieved by passing the cells through a 70 µm filter (BD Biosciences). To deplete macrophages, bone marrow cells were incubated for 30 minutes at 37°C in 5% CO_2 on Petri dishes. Non-adherent progenitor cells were collected from the dish, counted using trypan blue (Sigma Aldrich) and resuspended at 1.5 x 10^6/ml in culture media. GM-CSF was added to the bone marrow cells at 1% and 1 ml was added per well of a 24 well tissue culture plate (Thermo Fisher Scientific). On day 3 of culture, 75% of the media was removed and replaced with fresh culture media supplemented with 1% GM-CSF. On day 4, all the media was removed, the cells were washed and cultured with 1 ml fresh culture media supplemented with 1% GM-CSF. BMDCs were used between days 6 and 8, when they were at least 85% CD11c$^+$ as determined by flow cytometry. As the cultures are heterogenous, they were further phenotyped to identify GM-DCs and GM-macs, based on gating by Helft, J *et al*[234]. GM-DCs were identified as CD11c$^+$ MHCII^{hi} CD11b$^+$ live singlets and GM-macs were identified as CD11c$^+$ MHCII^{int} CD11b^{hi} live singlets.

2.2.2.3 Bone marrow derived DC (BMDC) culture using Flt3L

Bone marrow was flushed from femurs and tibias of WT and *Ptpn22*$^{-/-}$ mice with wash media (RPMI-1640 with L-glutamine supplemented with 1% heat-inactivated FBS and penicillin/streptomycin (100 µg/ml)) using a 23G needle and a 10ml syringe. Cells were pelleted for 5 minutes at 4°C and 1600 rpm and resuspended in 2 ml red blood cell lysis buffer (BioLegend) for 5 minutes at room temperature, washed with PBS and centrifuged for 5 minutes at 4°C and 1600 rpm. Cells were seeded at 1 x 10^6/ml in culture media (RPMI-1640 with

glutamine supplemented with 10% heat-inactivated FBS, penicillin/streptomycin (100 µg/ml) and β-Mercaptoethanol (50 µM) and HEPES (10 mM)) containing 0.2 µg/ml human recombinant Flt3L (BioLegend), and 5 mls was added per well of a 6 well plate (Thermo Fisher Scientific). Cells were cultured for 11-13 days at 37°C in 5% CO_2. To harvest cells for experiments, the media was removed, wells were washed with PBS and 1 ml Trypsin-EDTA was added per well and left at room temperature for 5-10 minutes, before cells were harvested by pipetting.

2.2.2.4 Isolation of splenic conventional DCs (cDCs)

Spleens from WT, *Ptpn22*$^{-/-}$, *Ptpn22*^{R619} and *Ptpn22*^{R619W} mice were digested in 1 ml RPMI-1640 containing DNase I and Liberase TL (both at 0.1 mg/ml, Roche) for 30 minutes at 37°C in 5% CO_2; 10 mM EDTA was added for the final 5 minutes. Spleens were mashed through gauze and centrifuged for 5 minutes at 4°C and 1600 rpm. Splenocytes were resuspended in 2 ml red blood cell lysis buffer (BioLegend) for 5 minutes at room temperature, washed with PBS and centrifuged for 5 minutes at 4°C and 1600 rpm. Splenic DCs were identified by flow cytometry as live, CD11c$^+$, MHCII$^+$ singlets and were used to measure FcγR cell surface expression and for receptor mediated endocytosis assays.

2.2.2.5 CD4$^+$ T cell isolation from lymph nodes and spleen

CD4$^+$ T cells were isolated from lymph nodes and spleens of 8-16 week old WT OT-II mice using a CD4$^+$ T cell isolation kit (Miltenyi Biotech). This technique uses negative selection, in which cells are first incubated with biotinylated antibodies against CD8α, CD11b, CD11c, CD19, CD45R, CD49b, CD105, MHCII, Ter119 and TCRγ/δ. This is followed by incubation with anti-biotin magnetic microbeads. By passing the cell suspension through a column mounted on a magnet, all non-CD4$^+$ cells will be retained by the magnet, and the CD4$^+$ T cells can be collected as they will pass through the column.

Single cell suspensions were made from lymph nodes and spleens by mashing them through 70 µm filters (BD Biosciences). Cells were centrifuged for 5 minutes at 4°C and 1600 rpm. Splenocytes were resuspended in 2 ml red blood cell lysis buffer (BioLegend) for 5 minutes at room temperature, washed with PBS and centrifuged for 5 minutes at 4°C and 1600 rpm. LN and spleen cells were combined, counted and resuspended in cold MACS buffer (0.5% BSA, 2mM EDTA in PBS) at 2.5 x 10^8/ml. 100 µl (per 1 x 10^8 cells) CD4$^+$ T cell biotin antibody cocktail was

added to the cells and incubated for 5 minutes at 4°C. 300 µl MACS buffer and 200 µl anti-biotin microbeads (per 1 x 10^8 cells) was then added to the cells and incubated for 10 minutes at 4°C. Cells were washed with MACS buffer, centrifuged for 5 minutes at 4°C and 1600 rpm and resuspended in 500 µl MACS buffer (per 1 x 10^8 cells). Cells were then loaded onto an LS column (Miltenyi Biotech), which had been pre-wetted with MACS buffer. The column was washed three times with MACS buffer and CD4$^+$ T cells were collected in the flow through.

To verify that the isolation had been successful, an aliquot of CD4$^+$ T cells were stained for flow cytometry, using antibodies against CD3, CD4, TCR Vα2 and TCR Vβ5 (all from BioLegend), and a fixable viability dye (eBioscience). In general, the proportion of cells that were CD4$^+$ after the sorting was at least 80%, and of those, approximately 90% were OT-II$^+$ (TCR Vα2$^+$, TCR Vβ5$^+$) (Figure 2-3).

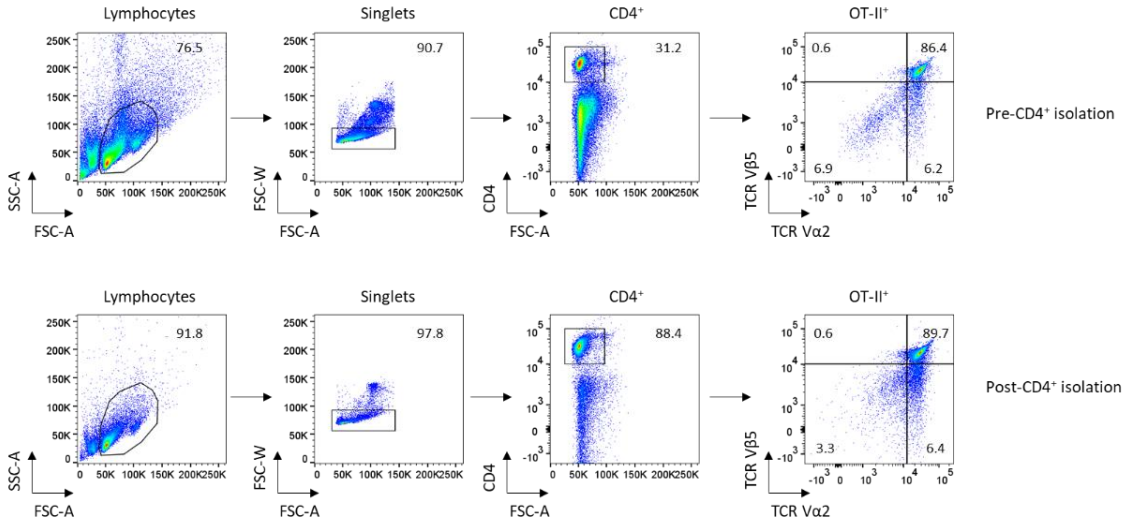

Figure 2-3: Representative flow cytometry plots showing CD4$^+$ T cell purity pre- and post-CD4$^+$ negative isolation.

Lymph nodes and spleens from WT OT-II mice were processed to make single cell suspensions, and CD4$^+$ T cells were isolated using a negative selection kit. An aliquot of cells were taken pre- and post-isolation and stained using CD4, TCR Vα2 and TCR Vβ5 antibodies, in addition to a viability dye. Cells were analysed by flow cytometry and the proportion of CD4$^+$ T cells that were OT-II$^+$ (TCR Vα2$^+$ TCR Vβ5$^+$) was determined by gating on live, CD4$^+$ singlets.

Once isolated, CD4$^+$ T cells were counted and resuspended at 2 x 10^7/ml in PBS and labelled with CellTrace Violet (2 µM, CTV, Invitrogen) in PBS for 20 minutes at 37°C, followed by quenching in culture media for 20 minutes at 37°C. CTV labelled WT CD4$^+$ OT-II T cells were used in co-cultures and conjugate assays.

2.2.2.6 Osteoclast culture

Bone marrow from WT and *Ptpn22*$^{-/-}$ mouse femurs were flushed with wash media (RPMI-1640 with L-glutamine supplemented with 1% heat-inactivated FBS and penicillin/streptomycin (100 µg/ml)) using a 25G needle and a 10 ml syringe. Bone marrow cells were centrifuged for 5 minutes at 4°C and 1600 rpm, and resuspended in 2 ml red blood cell lysis buffer (BioLegend) for 5 minutes at room temperature. Cells were then washed with PBS, centrifuged for 5 minutes at 4°C, resuspended in 8 ml osteoclast culture media (RPMI-1640 with L-glutamine supplemented with 10% heat-inactivated FBS, penicillin/streptomycin (100 µg/ml) and β-mercaptoethanol (50 µM)), containing 50 ng/ml recombinant mouse M-CSF (BioLegend) and seeded onto a 10 cm Petri dish at 37°C and 5% CO_2. Three days later, media was removed from Petri dishes, washed with PBS and adherent M-CSF dependent macrophages were harvested using a cell scraper. Harvested cells were centrifuged for 5 minutes at 4°C and 1600 rpm, resuspended and counted. Cells were resuspended at 1 x 10^6/ml in osteoclast culture media and 50 ng/ml M-CSF (as a negative control) or 50 ng/ml M-CSF and 50 ng/ml RANK-L (BioLegend) was added. 100 µl (1 x 10^5 cells) was added per well of a 96 well flat bottom plate or an OsteoLyse plate (Lonza). An additional 100 µl osteoclast culture media (containing M-CSF and RANK-L at the original concentrations) was added at day 6. Half of the media was replaced on day 9. Osteoclasts were used in experiments from days 6-12.

2.2.3 BMDC FcγR stimulation

2.2.3.1 Production of immune complexes and heat aggregated IgG

The protocol for immune complex production was based on Ellsworth, J *et al*[235]. A range of ratios of ova:anti-ova were initially tested for immune complex production. These were based on published data, and included 1:5, 1:20, 1:50 and 2:1. The upregulation of MHCII and co-stimulatory molecules on WT BMDCs after 24 hours of incubation was then assessed. A ratio of 1:20 was found to be most successful at inducing BMDC maturation, and was therefore used in all subsequent experiments.

For immune complexes that would bind to all FcγRs, EndoGrade ovalbumin (ova, Hyglos GmbH) and rabbit anti-chicken egg albumin (anti-ova, Sigma Aldrich) were combined at a ratio of 1:20

(ova:anti-ova, as utilised by Ellsworth, J *et al*) in PBS and incubated at 37°C for 1 hour. Insoluble ova immune complexes (ova ICs) were pelleted for 30 minutes at 4°C and 13,500 rpm and resuspended in PBS or culture media. Total protein concentration was determined by BCA assay (Thermo Fisher Scientific) as per the manufacturer's instructions, and added to BMDCs at 1 µM. In some experiments, ICs were added at 10 µg/ml. ICs were stored at 4°C and used within 1 week of production. As it was not possible to determine the proportion of ova and anti-ova in the final ICs, it was assumed that the initial 1:20 ratio was maintained.

For uptake assays, immune complexes were made using ova-AF488 (Invitrogen), instead of using EndoGrade ova. Using fluorescent ova allowed for receptor mediated endocytosis to be monitored by flow cytometry. For isotype specific immune complexes, 2,4,6-Trinitrophenyl-ovalbumin (TNP-ova, Santa Cruz Biotechnology) was combined with an IgG1 specific anti-TNP (Dr Michael Robson, King's College London), and produced as above.

To determine whether IgG glycosylation would affect the response of WT and *Ptpn22*$^{-/-}$ BMDCs, immune complexes were also made using TNP-ova and a panel of human IgG1 anti-TNP monoclonal antibodies with different glycoforms (Dr Gestur Vidarsson, University of Amsterdam). Immune complexes were made as per ova ICs. To produce these IgG1 glycoforms, the Vidarsson laboratory utilised decoy substrates to reduce fucosylation and galactosylation, overexpression of glycotransferases was used to increase levels of bisecting *N*-acetylglucosamine (GlcNAc linked to the mannose residue at the base of the N-glycan, referred to as 'bisection'), galactosylation and sialylation, and *in vitro* sialylation was used to increase sialylation. By using a combination of these techniques, they were able to engineer IgG1 molecules with specific glycosylation states[236]. See Table 2-7 for details.

Antibody number	Glycoform	Name
376	Unmodified	Anti-TNP IgG1
384	-G	Anti-TNP 2FG
341	+G	Anti-TNP IgG1 + B4GALT1 + D-galactose
353	+G +S	Anti-TNP IgG1 + B4GALT1 + ST6GALT + D-galactose
215	+B	Anti-TNP IgG1 + GNTIII
377	-F	Anti-TNP IgG1 + 2FF
212	-F +G	Anti-TNP + B4GALT1 + D-galactose + 2FF
302	-F +G +S	Anti-TNP IgG1 + B4GALT1 + ST6GALT + 2FF + D-galactose
218	-F +B	Anti-TNP IgG1 + GNTIII + 2FF

Table 2-7: IgG1 anti-TNP glycoforms.

2FG = 2-deoxy-2-fluoro-d-galactose, an analogue of galactose, used to prevent galactosylation (this also reduced sialylation and fucosylation). B4GALT1 = β-1,4-galactosyltransferase 1, which adds N-linked glycans, and is expressed in B cells. D-galactose = this increased levels of galactosylation by providing more substrate (this also slightly increases sialylation). ST6GALT = β-galactoside alpha-2,6-sialyltransferase 1, when co-transfected with B4GALT1 and D-galactose addition (to increase galactosylation), this increased levels of sialylation. BGNTIII = human N-acetylglucosamine (GlcNAc) transferase III, which is responsible for the addition of GlcNAc to glycans, therefore used to enhance levels of bisecting GlcNAc (bisection). 2FF = 2-deoxy-2-fluoro-1-fucose, added as a decoy substrate to reduce the incorporation of fucose into the IgG1-Fc glycan, thus decreasing fucosylation, without affecting the levels of galactosylation, sialylation and bisection. G = galactosylation, S = sialylation, B = bisection and F = fucosylation. IgG1 anti-TNP glycoforms were provided by Dr Gestur Vidarsson (University of Amsterdam).

As additional controls for some experiments, BMDCs were also stimulated with 1 µM ova pre-incubated with rabbit IgG (using the same procedure as making ova ICs), or with 1 µM ova added in combination with 1 µM heat aggregated (HA) rabbit IgG (Sigma Aldrich). HA rabbit IgG was made by incubating rabbit IgG at 62°C for 20 minutes, cooling to 4°C and centrifuging for 10 minutes at room temperature and 13,500 rpm to remove aggregates.

2.2.3.2 Immune complex induced BMDC maturation and cytokine secretion

To assess FcγR dependent BMDC maturation, 1 µM ova, anti-ova or ova ICs were added directly to WT, *Ptpn22*$^{-/-}$, *Ptpn22*^{R619} and *Ptpn22*^{R619W} culture wells on day 7 of culture. Polymyxin B (25µg/ml, Sigma Aldrich) was added to neutralise the effects of any potential endotoxin contamination. 24 hours later, BMDCs were harvested, washed, blocked with a non-fluorescent FcγRII/III antibody (BioLegend) and stained with anti-CD11c (BioLegend), anti-CD54 (BioLegend), anti-CD80 (BioLegend), anti-CD86 (BioLegened), anti-MHCII I-A^{b} (BioLegend) and a fixable viability dye (eBioscience) for 30 minutes at 4°C. Cells were washed and fixed using 1% PFA in PBS prior to flow cytometry. Cell surface CD54, CD80, CD86 and MHCII expression was determined by gating on live, CD11c^{+} singlets (Figure 2-4).

To determine FcγR induced cytokine secretion, WT, *Ptpn22*$^{-/-}$, *Ptpn22*^{R619} and *Ptpn22*^{R619W} BMDCs were harvested on day 6-7 of culture, counted and resuspended at 2 x 10^6/ml in culture media. 100 µl (2 x 10^5 cells) BMDCs were added per well of a 96 well round bottom plate (Thermo Fisher Scientific), and stimulated with 100 µl 2 x ova (10 µg/ml final concentration), rabbit anti-ova (200 µg/ml final concentration) or ova ICs (10 µg/ml ova final concentration) for 24 hours at 37°C and 5% CO_2. Polymyxin B (25µg/ml, Sigma Aldrich) was added to neutralise the effects of any potential endotoxin contamination (Figure 2-4). To analyse cytokine secretion as a result of signalling downstream of FcγRIII and FcγRIIb only, TNP-ova:IgG1 anti-TNP immune complexes were used. After 24 hours, cell-free supernatants were harvested from the wells and frozen at -20°C before use in IL-6, TNFα and IL-12/23p40 immunoassays (BioLegend).

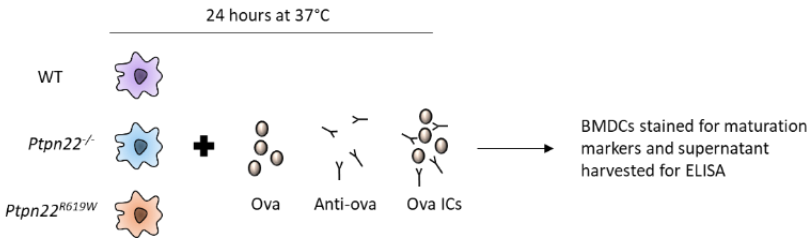

Figure 2-4: Schematic of ova immune complex stimulation of BMDCs for upregulation of MHCII and co-stimulatory molecules and secretion of cytokines.

WT, Ptpn22$^{-/-}$ and Ptpn22^{R619W} BMDCs or splenic DCs were incubated for 24 hours at 37°C, 5% CO_2 with ova, rabbit anti-ova or ova:anti-ova immune complexes (ova ICs). BMDCs were harvested, washed and stained with anti-CD11c, a viability dye and antibodies against MHCII and co-stimulatory molecules. Cell surface expression of these markers was determined by flow cytometry, gating on live, CD11c$^+$ singlets (for BMDCs) or live, CD11c$^+$ MHCII$^+$ singlets (for splenic conventional DCs). Alternatively, cell-free supernatants were collected and immunoassays were used to determine the secretion of cytokines including IL-6, TNFα and IL-12/23p40.

Immunoassays, which are generally enzyme-linked immunosorbent assays (ELISAs) can be used to measure the presence of an analyte in a serum, plasma or cell supernatant sample. The wells of a plate are first coated with a capture antibody, which will bind to the specific protein of interest in the sample. The proteins are then bound by labelled detection antibodies. This can then be detected on a plate reader, and using a standard curve, can be used to calculate the concentration of the analyte of interest in the original sample.

To carry out immunoassays using supernatants from stimulated BMDCs, 96 well flat bottom plates (Thermo Fisher Scientific) were coated overnight at 4°C with 50 µl per well of capture antibodies (IL-6, TNFα, or IL-12/23p40, BioLegend) in coating buffer (BioLegend). Wells were washed three times with immunoassay wash buffer (0.5% Tween in PBS) and blocked with 200 µl per well of immunoassay block buffer (2% BSA in PBS) at room temperature for 1 hour. During this time, supernatants were diluted 1:1 – 1:10 (depending on the expected secretion of the

cytokine being analysed) in culture media and standard serial dilutions were made. The top standard was generally 1-2 ng/ml, with 6 x 1:2 serial dilutions in culture media being made and 0 ng/ml as the bottom standard. Wells were washed three times with immunoassay wash buffer and 50 µl samples or standards were added per well for 2 hours at room temperature (added in duplicate). Wells were washed three times with immunoassay wash buffer and 50 µl per well of biotinylated detection antibodies (BioLegend) in immunoassay block buffer was added for 2 hours at room temperature. Wells were washed five times with Immunoassay wash buffer and 100 µl per well of Europium labelled streptavidin (Delfia) in immunoassay block buffer was added for 1 hour at room temperature. Wells were washed five times with immunoassay wash buffer and 100 µl per well of Enhancer solution (Delfia) was added for at least 10 minutes at room temperature. Emission was measured at 615 nm (using an excitation of 340 nm) on a Victor Wallac plate reader (Perkin Elmer).

The concentration of secreted cytokine was calculated using a standard curve, plotted using the standard concentration on the x-axis and the relative fluorescence unit on the y-axis, and the equation for the line of best fit, y = mx + c. The analyte concentration (x) could therefore be calculated using x = (y – c)/m, where y = relative fluorescence units, c = y-axis intercept and m = gradient of the slope. If the concentration was negative, this was manually adjusted to 0 (Figure 2-5).

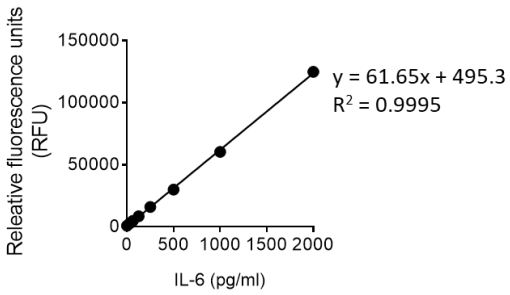

Figure 2-5: Example ELISA standard curve.

Relative fluorescence units (RFU) are averages of technical duplicates, and have been plotted against standard IL-6 concentrations, created by serial dilution. A line of best fit has been added. The equation of the line (y = 61.65x + 495.3) was used to calculate the IL-6 concentration in supernatant samples of unknown concentration.

To measure the secretion of a wider range cytokines and chemokines from immune complex stimulated BMDCs, a Bio-Plex pro cytokine assay (Bio-Rad) was also performed. This allowed for the identification of 23 analytes, and was carried out as per the manufacturer's instructions. Supernatants from WT and *Ptpn22*$^{-/-}$ BMDCs were harvested after 24 hours of stimulation with ova (10 µg/ml), rabbit anti-ova (200 µg/ml) or ova ICs (10 µg/ml ova final concentration), in the presence of polymyxin B (25 µg/ml, Sigma Aldrich). All supernatants were diluted 1:3 and set up

as technical duplicates for the multiplex assay. Samples were collected using a Luminex Flexmap3D and Xponent 4.0 software (Luminex).

2.2.3.3 BMDC calcium flux after immune complex stimulation

The dye indo-1 can be used to measure intracellular calcium flux in real time. Indo-1 emits at two wavelengths, both of which are detectable by flow cytometry, depending on whether it is in the presence of calcium (400 nm) or not (475 nm). In these experiments, the ionophore ionomycin was used as a positive control as it transports calcium from intracellular stores into the cytoplasm. The chelator ethylene glycol-bis(2-aminoethylether)-*N,N,N',*N'-tetraacetic acid (EGTA) was used as a negative control.

WT and *Ptpn22*$^{-/-}$ BMDCs were harvested, counted and resuspended at 1 x 10^7/ml in calcium flux assay buffer (0.5% BSA in HBSS containing calcium and magnesium). Cells were stained with indo-1 (2 µg/ml, Invitrogen) at 37°C for 30 minutes. Cells were washed with calcium flux assay buffer, centrifuged for 5 minutes at 4°C and 1600 rpm and resuspended at 1 x 10^7/ml in calcium flux assay buffer. Cells were stained with anti-CD11c (BioLegend) for 30 minutes at room temperature. 100 µl (1 x 10^6) cells was added per FACS tube and taken to the flow cytometer. BMDCs were collected for 7 minutes, and stimulated after 1 minute with ionomycin (10 µg/ml, Sigma Aldrich) followed by EGTA (2 mM, Sigma Aldrich) after 4 minutes, or with ova ICs (50 µg) after 1 minute. Calcium flux was determined by gating on CD11c$^+$ singlets (excluding really bright Indo-1 (violet and blue) cells) (Figure 2-6).

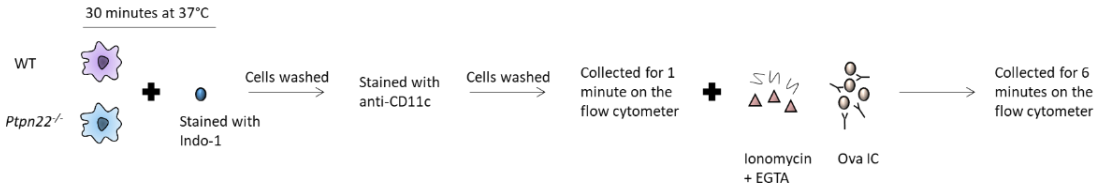

Figure 2-6: Schematic of calcium flux assay.

WT and Ptpn22$^{-/-}$ BMDCs were harvested, washed and resuspended at 1 x 10^7/ml and stained for 30 minutes at 37°C with indo-1. Cells were washed and stained with anti-CD11c and 1 x 10^6 cells (in 100 µl) were added per FACS tube. Samples were collected by flow cytometry for 1 minute before stimulations were added. Ionomycin was added, followed by EGTA 3 minutes later, or ova ICs were added. Calcium flux was determined by gating on CD11c$^+$ singlets.

2.2.3.4 Reactive oxygen species (ROS) production by *ex vivo* bone marrow neutrophils

Dihydrorhodamine 123 (DHR123) can be used to measure reactive oxygen species (ROS) production. DHR123 is an uncharged, non-fluorescent compound which can diffuse across membranes. When it becomes oxidised by the presence of ROS, it becomes fluorescent, which allows for the detection of ROS production by flow cytometry. DHR123 has an excitation wavelength of 507 nm and an emission wavelength of 529 nm.

To prevent unintended activation of *ex vivo* neutrophils, all reagents need to lack calcium and magnesium. In addition, incubations must be carried out at room temperature. WT and *Ptpn22*$^{-/-}$ bone marrow was flushed from mice using 0.1% gelatin in PBS and centrifuged for 5 minutes at room temperature and 1600 rpm and resuspended in 2 ml red blood cell lysis buffer (BioLegend) for 5 minutes at room temperature, washed in 0.1% gelatin in PBS and centrifuged for 5 minutes at room temperature and 1600 rpm. Bone marrow cells were resuspended at 1 x 10^7/ml in 0.1% gelatin in PBS and blocked with a non-fluorescent FcγRII/III antibody (BioLegend) and stained with anti-CD11b (BioLegend), anti-Ly6G (BioLegend) and a fixable viability dye (eBioscience) for 20 minutes at room temperature. Cells were washed, centrifuged for 5 minutes at room temperature and 1600 rpm and resuspended at 1 x 10^7/ml in 0.1% gelatin in PBS before being stained with 0.01 µM DHR123 (Sigma Aldrich) for 40 minutes at room temperature in the dark. Cells were washed, centrifuged for 5 minutes at room temperature and 1600 rpm and resuspended at 1 x 10^7/ml in 0.1% gelatin in PBS. 100 µl (1 x 10^6) cells was added per FACS tube and ova, anti-ova and ova ICs were added (all made in 0.1% gelatin in PBS) for 45 minutes at room temperature. Cells were washed, centrifuged for 5 minutes at room temperature and 1600 rpm and fixed using 1% PFA in PBS prior to flow cytometry. DHR123 expression was determined by gating on live, CD11b$^+$, Ly6G$^+$ singlets (Figure 2-7).

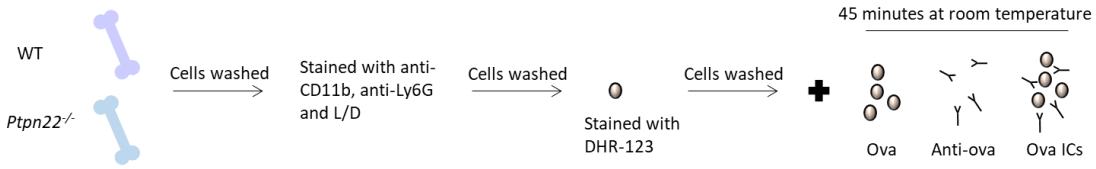

Figure 2-7: Schematic of reactive oxygen species (ROS) production by bone marrow neutrophils.

Bone marrow cells were flushed from WT and Ptpn22$^{-/-}$ mice, stained with anti-CD11c, anti-Ly6G and a viability dye (L/D). Cells were then washed and stained with DHR-123 and then stimulated with ova, rabbit anti-ova or ova:anti-ova immune complexes (ova ICs) for 45 minutes at room temperature. Cells were then washed and fixed and analysed by flow cytometry. ROS production was determined by gating on live, CD11b$^+$, Ly6G$^+$ singlets.

2.2.4 DC-T cell assays

2.2.4.1 *In vitro* DC-T cell co-cultures

WT, *Ptpn22*$^{-/-}$, *Ptpn22*^{R619} (WT) and *Ptpn22*^{R619W} BMDCs were incubated overnight at 37°C, 5% CO_2 with LPS (100 ng/ml, InvivoGen) and 0.01 µM or 1 µM $OVA_{323-339}$ (InvivoGen), 1 µM ova or 1 µM ova ICs. In some experiments, ova and ova IC pulsed BMDCs were also matured with LPS. The following day, BMDCs were harvested, washed and resuspended in culture media. OT-II $CD4^+$ T cells were isolated and CTV labelled as described in Section 2.2.2.5. BMDCs were co-cultured with CTV labelled $CD4^+$ T cells at 1:2 (1 x 10^5 BMDC:2 x 10^5 T cells) in 96 well round bottom plates (Thermo Fisher Scientific) for 1-6 days.

On day 1, cell-free supernatants were harvested, and IL-2 secretion was determined by immunoassay (BioLegend, as per Section 2.2.3.2). In addition, cells were harvested and stained with anti-CD3 (BioLegend), anti-CD4 (BioLegend), anti-CD25 (BioLegend), anti-CD69 (BioLegend) and a fixable viability dye (eBioscience) for 30 minutes at 4°C. Cells were washed and fixed using 1% PFA in PBS prior to flow cytometry. Cell surface CD25 and CD69 expression was determined by gating on live, $CD3^+$, $CD4^+$ singlets.

On days 3 and 6 of co-culture, cell-free supernatants were harvested, and IFNγ, TNFα and IL-17 secretion was determined by immunoassay (BioLegend, as per Section 2.2.3.2). In addition, cells were restimulated for 6 hours at 37°C, 5% CO_2 with phorbol 12-myristate 13-acetate (PMA, 10 ng/ml, Sigma Aldrich), ionomycin (500 ng/ml, Sigma Aldrich) and monensin (BioLegend). Cells were harvested and stained with anti-CD3 (BioLegend), anti-CD4 (BioLegend) and a fixable viability dye (eBioscience) for 30 minutes at 4°C. Cells were washed and incubated in fix/permeabilisation buffer (Foxp3/transcription factor staining buffer set, eBioscience) for 15 minutes at room temperature, washed with perm buffer (Foxp3/transcription factor staining buffer set, eBioscience) and stained with anti-IFNγ, anti-TNFα and anti-IL-17 (all from BioLegend) in permeabilisation buffer for 45 minutes at room temperature. Cells were washed in permeabilisation buffer and resuspended in PBS containing 5 x 10^4 counting beads (BioLegend) per FACS tube, prior to flow cytometry. T cell proliferation (via CTV dilution) and intracellular expression of IFNγ, TNFα and IL-17 were determined by gating on live, $CD3^+$, $CD4^+$ singlets (Figure 2-8). The total number of live, $CD3^+$, $CD4^+$ singlets per co-culture well was determined using cell

counts by trypan blue (Sigma Aldrich) exclusion and the proportion of live cells which were $CD3^+$, $CD4^+$ by flow cytometry.

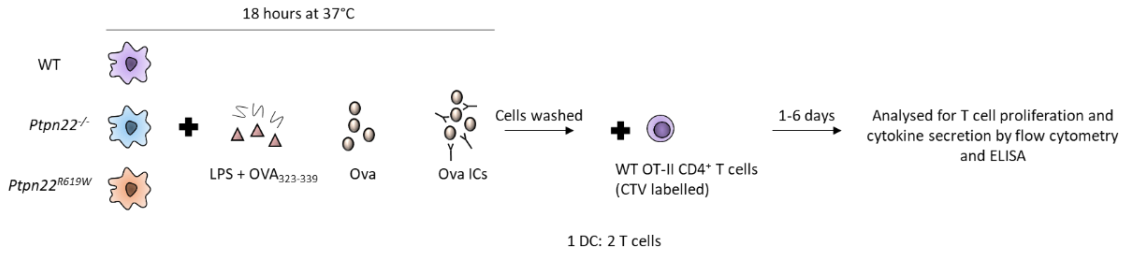

Figure 2-8: Schematic of in vitro BMDC:T cell co-cultures.

WT, Ptpn22$^{-/-}$ and Ptpn22^{R619W} BMDCs were incubated for 18 hours at 37°C, 5% CO_2 in the presence of 100 ng/ml LPS and 10 µM $OVA_{323-339}$, or 1 µM ova or 1 µM ova:anti-ova ICs (ova ICs). . BMDCs were harvested, washed and co-cultured with WT CTV labelled $CD4^+$ OT-II T cells for 1-6 days, at 1 DC: 2 T cells (1 x 10^5:2 x 10^5). Cell-free supernatants were collected on days 1, 3 and 6 and analysed for secretion of IL-2 (day 1), IFNγ, TNFα and IL-17 (days 3 and 6). Intracellular cytokines were detected after 6 hours of restimulation with PMA, ionomycin and monensin. Finally, T cell proliferation was assessed by CTV dilution and by calculating the total number of T cells in the co-culture wells (days 3 and 6).

As additional controls for some experiments, BMDCs were also stimulated with 1 µM ova pre-incubated with rabbit IgG (using the same procedure as making ova ICs), or with 1 µM ova added in combination with 1 µM HA rabbit IgG (Sigma Aldrich), prior to co-culture with WT $CD4^+$ OT-II T cells.

2.2.4.2 DC:T-cell conjugate assay

WT and *Ptpn22*$^{-/-}$ BMDCs were incubated overnight at 37°C, 5% CO_2 with LPS (100 ng/ml, InvivoGen) and 10 µM $OVA_{323-339}$ (InvivoGen), 1 µM ova or 1 µM ova ICs. The following day, BMDCs were harvested, washed and resuspended at 1 x 10^7/ml in PBS prior to staining with 1 µM CellTrace Far Red (CTFR, Invitrogen) for 20 minutes at 37°C, followed by quenching in culture media for 20 minutes at 37°C. 1 x 10^5 CTFR labelled BMDCs and 2 x 10^5 CTV labelled WT OT-II T cells (in a total volume of 50 µl) were added to each 1.5 ml tube, centrifuged for 2 minutes at 500 rpm and incubated at 37°C for 0-120 minutes. Cells were fixed with 3% PFA for 15 minutes at room temperature, transferred to FACS tubes and acquired by flow cytometry using a medium flow rate. Conjugates were identified as CTV^+ $CTFR^+$ events (Figure 2-9).

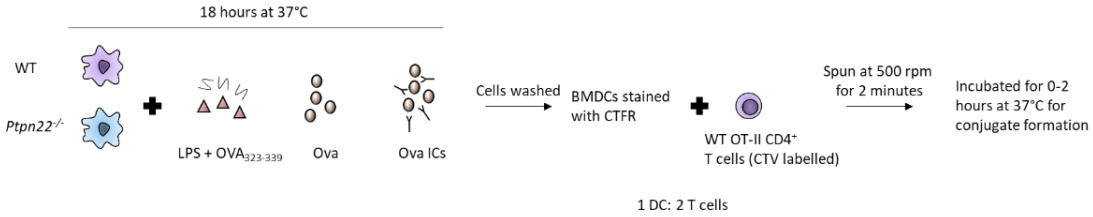

Figure 2-9: Schematic of DC-T cell conjugate assay.

WT and Ptpn22$^{-/-}$ BMDCs were incubated for 18 hours at 37°C, 5% CO_2 in the presence of 100 ng/ml LPS and 10 µM $OVA_{323-339}$, or 1 µM ova or 1 µM ova:anti-ova ICs (ova ICs). The following day, BMDCs were washed and stained with CellTrace Far Red (CTFR). WT OT-II CD4$^+$ T cells were isolated from the spleen and lymph nodes of OT-II mice and stained with CellTrace Violet (CTV). BMDCs and T cells were mixed at 1 DC: 2 T cells (1 x 10^5:2 x 10^5) and centrifuged for 2 minutes at 500 rpm. Cells were incubated at 37C for 0-2 hours for conjugates to form. Conjugates were identified as CTFR$^+$ CTV$^+$ events.

To determine the role of Src and Syk family kinases in immune complex induced conjugate formation, WT BMDCs were incubated overnight at 37°C, 5% CO_2 with 1 µM ova ICs. The following day, BMDCs were harvested and CTFR stained as above, before being incubated with Src inhibitor-1 (5 µM, Sigma Aldrich) or Syk inhibitor II (5 µM, Calbiochem) for 15 minutes at 37°C. The conjugate assay was then carried out as described above.

2.2.5 *In vivo* experiments

2.2.5.1 FITC painting assay

FITC (Invitrogen) was resuspended in DMSO and diluted in 1:1 acetone:dibutyl phthalate (irritant, Sigma Aldrich) at 1 mg/ml. WT and *Ptpn22$^{-/-}$* mice were anaesthetised and 10 µl FITC in irritant was added to the dorsal side of their left ears. 10 µl irritant alone (as a negative control) was added to the dorsal side of their right ears. After 24 hours, auricular draining lymph nodes were harvested, ripped open using 26G needles and digested in RPMI-1640 containing DNase I and Liberase TL (both at 0.1mg/ml, Roche) for 30 minutes at 37°C in 5% CO_2; 10 mM EDTA was added for the final 5 minutes. Single cell suspensions were obtained by mashing the digested lymph nodes through gauze. Cells were counted and stained with anti-CD11c (BioLegend), anti-MHCII I-A^b (BioLegend) and a fixable viability marker (eBioscience) for 30 minutes at 4°C. Cells were washed and fixed using 1% PFA in PBS prior to flow cytometry. FITC uptake was measured in migratory DCs by gating on live, CD11c$^+$, MHCII^{hi} singlets and in resident DCs by gating on live, CD11c^{hi}, MHCII$^+$ singlets (Figure 2-10).

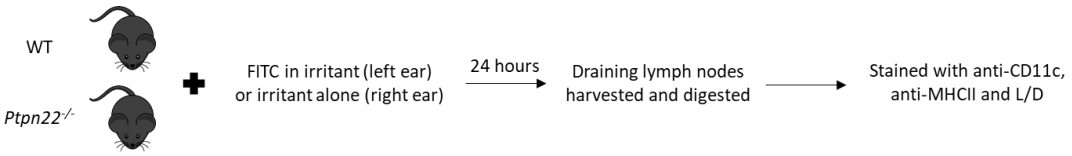

Figure 2-10: Schematic of FITC painting assay.

FITC in acetone:dibutyl phthalate (irritant) or irritant alone was added to the dorsal sides of the left and right ears respectively of WT and Ptpn22$^{-/-}$ mice. 24 hours later, draining lymph nodes were removed, digested and stained with anti-CD11c, anti-MHCII and a viability dye (L/D). FITC uptake by resident (gated on live, CD11c^{hi}, MHCII^{+} singlets) and migratory (gated on live, CD11c^{+}, MHCII^{hi} singlets) DCs was determined by flow cytometry.

2.2.5.2 Ova and ova IC induced *in vivo* T cell proliferation

To determine if PTPN22 played a role in regulating immune complex induced T cell proliferation *in vivo*, CD4^{+} OT-II T cells were transferred into WT and *Ptpn22*$^{-/-}$ recipient mice. The mice were later immunised with ova ICs, which would be processed and presented by endogenous antigen presenting cells, and T cell proliferation could be monitored after 3 days by CTV dilution and by calculating the total number of transferred T cells in the draining lymph nodes.

WT CD4^{+} OT-II T cells were isolated from the lymph nodes and spleens of OT-II CD45.1^{+} mice and stained with CTV, as described in Section 2.2.2.5. An aliquot of cells was stained with anti-CD4 (BioLegend), anti-TCR Vα2 (BioLegend) and anti-TCR Vβ5 (BioLegend) for 30 minutes at 4 °C. Samples were washed with FACS buffer and fixed using 1% PFA in PBS prior to flow cytometry. The proportion of total cells which were OT-II^{+} was determined by gating on live, CD4^{+}, TCR Vα2^{+}, TCR Vβ5^{+} singlets. 1 x 10^{6} CTV labelled WT CD4^{+} OT-II T cells were injected (i.v.) into WT or *Ptpn22*$^{-/-}$ mice (CD45.2^{+}). The following day mice were immunised (s.c.) with 1 µg ova, 20 µg anti-ova or ova ICs (containing 1 µg ova and 20 µg anti-ova), into the right footpad (in a total volume of 20 µl). After 3 days, draining popliteal lymph nodes (right) and non-draining popliteal lymph nodes (left) were harvested. Single cell suspensions were made by mashing lymph nodes through gauze. Cells were washed with PBS and centrifuged for 5 minutes at 4°C and 1600 rpm. Cells were counted, blocked with a non-fluorescent FcγRII/III antibody (BioLegend) and stained using antibodies against CD4, TCR Vα2, TCR Vβ5, CD45.1, CD45.2 (all from BioLegend), and a fixable viability dye (eBioscience). CTV dilution was determined by gating on the live, CD4^{+}, TCR Vα5^{+}, TCR Vβ2^{+}, CD45.1^{+}, CD45.2^{-} singlets (Figure 2-11). In addition, the total number of transferred OT-II T cells was calculated using cell counts by trypan blue (Sigma Aldrich) exclusion and the proportion of live cells which were OT-II T cells by flow cytometry.

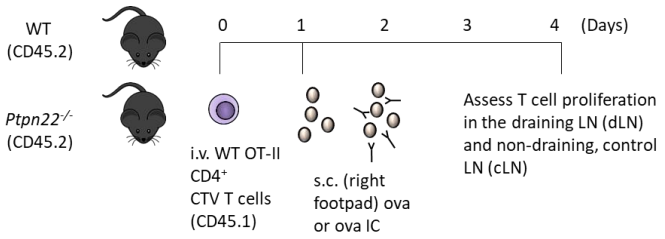

Figure 2-11: Schematic of in vivo T cell proliferation assays.

WT and Ptpn22$^{-/-}$ (CD45.2) mice were injected (i.v.) with CTV labelled WT CD4^{+} OT-II T cells (CD45.1). The following day, mice were injected (s.c.) into their right footpad with ova or ova ICs. 3 days later, draining (right) and non-draining (left) popliteal lymph nodes were removed and T cell proliferation was assessed by flow cytometry.

2.2.5.3 Transfer of ova IC pulsed BMDCs into recipient mice for *in vivo* T cell proliferation

An alternative assay to investigate the role of PTPN22 in immune complex induced T cell proliferation *in vivo* was to transfer ova IC pulsed WT and *Ptpn22*$^{-/-}$ BMDCs into OT-II recipient mice and to monitor T cell proliferation in the draining lymph nodes.

WT and *Ptpn22*$^{-/-}$ BMDCs were pulsed overnight with 1 µM ova ICs. The following day, BMDCs were harvested, washed, counted and resuspended at 2.5 x 10^7/ml in PBS. 5 x 10^5 BMDCs were injected (s.c.) into the right footpad of recipient WT OT-II mice (in a total volume of 20 µl). After 6 days, draining (right) and non-draining (left) popliteal lymph nodes were harvested. Single cell suspensions were made by mashing the lymph nodes through gauze. Cells were counted, blocked with a non-fluorescent FcγRII/III antibody (BioLegend) and stained using antibodies against CD4, TCR Vα2, TCR Vβ5 (all from BioLegend) and a fixable viability dye (eBioscience). Cells were washed with FACS buffer and resuspended in PBS containing 5 x 10^4 counting beads (BioLegend) per FACS tube, prior to flow cytometry (Figure 2-12). The total number of OT-II T cells per lymph node was calculated using cell counts by trypan blue (Sigma Aldrich) exclusion and the proportion of live cells which were OT-II T cells by flow cytometry.

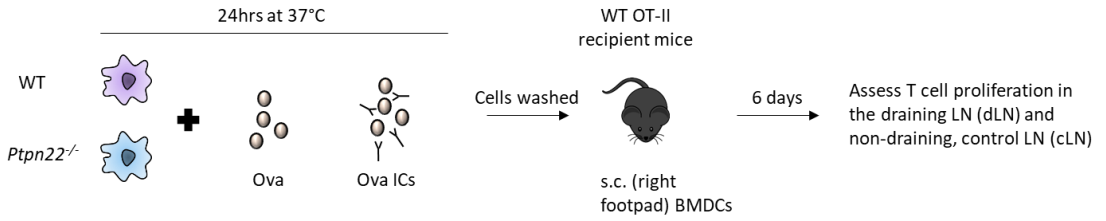

Figure 2-12: Schematic of in vivo T cell proliferation assay.

WT and Ptpn22$^{-/-}$ BMDCs DCs were incubated for 24 hours at 37°C, 5% CO_2 with ova or ova:anti-ova immune complexes (ova ICs). The following day, BMDCs were harvested, washed and injected (s.c.) into the right footpad of recipient WT OT-II mice. 6 days later, draining (right) and non-draining (left) popliteal lymph nodes were removed and T cell proliferation was assessed by flow cytometry.

2.2.6 Uptake, processing and presentation assays

2.2.6.1 Macropinocytosis assay

In order to identify whether PTPN22 was required for BMDC macropinocytosis, assays were conducted using Lucifer yellow CH (LY), a water-soluble dye. The polar properties of LY mean that it cannot passively pass through cell membranes, however it can be internalised by DCs during non-specific uptake of their surrounding environments, via macropinocytosis. LY is fluorescent and can therefore be detected by flow cytometry and thus provides a simple method for monitoring macropinocytosis.

WT, *Ptpn22*$^{-/-}$, *Ptpn22*^{R619} and *Ptpn22*^{R619W} BMDCs were stimulated overnight in the presence or absence of LPS (100 ng/ml, InvivoGen). The following day, BMDCs were harvested, washed and counted and 2 x 10^5 were added to each FACS tube. BMDCs were cooled on ice and incubated with Lucifer yellow (1 mg/ml, Invitrogen) at 37°C for 0-30 minutes. Samples were returned to ice and washed twice with cold PBS to prevent further uptake. Cells were blocked with a non-fluorescent FcγRII/III antibody (BioLegend) and stained with anti-CD11c and a fixable viability dye (BioLegend) for 30 minutes on ice. Cells were washed with FACS buffer and fixed using 1% PFA in PBS prior to flow cytometry. BMDCs were identified as live, CD11c$^+$ singlets (Figure 2-13).

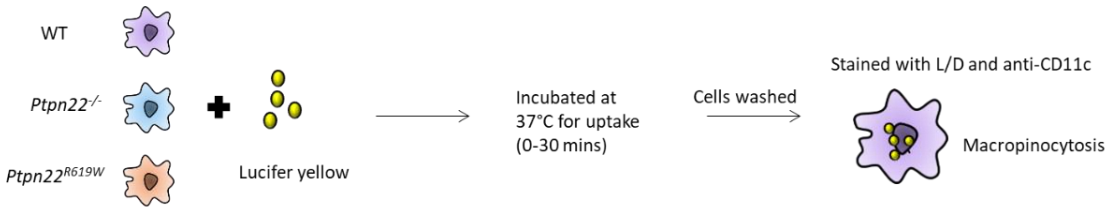

Figure 2-13: Schematic of Lucifer yellow uptake.

WT, Ptpn22$^{-/-}$ and Ptpn22^{R619W} BMDCs were incubated with Lucifer yellow for 0-30 minutes at 37°C. In some experiments, BMDCs were matured overnight with 100 ng/ml lipopolysaccharide (LPS) prior to the uptake assay. Cells were washed with cold PBS to prevent further uptake, and were stained with anti-CD11c and a viability dye (L/D). Internalisation was measured by flow cytometry, gating on live, CD11c^{+} singlets.

2.2.6.2 Receptors mediated endocytosis of heat killed *Listeria monocytogenes* and heat killed *Candida albicans*

Listeria monocytogenes is a Gram-positive bacteria which is mainly recognised by Toll-like receptor 2 (TLR2). *Candida albicans* is a fungus which contains β-glucans in its cell wall. β-glucans are recognised by the C-type lectin receptor, dectin-1. Heat killed preparations of these agonists can be used to monitor receptor mediated endocytosis via TLR2 and dectin-1 respectively.

Heat killed *Listeria monocytogenes* (HKLM, InvivoGen) or heat killed *Candida albicans* (HKCA, InvivoGen) were stained with Zombie UV Fixable Viability dye (BioLegend, diluted 1:50 in PBS) at room temperature in the dark for 20 minutes. Labelled HKLM and HKCA was then washed with PBS, centrifuged for 5 minutes at room temperature and 13,500 rpm and resuspended in PBS at 1 x 10^8/ml.

WT, *Ptpn22$^{-/-}$*, *Ptpn22^{R619}* and *Ptpn22^{R619W}* BMDCs were harvested, counted and resuspended in FACS buffer at 8 x 10^6/ml. 2 x 10^5 BMDCs were added to FACS tubes, cooled on ice and incubated with 6 x 10^6 UV labelled heat killed *Listeria monocytogenes* (1 DC:30 HKLM) or 2 x 10^6 heat killed *Candida albicans* (1 DC:10 HKCA) on ice for 45 minutes. Cells were washed with cold FACS buffer and incubated at 37°C for 0-60 minutes. Samples were returned to ice and washed with cold PBS to prevent further uptake. Cells were blocked with a non-fluorescent FcγRII/III antibody (BioLegend) and stained with anti-CD11c (BioLegend) for 30 minutes on ice. Cells were washed with FACS buffer and fixed using 1% PFA in PBS prior to flow cytometry. Uptake was identified as CD11c^{+} UV^{+} events (Figure 2-14).

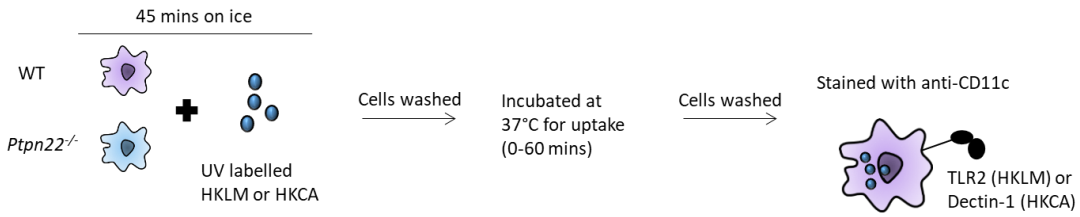

Figure 2-14: Schematic of HKLM and HKCA antigen uptake assays.

WT and Ptpn22$^{-/-}$ BMDCs were incubated with heat killed Listeria monocytogenes (HKLM) or heat killed Candida albicans (HKCA) on ice for 45 minutes, before being washed and incubated at 37°C for 0-60 minutes. Cells were washed with cold PBS to prevent further uptake, and were stained with anti-CD11c and a viability dye (L/D). Internalisation was measured by flow cytometry, gating on live, CD11c^{+} singlets.

2.2.6.3 Receptor mediated endocytosis of ovalbumin

Ovalbumin (ova) is internalised via mannose receptor mediated endocytosis. By pre-incubating BMDCs with fluorescent ova on ice, this allows for binding to the mannose receptors. Transfer of the DCs to 37°C allows for receptor mediated endocytosis. This assay can therefore be used to identify whether PTPN22 is required for receptor mediated endocytosis of ova.

WT, *Ptpn22*$^{-/-}$, *Ptpn22*^{R619} and *Ptpn22*^{R619W} BMDCs were stimulated overnight in the presence or absence of LPS (100 ng/ml, InvivoGen). The following day, BMDCs were harvested, counted and resuspended in FACS buffer at 8 x 10^6/ml. 2 x 10^5 BMDCs were added to FACS tubes, cooled on ice and incubated with ova-AF488 (10 µg/ml, Invitrogen) on ice for 45 minutes. Cells were then incubated at 37°C for 0-60 minutes. Samples were returned to ice and washed with cold PBS to prevent further uptake. Cells were blocked with a non-fluorescent FcγRII/III antibody (BioLegend) and stained with anti-CD11c (BioLegend) and a fixable viability dye (eBioscience) for 30 minutes on ice. Cells were washed with FACS buffer and fixed using 1% PFA in PBS prior to flow cytometry. BMDCs were identified as live, CD11c^{+} singlets (Figure 2-15).

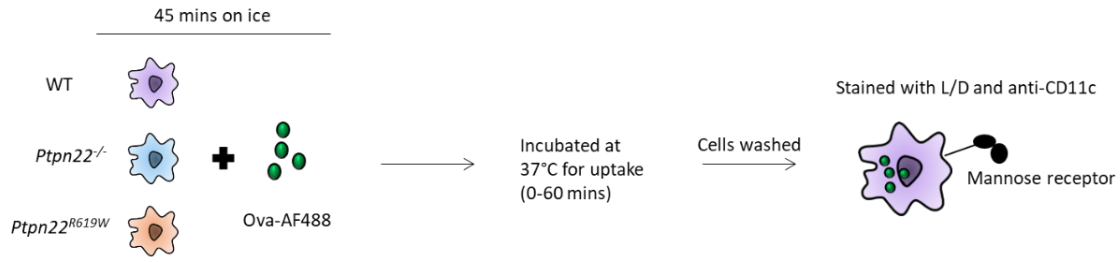

Figure 2-15: Schematic of ova uptake assays.

WT, Ptpn22$^{-/-}$ and Ptpn22^{R619W} BMDCs or splenocytes were incubated with ova-AF488 or ova-AF647 on ice for 45 minutes, before being incubated at 37°C for 0-60 minutes. In some experiments, BMDCs were matured overnight with 100 ng/ml lipopolysaccharide (LPS) prior to the uptake assay. Cells were washed with cold PBS to prevent further uptake, and were stained with anti-CD11c and a viability dye (L/D) for BMDCs or with anti-CD11c, anti-MHCII and a viability dye (L/D) for splenocytes. Internalisation was measured by flow cytometry, gating on live, CD11c$^+$ singlets (for BMDCs) or gating on live, CD11c$^+$, MHCII$^+$ singlets (for splenic conventional DCs).

To measure ova uptake by splenic DCs, spleens from WT, *Ptpn22*$^{-/-}$, *Ptpn22*^{R619} and *Ptpn22*^{R619W} mice were digested in 1 ml RPMI-1640 containing DNase I and Liberase TL (both at 0.1mg/ml, Roche) for 30 minutes at 37°C in 5% CO_2; 10 mM EDTA was added for the final 5 minutes. Splenocyte cell suspensions were resuspended in 2 ml red blood cell lysis buffer (BioLegend), washed in PBS and centrifuged for 5 minutes at 4°C and 1600 rpm. Splenocytes were counted and 5 x 10^6 were added per FACS tube. Splenocytes were cooled on ice and incubated with ova-AF647 (50 µg/ml, Invitrogen) for 45 minutes on ice. Cells were washed and transferred to 37°C for 45 minutes to allow for uptake. Samples were returned to ice and washed with cold PBS to prevent further uptake. Cells were blocked with a non-fluorescent FcγRII/III antibody (BioLegend) and stained to identify splenic DCs, washed with FACS buffer and fixed using 1% PFA in PBS prior to flow cytometry. Splenic DCs were identified as live, lineage$^-$ (to exclude CD3$^+$, CD19$^+$, Ter119$^+$, NK1.1$^+$, GR1$^+$, B220$^+$ splenocytes), CD11c$^+$, MHCII$^+$ singlets.

2.2.6.4 Receptor mediated endocytosis of ova immune complexes

Ova:anti-ova immune complexes (ova ICs) were made as described in Section 2.2.3.1. As rabbits do not have IgG subtypes, these ova ICs will bind to all FcγRs expressed on the cell surface of BMDCs. By using fluorescent ova (ova-AF488) in the ova ICs, FcγR mediated endocytosis could be monitored by flow cytometry.

WT and *Ptpn22*$^{-/-}$ BMDCs were harvested, counted and resuspended in FACS buffer at 8 x 10^6/ml. 2 x 10^5 BMDCs were added to FACS tubes, cooled on ice and incubated with ova-AF488 (10

µg/ml, Invitrogen) immune complexes (ova ICs) on ice for 45 minutes. Cells were washed with cold FACS buffer and incubated at 37°C for 0-60 minutes. Samples were returned to ice and washed with cold PBS to prevent further uptake. Cells were blocked with a non-fluorescent FcγRII/III antibody (BioLegend) and stained using anti-CD11c (BioLegend), F(ab')2 goat anti-rabbit IgG-AF647 (Invitrogen) and a fixable viability dye (BioLegend). Cells were washed and fixed using 1% PFA in PBS prior to flow cytometry. Cell surface ova-AF488 ICs were identified as F(ab')2 goat anti-rabbit IgG-AF647^{+}, as this would bind to rabbit anti-ova-containing ICs. BMDCs with internalised ova ICs were identified as live, CD11c^{+}, F(ab')2 goat anti-rabbit IgG-AF647^{-} singlets (Figure 2-16).

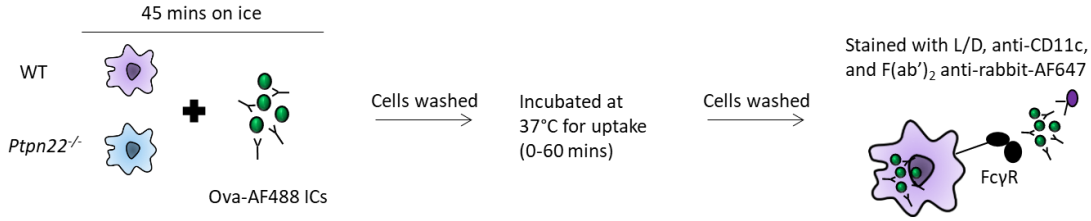

Figure 2-16: Schematic of ova:anti-ova immune complex uptake assays.

WT and Ptpn22$^{-/-}$ BMDCs were incubated with ova-AF488:anti-ova immune complexes (ova-AF488 ICs) on ice for 45 minutes, before being washed and incubated at 37°C for 0-60 minutes. Cells were washed with cold PBS to prevent further uptake, and were stained with anti-CD11c, a viability dye (L/D) and F(ab')$_2$ anti-rabbit-AF647 (to identify non-internalised ova-AF488 ICs). Internalisation was measured by flow cytometry, gating on live, CD11c^{+}, F(ab')$_2$ anti-rabbit-AF647^{-} singlets.

2.2.6.5 Ova and ova immune complex degradation assay

To investigate whether PTPN22 may regulate the degradation of internalised antigens by BMDCs, polystyrene beads were coated with fluorescent ova and rabbit anti-ova. The intensity of the ova signal is lost over time, which can be used as a measure of antigen degradation.

3µm polystyrene beads (Polysciences) were coated overnight at 4°C with ovalbumin-AF594 (0.5 mg/ml, Invitrogen). For ova-AF594:anti-ova coated beads, beads were washed the following day and incubated with rabbit anti-ova (50 µg/ml, Sigma Aldrich) for 20 minutes on ice. 1 x 10^5 BMDCs and 2 x 10^6 beads were added to wells of a 96 well round bottom plate (1 DC:20 beads, Thermo Fisher Scientific), centrifuged for 5 minutes at 2000 rpm and incubated at 37°C and 5% CO_2 for 0-7 hours. To exclude non-internalised beads, BMDCs were washed and stained with rabbit anti-ova (50 µg/ml, Sigma Aldrich, only for ova coated beads), and F(ab')2 goat anti-rabbit IgG-AF647 (4 µg/ml, Invitrogen) for 20 minutes on ice. Cells were washed with FACS buffer and

lysed for 10 minutes on ice in lysis buffer (0.5% NP-40, 50mM Tris, 150 mM NaCl). Beads were washed twice with FACS buffer and transferred to FACS tubes. Internalised beads were identified as F(ab')2 goat anti-rabbit IgG-AF647$^-$ (Figures 2-17 and 2-18).

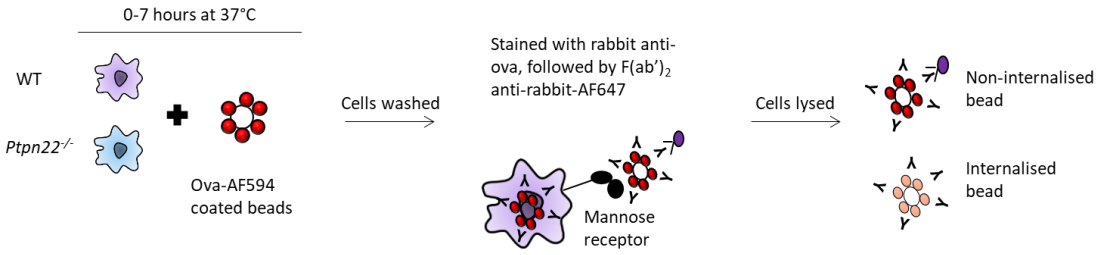

Figure 2-17: Schematic of ova coated bead degradation assay.

WT and Ptpn22$^{-/-}$ BMDCs were incubated with ova-AF594 coated beads for 0-7 hours at 37°C, 5% CO_2. BMDCs were washed and stained with rabbit anti-ova, followed by F(ab')$_2$ anti-rabbit-AF647 (to identify non-internalised beads). BMDCs were lysed and beads were analysed by flow cytometry. The ova-AF594 fluorescence was determined on internalised beads by gating on single, F(ab')$_2$ anti-rabbit-AF647$^-$ beads.

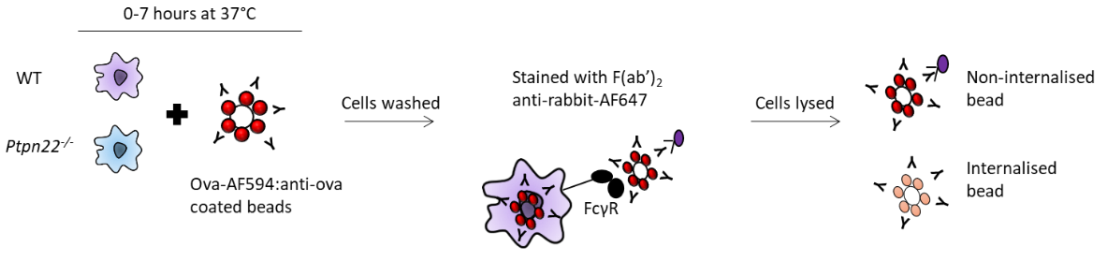

Figure 2-18: Schematic of ova:anti-ova coated bead degradation assay.

WT and Ptpn22$^{-/-}$ BMDCs were incubated with ova-AF594:anti-ova coated beads for 0-7 hours at 37°C, 5% CO_2. BMDCs were washed and stained with followed by F(ab')$_2$ anti-rabbit-AF647 (to identify non-internalised beads). BMDCs were lysed and beads were analysed by flow cytometry. The ova-AF594 fluorescence was determined on internalised beads by gating on single, F(ab')$_2$ anti-rabbit-AF647$^-$ beads.

2.2.6.6 Immune complex derived antigen presentation assay

The antibody YAe can be used to monitor cell surface presentation of immune complex derived antigens. The antibody is specific for I-A^b restricted presentation of a peptide from Eα (Eα$_{52-68}$), so by incubating BMDCs with immune complexes containing Eα, the antibody can be utilised to compare expression of processed antigens on the surface of BMDCs, in the presence or absence of PTPN22.

WT and *Ptpn22$^{-/-}$* BMDCs were harvested, counted and resuspended in culture media at 2 x 10^6/ml. 100 µl (2 x 10^5) BMDCs were incubated on 96 well round bottom plates (Thermo Fisher

Scientific) with GFP, GFP-Eα (Erwan Boëdec, Paris 7 University), GFP:anti-GFP immune complexes or immune complexes containing 0.3 mg/ml GFP-Eα and anti-GFP (Invitrogen) for 18 hours at 37°C, 5% CO_2. BMDCs were harvested, washed and stained with anti-CD11c (BioLegend), anti-$E\alpha_{52\text{-}68}$-biotin (YAe, eBioscience) and a fixable viability dye (eBioscience) for 30 minutes on ice. Cells were washed with FACS buffer and stained with PBS containing streptavidin-APC (BioLegend) at room temperature for 10 minutes. Cells were washed and fixed using 1% PFA in PBS prior to flow cytometry. BMDCs were identified as live, $CD11c^+$ singlets (Figure 2-19). To determine MHCII cell surface expression on WT and *Ptpn22*$^{-/-}$ BMDCs, separate wells (which did not receive any antigen or immune complex) were also stained with anti-CD11c (BioLegend), anti-MHCII I-A^b (BioLegend) and a fixable viability dye (eBioscience).

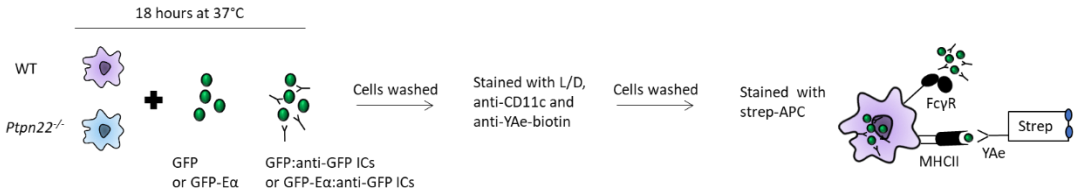

Figure 2-19: Schematic of immune complex derived antigen presentation assay.

WT and Ptpn22$^{-/-}$ BMDCs were incubated with GFP, GFP-Eα, GFP:anti-GFP ICs or GFP-Eα:anti-GFP ICs for 18 hours at 37°C, 5% CO_2. BMDCs were washed and stained with anti-CD11c, anti-YAe-biotin (which recognises $E\alpha_{52\text{-}68}$ in I-A^b) and a viability dye (L/D). BMDCs were washed and incubated with streptavidin-APC. Antigen or IC internalisation was determined by measuring GFP expression on live, $CD11c^+$ singlets. Cell surface presentation of $E\alpha_{52\text{-}68}$ in I-A^b was determined by YAe fluorescence, after gating on live, $CD11c^+$ singlets.

2.2.6.7 Using blocking antibodies and kinase inhibitors in uptake and degradation assays

To verify that the ova ICs were being internalised via FcγRs, BMDCs were pre-incubated with anti-FcγRI (BioLegend), FcγRII/III (BioLegend) and FcγRIV (Professor Jeffrey Ravetch, Rockefeller University) for 15 minutes at 4°C, prior to incubation with ova ICs. To determine the role of Src and Syk family kinases in ova IC uptake, BMDCs were pre-incubated with Src inhibitor-1 (5 µM, Sigma Aldrich) for 15 minutes at 37°C, or Syk inhibitor II (5 µM, Calbiochem) for 15 minutes at 37°C, prior to incubation with LY, ova or ova ICs. To verify that the HKCA was being internalised via dectin-1, BMDCs were pre-incubated with anti-dectin-1 (10 µg/ml, InvivoGen) for 30 minutes on ice, prior to incubation with the UV labelled HKCA.

2.2.7 FcγR expression on BMDCs

2.2.7.1 Cell surface expression of FcγRs on DCs by flow cytometry

For cell surface FcγR expression, isolated splenocytes and BMDCs from WT, *Ptpn22*$^{-/-}$, *Ptpn22*^{R619} and *Ptpn22*^{R619W} mice were harvested, washed and stained using the following antibodies: FcγRI-APC (BioLegend), FcγRII/III-FITC (BioLegend), FcγRIIb (Professor Jeffrey Ravetch, Rockefeller University) followed by goat anti-mouse AF488 (Invitrogen) and FcγRIV (Professor Jeffrey Ravetch, Rockefeller University) followed by goat anti-hamster FITC (AbD Serotec). FcγRIII expression was determined by using anti-FcγRIIb followed by FcγRII/III-FITC. Cells were washed with FACS buffer and fixed using 1% PFA in PBS prior to flow cytometry. FcγR expression was determined by gating on live, CD11c^{+} singlets (for BMDCs) and live, CD11c^{+}, MHCII^{+} singlets (for splenic cDCs).

Cell surface expression of FcγRIIb on bone marrow preDCs and CDPs was also investigated. Bone marrow was flushed from WT and *Ptpn22*$^{-/-}$ mice, centrifuged for 5 minutes at room temperature and 1600 rpm and resuspended in 2 ml red blood cell lysis buffer (BioLegend) for 5 minutes at room temperature, washed with PBS and centrifuged for 5 minutes at room temperature and 1600 rpm. 5 x 10^{6} bone marrow cells were stained with FcγRIIb (Professor Jeffrey Ravetch, Rockefeller University) followed by goat anti-mouse AF488 (Invitrogen), washed, blocked with a non-fluorescent FcγRII/III antibody (BioLegend) and stained with antibodies to identify common DC precursors (CDPs) and preDCs. Cells were washed and fixed using 1% PFA in PBS prior to flow cytometry. FcγRIIb expression was determined by gating on live, CD115^{+}, cKit (CD117)$^{-}$, Flt3 (CD135)$^{+}$ singlets (for CDPs) and live, CD11c^{+}, MHCII^{-}, SIRPα^{low}, Flt3 (CD135)$^{+}$ singlets (for preDCs).

2.2.7.2 Cell surface bone marrow neutrophil FcγR expression by flow cytometry

To determine cell surface FcγR expression on neutrophils, WT, *Ptpn22*$^{-/-}$, *Ptpn22*^{R619} and *Ptpn22*^{R619W} bone marrow was flushed from mice, centrifuged for 5 minutes at room temperature and 1600 rpm and resuspended in 2 ml red blood cell lysis buffer (BioLegend) for 5 minutes at room temperature, washed with PBS and centrifuged for 5 minutes at room temperature and 1600 rpm. Bone marrow cells were stained as described above (Section

2.2.7.1). Cells were washed and fixed using 1% PFA in PBS prior to flow cytometry. FcγR expression was determined by gating on live, $CD11b^+$, $Ly6G^+$ singlets.

2.2.7.3 BMDC *Fcgr* mRNA expression

To determine mRNA levels of *Fcgrs*, BMDCs were harvested, washed with PBS and lysed in 700 µl QIAzol (Qiagen) for 5 minutes at room temperature, before being stored at -80°C. To extract RNA, samples were thawed and 200 µl chloroform was added per sample and shaken vigorously by hand for 15 seconds before being incubated at room temperature for 5 minutes. Samples were centrifuged for 20 minutes at 4°C and 13,500 rpm and the clear aqueous phase (containing the RNA) was transferred to a new RNase free eppendorf tube on ice (carried out in the fume hood). 500 µl ice-cold isopropanol and 1 µl Glycoblue (Invitrogen) was added per tube and shaken for 15 seconds. Samples were incubated for at least 30 minutes at -20°C before being centrifuged for 30 minutes at 4°C and 13,500 rpm. The supernatants were discarded and replaced with 1 ml ice-cold 70% ethanol and mixed. Samples were centrifuged for 10 minutes at 4°C and 13,500rpm before discarding the supernatant. RNA was washed twice with 250 µl 70% ice-cold ethanol. RNA was air dried for at least 15 minutes on ice and resuspended in 20-30 µl cooled nuclease free water for at least 15 minutes on ice. Finally, the NanoDrop (Thermo Fisher Scientific) was used to determine the amount and quality of RNA present.

cDNA was reverse transcribed using a First Strand cDNA synthesis kit (Thermo Fisher Scientific). Each reaction was in a final volume of 20 µl, composed of 10 µl mastermix (reaction buffer, RNase inhibitor, dNTPs, reverse transcriptase and oligo (dT) 18 primer) and 1 µg mRNA (in 10 µl nuclease free water). Samples were incubated at 37°C for 60 minutes followed by 5 minutes at 70°C on a Thermal Cycler. cDNA was stored at -20C before use in qPCR.

Gene expression was measured by TaqMan quantitative real-time PCR. qPCRs were set up on ice, with each reaction containing 5 µl 2 x qPCRBIO probe (PCR Biosystems), 0.5 µl probe (FAM labelled *Fcgr1*: Mm00438874_m1, *Fcgr2b*: Mm00438875_m1 or *Fcgr3:* Mm00438882_m1, or a VIC labelled eukaryotic *18S* probe: Hs99999901_s1, all from Applied Biosystems), 3.5 µl nuclease free water and 1µl cDNA. Each condition was set up on a 384 well plate (Thermo Fisher Scientific) in duplicate.

Acquisition was conducted using the ABI 7900HT fast real-time PCR system (Applied Biosystems), using the following settings: 94°C for 2 minutes, 50 x (95°C for 5 seconds and 65°C

for 30 seconds), 95°C for 15 seconds, 60°C for 1 minute and 95°C for 15 seconds. Relative abundance of gene expression was calculated using 18S as the endogenous control, and the formula: relative abundance = $2^{(-\Delta CT)}$.

2.2.8 Osteoclast analysis

2.2.8.1 Tartrate-resistant alkaline phosphatase (TRAP) staining

To ascertain whether PTPN22 was required for osteoclast differentiation *in vitro*, bone marrow cultures from WT and *Ptpn22*$^{-/-}$ mice were grown in the presence of M-CSF only or M-CSF and RANK-L (to induce osteoclast differentiation). A commercial staining kit was used to identify cells which expressed the osteoclast enzyme tartrate-resistant acid phosphatase (TRAP). The assay utilises Naphthol AS-BI phosphoric acid solution which is hydrolysed by TRAP to produce naphthol AS-BI, which then couples with fast garnet GBC to form insoluble maroon coloured crystals at the location of TRAP activity. As osteoclasts fuse and become multinucleated during differentiation, the cells could also be assessed for the number of nuclei they had. This therefore provided a simple assay to measure osteoclast differentiation *in vitro*. Using this method, osteoclasts were defined as TRAP^{+} and having 3 or more nuclei.

On day 10 of osteoclast culture (see Section 2.2.2.6 for culture details), media was removed from the wells and cells were fixed for 5 minutes at room temperature using 150 µl per well of 4% PFA in dI water. Wells were washed three times with dI water. 150 µl per well of a solution to identify TRAP (Sigma Aldrich) was added, which contained 1.5 µl naphthol AS-BI phosphate solution, 6 µl acetate solution, 3 µl fast garnet GBC base solution, 3 µl sodium nitrite solution, 7 µl tartrate solution and 129.5 µl dI water. After 5 minutes, the wells were washed with dI water and left in dI water to image. Cells were scored using a light microscope by assigning them into 3 categories: TRAP^{-}, TRAP^{+} with 1-2 nuclei and TRAP^{+} with 3 or more nuclei (osteoclasts).

2.2.8.2 Expression of osteoclast specific genes

In order to investigate if PTPN22 was required for osteoclast differentiation in a more quantitative manner than TRAP staining, the expression of osteoclast specific genes was measured in WT and *Ptpn22*$^{-/-}$ osteoclast cultures. On day 12 of osteoclast culture (see Section

2.2.2.6 for culture details), media was removed from the wells and the cells were washed with PBS. 200 µl per well 0.05M EDTA in PBS was added for 30 minutes at room temperature. To harvest the cells, they were pipetted up and down, centrifuged at 1600 rpm for 5 minutes at 4°C and lysed in 700 µl QIAzol for 5 minutes at room temperature. Samples were then stored at -80°C before use. To extract RNA, samples were thawed and 200 µl chloroform was added per sample and shaken vigorously by hand for 15 seconds before being incubated at room temperature for 5 minutes. Samples were centrifuged for 20 minutes and 4°C at 13,500 rpm and the clear aqueous phase (containing the RNA) was transferred to a new RNase free eppendorf tube on ice. 500 µl ice-cold isopropanol and 1 µl Glycoblue (Invitrogen) was added per tube and shaken for 15 seconds. Samples were incubated for at least 30 minutes at -20°C before being centrifuged for 30 minutes and 4°C at 13,500 rpm. The supernatants were discarded and replaced with 1 ml ice-cold 70% ethanol and mixed. Samples were centrifuged for 10 minutes and 4°C at 13,500rpm before discarding the supernatant. RNA was washed twice with 250 µl 70% ice-cold ethanol. RNA was air dried for at least 15 minutes on ice and resuspended in 20 – 30 µl cooled nuclease free water for at least 15 minutes on ice. Finally, the nanodrop was used to determine the amount and quality of RNA present.

cDNA was reverse transcribed using first strand cDNA synthesis using random hexamers (PCR Biosystems). Each reaction was in a final volume of 20 µl, composed of 4 µl 5 x cDNA synthesis mix, 1 µl 20 x RTase and 100 ng mRNA (made up to 20 µl using nuclease free water). Samples were incubated at 42°C for 30 minutes followed by 10 minutes at 85°C on a Thermal Cycler. cDNA was stored at 4°C before use in qPCRs. qPCRs were set up on ice, with each reaction containing 5 µl 2 x mastermix (Applied Biosystems PowerUp SYBR green), 0.5 µl forward and reverse primers (at 100 µM, see table 2-8 for details), 3 µl nuclease free water and 1µl cDNA (diluted 1:5). Each condition was set up on a 384 well plate (Thermo Fisher Scientific) in duplicate.

Primer pairs	Primer sequence	PCR cycle
Ptpn22 (spanning exon 1-2 junction)	Forward: 5' AGT TTG CCA GTG AAT TTC TGA AGC 3' Reverse: 5' TGA TAT TCT TGG GCC TCT GAG C 3'	50°C for 2 mins 95°C for 2 mins 40 x 95°C for 15s 58°C for 15s 72°C for 1 min 95°C for 15s 60°C for 1 min 95°C for 15s
Acp5	Forward: 5' TCC TCG GAG AAA ATG CAT CAT 3'	50°C for 2 mins 95°C for 2 mins

	Reverse: 5’ GCA GTT AAG CTC CTG GAC CAA 3’	40 x 95°C for 15s 50°C for 15s 72°C for 1 min 95°C for 15s 60°C for 1 min 95°C for 15s
Mmp9	Forward: 5’ CAC CTT CAC CCG CGT GTA C 3’ Reverse: 5’ GCT CCG CGA CAC CAA ACT 3’	50°C for 2 mins 95°C for 2 mins 40 x 95°C for 15s 50°C for 15s 72°C for 1 min 95°C for 15s 60°C for 1 min 95°C for 15s
Ctsk	Forward: 5’ GCT GTG GAG GCG GCT ATA TG 3’ Reverse: 5’ AGA GTC AAT GCC TCC GTT CTG 3’	50°C for 2 mins 95°C for 2 mins 40 x 95°C for 15s 51°C for 15s 72°C for 1 min 95°C for 15s 60°C for 1 min 95°C for 15s
Itgb3	Forward: 5’ GGA AGC AGC GCC CAG ATC AC 3’ Reverse: 5’ TTG TCC ACG AAG GCC CCA AA 3’	50°C for 2 mins 95°C for 2 mins 40 x 95°C for 15s 51°C for 15s 72°C for 1 min 95°C for 15s 60°C for 1 min 95°C for 15s
Tnfsf11a	Forward: 5’ TGC CTA CAG CAT GGG CTT T 3’ Reverse: 5’ AGA GAT GAA CGT GGA GTT ACT GTT T 3’	50°C for 2 mins 95°C for 2 mins 40 x 95°C for 15s 50°C for 15s 72°C for 1 min 95°C for 15s 60°C for 1 min 95°C for 15s

B2m	Forward: 5‘ CAG CAA GGA CTG GTC TTT CTA TAT CCT GGC 3’ Reverse: 5‘ TCT CGA TCC CAG TAG ACG GTC TTG GG 3‘	50°C for 2 mins 95°C for 2 mins 40 x 95°C for 15s 50-58°C for 15s (depending on what other primers were being used) 72°C for 1 min 95°C for 15s 60°C for 1 min 95°C for 15s

Table 2-8: PCR primer sequences and cycles used for Fcgr mRNA expression in BMDCs.

Acquisition was conducted using the ABI 7900HT fast real-time PCR system (Applied Biosystems). Relative abundance of gene expression was calculated using *B2m* mRNA as an endogenous control, and the formula: relative abundance = $2^{(-\Delta Ct)}$.

2.2.8.3 OsteoLyse assay

The OsteoLyse assay kit allows for the measurement of collagen degradation by osteoclasts. The OsteoLyse plate contains wells which are coated with Europium labelled collagen. As the osteoclasts differentiate and become resorptive, they will degrade the underlying collagen. This leads to the release of Europium labelled collagen fragments into the media. The media can be harvested and the amount of collagen in the media can be measured on a plate reader.

On days 6 and 11 of osteoclast culture (see Section 2.2.2.6 for culture details), 20 µl cell-free supernatant was removed from the wells of WT and *Ptpn22*$^{-/-}$ bone marrow cells grown in the presence of M-CSF only, or M-CSF and RANK-L, on an OsteoLyse plate (Lonza). Supernatants were stored at -20°C before use.

To carry out the OsteoLyse assay, 10 µl cell-free supernatant was added per well of a black 96 well flat bottom assay plate (Corning). 200 µl room temperature Fluorophore Releasing Reagent (Lonza) was added per well and the plate was rotated for 5 minutes at room temperature to mix. The fluorescence of each well was determined using an excitation of 340 nm and an emission of 615 nm, using a Victor Wallac plate reader (Perkin Elmer).

2.2.9 K/BxN serum transfer model of arthritis

The K/BxN serum transfer model is described in Kouskoff V et al., 1996[178]. The model can be established in a wide range of mouse strains, and is initiated by the transfer of arthritogenic serum containing IgG1 autoantibodies to glucose-6-phosphate isomerase (GPI). The arthritogenic serum is harvested from K/BxN mice, which express the KRN TCR transgene and the MHCII I-A^{g7} and develop spontaneous disease. The KRN TCR transgene recognises a peptide from the bovine pancreas ribonuclease when presented in MHCII I-A^{k} and also a peptide of GPI when presented in MHCII I-A^{g7}. The K/BxN model is similar to human RA in that they both show symmetrical distribution and a chronic progressive disease with joint destruction.

2.2.9.1 Arthritogenic serum collection and anti-GPI ELISA

Mice expressing the KRN TCR transgene were bred to NOD mice, which express I-A^{g7}. The offspring of this cross (K/BxN mice) spontaneously develop arthritis at 4-6 weeks of age. At 8 weeks of age, cardiac punctures (under anaesthetic) were performed on arthritic mice. The arthritogenic serum, containing autoantibodies to GPI was pooled, aliquoted and stored at -80°C before use (Figure 2-20).

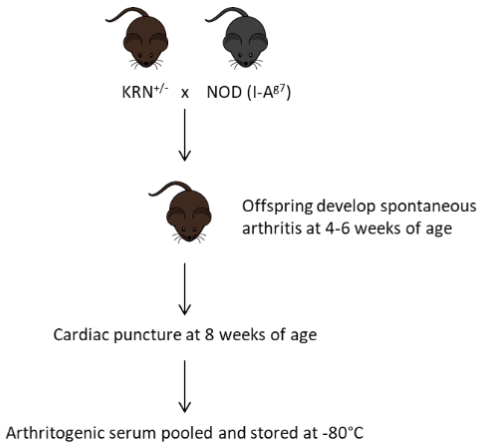

Figure 2-20: Schematic showing production of arthritogenic serum for the K/BxN serum transfer model of arthritis.

Male mice expressing the KRN transgene are bred with female NOD mice expressing I-A^{g7}. Offspring from this cross develop spontaneous arthritis between 4-6 weeks of age. Cardiac punctures are performed on arthritic mice at 8 weeks of age. The blood is centrifuged and the arthritogenic serum is pooled and stored at -80°C. This serum can be used to induce arthritis in recipient mice.

To ensure that the arthritogenic serum contained autoantibodies to GPI, an ELISA was performed, comparing the anti-GPI levels in different batches of serum. A 96 well flat bottom plate (Thermo Fisher Scientific) was coated overnight at 4°C with 50 µl 5 µg/ml recombinant human glucose-6-phosphate isomerase (GPI, RayBiotech). The following day, the wells were washed three times with wash buffer (0.05% Tween in PBS). Wells were then blocked with 250 µl ELISA block buffer (1% BSA in PBS) for 30 minutes at room temperature, and washed three times with wash buffer. 50 µl serum samples (diluted 1:2700, 1:5400, 1:21600 and 1:86400 with PBS) were added to the wells and incubated for 1 hour at room temperature. Wells were washed 3 times with wash buffer and 50 µl alkaline phosphatase-conjugated F(ab')2 goat anti-mouse IgG (1:2000 in PBS, Jackson ImmunoResearch) added per well for 30 minutes at room temperature. The wells were washed 3 times with wash buffer and 100 µl phosphatase substrate was added per well and incubated for 10 minutes at room temperature, before measuring the absorbance at 405 nm on a Victor Wallac plate reader (Perkin Elmer).

2.2.9.2 Establishing disease using the K/BxN serum transfer model of arthritis

Arthritogenic serum was diluted 1:1 with PBS and 150 µl was injected (i.p.) into WT, *Ptpn22*$^{-/-}$, *Ptpn22*^{R619} and *Ptpn22*^{R619W} mice on days 0 and 2. Mice receiving PBS were used as controls. Disease progression was monitored daily for 10 days by assigning clinical scores to each limb, using a scale of 0-3 per paw, where 0 = no reddening or swelling, 1 = slight swelling and/or reddening, 2 = pronounced swelling, 3 = pronounced swelling leading to joint stiffness (maximum per mouse = 12). Paw swelling was also measured using calipers (Kroeplin) and mice were weighed (Figure 2-21 and 2-22).

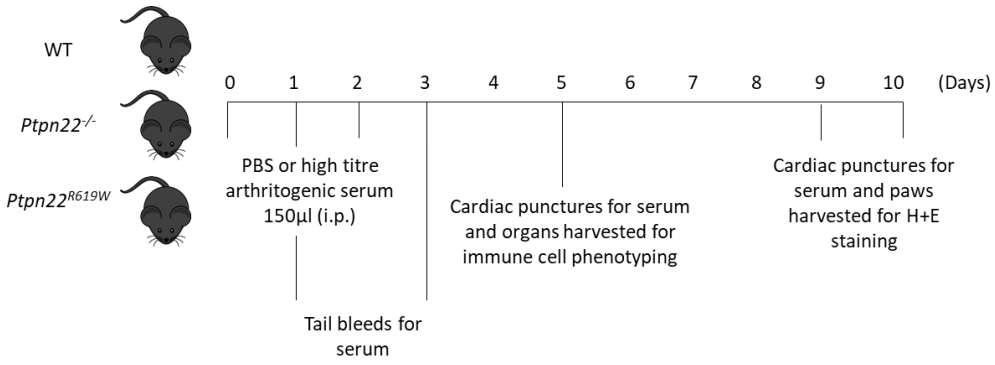

Figure 2-21: Schematic showing the K/BxN serum transfer model of arthritis.

WT, Ptpn22$^{-/-}$ and Ptpn22^{R619W} mice were injected (i.p) with 150 µl PBS or arthritogenic serum (diluted 1:1 with PBS) on days 0 and 2. Tail bleeds for serum were performed on days 1 and 3. At the peak of disease (on day 5), LNs, spleens and joints were harvested for immune cell phenotyping. Cardiac punctures were performed on days 5, 9 and 10 for serum. Paws were harvested on days 9 and 10 for histology. Mice were monitored daily by assigning clinical scores, taking paw caliper measurements and taken their weights.

Figure 2-22: Example photos showing paws of WT healthy and arthritic mice on day 6 of the K/BxN serum transfer model of arthritis.

2.2.9.3 Serum collection from healthy and arthritic mice

Tail bleeds were performed on days 1 and 3 of the model, or cardiac punctures (under anaesthetic) were performed on days 5 and 9 (at the end of the experiments) from WT and *Ptpn22*$^{-/-}$ mice who had received arthritogenic serum or PBS. Blood was transferred to 1.5 ml tubes, allowed to clot at room temperature for at least 30 minutes, centrifuged for 20 minutes at room temperature and 13,500 rpm and the serum was transferred to new tubes and stored at -80°C.

2.2.9.4 Analysis of serum cytokines and chemokines

Serum cytokines and chemokines were measured using a LEGENDplex mouse proinflammatory chemokine panel and a LEGENDplex mouse inflammation panel, each of which could identify 13 analytes (both from BioLegend). These are bead based immunoassays in which differentially sized and fluorescent beads are bound to antibodies specific for each analyte. These act as capture beads for the analytes present in the samples. A biotinylated detection antibody cocktail is then added, which contains antibodies specific for each analyte bound to a capture antibody on the beads. Finally, streptavidin-PE is added, which will bind to the biotinylated detection antibodies, which allows for fluorescent detection of each analyte, proportional to the amount of analyte present in the original sample. This fluorescence can be detected using flow cytometry.

The assays were carried out as per the manufacturer's instructions. Serum samples were thawed, vortexed for 5 seconds and centrifuged for 2 mins and 4°C at 13,500 rpm, before being diluted 1:1 with assay buffer. The top standard was reconstituted and serially diluted 1:4 to create the standards. 25 µl diluted samples and standards were loaded onto a 96 well V bottom plate in duplicate. Beads were vortexed and 25 µl was added to each well and the plate was rotated for 2 hours at room temperature at 800 rpm. The plate was centrifuged for 5 minutes at 1050 rpm and the supernatant was flicked out. The beads were washed with wash buffer and centrifuged as above. 25 µl detection antibodies were added to each well and the plate was rotated for 1 hour at room temperature at 800 rpm. 25 µl streptavidin-PE was added to each well and the plate was rotated for 30 minutes at room temperature at 800 rpm. The plate was centrifuged for 5 minutes at 1050 rpm and the supernatant was removed. The beads were washed with wash buffer and transferred to microFACS tubes, before being collected by flow cytometry. Cytokine and chemokine serum concentrations were determined using standard curves for each analyte.

2.2.9.5 Hematoxylin and eosin staining of joint sections

Hematoxylin and eosin staining is a histological stain which allows for the visualisation of joint architecture and cell infiltration. Hematoxylin in combination with a metal cation (for example aluminium ions) is positively charged and can interact with negatively charged, acidic cell components including nucleic acids. This results in purple/blue nuclei, ribosomes and the rough endoplasmic reticulum. Eosin is acidic and negatively charged and can therefore react with

positively charged, basic parts of the tissue, such as amino groups in proteins in the cytoplasm, which become pink/red. As a result, different immune cells can be identified using this staining technique.

On day 9 or 10 of the K/BxN serum transfer model of arthritis, WT, *Ptpn22*$^{-/-}$, *Ptpn22*^{R619} and *Ptpn22*^{R619W} mice were culled and hind paws were removed and fixed in formalin. 1-2 weeks later, fixed paws were transferred to tubes containing PBS and sent to Pathology Core Facilities at either Imperial College London or Queen Mary University London. Here the paws were decalcified over a period of 2 weeks, using EDTA, embedded into paraffin blocks, sectioned along the sagittal plane of the ankle joint, and stained using hematoxylin and eosin. Joints were scored in a blinded fashion using a light microscope by Professor Andrew Cope (King's College London) using a scale of 0-3 for cell infiltration and joint erosion.

2.2.9.6 Immunophenotyping of joints and joint draining LNs

At day 5 of the K/BxN serum transfer model of arthritis WT and *Ptpn22*$^{-/-}$ mice were culled and spleens, popliteal dLNs, brachial/axiallary dLNs, wrist and ankle joints were removed. Joints were only removed if they were visibly arthritic. If two wrists (or two ankles) of a mouse were both similarly arthritic, these were combined into one sample. If only one ankle (or one wrist) was arthritic, then this joint was processed individually. Tissue from ankle and wrists joints were not combined. As each joint sample was from a different amount of tissue, I did not calculate the absolute cell numbers for each of the immune cell populations. To process the joints, they were first cut into small pieces, before being digested in 1ml RPMI-1640 containing DNase I and Liberase TL (both at 0.1mg/ml, Roche) for 2 hours at 37°C in 5% CO_2; 10 mM EDTA was added for the final 5 minutes. Single cell suspensions were made by mashing the joint pieces and released cells through gauze. All the recovered cells were then transferred into FACS tubes, washed in PBS and centrifuged for 5 minutes at 4°C and 1600 rpm, and stained as described below.

To process lymph nodes and spleens, the lymph nodes were first disrupted using 26G needles and then both lymph nodes and spleens were digested in 1 ml RPMI-1640, containing DNase I and Liberase TL (both at 0.1mg/ml, Roche) for 30 minutes at 37°C in 5% CO_2; 10 mM EDTA was added for the final 5 minutes. Single cell suspensions were obtained by mashing the digested organs through gauze. Splenocyte cell suspensions were resuspended in 2 ml red blood cell lysis buffer (BioLegend) for 5 minutes at room temperature, washed in PBS and centrifuged for 5 minutes 4°C and 1600 rpm. Splenocytes were counted and 5 x 10^6 were added per FACS tube.

Lymphocyte cell suspensions were transferred into FACS tubes, counted, washed in PBS and centrifuged for 5 minutes at 4°C and 1600 rpm. Cells were then stained as described below.

For staining, cells were blocked with a non-fluorescent FcγRII/III antibody (BioLegend) and stained with 100 µl per tube of an antibody cocktail containing anti-Ter119, anti-CD19, anti-B220, anti-NK1.1, anti-MHCII I-A^b, anti-CD11b, anti-CD11c, anti-Ly6G, anti-Ly6C, anti-CD3, anti-CD4, anti-CD8 (all from BioLegend) and a fixable viability dye (eBioscience) in PBS for 30 minutes at 4°C. Cells were washed with FACS buffer and stained with 100 µl per tube streptavidin in FACS buffer for 10 minutes at room temperature. Finally, cells were washed with FACS buffer and fixed using 1% PFA in PBS containing 5 x 10^4 counting beads (BioLegend), prior to flow cytometry. Cell were first gated on live, lineage$^-$ (to exclude Ter119$^+$, CD19$^+$, B220$^+$ and NK1.1$^+$ cells) singlets and then the following cell subsets were identified: Ly6C$^{lo\ to\ med}$ monocytes (CD11c$^-$ Ly6C$^{low\ to\ med}$, SSC-A^{lo}), Ly6C^{hi} monocytes (CD11c$^-$, Ly6C^{hi}, SSC-A^{lo}), neutrophils (CD11c$^-$, CD11b$^+$, Ly6G$^+$), CD4$^+$ T cells (CD3$^+$, CD4$^+$), CD8$^+$ T cells (CD3$^+$, CD8$^+$), conventional DCs (cDCs, CD11c$^+$, MHCII$^+$), cDC1s (CD11c$^+$, MHCII$^+$, CD8$^+$) and cDC2s (CD11c$^+$, MHCII$^+$, CD11b$^+$) (Figure 2-23).

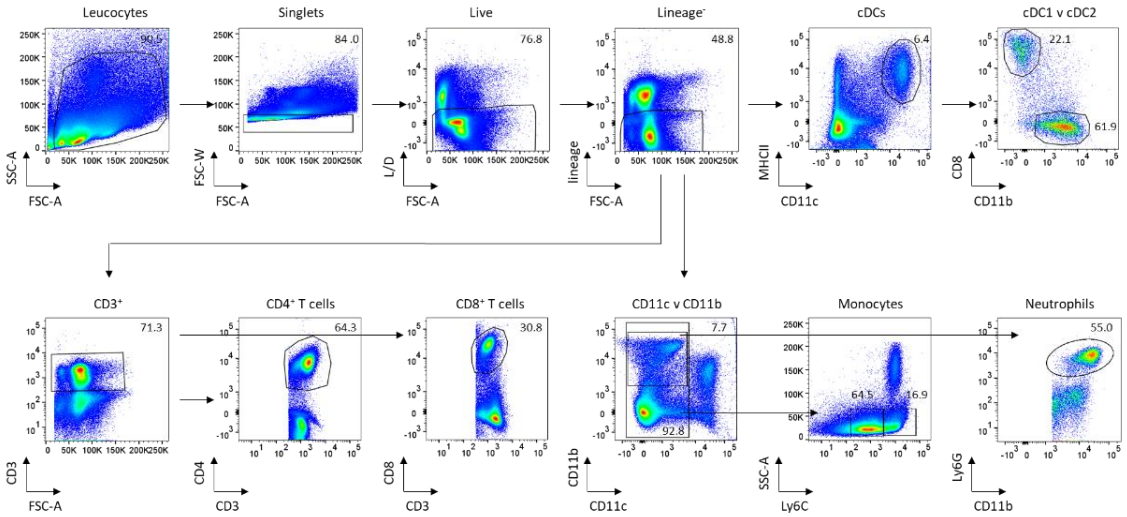

Figure 2-23: Flow cytometry plots showing example gating for K/BxN immune cell phenotyping at the peak of disease (day 5).

Single cell suspensions were made from spleens, lymph nodes and joints of WT and Ptpn22$^{-/-}$ mice on day 5 of the K/BxN serum transfer model of arthritis. Cells were stained with antibodies for detection of immune cell subsets by flow cytometry. Cell were first gated on live, lineage- (to exclude Ter119$^+$, CD19$^+$, B220$^+$ and NK1.1$^+$ cells) singlets and then the following cell subsets were identified: Ly6C$^{lo\ to\ med}$ monocytes (CD11c$^-$ Ly6C$^{low\ to\ med}$, SSC-A^{lo}), Ly6C^{hi} monocytes (CD11c$^-$, Ly6C^{hi}, SSC-A^{lo}), neutrophils (CD11c$^-$, CD11b$^+$, Ly6G$^+$), CD4$^+$ T cells (CD3$^+$, CD4$^+$), CD8$^+$ T cells (CD3$^+$, CD8$^+$), conventional DCs (cDCs, CD11c$^+$, MHCII$^+$), cDC1s (CD11c$^+$, MHCII$^+$, CD8$^+$) and cDC2s (CD11c$^+$, MHCII$^+$, CD11b$^+$).

2.2.9.7 Micro-computed tomography analysis

Leg bones were removed from WT and *Ptpn22*$^{-/-}$ mice on day 10 of the K/BxN serum transfer model of arthritis. Bones were fixed overnight at room temperature in 4% PFA in PBS and then transferred to 70% ethanol the following day. Bones were shipped to the lab of Dr Nicole Horwood (University of Oxford) where micro-computed tomography (micro-CT) analysis was carried out. Bones were scanned using a Skyscan 1174 scanner (Bruker) and images were analysed using Skyscan CT analyser software version 1.13.2.1.

2.2.9.8 Positron emission tomography/computed tomography (PET/CT imaging of arthritic mice using the radiotracer $^{68}Ga(HP_3\text{-}RGD_3)$

In order to visualise areas of inflammation in whole mice, we utilised a Galium-68 labelled RGD trimeric peptide ($^{68}Ga(HP_3\text{-}RGD_3)$). The RGD (arginine-glycine-aspartic acid) peptide, found in multiple extracellular matrix proteins binds to the integrin αvβ3, which is expressed at low levels in the steady state, but is upregulated in areas of angiogenesis and inflammation. Radiolabelling of the RGD trimeric peptide was carried out by Dr Michelle Ma (King's College London). Hydrochloric acid (0.1 M, 5 mls) was passed through a $^{68}Ge/^{68}Ga$ generator (Eckert and Ziegler) and the eluate was fractionated into 1 ml fractions. The second 1 ml fraction was added to $HP_3\text{-}RGD_3$ in a 1:1 ethanol:water solution (50-100 µl), immediately followed by ammonium acetate (1 M, 300 µl). High performance liquid chromatography was used to determine the labelling efficiency.

The K/BxN serum transfer model of arthritis was established in WT and *Ptpn22*$^{-/-}$ mice, and on day 6 the mice were injected (i.v.) with 4 µg $^{68}Ga(HP_3\text{-}RGD_3)$, containing 8-14 Mbq (under anaesthetic). One hour post injection, mice were either culled and imaged dead, or mounted onto the nanoScan PET/CT bed (Mediso Medical Imaging Systems) set at 37°C with continuous anaesthetic. PET images were collected for 15 minutes, followed by a CT image (to gain anatomical information). After imaging (or using separate mice), mice were culled and organs were collected for biodistribution. All organ collection tubes were weighed before and after adding the organ, so that the weight of each organ could be calculated. The radioactivity of each organ was determined using a gamma counter. These experiments were carried out with Dr Samantha Terry and Dr Michelle Ma (King's College London) (Figure 2-24).

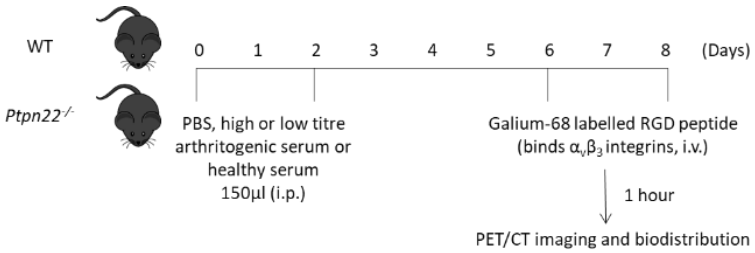

Figure 2-24: Schematic showing induction and experimentation of PET/CT and biodistribution analysis of arthritis in WT and Ptpn22$^{-/-}$ mice using the K/BxN serum transfer model of arthritis.

WT and Ptpn22$^{-/-}$ mice were injected (i.p) with 150 µl PBS or high titre arthritogenic serum (diluted 1:1 with PBS) or low titre arthritogenic serum (diluted 1:8 with PBS on days 0 and 2. On day 6 or 8, mice were injected (i.v.) with gallium-68 labelled RGD peptide. 1 hour later, mice were culled and imaged using PET/CT and organs were harvested for biodistribution. Mice were monitored daily by assigning clinical scores, taking paw caliper measurements and taken their weights.

2.2.10 Data acquisition and analysis

Flow cytometry samples were acquired using a Fortessa II or FACSCanto II with FACS Diva software (all from BD). Data were analysed using FlowJo software version 10 (TreeStar). Gates were determined by fluorescence minus one (FMO) controls. All graphs were plotted using Prism version 7 (GraphPad) and analysed for statistical significance using a 2-way ANOVA followed by Sidak's or Tukey's multiple comparisons test, Wilcoxon matched-pairs signed ranks test, or paired or unpaired t-tests. $p<0.05$ was deemed statistically significant.

3. Results: Investigating the regulation of immune complex induced DC effector functions by PTPN22

3.1 Introduction

PTPN22 is a non-receptor protein tyrosine phosphatase which regulates signalling downstream of a range of immunoreceptors, generally via its ability to dephosphorylate Src and Syk family kinases[237]. DCs (DCs) express a range of pattern recognition receptors (PRRs) including Toll-like receptors (TLRs), C-type lectin receptors (CLRs), nucleotide oligomerisation domain (NOD)-like receptors (NLRs), retinoic acid-inducible gene I (RIG-I)-like receptors (RLRs) and Fc gamma receptors (FcγRs), and use these to bind and internalise soluble and particulate matter from their surroundings[238]. FcγRs are expressed on most innate immune cells and recognise the Fc region of IgG immunoglobulins. These can be as part of an antibody:antigen immune complex or as part of an opsonised particle, and engagement of these with FcγRs leads to receptor crosslinking and downstream signalling involving Src and Syk family kinases. This ultimately leads to a variety of cellular processes including immune complex internalisation, antigen processing and presentation, antibody-dependent cellular cytotoxicity (ADCC), cytokine and chemokine secretion, cell maturation and release of reactive oxygen species (ROS)[125]; all of which shape the immune response. As polymorphisms in PTPN22 are associated with autoimmune diseases, and the majority of the associated diseases have an autoantibody component to their pathology, the experiments described in this Chapter set out to investigate whether PTPN22 regulates DC effector responses after FcγR engagement. Firstly, I compared immune complex induced effector functions in WT and *Ptpn22*$^{-/-}$ bone marrow derived DCs (BMDCs), including DC upregulation of co-stimulatory molecules, cytokine secretion and T cell activation. BMDCs from mice expressing the autoimmune associated variant of *Ptpn22* (*Ptpn22*^{R619W}) were then studied, to investigate whether FcR stimulation was dysregulated by the autoimmune associated variant of PTPN22 (PTPN22^{R620W}). Finally, the role of PTPN22 in antigen processing and presentation *in vivo* was investigated.

3.2 Aims

This Chapter aimed to determine whether PTPN22 is required for:

1. BMDC differentiation and FcγR expression.
2. Immune complex induced BMDC maturation.
3. Immune complex induced T cell proliferation *in vitro* and *in vivo.*

3.3 Results

3.3.1 PTPN22 does not regulate BMDC differentiation *in vitro*

As BMDCs have been extensively used throughout this thesis, I first wanted to ascertain whether PTPN22 affected differentiation of BMDCs from bone marrow. Wild type (WT) and *Ptpn22*$^{-/-}$ bone marrow was cultured in the presence of granulocyte-macrophage colony stimulating factor (GM-CSF) for 7 days and flow cytometry was used to identify the proportion of the cultures that had differentiated into CD11c^{+} DCs. This was found to be similar in the presence or absence of PTPN22 (Figure 3-1b). As GM-CSF induced BMDC cultures do not form a homogenous population, additional analysis was carried out to distinguish between cells which were more DC-like (GM-DCs, identified as CD11c^{+}, MHCII^{hi}, CD11b^{+} live singlets) and macrophage-like (GM-macs, identified as CD11c^{+}, MHCII^{int}, CD11b^{hi} live singlets), based on gating by Helft J. *et al*[234]. Verification of these distinct populations was also achieved by measuring the expression of DC and macrophage specific cell surface markers including CD24 and CD64 respectively (Figure 3-1d). The proportions of both GM-DCs and GM-macs were similar in WT and *Ptpn22*$^{-/-}$ bone marrow cultures (Figure 3-1b), indicating that PTPN22 does not regulate bone marrow differentiation into BMDCs in the presence of GM-CSF *in vitro*.

Bone marrow differentiation was also assessed from mice expressing the orthologue of the human associated variant of *Ptpn22* (*Ptpn22*^{R619W}). As with the *Ptpn22*$^{-/-}$ cultures, *Ptpn22*^{R619W} bone marrow cultures differentiated similarly to *Ptpn22*^{R619} (WT) cultures (Figure 3-1c).

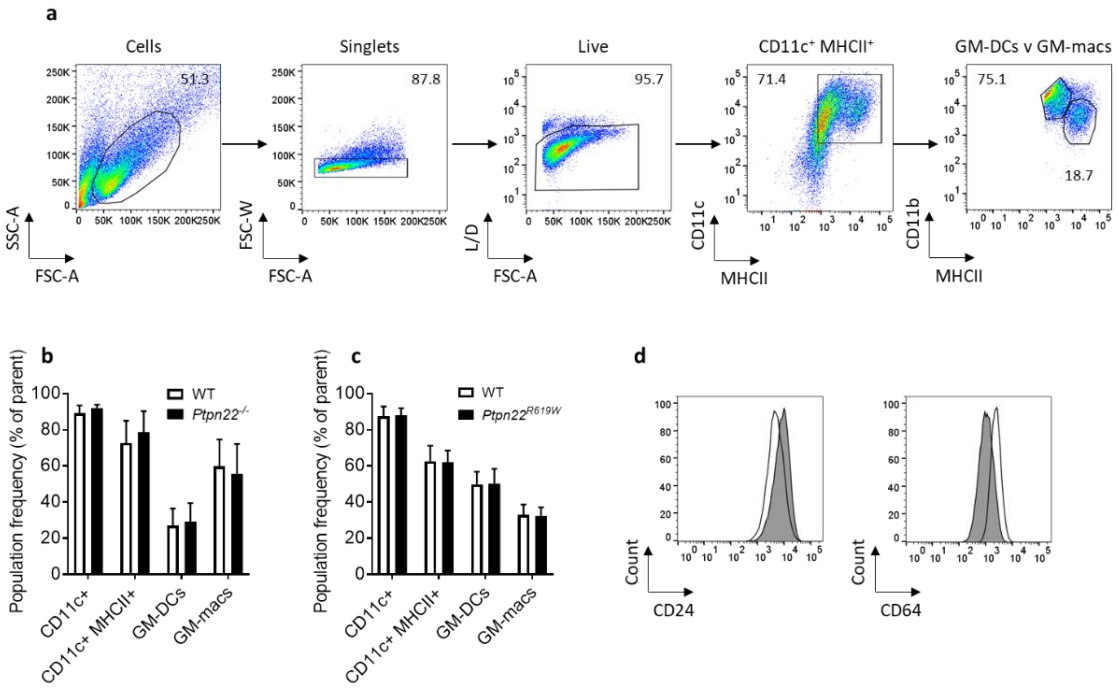

Figure 3-1: PTPN22 does not affect BMDC differentiation in vitro.

(a-d) Bone marrow from WT (white) and Ptpn22$^{-/-}$ (black) (a-b) or Ptpn22^{R619} (WT, white) and Ptpn22^{R619W} (black) (c) mice was cultured in the presence of GM-CSF for 7 days. Cells were stained to identify CD11c^{+} cells, CD11c^{+} MHCII^{+} cells, CD11c^{+} MHCII^{hi} CD11b^{+} (GM-DCs) and CD11c^{+} MHCII^{int} CD11b^{hi} (GM-macs), all gated on live singlets. Representative flow cytometry plots (a) and combined data (b-c) are shown. n = 6-7 $\pm$ s.d. (d) Representative flow cytometry plots of CD24 (left, GM-DC marker) and CD64 (right, GM-mac marker), gated on CD11c^{+} MHCII^{hi} CD11b^{+} (GM-DCs, grey) and CD11c^{+} MHCII^{int} CD11b^{hi} (GM-macs, white) live singlets.

These observations show that PTPN22 does not modulate BMDC differentiation *in vitro*, which indicated that any differences found in the response of WT and *Ptpn22*$^{-/-}$ BMDCs in subsequent experiments is not due to any initial differences in their differentiation.

3.3.2 *Ptpn22*$^{-/-}$ BMDCs express normal levels of activating FcγRs, but reduced expression of the inhibitory receptor FcγRIIb

Four FcγRs are expressed in mice: FcγRI, FcγRIIb, FcγRIII and FcγRIV[126]. Before beginning to investigate a potential role of PTPN22 in regulating FcγR dependent effector responses in DCs, BMDC cell surface expression of FcγRs was measured. Cell surface expression of the activating receptors FcγRI, FcγRIII and FcγRIV was similar on WT and *Ptpn22*$^{-/-}$ BMDCs (as judged by % positive and geometric mean fluorescence intensity, GMFI), however *Ptpn22*$^{-/-}$ BMDCs were found to have reduced expression of the inhibitory FcγRIIb on their cell surface (Figure 3-2a),

while the proportion of WT and *Ptpn22*$^{-/-}$ BMDCs expressing FcγRIIb was similar (Figure 3-2b). Expression of the autoimmune associated variant of *Ptpn22* (*Ptpn22*^{R619W}) did not affect BMDC FcγR expression (Figure 3-2c). Despite the reduced expression of FcγRIIb on *Ptpn22*$^{-/-}$ BMDCs, when WT and *Ptpn22*$^{-/-}$ BMDCs were matured with LPS, their FcγR expression was found to be similar (Figure 3-2d).

To identify at what point during DC differentiation the difference in FcγRIIb expression occurred, bone marrow from WT and *Ptpn22*$^{-/-}$ mice was harvested and stained to identify common DC progenitors (CDPs) and preDCs. FcγRIIb expression was similar on WT and *Ptpn22*$^{-/-}$ CDPs and preDCs (Figure 3-2e), indicating that PTPN22 may regulate FcγRIIb expression at a later stage of DC development.

To investigate this further, WT and *Ptpn22*$^{-/-}$ BMDCs were lysed, mRNA was extracted, cDNA was reverse transcribed, and expression of *Fcgr1*, *Fcgr2b* and *Fcgr3* was determined using qRT-PCR. Expression of these genes was found to be similar between WT and *Ptpn22*$^{-/-}$ BMDCs (Figure 3-2f), indicating that the difference in cell surface expression of FcγRIIb between WT and *Ptpn22*$^{-/-}$ BMDCs was not due to differences in *Fcgr2b* gene expression.

Expression of FcγRs was also measured on conventional DCs derived from the spleens of WT, *Ptpn22*$^{-/-}$ and *Ptpn22*^{R619W} mice. As with the BMDCs, splenic DCs from the different genotypes of mice expressed similar levels of the activating receptors (Figure 3-2g-h). Although there was a trend in some experiments towards reduced expression of FcγRIIb on *Ptpn22*$^{-/-}$ splenic DCs compared to WT splenic DCs, overall, the difference was not significant (Figure 3-2g). Similar FcγR expression was also seen on splenic DCs from *Ptpn22*^{R619} (WT) and *Ptpn22*^{R619W} mice (Figure 3-2h). This indicates that PTPN22 does not regulate expression of FcγRs on DCs *in vivo*.

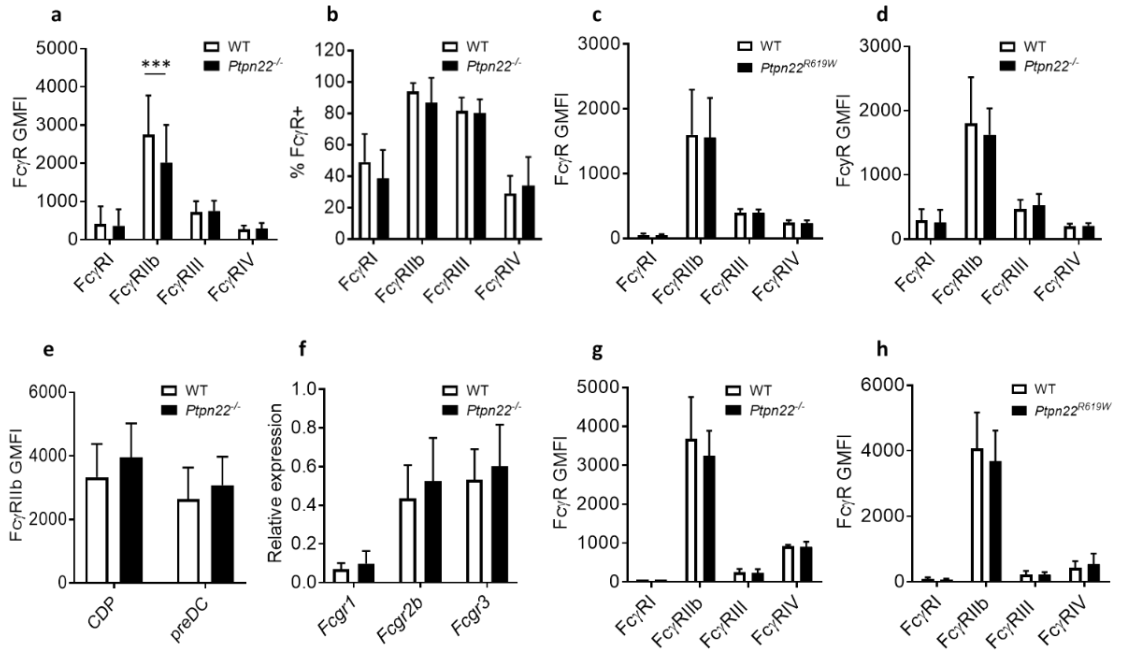

Figure 3-2: Ptpn22$^{-/-}$ BMDCs express normal levels of activating FcγRs, but reduced expression of the inhibitory receptor FcγRIIb.

*(a) FcγR surface expression on WT (white) and Ptpn22$^{-/-}$ (black) BMDCs (geometric mean fluorescence intensity, GMFI, gated on CD11c^{+} live singlets). n = 16-18 ± s.d; ***p<0.005 using a 2-way ANOVA with Sidak's multiple comparisons test. (b) FcγR surface expression on WT (white) and Ptpn22$^{-/-}$ (black) BMDCs (% positive, gated on CD11c^{+} live singlets). n = 10 ± s.d. (c) FcγR surface expression on Ptpn22^{R619} (WT, white) and Ptpn22^{R619W} (black) BMDCs (GMFI, gated on CD11c^{+} live singlets). n = 7 ± s.d. (d) FcγR surface expression on WT (white) and Ptpn22$^{-/-}$ (black) LPS matured BMDCs (GMFI, gated on CD11c^{+} live singlets). n = 4 ± s.d. (e) FcγRIIb surface expression on WT (white) and Ptpn22$^{-/-}$ (black) CDPs and preDCs (GMFI, gated on CD115^{+}, cKit^{-}, Flt3^{+} live singlets for CDPs and CD11c^{+}, MHCII^{-}, SIRPα^{low}, Flt3^{+} live singlets for preDCs). n = 6 ± s.d. (f) Fcgr mRNA expression from WT (white) and Ptpn22$^{-/-}$ (black) BMDCs, relative to 18S. n = 5 ± s.d. (g) FcγR surface expression on WT (white) and Ptpn22$^{-/-}$ (black) splenic DCs (gated on CD11c^{+}, MHCII^{+} live singlets). n = 1 (for FcγRI), 3 (for FcγRIII and IV), 11 (for FcγRIIb) ± s.d. (h) FcγR surface expression on Ptpn22^{R619} (WT, white) and Ptpn22^{R619W} (black) splenic DCs (gated on CD11c^{+}, MHCII^{+} live singlets). n = 5 (for FcγRI), 8 (for FcγRIIb, III and IV) ± s.d.*

3.3.3 PTPN22 does not regulate FcγR expression on bone marrow neutrophils

In addition to DCs, most other innate immune cells also express FcγRs. Bone marrow neutrophils from WT, *Ptpn22$^{-/-}$* and *Ptpn22^{R619W}* mice were analysed to determine their FcγR expression. This was found to be similar between the different genotypes (Figure 3-3a-b), indicating that PTPN22 does not regulate FcγR expression on bone marrow neutrophils.

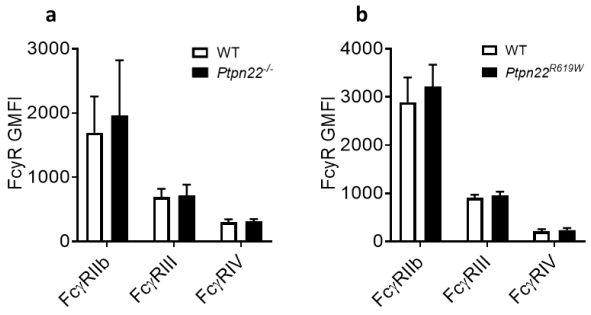

Figure 3-3: Ptpn22$^{-/-}$ and Ptpn22^{R619W} neutrophils express normal levels of FcγRs.

(a) FcγR surface expression on WT (white) and Ptpn22$^{-/-}$ (black) bone marrow neutrophils (geometric mean fluorescence intensity, GMFI, gated on CD11b^{+}, Ly6G^{+} live singlets). n = 10 ± s.d. (b) FcγR surface expression on Ptpn22^{R619} (WT, white) and Ptpn22^{R619W} (black) bone marrow neutrophils (GMFI, gated on CD11b^{+}, Ly6G^{+} live singlets). n = 8 ± s.d.

3.3.4 PTPN22 is dispensable for FcγR induced BMDC maturation

Immune complex crosslinking of FcγRs causes BMDC maturation, which leads to increased cell surface expression of the major histocompatibility complex class II (MHCII) and co-stimulatory molecules including CD54, CD80 and CD86; expression of which can affect T cell activation[166]. WT and *Ptpn22$^{-/-}$* BMDCs were incubated with ovalbumin (ova), rabbit anti-ova (anti-ova), ova pre-incubated with rabbit IgG (ova + rabbit IgG, and produced as per an immune complex), ova and heat aggregated (HA) rabbit IgG (ova + HA IgG) and ova:anti-ova immune complexes (ova ICs) for 24 hours at 37°C, 5% CO_2. After 24 hours, BMDCs were harvested and stained for cell surface expression of MHCII and co-stimulatory molecules (see Materials and Methods Figure 2-4 for experimental setup). Expression of these molecules was unchanged from unstimulated conditions after incubation with ova, anti-ova, ova pre-incubated with rabbit IgG, and ova added in combination with HA IgG (Figure 3-4a-f). Only incubation with ova ICs caused BMDC maturation, as determined by a moderate increase in CD54, CD80 and CD86 expression (Figure 3-4a-f). This indicates that the addition of an antigen and antibody is insufficient to induce BMDC maturation, but that it requires the presence of an antigen:antibody immune complex. The response to ova IC stimulation between WT and *Ptpn22$^{-/-}$* BMDCs was similar (Figure 3-4a-f), indicating that PTPN22 is dispensable for this process.

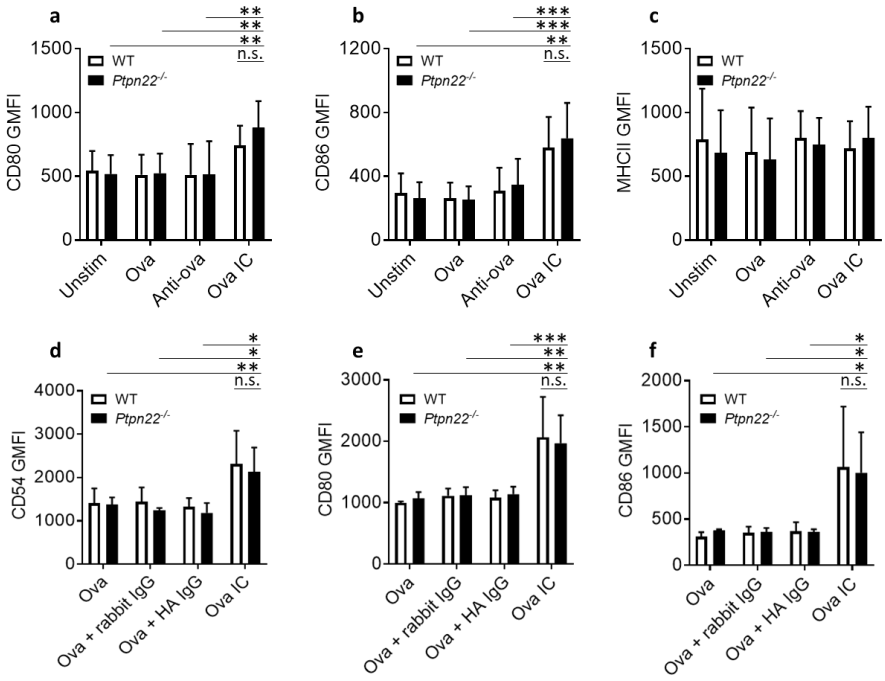

Figure 3-4: PTPN22 does not regulate immune complex induced maturation of BMDCs.

*(a-c) WT and Ptpn22$^{-/-}$ BMDCs were stimulated in the presence of ova, anti-ova or ova IC. After 24 hours, BMDCs were harvested and surface stained for CD80, CD86 and MHCII. WT (white) and Ptpn22$^{-/-}$ (black) BMDC cell surface expression (geometric mean fluorescence intensity, GMFI, gated on CD11c^{+} live singlets) of CD80 (a), CD86 (b) and MHCII (c). n = 6-8 ± s.d. ***p<0.005, **p<0.01 using a 2-way ANOVA with Tukey's multiple comparisons test. All WT v Ptpn22$^{-/-}$ comparisons were non-significant (n.s.). Bars on graphs only show comparisons of ova IC v unstim/ova/anti-ova for Ptpn22$^{-/-}$ BMDCs (for simplicity). (d-f) WT and Ptpn22$^{-/-}$ BMDCs were stimulated in the presence of ova, ova pre-incubated with rabbit IgG (ova + rabbit IgG), ova with heat aggregated IgG (ova + HA IgG), or ova IC. After 18 hours, BMDCs were harvested and surface stained for CD54, CD80 and CD86. GMFI (gated on CD11c^{+} live singlets) are shown for WT (white) and Ptpn22$^{-/-}$ (black) BMDC CD54 (d), CD80 (e) and CD86 (f) expression. n = 4 ± s.d. ***p<0.005, **p<0.01, *p<0.05 using a 2-way ANOVA with Tukey's multiple comparisons test. All WT v Ptpn22$^{-/-}$ comparisons were non-significant (n.s.). Bars on graphs only show comparisons of ova IC v ova/ova + rabbit IgG/ova + HA IgG for Ptpn22$^{-/-}$ BMDCs (for simplicity).*

To determine whether expression of the autoimmune associated variant of PTPN22 would affect BMDC maturation in response to immune complex stimulation, *Ptpn22^{R619}* (WT) and *Ptpn22^{R619W}* BMDCs were stimulated with ova ICs for 24 hours (with ova and anti-ova being used as controls). Although immune complex stimulation did cause a subtle increase in CD54 and CD86 expression, the expression was similar between WT and *Ptpn22^{R619W}* BMDCs (Figure 3-5a-c). This indicates that PTPN22 does not regulate expression of co-stimulatory molecules after FcγR crosslinking in BMDCs.

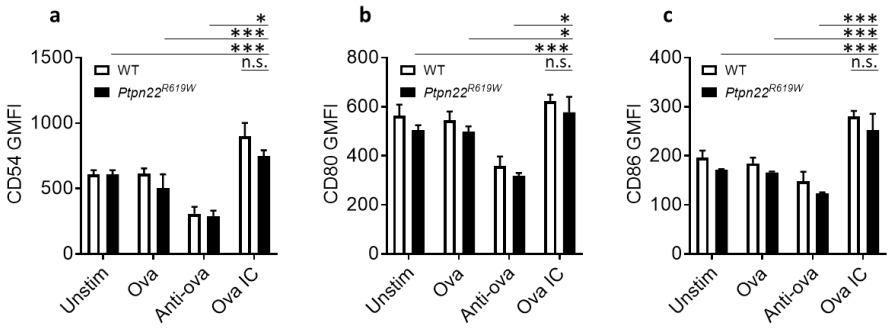

Figure 3-5: PTPN22^{R619W} expression does not affect immune complex induced maturation of BMDCs.

*(a-c) Ptpn22^{R619} (WT) and Ptpn22^{R619W} BMDCs were stimulated in the presence of ova, anti-ova or ova IC. After 24 hours, BMDCs were harvested and surface stained for CD54, CD80 and CD86. (a-c) WT (white) and Ptpn22^{R619W} (black) BMDC cell surface expression (geometric mean fluorescence intensity, GMFI, gated on CD11c^{+} live singlets) of CD54 (a), CD80 (b) and CD86 (c). n = 4 ± s.d. ***p<0.005, *p<0.05 using a 2-way ANOVA with Tukey's multiple comparisons test. All WT v Ptpn22^{R619W} comparisons were non-significant (n.s.). Bars on graphs only show comparisons of ova IC v unstim/ova/anti-ova for Ptpn22^{R619W} BMDCs (for simplicity).*

As GM-CSF induced BMDCs are not equivalent to *in vivo* DCs, I wanted to test whether PTPN22 may be playing a role in FcγR BMDC effector functions in Flt3L induced BMDCs, which are more reflective of *in vivo* DCs. WT and *Ptpn22$^{-/-}$* Flt3L cultures differentiated similarly to produce DC1-like (CD24^{+}) and DC2-like (SIRPα^{+}) DCs (Figure 3-6a). WT and *Ptpn22$^{-/-}$* Flt3L BMDCs were stimulated for 24 hours with ova, ova ICs or LPS and expression of CD54, CD80 and MHCII was determined by flow cytometry. Ova ICs only induced a modest upregulation of these markers, whereas expression was highly upregulated after LPS stimulation. In agreement with the GM-CSF BMDCs, both WT and *Ptpn22$^{-/-}$* Flt3L BMDCs responded similarly to stimulation (Figure 3-6b-c).

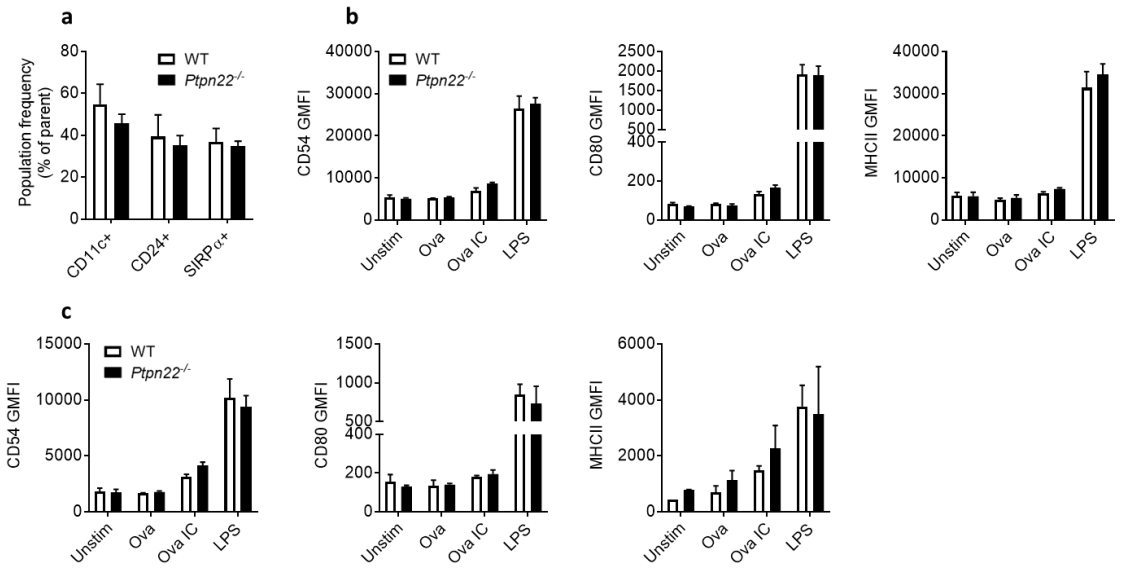

Figure 3-6: PTPN22 is dispensable for Flt3L BMDC differentiation and effector functions.

(a-d) WT (white) and Ptpn22$^{-/-}$ (black) bone marrow cells were grown in the presence of Flt3L for 12-13 days. (a) BMDCs were harvested and stained for immunophenotyping, by gating on CD11c^{+} live singlets, CD11c^{+} CD24^{+} live singlets (DC1-like cells) and CD11c^{+} SIRPα^{+} (DC2-like cells) live singlets. n = 3 ± s.d. (representative of 8 independent experiments). (b-c) BMDCs were stimulated for 24 hours with ova, ova ICs or LPS, harvested and stained for expression of CD54, CD80 and MHCII (gated on CD11c^{+}, CD24^{+} (b) or CD11c^{+}, SIRPα^{+} (c) live singlets). n = 3 ± s.d.

3.3.5 PTPN22 does not regulate immune complex induced maturation of splenic DCs

Splenic DCs from WT and *Ptpn22$^{-/-}$* mice were stimulated *ex vivo* with ova or ova ICs. After 24 hours, cell surface upregulation of CD40, CD54 and CD86 was measured. As with the *in vitro* BMDCs, lack of PTPN22 did not affect expression of these molecules on splenic DCs (Figure 3-7a-c). Taken together, this indicates that PTPN22 does not play a role in modulating splenic DC surface expression of co-stimulatory molecules in response to immune complex stimulation.

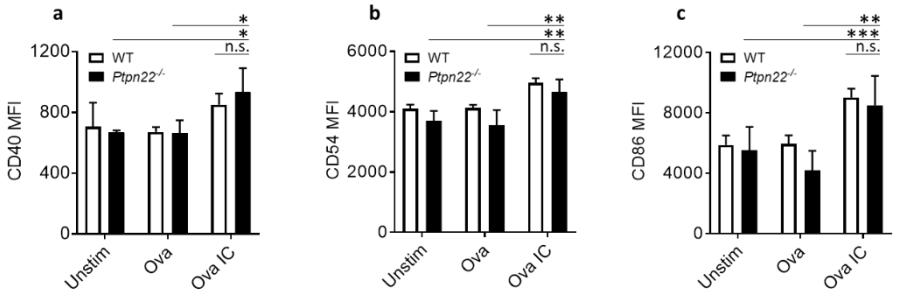

Figure 3-7: PTPN22 does not regulate immune complex induced maturation of splenic DCs.

*(a-c) WT and Ptpn22$^{-/-}$ splenic DCs were stimulated in the presence of ova or ova IC. After 24 hours, splenic DCs were harvested and surface stained for CD40, CD54 and CD86. Data shows WT (white) and Ptpn22$^{-/-}$ (black) splenic DC cell surface expression (mean fluorescence intensity, MFI, gated on CD11c^{+}, MHCII^{+} live singlets) of CD40 (a), CD54 (b) and CD86 (c). n = 4 ± s.d. ***p<0.005, **p<0.01, *p<0.05 using a 2-way ANOVA with Tukey's multiple comparisons test. All WT v Ptpn22$^{-/-}$ comparisons were non-significant (n.s.). Bars on graphs only show comparisons of ova IC v unstim/ova for Ptpn22$^{-/-}$ BMDCs (for simplicity).*

3.3.6 PTPN22 is dispensable for FcγR induced BMDC cytokine secretion

In addition to causing upregulation of MHCII and co-stimulatory molecules, immune complex stimulation also induces the secretion of T cell polarising cytokines by BMDCs[127,239]. To determine whether PTPN22 was required for this process, WT and *Ptpn22$^{-/-}$* BMDCs were harvested, counted and stimulated in the presence of ova, anti-ova or ova ICs for 24 hours at 37°C, 5% CO_2. After 24 hours, supernatants were harvested and the secretion of interleukin-6 (IL-6), tumour necrosis factor α (TNFα) and interleukin-12/23p40 (IL-12/23p40) was measured by immunoassay (see Materials and Methods Figure 2-4 for experimental setup). Ova and anti-ova stimulation caused very low levels of cytokine secretion from both WT and *Ptpn22$^{-/-}$* BMDCs (Figure 3-8a-c). BMDCs stimulated with ova ICs secreted significantly more IL-6, TNFα and IL-12/23p40 compared to BMDCs incubated with ova or anti-ova alone, however, both WT and *Ptpn22$^{-/-}$* BMDCs secreted similar levels of these cytokines in response to immune complex stimulation (Figure 3-8a-c).

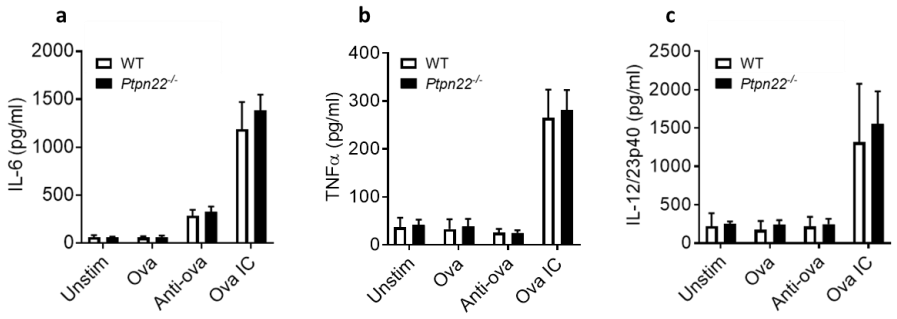

Figure 3-8: PTPN22 is dispensable for BMDC cytokine secretion after immune complex stimulation.

(a-c) WT (white) and Ptpn22$^{-/-}$ (black) BMDCs were stimulated with ova, anti-ova or ova IC, in the presence of polymyxin B. After 24 hours, cell-free supernatants were harvested and secretion of IL-6 (a), TNFα (b) and IL-12/23p40 (c) was determined by immunoassay. n = 3 ± s.d. (representative of 10 independent experiments).

Cytokine secretion was also measured from immune complex stimulated *Ptpn22^{R619}* (WT) and *Ptpn22^{R619W}* BMDCs. Only low levels of IL-6, TNFα and IL-12/23p40 were detected in the supernatants of BMDCs incubated in the presence of ova alone for 24 hours (Figure 3-9a-c). Whilst enhanced cytokine secretion was observed after stimulation with ova ICs, WT and *Ptpn22^{R619W}* BMDCs secreted similar levels (Figure 3-9a-c).

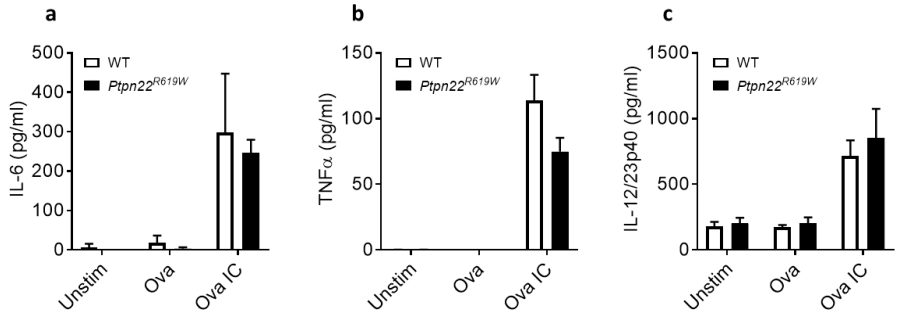

Figure 3-9: Expression of Ptpn22^{R619W} does not affect BMDC cytokine secretion after immune complex stimulation.

(a-c) Ptpn22^{R619} (WT, white) and Ptpn22^{R619W} (black) BMDCs were stimulated with ova or ova IC, in the presence of polymyxin B. After 24 hours, cell-free supernatants were harvested and secretion of IL-6 (a), TNFα (b) and IL-12/23p40 (c) was determined by immunoassay. n = 4 ± s.d.

In order to look at the secretion of a wider array of cytokines and chemokines after immune complex stimulation, a Luminex assay was performed. Of the 23 analytes that were detected, 8 showed immune complex induced secretion, above that secreted by ova or anti-ova stimulated BMDCs. These were IL-6, monocyte chemoattractant protein-1 (MCP-1), interleukin-1α (IL-1α), regulated on activation, normal T cell expressed and secreted (RANTES, CCL5), keratinocyte chemoattractant (KC, CXCL1), macrophage inflammatory protein-1β (MIP-1β), interleukin-12p40 (IL-12p40) and macrophage inflammatory protein-1α (MIP-1α). However, the secretion of these analytes was similar between WT and *Ptpn22$^{-/-}$* ova IC stimulated BMDCs (Figure 3-10a-

h). This again indicates that PTPN22 is dispensable for cytokine and chemokine secretion after immune complex stimulation.

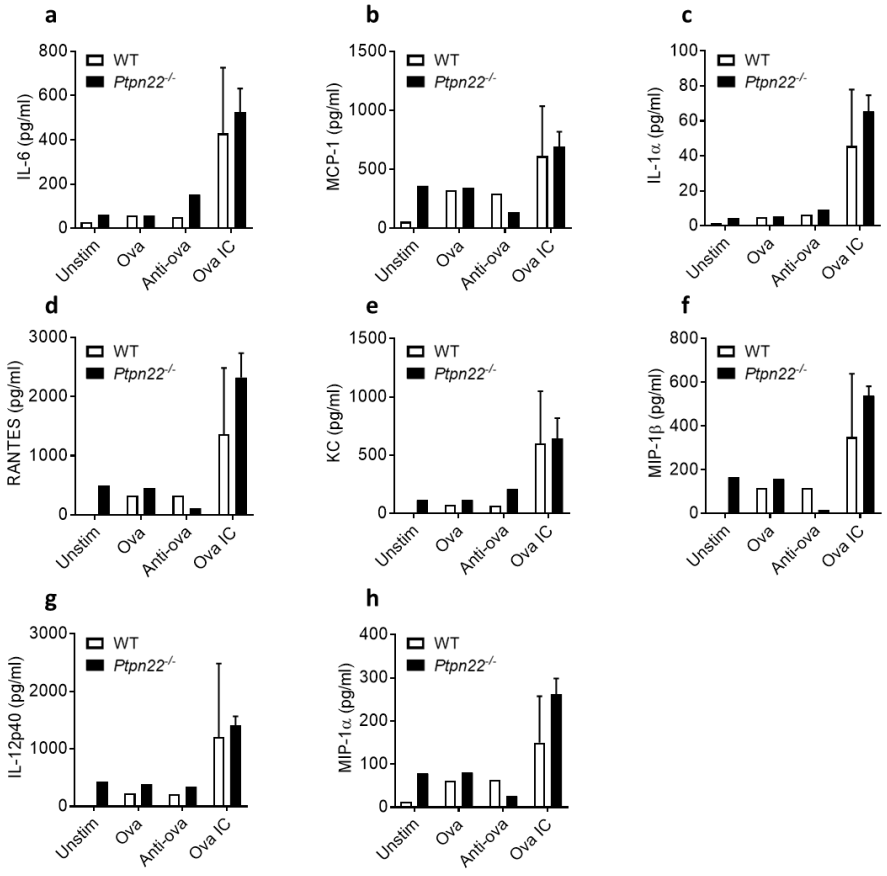

Figure 3-10: PTPN22 is dispensable for BMDC cytokine secretion after immune complex stimulation.

(a-h) WT (white) and Ptpn22$^{-/-}$ (black) BMDCs were stimulated with ova, anti-ova or ova IC. After 24 hours, cell-free supernatants were harvested and secretion of IL-6 (a), MCP-1 (b), IL-1α (c), RANTES (d), KC (e), MIP-1β (f), IL-12p40 (g) and MIP-1α (h) was determined using a Luminex assay. n = 1 (unstim, ova, anti-ova) and 3 (ova IC) ± s.d.

Ova ICs bind to all FcγRs expressed on the surface of mouse BMDCs because the anti-ova is raised in rabbits, and rabbit IgG does not have different subclasses. To further investigate whether PTPN22 may be required for cytokine secretion downstream of specific FcγRs, monoclonal anti-TNP antibodies of the IgG1 isotype were combined with TNP-ova to form TNP-ova:IgG1 anti-TNP immune complexes. These ICs preferentially bind to FcγRIIb and FcγRIII[126], and were used to induce cytokine secretion from WT and *Ptpn22*$^{-/-}$ BMDCs. As with the ova ICs, the TNP-ova:IgG1 anti-TNP immune complex stimulation led to enhanced secretion of IL-6 and TNFα, but the magnitudes were similar between WT and *Ptpn22*$^{-/-}$ BMDCs (Figure 3-11a-b).

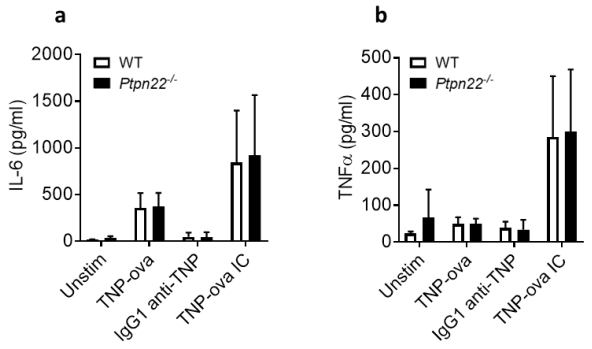

Figure 3-11: PTPN22 is dispensable for BMDC cytokine secretion after IgG1 specific immune complex stimulation.

(a-b) WT (white) and Ptpn22$^{-/-}$ (black) BMDCs were stimulated with TNP-ova, IgG1 anti-TNP or TNP-ova:IgG1 anti-TNP IC (TNP-ova IC), in the presence of polymyxin B. After 24 hours, cell-free supernatants were harvested and secretion of IL-6 (a) and TNFα (b) was determined by immunoassay. n = 3 ± s.d.

In contrast to rabbits, there are four IgG subclasses in mice: IgG1, IgG2a, IgG2b and IgG3. These have different affinities for FcγRs, for example, FcγRI is a high affinity receptor for IgG2a, whereas FcγRIV has no affinity for IgG3[127]. An additional factor that affects IgG binding to FcγRs is the presence of an *N*-linked glycan at asparagine 297 in the Fc domain of IgGs. The glycan is composed of fucose, galactose, sialic acid and bisecting *N*-acetylglucosamine, in varying proportions[128]. The composition of the glycan affects IgG binding to FcγRs, for example, the lack of fucose in the glycan enhances IgG binding to human FcγRIII[240]. The lab of Dr Gestur Vidarsson (University of Amsterdam) kindly provided me with engineered human IgGs with defined Fc-glycans[236] (see Materials and Methods Table 2-7 for antibody details). Although they have been verified to bind to mouse FcγRs, not many of the IgG glycoforms caused BMDC cytokine secretion as part of an immune complex that was higher than the secretion caused by the IgG antibody alone. Focussing on those IgG glycoforms which did induce BMDC cytokine secretion, there was no difference in the response of WT and *Ptpn22$^{-/-}$* BMDCs (Figure 3-12a-c). This is in agreement with my previous experiments showing that PTPN22 does not regulate immune complex induced BMDC cytokine secretion.

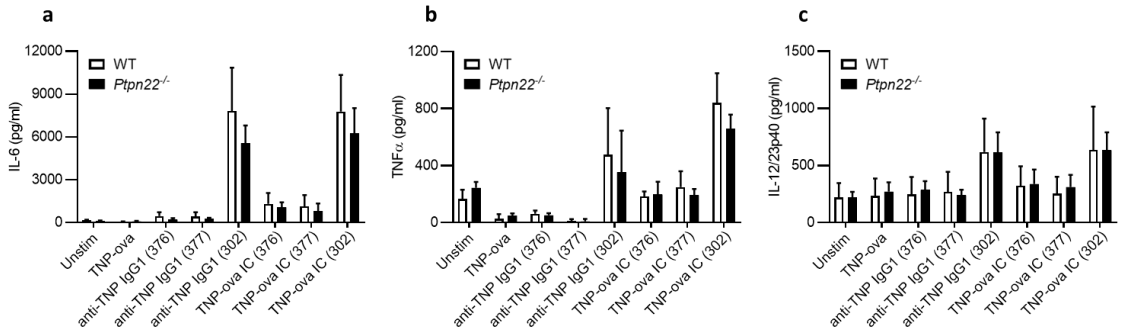

Figure 3-12: PTPN22 is dispensable for BMDC cytokine secretion after IgG1 specific immune complex stimulation.

(a-c) WT (white) and Ptpn22$^{-/-}$ (black) BMDCs were stimulated with TNP-ova, glycosylation variants of IgG1 anti-TNP or TNP-ova:IgG1 anti-TNP ICs, in the presence of polymyxin B. IgG1 anti-TNP glycosylation variants used were unmodified IgG1 anti-TNP (376), IgG1 anti-TNP +2FF (377) and IgG anti-TNP + B4galT1 + St6galT + 2FF + d-gal (302); see Materials and Methods Table 2-7 for more details. After 24 hours, cell-free supernatants were harvested and secretion of IL-6 (a), TNFα (b) and IL-12/23p40 (c) was determined by immunoassay. n = 3 ± s.d. IgG1 anti-TNP glycoforms were provided by Dr Gestur Vidarsson (University of Amsterdam).

Taken together, this data therefore indicates that PTPN22 is not required for immune complex induced BMDC maturation, including upregulation of co-stimulatory molecules and cytokine secretion.

3.3.7 Immune complex stimulation can induce calcium flux in BMDCs

An earlier response to FcγR crosslinking than DC cytokine secretion and maturation, is calcium flux. After receptor crosslinking, phospholipase Cγ2 becomes stimulated which then cleaves phosphatidylinositol-(4,5)-bisphosphate to diacylglycerol and inositol-(1,4,5)-trisphosphate. Inositol-(1,4,5)-trisphosphate binds to IP_3 receptors located in the endoplasmic reticulum, resulting in the release of calcium from intracellular stores. Indo-1 is a sensitive ratiometric dye which can be used to measure intracellular calcium flux as it emits light at different wavelengths depending on whether it is in the absence or presence of calcium. In the absence of calcium, indo-1 displays a main emission peak at 500 nm, whereas in the presence of calcium, this shifts to 390 nm. By staining BMDCs with indo-1, the calcium flux in response to stimulation can be monitored in real time by flow cytometry. The response of WT and *Ptpn22$^{-/-}$* BMDCs to immune complex stimulation was measured in multiple experiments, however, the results were not consistent. Although the ionophore ionomycin always induced a robust calcium flux, and the chelator EGTA reduced this back to baseline, immune complex stimulation only caused a measurable flux in calcium in some experiments (Figure 3-13). Therefore, it was not possible

from these experiments to conclude whether PTPN22 was required for calcium flux after FcγR crosslinking.

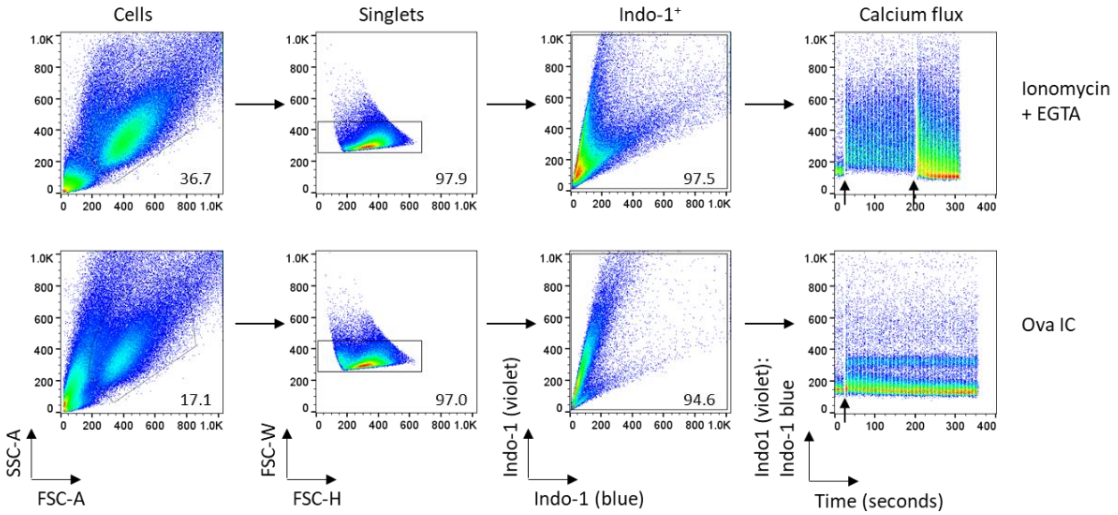

Figure 3-13: Immune complex stimulation can cause calcium flux in BMDCs.

BMDCs were stained with indo-1 and collected by flow cytometry. Ionomycin, followed by EGTA (top) or ova ICs (bottom) were used added to BMDCs (arrows on the right hand plots indicate the time of addition of stimulations), and calcium flux was measured in real time.

3.3.8 PTPN22 does not regulate immune complex induced reactive oxygen species production by neutrophils

The production of reactive oxygen species (ROS) is one of the mechanisms that phagocytes use to destroy invading pathogens. Although DCs can produce ROS, neutrophils and macrophages are far more efficient at using this to destroy pathogens[241]. This is because the phagocytic pathway in DCs focuses more on antigen presentation as opposed to pathogen killing[238]. I therefore compared the ability of *ex vivo* neutrophils (identified as $CD11b^+$, $Ly6G^+$ live singlets) from the bone marrow of WT and *Ptpn22*$^{-/-}$ mice to produce ROS after immune complex stimulation, using dihydrorhodamine 123 (DHR123). DHR123 is a derivative of rhodamine and is an uncharged and non-fluorescent dye. When it is incubated with cells, it can passively diffuse across membranes, and when it becomes oxidised by ROS, it is converted into rhodamine 123, which fluoresces green and can be detected by flow cytometry. Ova and anti-ova stimulation caused no increase in ROS production (as shown by no change in the percentage of $DHR123^+$ neutrophils) relative to unstimulated bone marrow cells (Figure 3-14). Although ova ICs caused a subtle increase in ROS production, a similar increase was observed in both WT and *Ptpn22*$^{-/-}$ neutrophils (Figure 3-14).

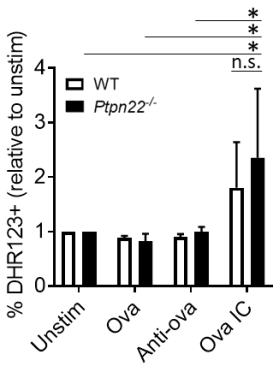

Figure 3-14: PTPN22 is not required for immune complex induced ROS production by bone marrow neutrophils.

*Bone marrow from WT and Ptpn22$^{-/-}$ mice was flushed, red blood cell lysed, stained with DHR123 and incubated with ova, anti-ova and ova ICs for 45 minutes at room temperature. DHR123 expression (% positive, relative to the unstimulated condition) in WT (white) and Ptpn22$^{-/-}$ (black) neutrophils was determined by flow cytometry (gated on CD11b^{+}, Ly6G^{+} live singlets). n = 3 ± s.d. *p<0.05 using a 2-way ANOVA with Tukey's multiple comparisons test. All WT v Ptpn22$^{-/-}$ comparisons were non-significant (n.s.). Bars on graphs only show comparisons of ova IC v unstim/ova/anti-ova for Ptpn22$^{-/-}$ BMDCs (for simplicity).*

3.3.9 PTPN22 is dispensable for T cell proliferation after co-culture with LPS matured, OVA$_{323-339}$ peptide pulsed BMDCs

Before identifying whether PTPN22 was required for presentation of immune complex derived peptide to T cells, its potential role in the presentation of a non-internalised antigen was first investigated. LPS matured BMDCs are more efficient at causing T cell proliferation when presenting OVA$_{323-339}$ peptide, than immature BMDCs[242]. This is due to the increased expression of MHCII on the surface of mature DCs, allowing for enhanced presentation of OVA$_{323-339}$ peptide. Therfore, I first wanted to determine whether PTPN22 was required for T cell proliferation by mature BMDCs presenting OVA$_{323-339}$ peptide. WT and *Ptpn22$^{-/-}$* BMDCs were LPS matured and pulsed with OVA$_{323-339}$ peptide overnight, prior to co-culture with ova specific WT CD4^{+} OT-II T cells for 1-6 days (see Materials and Methods Figure 2-8 for experimental setup).

Increasing concentrations of OVA$_{323-339}$ peptide caused enhanced upregulation of CD25 and CD69 on T cells after 1 day of co-culture, but expression of these early activation markers was not dependent on the genotype of the BMDC (Figure 3-15a-b). In addition, interleukin-2 (IL-2) secretion was measured at day 1 and found to be similar between WT T cells co-cultured with WT or *Ptpn22$^{-/-}$* BMDCs (Figure 3-15c). T cell proliferation after 6 days of co-culture, measured by CellTrace Violet (CTV) dilution was similar regardless of the BMDC genotype (Figure 3-15d-e), and secretion of interferon γ (IFNγ) was also found to be similar (Figure 3-15f). This indicates

that PTPN22 is not required for the presentation to T cells of $OVA_{323-339}$ peptide by LPS matured BMDCs. Consistent with these data, I have previously observed no differences in MHCII expression on LPS matured WT or *Ptpn22*$^{-/-}$ BMDCs (Figure 3-16).

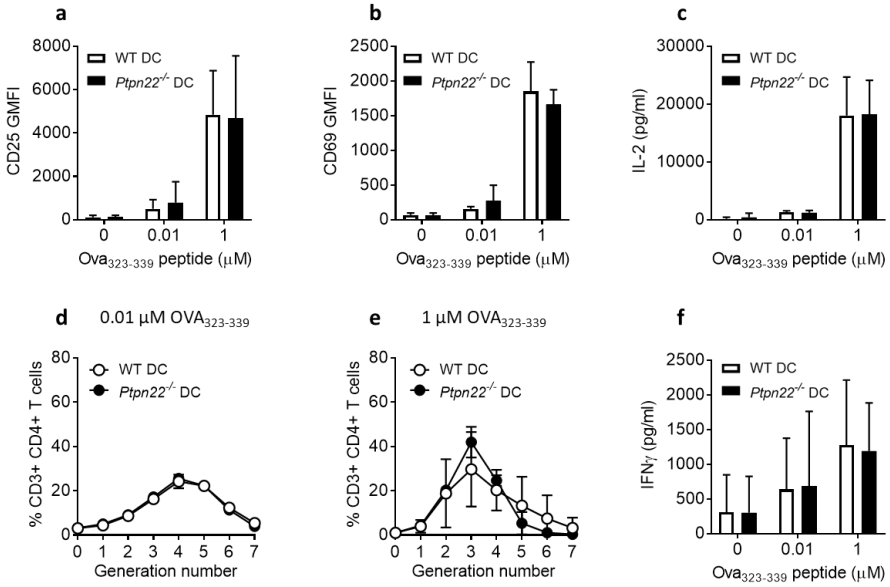

Figure 3-15: PTPN22 is dispensable for T cell proliferation caused by LPS matured, $OVA_{323-339}$ peptide pulsed BMDCs.

(a-f) WT and Ptpn22$^{-/-}$ BMDCs were LPS matured and pulsed overnight in the presence of $OVA_{323-339}$ peptide (or left unpulsed) prior to co-culture with CTV labelled WT CD4^{+} OT-II T cells for 6 days. (a-b) CD25 (a) and CD69 (b) cell surface expression (geometric mean fluorescence intensity, GMFI) on WT OT-II T cells after 1 day of co-culture with WT (white) or Ptpn22$^{-/-}$ (black) BMDCs (gated on CD3^{+}, CD4^{+} live singlets). n = 2-3 ± s.d. (c) At day 1 of co-culture, cell-free supernatants were assessed for IL-2 by immunoassay. n = 3 ± s.d. (d-e) Proportions of WT OT-II T cells in each generation of cell division after 6 days of co-culture with 0.01 μM (d) and 1 μM (e) $OVA_{323-339}$ peptide pulsed WT (white) or Ptpn22$^{-/-}$ (black) BMDCs (gated on CD3^{+}, CD4^{+} live singlets). n = 2-3 ± s.d. (f) At day 6 of co-culture, cell-free supernatants were assessed for IFNγ by immunoassay. n = 3 ± s.d. Experiments were carried out with Dr Harriet Purvis (Cope laboratory, King's College London).

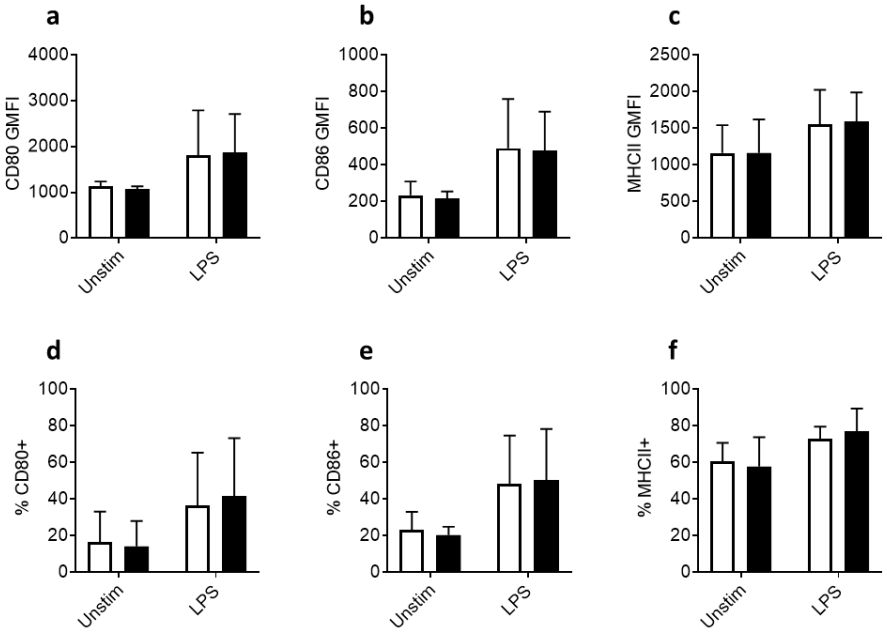

Figure 3-16: PTPN22 does not regulate LPS induced maturation of BMDCs.

WT and Ptpn22$^{-/-}$ BMDCs were stimulated in the presence or absence (unstim) of LPS. After 24 hours, BMDCs were harvested and surface stained for CD80, CD86 and MHCII. (a-c) WT (white) and Ptpn22$^{-/-}$ (black) BMDC cell surface expression (geometric mean fluorescence intensity, GMFI, gated on CD11c^{+} live singlets) of CD80 (a), CD86 (b) and MHCII (c). (d-f) WT (white) and Ptpn22$^{-/-}$ (black) BMDC cell surface expression (% positive, gated on CD11c^{+} live singlets) of CD80 (d), CD86 (e) and MHCII (f). n = 5 ± s.d.

To determine whether expression of the autoimmune associated variant of PTPN22 would affect BMDC presentation of $OVA_{323-339}$ peptide to T cells, co-cultures were also carried out using *Ptpn22^{R619}* (WT) and *Ptpn22^{R619W}* LPS matured BMDCs. IL-2 secretion after 1 day of co-culture and IFNγ secretion after 6 days of co-culture were similar between T cells co-cultured with WT and *Ptpn22^{R619W}* LPS matured BMDCs (Figure 3-17a-b), indicating that expression of PTPN22^{R619W} does not affect the ability of BMDCs to present $OVA_{323-339}$ peptide to T cells.

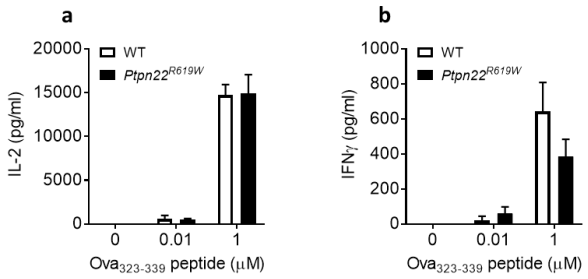

Figure 3-17: Expression of PTPN22^{R619W} does not affect T cell cytokine secretion after co-culture with LPS matured, OVA$_{323-339}$ peptide pulsed BMDCs.

(a-b) Ptpn22^{R619} (WT) and Ptpn22^{R619W} BMDCs were LPS matured and pulsed overnight in the presence of OVA$_{323-339}$ peptide (or left unpulsed) prior to co-culture with CTV labelled WT CD4$^+$ OT-II T cells for 6 days. (a) At day 1 of co-culture, cell-free supernatants from T cells co-cultured with Ptpn22^{R619} (WT, white) and Ptpn22^{R619W} (black) BMDCs were assessed for IL-2 by immunoassay. n = 4 ± s.d. (b) At day 6 of co-culture, cell-free supernatants from T cells co-cultured with Ptpn22^{R619} (WT, white) and Ptpn22^{R619W} (black) BMDCs were assessed for IFNγ by immunoassay. n = 4 ± s.d.

3.3.10 Immune complex pulsed *Ptpn22*$^{-/-}$ BMDCs cause enhanced T cell proliferation

Once immune complexes have been internalised via FcγRs, they enter the endosomal processing pathway such that immune complex derived antigens can be presented to CD4$^+$ T cells on MHCII. The cross-presentation pathway also allows for the presentation of antigens derived from exogenous material on MHCI to CD8$^+$ T cells, but this process was not investigated here. To determine whether PTPN22 modulates the ability of BMDCs to present immune complex derived antigens and in turn activate CD4$^+$ T cells, *in vitro* co-culture assays were performed. WT and *Ptpn22*$^{-/-}$ BMDCs were pulsed overnight with ova, ova pre-incubated with rabbit IgG (ova + rabbit IgG), ova added in combination with heat aggregated rabbit IgG (ova + HA IgG), or ova ICs and the following day were co-cultured with ova specific WT CD4$^+$ OT-II T cells for 1-6 days (see Materials and Methods Figure 2-8 for experimental setup).

At early stages of the co-culture, T cells co-cultured with ova IC pulsed BMDCs responded more robustly that those co-cultured with ova alone, as judged by an increase in CD25 and CD69 expression, IL-2 and IFNγ secretion, and T cell proliferation (Figure 3-18a-e). On day 1 of culture, WT T cells that had been co-cultured with ova IC pulsed *Ptpn22*$^{-/-}$ BMDCs expressed higher levels of the early activation markers CD25 and CD69, and secreted enhanced levels of IL-2, in comparison to T cells co-cultured with ova IC pulsed WT BMDCs (Figure 3-18a-c). At day 3, T cell proliferation was measured by calculating the total number of T cells per co-culture well. Enhanced T cell proliferation was found after co-culture with ova IC pulsed *Ptpn22*$^{-/-}$ BMDCs

(Figure 3-18d), but this was not accompanied by changes in IFNγ cytokine secretion (Figure 3-18e).

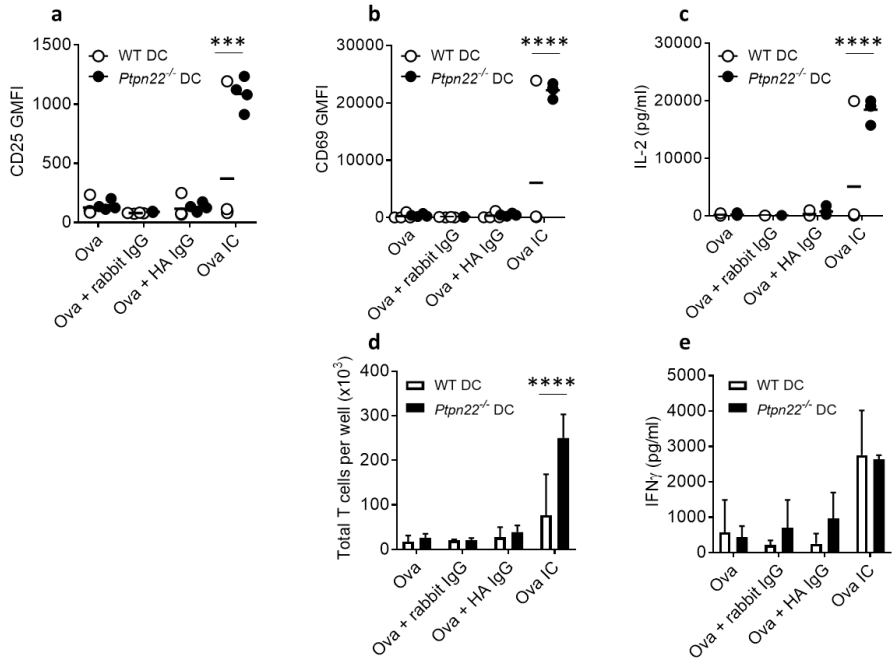

Figure 3-18: Ova IC pulsed Ptpn22$^{-/-}$ BMDCs cause enhanced T cell activation and proliferation after 1-3 days of co-culture.

*(a-e) WT and Ptpn22$^{-/-}$ BMDCs were pulsed overnight in the presence of ova, ova pre-incubated with rabbit IgG (ova + rabbit IgG), ova with heat aggregated IgG (ova + HA IgG), or ova IC prior to co-culture with CTV labelled WT CD4^{+} OT-II T-cells for 1-3 days. (a-b) CD25 (a) and CD69 (b) cell surface expression (geometric mean fluorescence intensity, GMFI) on WT OT-II T cells after 1 day of co-culture with WT (white) or Ptpn22$^{-/-}$ (black) BMDCs (gated on CD3^{+}, CD4^{+} live singlets). n = 4; ****p<0.001, ***p<0.005 using a 2-way ANOVA with Sidak's multiple comparisons test. (c) At day 1 of co-culture, cell-free supernatants were assessed for IL-2 by immunoassay. n = 4; ****p<0.001 using a 2-way ANOVA with Sidak's multiple comparisons test. (d) The number of T cells per co-culture well was counted after 3 days of co-culture with WT (white) or Ptpn22$^{-/-}$ (black) BMDCs (gated on CD3^{+}, CD4^{+} live singlets). n = 4 ± s.d; ****p<0.001 using a 2-way ANOVA with Sidak's multiple comparisons test. (e) At day 3 of co-culture, cell-free supernatants were assessed for IFNγ by immunoassay. n = 4 ± s.d.*

After 6 days, T cell proliferation was assessed by CTV dilution. It has been previously demonstrated that complexed antigen is more efficient at inducing T cell proliferation than antigen alone[243]. This was confirmed as T cells co-cultured with ova IC pulsed BMDCs proliferated more than those with ova pulsed BMDCs (Figure 3-19b-c). I next compared the ability of ova IC pulsed WT or *Ptpn22$^{-/-}$* BMDCs to induce T cell proliferation. In agreement with the findings from days 1 and 3 of co-culture, ova IC pulsed *Ptpn22$^{-/-}$* BMDCs induced enhanced T cell proliferation after 6 days, in comparison to WT BMDCs (Figure 3-19c). This was also accompanied by augmented total cell numbers in the co-culture wells on day 6 (Figure 3-19d).

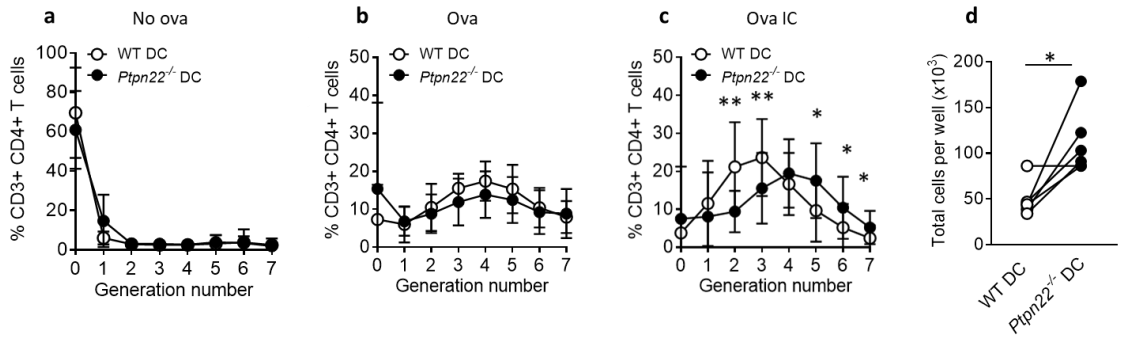

Figure 3-19: Ptpn22$^{-/-}$ BMDCs enhance immune complex induced T cell proliferation after 6 days of co-culture.

*(a-d) WT and Ptpn22$^{-/-}$ BMDCs were pulsed overnight in the presence of ova or ova IC (or left unpulsed, no ova) prior to co-culture with CTV labelled WT CD4^{+} OT-II T cells for 6 days. Proportions of WT OT-II T cells in each generation of cell division after 6 days of co-culture with unpulsed (a), ova (b) and ova IC (c) pulsed WT (white) or Ptpn22$^{-/-}$ (black) BMDCs (gated on CD3^{+}, CD4^{+} live singlets). n=7-11 ± s.d.; **p<0.01, *p<0.05 using a Wilcoxon matched-pairs signed ranks test. (d) The number of cells per well were counted after 6 days of co-culture with ova IC pulsed WT (white) or Ptpn22$^{-/-}$ (black) BMDCs. n = 6; *p<0.05 using a paired t-test.*

As a control, unpulsed BMDCs were also co-cultured with ova specific T cells, and, as expected, these caused very little T cell proliferation or cytokine secretion (Figure 3-19a, 3-20a-c and 3-21a-c). As additional controls, BMDCs were pulsed with ova pre-incubated with rabbit IgG, or ova added in combination with HA rabbit IgG. BMDCs pulsed with these antigen/antibody combinations did not induce T cell proliferation, upregulation of CD25 or CD69, or cytokine secretion, higher than those seen by ova pulsed BMDCs alone (Figure 3-18a-e). This indicates that it is the presence of an antibody:antigen immune complex which is causing enhanced T cell responses by *Ptpn22$^{-/-}$* BMDCs, and that just the combined presence of an antibody and antigen is not sufficient.

Although T cells co-cultured for 6 days with ova IC pulsed BMDCs secreted enhanced levels of IFNγ, TNFα and IL-17 in comparison to those induced by ova pulsed BMDCs (Figure 3-20a-c), expression or secretion of these cytokines was not dependent on the genotype of the BMDC (Figures 3-20a-c and 3-21a-c). Together, these data demonstrate that PTPN22 negatively regulates the ability of BMDCs to induce immune complex dependent T cell activation and proliferation, but that it has no effect on cytokine expression.

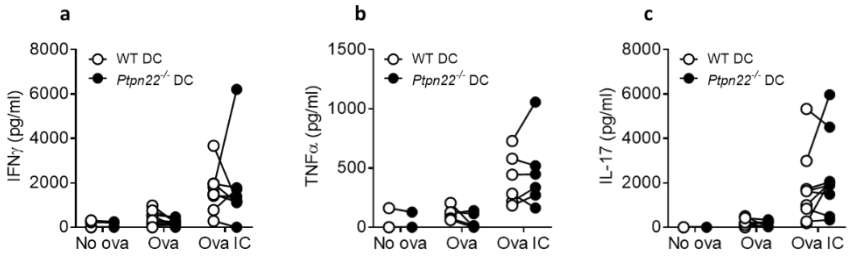

Figure 3-20: PTPN22 is dispensable for T cell cytokine secretion after 6 days of co-culture with BMDCs.

(a-c) WT and Ptpn22$^{-/-}$ BMDCs were pulsed overnight in the presence of ova or ova IC prior to co-culture with CTV labelled WT CD4^{+} OT-II T-cells for 6 days. At day 6 of co-culture, cell-free supernatants were assessed for IFNγ (a), TNFα (b) and IL-17 (c) by immunoassay. n = 3-9. Connecting lines indicate WT or Ptpn22$^{-/-}$ BMDCs co-cultured with the same WT OT-II T cells.

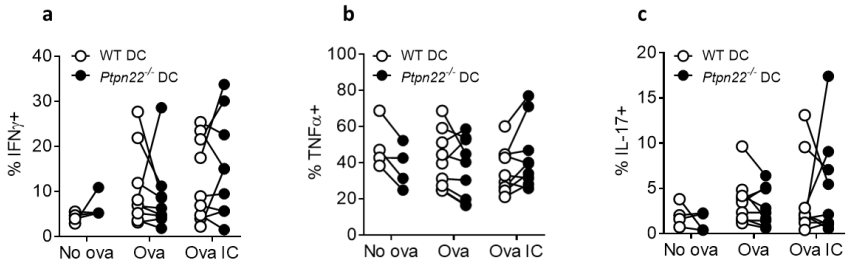

Figure 3-21: PTPN22 is dispensable for T cell cytokine expression after 6 days of co-culture with BMDCs.

(a-c) WT and Ptpn22$^{-/-}$ BMDCs were pulsed overnight in the presence of ova or ova IC prior to co-culture with CTV labelled WT CD4^{+} OT-II T-cells for 6 days. At day 6, T cells co-cultured with ova or ova IC pulsed WT (white) or Ptpn22$^{-/-}$ (black) BMDCs were restimulated for 6 hours with PMA and ionomycin in the presence of monensin and intracellular expression of IFNγ (a), TNFα (b) and IL-17 (c) was determined (gated on CD3^{+}, CD4^{+} live singlets). n = 4-9. Connecting lines indicate WT or Ptpn22$^{-/-}$ BMDCs co-cultured with the same WT OT-II T cells.

To determine whether lacking PTPN22 expression in the T cell would cause an additive or synergistic effect to lacking PTPN22 expression in the BMDC, co-cultures were performed using ova IC pulsed *Ptpn22$^{-/-}$* BMDCs and WT or *Ptpn22$^{-/-}$* CD4^{+} OT-II T cells. The lack of PTPN22 in the T cell did not further enhance the rate of T cell proliferation (Figure 3-22), indicating that PTPN22 plays an important role in BMDCs to regulate T cell proliferation, regardless of the genotype of the T cell.

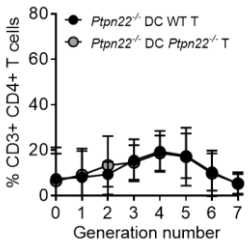

Figure 3-22: Lacking PTPN22 expression in T cells does not affect T cell proliferation after co-culture with ova IC pulsed Ptpn22$^{-/-}$ BMDCs.

Ptpn22$^{-/-}$ BMDCs were pulsed overnight in the presence of ova ICs prior to co-culture with CTV labelled WT (black) or Ptpn22$^{-/-}$ (dark grey) CD4^{+} OT-II T cells for 6 days. Data shows proportions of OT-II T cells in each generation of cell division (gated on CD3^{+}, CD4^{+} live singlets). n = 6-10 ± s.d.

3.3.11 PTPN22 is dispensable for immune complex induced T cell proliferation and cytokine secretion by LPS matured BMDCs

During infection, or autoimmunity, it is unusual for immune cells to be exposed to immune complexes alone, as the co-cultures discussed above have modelled. Instead, it is more likely that immune cells will interact with both TLR and FcγR ligands. For example, endogenous ligands such as damage associated molecular patterns (DAMPs) and autoantibodies are often present simultaneously in rheumatoid arthritis patients. To investigate whether PTPN22 also played a role in the presentation of immune complex derived antigens by LPS matured BMDCs, co-cultures were performed using ova and ova IC pulsed LPS matured WT and *Ptpn22$^{-/-}$* BMDCs and WT CD4^{+} OT-II T cells. Although I have found that PTPN22 negatively regulates immune complex induced T cell proliferation (Figure 3-19c), in the presence of LPS, PTPN22 was no longer required. Both ova IC pulsed WT and *Ptpn22$^{-/-}$* LPS matured BMDCs caused similar T cell proliferation after 6 days of co-culture (Figure 3-23c).

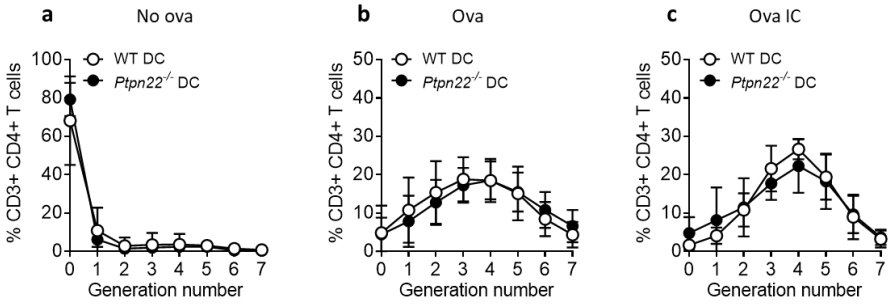

Figure 3-23: LPS matured Ptpn22$^{-/-}$ BMDCs cause normal immune complex induced T cell proliferation.

(a-c) WT and Ptpn22$^{-/-}$ BMDCs were LPS matured and pulsed overnight in the presence of ova or ova IC (or left unpulsed, no ova) prior to co-culture with CTV labelled WT CD4^{+} OT-II T cells for 6 days. Proportions of WT OT-II T cells in each generation of cell division after 6 days of co-culture with unpulsed (a), ova (b) and ova IC (c) pulsed WT (white) or Ptpn22$^{-/-}$ (black) BMDCs (gated on CD3^{+}, CD4^{+} live singlets). n= 6-7 ± s.d.

In addition, production and secretion of IFNγ, TNFα and IL-6 was similar between T cells co-cultured with mature WT and *Ptpn22$^{-/-}$* BMDCs (Figures 3-24a-c and 3-25a-c).

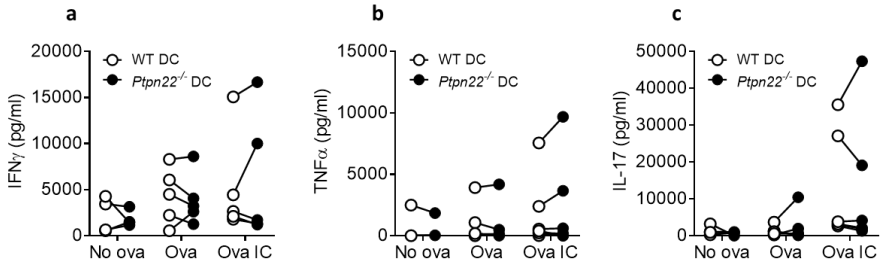

Figure 3-24: PTPN22 is dispensable for T cell cytokine secretion after 6 days of co-culture with LPS matured BMDCs.

(a-f) WT and Ptpn22$^{-/-}$ BMDCs were LPS matured and pulsed overnight in the presence of ova or ova IC prior to co-culture with CTV labelled WT CD4^{+} OT-II T-cells for 6 days. At day 6 of co-culture, cell-free supernatants were assessed for IFNγ (a), TNFα (b) and IL-17 (c) by immunoassay. n = 4-7. Connecting lines indicate WT or Ptpn22$^{-/-}$ BMDCs co-cultured with the same WT OT-II T cells.

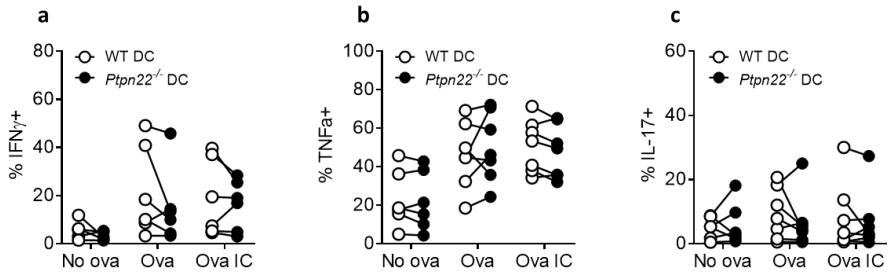

Figure 3-25: PTPN22 is dispensable for T cell cytokine expression after 6 days of co-culture with LPS matured BMDCs.

(a-c) WT and Ptpn22$^{-/-}$ BMDCs were LPS matured and pulsed overnight in the presence of ova or ova IC prior to co-culture with CTV labelled WT CD4^{+} OT-II T-cells for 6 days. At day 6, T cells co-cultured with ova or ova IC pulsed LPS matured WT (white) or Ptpn22$^{-/-}$ (black) BMDCs were restimulated for 6 hours with PMA and ionomycin in the presence of monensin and intracellular expression of IFNγ (d), TNFα (e) and IL-17 (f) was determined (gated on CD3^{+}, CD4^{+} live singlets). n = 4-6. Connecting lines indicate WT or Ptpn22$^{-/-}$ BMDCs co-cultured with the same WT OT-II T cells.

3.3.12 PTPN22 is dispensable for immune complex induced T cell proliferation *in vivo*

I next wanted to determine whether PTPN22 was required for antigen presenting cell (APC) mediated T cell proliferation *in vivo*. For this, I took two approaches, firstly, CTV labelled WT CD4^{+} CD45.1^{+} OT-II T cells were adoptively transferred into WT or *Ptpn22*$^{-/-}$ CD45.2^{+} recipient mice and the following day mice were injected with ova or ova ICs into their right footpad. Three days later, the draining (right) and non-draining (left) popliteal lymph nodes were extracted and proliferation of the transferred T cells was assessed (see Materials and Methods Figure 2-11 for experimental setup). Only low numbers of transferred T cells were found in the non-draining lymph nodes, as expected (Figure 3-26b). More transferred T cells were found in the draining LNs, and ova IC immunisation enhanced T cell proliferation in comparison with ova alone (Figure 3-26c), consistent with my *in vitro* experiments. Despite this, proliferation of the transferred WT OT-II T cells was similar in WT and *Ptpn22*$^{-/-}$ mice (Figure 3-26b-c). This indicates that PTPN22 is not required for ova IC induced T cell proliferation *in vivo*.

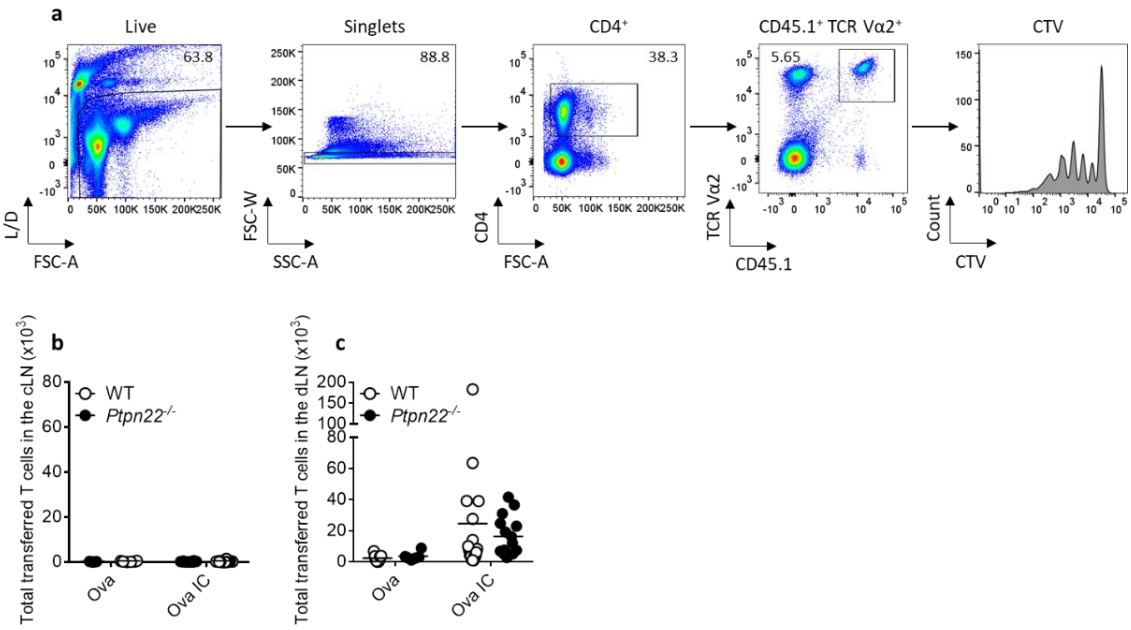

Figure 3-26: PTPN22 is dispensable for immune complex induced antigen presentation and T cell proliferation in vivo.

(a-c) CTV labelled WT CD4$^+$ OT-II CD45.1$^+$ T cells were transferred (i.v.) into WT and Ptpn22$^{-/-}$ CD45.2$^+$ recipient mice. The following day, ova or ova IC were injected (s.c.) into the right footpad. 3 days later, T cell proliferation was measured in the draining (right, dLN) and non-draining, control (left, cLN) popliteal lymph nodes. (a) Representative flow cytometry plots showing gating to identify transferred WT CD4$^+$ TCR Vα2$^+$ CD45.1$^+$ T cells in the dLNs of CD45.2$^+$ recipient mice. (b-c) Total number of transferred WT CD4$^+$ TCR Vα2$^+$ CD45.1$^+$ T cells in the non-draining (b) and draining (c) lymph nodes of WT (white) and Ptpn22$^{-/-}$ (black) CD45.2$^+$ recipient mice (gated on CD4$^+$, TCR Vα2$^+$, CD45.1$^+$ live singlets). n = 6-9 (ova) and 15-17 (ova IC) recipient mice.

Secondly, to try to ascertain whether PTPN22 may regulate BMDC ova IC induced T cell proliferation in a more *in vivo* setting, WT and *Ptpn22*$^{-/-}$ BMDCs were pulsed with ova ICs *in vitro* and then transferred into the right footpad of WT OT-II recipient mice (see Materials and Methods Figure 2-12 for experimental setup). As the responding T cells were endogenous in the recipient mice, CTV could not be used to track T cell proliferation. Instead, the total number of OT-II T cells were calculated in the draining (right) and non-draining (left) popliteal lymph nodes 6 days after BMDC transfer. Only a low number of T cells were present in the non-draining lymph node compared to the draining LN (Figure 3-27). Similar numbers of T cells were present in the draining LNs of mice that received WT and *Ptpn22*$^{-/-}$ ova IC pulsed BMDCs (Figure 3-27), indicating that PTPN22 does not regulate ova IC induced T cell proliferation *in vivo*.

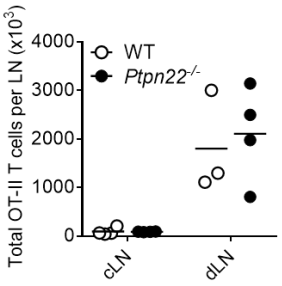

Figure 3-27: PTPN22 is dispensable for ova IC pulsed BMDC induced T cell proliferation in vivo.

WT (white) and Ptpn22$^{-/-}$ (black) BMDCs were stimulated in the presence of ova ICs. The following day, BMDCs were injected (s.c.) into the right footpad of WT OT-II recipient mice. 6 days later, T cell proliferation was measured in the draining (dLN) and non-draining, control (cLN) popliteal lymph nodes. Data shows the total number of transferred WT CD4^{+} OT-II T cells in the lymph nodes (gated on CD4^{+}, TCR Vα2^{+}, TCR Vα2^{+} live singlets). n = 3-4 recipient mice.

3.3.13 PTPN22 is dispensable for *in vivo* migration of migratory DCs

Not only do DCs need to be able to recognise, internalise, process and present antigens in order to cause T cell activation, they must also be capable of migrating from peripheral tissues to lymph nodes, so that they can interact with T cells[244]. Therefore, the role of PTPN22 in DC migration was assessed. FITC in 1:1 acetone:dibutyl phthalate (irritant) was added to the dorsal side of the left ears of WT and *Ptpn22$^{-/-}$* mice (irritant alone was added as a negative control to the right ears). 24 hours later, the proportion of FITC^{+} migratory and resident DCs in the draining auricular lymph nodes was assessed (see Materials and Methods Figure 2-10 for experimental setup). Similar proportions of FITC^{+} migratory DCs were found in the draining lymph nodes of both WT and *Ptpn22$^{-/-}$* mice (Figure 3-28b). This indicates that PTPN22 is dispensable for DC migration *in vivo*.

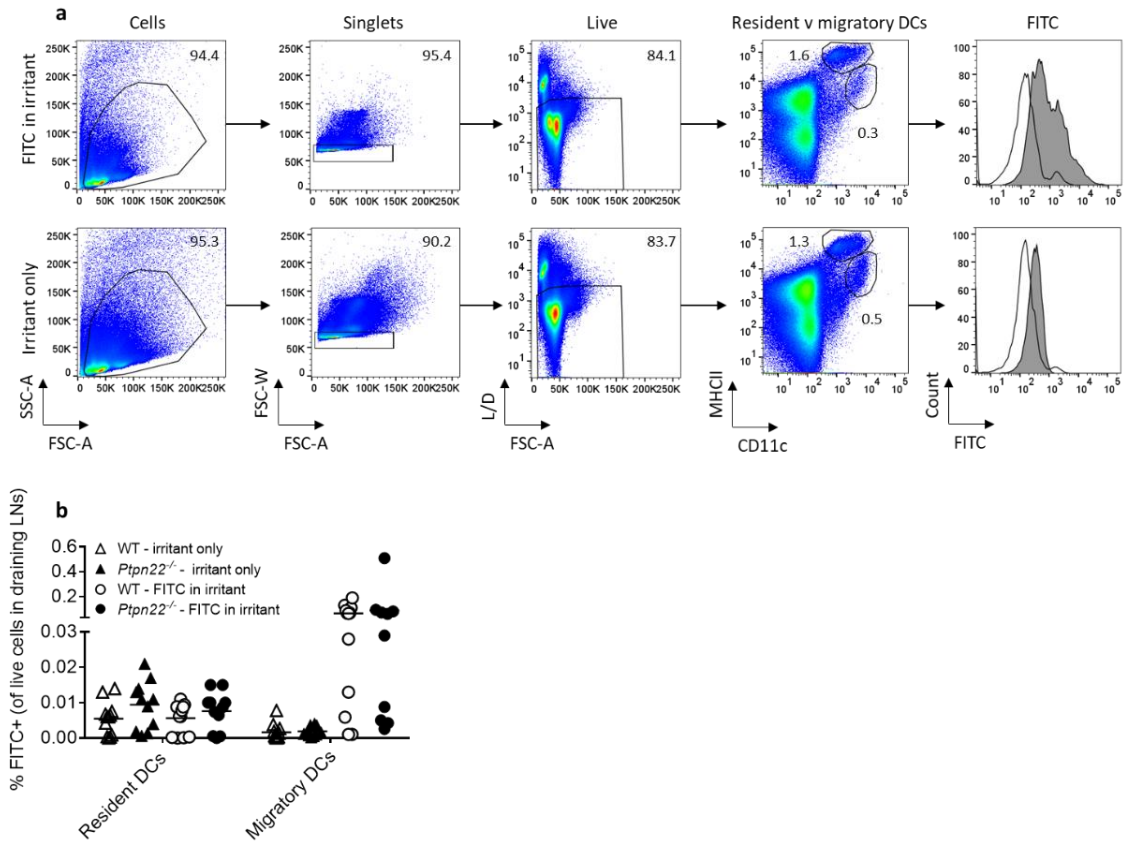

Figure 3-28: PTPN22 is not required for in vivo migration of skin resident DCs to the draining lymph nodes.

(a-b) FITC in 1:1 acetone:dibutyl phthalate (FITC in irritant) was added to the dorsal side of the left ears of WT and Ptpn22$^{-/-}$ mice. Irritant alone (as a negative control) was added to the dorsal side of the left ears of WT and Ptpn22$^{-/-}$ mice. After 24 hours, auricular draining lymph nodes were harvested, digested and stained to identify resident and migratory DCs. (a) Representative flow cytometry plots showing FITC expression in resident (white) and migratory (grey) DCs in the draining LNs of a mouse receiving FITC in irritant (top) or irritant alone (bottom). (b) Combined data showing FITC uptake in resident (gated on CD11c^{hi}, MHCII^{+} live singlets) and migratory DCs (gated on CD11c^{+}, MHCII^{hi} live singlets) in WT (white) and Ptpn22$^{-/-}$ (black) mice, after receiving FITC in irritant (circle) or irritant alone (triangle). n = 10-12 recipient mice.

3.4 Overall findings

The main findings of this Chapter were:

1. PTPN22 is dispensable for BMDC differentiation *in vitro*.
2. *Ptpn22*$^{-/-}$ BMDCs express reduced cell surface FcγRIIb.
3. PTPN22 is dispensable for immune complex induced upregulation of co-stimulatory molecules and cytokine secretion.
4. PTPN22 negatively regulates immune complexed induced T cell proliferation *in vitro*.

This data has been published in:

1. **Clarke F**, Purvis HA, Sanchez-Blanco C, Gutiérrez-Martinez E, Cornish GH, Zamoyska R, Guermonprez P, Cope AP. The protein tyrosine phosphatase PTPN22 negatively regulates presentation of immune complex derived antigens. *Scientific Reports* **8** (2018).

3.5 Discussion

The aim of this Chapter was to investigate whether PTPN22 was regulating DC effector functions after FcγR engagement. Src and Syk family kinases are downstream of FcγRs and have been shown to be dephosphorylated after ligand engagement with other immunoreceptors. In addition, autoantibodies are present in most of the $PTPN22^{R620W}$ associated autoimmune diseases. Together, these suggested a potential role of PTPN22 in regulating cellular processes after FcγR crosslinking.

The data presented in this Chapter demonstrate that PTPN22 is dispensable for immune complex induced BMDC effector functions, including upregulation of co-stimulatory molecules and cytokine secretion. This finding is somewhat surprising, as Syk, a target of PTPN22, has previously been shown to be required for upregulation of CD40 and CD86 on BMDCs after FcγR crosslinking[245]. In addition, my data contrasts with the role identified for PTPN22 in regulating FcγR signalling in mouse neutrophils. In this cell type, PTPN22 is required for immune complex induced effector responses including ROS production, adhesion and degranulation[63]. This difference may reflect cell specific roles for PTPN22, or it may be due to different immune complex stimulations being used. I did however find that PTPN22 negatively regulates immune complex induced T cell proliferation.

3.5.1 Using GM-CSF induced BMDCs as an *in vitro* model of DCs

Most of the data presented in this Chapter was generated using GM-CSF induced BMDCs. These cultures have the major advantage of being able to produce millions of cells from the bones of a single mouse. They also provide a simple model to investigate DC function *in vitro.* However, they do not directly model an *in vivo* DC population, meaning that extrapolation from BMDC cultures to the situation *in vivo* should be undertaken with caution. As shown in the phenotyping

in Figure 3-1, the GM-CSF bone marrow cultures are comprised of both conventional DCs and monocyte-derived macrophages (referred to as GM-DCs and GM-macs respectively). An alternative cell culture protocol is the differentiation of bone marrow progenitors using Flt3 ligand (Flt3L)[246]. These cultures more closely mirror *in vivo* DC populations as they differentiate into the 3 main DC subsets: pDCs, cDC1s and cDC2s. Alternatively, in the future, it would be interesting to see the response of *in vivo* DC populations to immune complex stimulation. This could be achieved by injecting WT and *Ptpn22*$^{-/-}$ mice with immune complexes and measuring upregulation of MHCII and co-stimulatory molecules on the DCs present in the draining lymph nodes.

Despite the caveats associated with the use of GM-CSF induced BMDCs, I did nevertheless find that PTPN22 did not affect their differentiation into CD11c^{+} cells, or when they were further classified as GM-DCs and GM-macs. In the future, it would be worthwhile sorting the GM-DCs and GM-macs from WT and *Ptpn22*$^{-/-}$ cultures to see if they responded differently to immune complex stimulation. It is possible that the requirement for PTPN22 to negatively regulate immune complex induced T cell proliferation may be due to its role in more DC or macrophage like cells. Despite there being a shift in the balance of GM-DCs and GM-macs between WT v *Ptpn22*$^{-/-}$ and WT v *Ptpn22*^{R619W} cultures, the composition of the cultures were always similar when comparing cultures produced side-by-side.

3.5.2 FcγR expression

Ptpn22$^{-/-}$ BMDCs do show a different balance in their cell surface expression of activating and inhibitory FcγRs compared to WT BMDCs. As the expression of *Fcgr1, Fcgr2b and Fcgr3* were found to be similar between WT and *Ptpn22*$^{-/-}$ BMDCs, this indicates that PTPN22 may be regulating FcγRs post-transcriptionally. This may include regulating trafficking of FcγRs to the cell surface, their retention there, or rates of receptor internalisation. Intracellular expression of FcγRs and their transport was not investigated, so it is not possible to determine exactly why *Ptpn22*$^{-/-}$ BMDCs express a lower level of the inhibitory receptor, FcγRIIb on their cell surface. Reduced expression of the inhibitory receptor may alter the activating/inhibitory (A/I) ratio, which could lead to an overall increase in positive signalling downstream of FcγRs in *Ptpn22*$^{-/-}$ BMDCs, and this could partly be responsible for the enhanced immune complex induced T cell proliferation that I have observed. However, as the difference in FcγRIIb expression is subtle, and only observed at the level of expression and not percent positivity, it is unlikely that this is the only mechanism. In addition, if PTPN22 is regulating the expression of FcγRIIb, this only

appears to occur in differentiated DCs, as FcγRIIb expression was found to be similar on the cell surface of bone marrow preDCs and CDPs. Other phosphatases have been shown to regulate the cell surface expression of receptors. For example, the non-receptor tyrosine phosphatase PTP-MEG2 is required for the transport of the neurotrophin receptor tropomyosin receptor kinase A (TrkA) to the cell surface of neurons[247]. PTP-MEG2 contains a Sec14 domain in its N-terminal which targets it to secretory vesicles[248], PTP-MEG2 can then dephosphorylate *N*-ethylmaleimide-sensitive fusion factor which causes vesicle fusion and transport to the plasma membrane. PTPN22 does not contain a Sec14 domain, so it may not be capable of regulating expression of FcγRIIb via this mechanism.

3.5.3 FcγR signalling and effector responses

Some of the responses I detected after immune complex stimulation, including the upregulation of co-stimulatory molecules, ROS production and calcium flux, were subtle. This may have been because the ova ICs bind to all FcγRs present on the cells, so these will crosslink both the activating and inhibitory receptors. As a result, the inhibitory receptor FcγRIIb may dampen down the response through the activating receptors. To circumvent this issue, it would have been interesting to repeat these assays in the presence of a FcγRIIb blocking antibody, such that only signalling downstream of the activating receptors would be measured.

Due to the unavailability of reagents, I had to use an ova antibody to make the ova ICs which was not guaranteed to be endotoxin free. For this reason, I also included polymyxin B in the stimulations to try to reduce the potential endotoxin contamination. This allowed me to be more confident that I was looking at FcγR signalling, and not a combination of responses downstream of FcγRs and TLR4. Although I did not directly test the level of endotoxin in the anti-ova, when the anti-ova was given to the cells with polymyxin B, the resulting BMDC maturation and cytokine secretion was similar to unstimulated conditions, indicating that the majority of the results seen with the ova ICs were due to FcγR dependent responses, as opposed to any potential endotoxin contamination. Also, PTPN22 was found to be dispensable for immune complex induced T cell proliferation when the BMDCs were LPS matured, whereas it was required to modulate T cell proliferation in the absence of LPS. This indicates that LPS is not contributing greatly to the results seen in the assays using ova ICs alone.

For analysing BMDC immune complex induced calcium flux, I was not able to get consistent results. In addition to using ova ICs added in suspension as the stimulation, I also tried heat aggregated rabbit IgG (which should efficiently crosslink FcγRs) and a commercial BSA:anti-BSA

IC (OxyBURST), but I was still unsuccessful in measuring robust immune complex induced calcium flux. The role of PTPN22 in neutrophil ROS production after FcγR engagement was investigated in a recent paper. They found that *Ptpn22*$^{-/-}$ bone marrow neutrophils showed lower calcium flux in response to immobilised BSA:anti-BSA immune complexes[63]. I did not try to use immobilised immune complexes, but it would be interesting to see if I could observe robust BMDC calcium flux using this protocol.

If time had permitted, it would have been worthwhile to look at signalling after FcγR engagement in the presence or absence of PTPN22. This could be achieved by using immune complexes or antibodies to crosslink FcγRs and then monitoring the phosphorylation status of signalling intermediates including Src, Syk and ERK by western blotting. I would hypothesise that in the absence of PTPN22, you would see enhanced phosphorylation of signalling intermediates after FcγR engagement.

3.5.4 The role of PTPN22 in DCs on T cell proliferation

I did not find a role for PTPN22 in inducing T cell proliferation after BMDC ova or $OVA_{323-339}$ peptide pulsing. It has been shown previously that $CD11b^{+}$ splenic macrophages expressing *Ptpn22*^{R619W} and pulsed with ova, are more efficient at causing T cell activation and proliferation[67]. This was attributed to enhanced macrophage expression of MHCII, CD80 and CD86, and an enhanced phagocytic capacity after LPS treatment. This is in contrast to my data using *Ptpn22*$^{-/-}$ BMDCs. In addition, I have not observed any differences in cell surface expression of MHCII and co-stimulatory molecules on WT and *Ptpn22*$^{-/-}$ BMDCs in response to LPS (Figure 3-16). These differences may be due to PTPN22 playing a different role in macrophages and DCs, and/or it may be that lacking the gene has no affect whereas expression of the autoimmune associated variant of PTPN22 is important. For example, B cell receptor signalling is unaffected in *Ptpn22*$^{-/-}$ mice, but is enhanced in *Ptpn22*^{R619W} mice[13].

Despite finding that PTPN22 is dispensable for immune complex induced BMDC maturation, and in inducing T cell proliferation after ova and $OVA_{323-339}$ pulsing, I did find that PTPN22 negatively regulates processes leading to immune complex induced T cell activation. It was somewhat surprising that the lack of BMDC PTPN22 expression affected T cell proliferation and CD25 and CD69 expression, but that it had no effect on cytokine secretion after 6 days of co-culture. It has however been shown that T cell proliferation and cytokine secretion can be uncoupled. For example, the TCR-CD3 complex contains ten ITAMs, and phosphorylation of the tyrosine residues in the CD3 ITAMs leads to the recruitment of ZAP-70. In turn, this aids the

phosphorylation of SLP-76 and Lat, allowing for further downstream signalling involving Vav1 (for cytoskeletal rearrangement), Erk and the translocation of transcription factors such as NFAT to the nucleus. Although lots of these signalling events are required for cytokine production, the exact signals required for T cell proliferation are less well understood. It has however been shown that the number of ITAMs present in the TCR-CD3 complex directly correlates with T cell proliferation, but that this is not the case for cytokine production[249]. This indicates that depending on the signal strength received by the T cell from the APC, T cell proliferation and cytokine secretion could be differentially affected. In addition, it has been shown that T cells *in vivo* which are in the G1 phase of the cell cycle (i.e. not actively cycling) are still capable of producing IFNγ, showing that proliferation and cytokine secretion are not always linked[250]. Finally, it has been demonstrated using LPS stimulated human DCs that inhibition of the kinases c-Src and Lyn (using the small molecular inhibitor PP1) leaves the cells less capable of inducing T cell IFNγ secretion, while still being able to cause T cell proliferation. This was shown to be due to a role of Src family kinases in stabilising the transcription factor c-Jun, which is needed for the transcription of cytokine genes[251].

Although PTPN22 has been previously shown to play an important regulatory role downstream of the TCR in T cells, by dephosphorylating kinases including Lck and ZAP-70, I found that lacking expression of PTPN22 in the OT-II T cells used in the co-cultures did not further effect their ova IC induced proliferation. I had hypothesised that *Ptpn22*$^{-/-}$ T cells would show enhanced proliferation after presentation of immune complexed derived peptides by *Ptpn22*$^{-/-}$ BMDCs, as compared to WT T cells, but this is not what I have found. This indicates that in relation to immune complex induced T cell proliferation, PTPN22 may be playing a more important role in the BMDC compared to the T cell.

When immune complex induced T cell proliferation assays were conducted *in vivo*, I found that PTPN22 expression in BMDCs or endogenous APCs was not required to modulate T cell proliferation. There are many reasons why the results from the *in vitro* co-cultures were not corroborated *in vivo.* These include the fact that the *in vitro* co-cultures are a reductionist approach where only BMDCs and ova specific T cells are present. The situation *in vivo* is a lot more complex, with multiple cell types being capable of presenting antigen to the responding T cells. If PTPN22 is not required for antigen processing and presentation in certain cell types, then this may compensate for a potential role of PTPN22 in a different cell type *in vivo.* Another difference between the *in vitro* co-cultures and the *in vivo* situation is that GM-CSF induced BMDCs do not represent an *in vivo* DC population, and as PTPN22 has been shown to play different roles in different immune cell subsets, this discrepancy may be explained by the fact that PTPN22 may function differently in GM-CSF induced BMDCs compared to *in vivo* DC

populations. In addition, the results from the FITC painting experiment indicated that PTPN22 was not required for migration of APCs from the footpad to the draining popliteal LN. This may go some way towards explaining why transferred T cells proliferated normally *in vivo* in WT and *Ptpn22*$^{-/-}$ mice after immunisation with ova ICs, as the APCs would have been capable of internalising the immune complexes, and migrating to the draining LNs, in order to come into contact with the ova specific T cells.

3.5.5 Crosstalk between FcγR and TLR4 signalling

The difference in the requirement for PTPN22 to regulate T cell proliferation in the absence or presence of LPS may be due to a variety of factors. The strength of signalling downstream of TLR4 engagement may be more than downstream of FcγR engagement, therefore the presence of LPS may mask the role that PTPN22 is playing in regulating FcγR signalling. Signal strength would be affected by the proportion of TLR4 and FcγRs which are bound by their ligands, and also on the affinity of the receptors for their ligands. It has been demonstrated that TLR4 is involved in FcγRIII signalling. This indicates that these receptor signalling pathways are connected. Lysates from immune complex stimulated neutrophils and macrophages were immunoprecipitated with anti-TLR4 and by immunoblotting, FcγRIII was found to be associated. This association was not detected after LPS stimulation alone, but was enhanced by combined LPS and immune complex stimulation. In addition, IL-6 and TNFα secretion after immune complex stimulation was diminished from neutrophils and macrophages from TLR4 mutant mice (which have a missense mutation in *Tlr4*). This was accompanied by reduced tyrosine phosphorylation of FcRγ in TLR4 mutant cells. However, neutrophils and macrophages from *FcγRIII*$^{-/-}$ mice were equally capable as WT cells to secrete cytokines in response to LPS treatment. This indicates that a functional TLR4 is required for phagocytes to respond to immune complex stimulation, but that FcγRIII is not required for TLR4 signalling[252]. In addition, BMDCs treated with LPS for 48 hours have been shown to have a reduced ability to subsequently cause immune complex induced $CD8^+$ T cell proliferation, whereas 18 hours of LPS pre-treatment enhanced immune complex induced $CD8^+$ T cell proliferation[253]. This demonstrates that FcγR and TLR signalling are linked.

3.5.6 PTPN22 potential redundancy with other phosphatases

A potential reason why some of the data presented in this Chapter show that PTPN22 is not required, may be due to the presence of other phosphatases with functional redundancy. For example, PTPN12 is a protein tyrosine phosphatase which belongs to the same family as PTPN22[254]. As I have found for PTPN22, PTPN12 is also dispensable for ova induced T cell proliferation, but it is required for the induction of optimal IFNγ secretion by T cells[232]. This may explain why there was no difference in IFNγ secretion by T cells co-cultured with *Ptpn22*$^{-/-}$ BMDCs compared to WT BMDCs, as both will express PTPN12. The Src homology region 2 domain-containing phosphatase-1 (SHP-1, also known as PTPN6) is also expressed in DCs and has been shown to regulate T cell proliferation after DC ova pulsing. Splenic CD11c^{+} DCs lacking SHP-1 expressed higher levels of CD86 and CCR7 (but not MHCII, CD40 or CD80) *ex vivo*. These SHP-1 deficient DCs also secreted enhanced TNFα, IL-6, IL-1β, IL-10 and IFNβ at steady state, but also after 24 hours of LPS treatment. Overtime, these mice lacking expression of SHP-1 in DCs, showed an expansion of activated (CD62L^{lo} CD44^{hi}) CD4^{+} and CD8^{+} T cells in the spleen, which was accompanied by an increased ability of SHP-1 deficient DCs to induce OT-II T cell proliferation after ova pulsing *in vitro*[255].

The SH2-containing inositol 5'-phosphatase 1 (SHIP-1) has been shown to negatively regulate signalling downstream of the Fc receptor for IgE, FcεR1, such that SHIP-1 deficient mast cells require less stimulation to degranulate, flux calcium and phosphorylate ERK[256]. The SH2-containing inositol 5'-phosphatase 2 (SHIP-2) has also been found to regulate signalling downstream of FcγRs. Over expression of SHIP-2 in the human monocyte THP-1 cell line prevented *Nfkb* mediated gene transcription and activation of the serine/threonine kinase Akt (also known as protein kinase B) after FcγRIIa clustering[257].

An additional protein tyrosine phosphatase which is expressed in DCs is CD45. The role of CD45 in FcγR induced effector functions has been investigated in neutrophils. Crosslinking CD45 caused a reduction in FcγR induced calcium flux by human neutrophils[258]. A later study found that the addition of anti-CD45 to human neutrophils on which FcγRs had been crosslinked, led to a reduction in antibody-dependent cell-mediated cytotoxicity (ADCC), indicating that CD45 negatively regulates this neutrophil effector function after FcγR signalling. Crosslinking CD45 also led to an overall reduction in protein tyrosine phosphorylation and F-actin polymerisation after FcγR stimulation[259].

The inositol 3-phosphatase, phosphatase and tensin homologue (PTEN) has been shown to regulate FcγR signalling in mouse macrophages. In the absence of PTEN, mouse peritoneal

macrophages display enhanced Akt and ERK phosphorylation after FcγR signalling. Additionally, FcγR induced cytokine secretion, including TNFα, IL-6 and IL-10 was enhanced in the absence of PTEN expression[260].

As *Ptpn22*$^{-/-}$ BMDCs would express SHP-1, SHIP-1, SHIP-2, CD45 and PTEN, this indicates that other phosphatases may be compensating for the lack of PTPN22, and could partially explain why PTPN22 was not required for some of the immune complex induced effector functions which were investigated in this Chapter.

3.5.7 Differences between *Ptpn22*$^{-/-}$ and *Ptpn22*^{R619W} BMDCs

The data presented in this Chapter indicates that expression of the autoimmune associated variant of PTPN22 does not affect the ability of BMDCs to differentiate, express FcγRs, or to upregulate co-stimulatory molecules, secrete cytokines or induce T cell proliferation in response to immune complex stimulation. Therefore, the variant is not working as a gain- or loss-of-function variant in these instances. The immune cell phenotypes in *Ptpn22*$^{-/-}$ and *Ptpn22*^{R619W} mice do not always match, for example, *Ptpn22*$^{-/-}$ mice show an expansion of T_{regs} with age[57,58], but this is not found in *Ptpn22*^{R619W} mice[13].

4. Results: Investigating the role of PTPN22 in antigen uptake, processing and presentation in BMDCs

4.1 Introduction

DCs are professional antigen presenting cells, sampling their surroundings and scanning for antigens. They are able to initiate an immune response, or cause tolerance, by internalising, processing and presenting antigens to T cells on MHCI and MHCII. If the antigens are recognised in the context of an inflammatory signal, then the DC begins a process known as maturation[261]. This includes upregulating cell surface expression of MHCII and co-stimulatory molecules, acidification of lysosomal compartments, a reduction in macropinocytosis, and migration to draining lymph nodes – all of which aid in the initiation of an effective adaptive immune response. Although mature DCs downregulate their macropinocytotic capacity, they are still capable of receptor mediated endocytosis[242].

In Chapter 3, I demonstrated that *Ptpn22*$^{-/-}$ BMDCs pulsed with ova IC are more efficient at inducing ova specific T cell proliferation. In this Chapter, the potential mechanism(s) behind this were explored in more detail. The ability of WT and *Ptpn22*$^{-/-}$ BMDCs to bind, internalise, process and present a variety of antigens, including immune complexes was investigated. Regulation of any of these processes by PTPN22 would provide a mechanism by which ova IC pulsed *Ptpn22*$^{-/-}$ BMDCs cause augmented T cell proliferation.

4.2 Aims

This Chapter aimed to determine specifically whether PTPN22 is required for:

1. BMDC antigen binding and uptake.
2. BMDC antigen processing.
3. BMDC antigen presentation in MHCII and BMDC-T cell conjugate formation.

4.3 Results

4.3.1 PTPN22 is dispensable for Lucifer yellow macropinocytosis

Before studying immune complex uptake via FcyRs, I explored pathways of BMDC antigen uptake via macropinocytosis and receptor mediated endocytosis, starting with macropinocytosis. BMDCs utilise macropinocytosis to constitutively and non-selectively engulf particles. These include nutrients, soluble molecules and circulating antigens from their surrounding environment[262,263]. The process requires the actin cytoskeleton for the production of lamellipodia. These extend and retract from the plasma membrane and a proportion fold back and fuse with the membrane, thus forming a vesicle called a macropinosome which engulfs particles from the environment. Macropinocytosis does not require the expression of specific cell surface receptors and is also independent of clathrin[264]. Once particles are internalised via macropinocytosis, they can be presented on MHCI and MHCII molecules[103,105,263]. I chose as a model for studying this process Lucifer yellow (LY) because it is a water-soluble dye which can also function as a fluid phase marker for macropinocytosis, where uptake can be easily measured by flow cytometry.

The requirement for Src and Syk family kinases for macropinocytosis was first determined. WT BMDCs were pre-incubated with Src and Syk family kinase inhibitors before being incubated with LY for 0-30 minutes at 37°C. Inhibition of Src and Syk kinases had no effect on LY uptake by WT BMDCs, indicating that these kinases are not involved in the process (Figure 4-1a). Next, to determine whether PTPN22 was required for macropinocytosis, WT and *Ptpn22*$^{-/-}$ BMDCs were incubated with LY for 0-30 minutes at 37°C (see Materials and Methods Figure 2-13 for experimental setup). Over time, the LY geometric mean fluorescent intensity (GMFI) signal increased, as expected (Figure 4-1b). However, LY internalisation was similar between WT and *Ptpn22*$^{-/-}$ BMDCs (Figure 4-1b).

Following Toll-like receptor (TLR) induced BMDC maturation, the rate of macropinocytosis is decreased[103,242,262], although there is a transient increase in macropinocytosis within 30-45 minutes of TLR stimulation, due to enhanced membrane ruffling. This allows for a temporary enhancement in antigen capture and presentation in the presence of an inflammatory signal[265]. Given that PTPN22 regulates signals transduced by pattern recognition receptors, notably dectin-1, I tested whether *Ptpn22*$^{-/-}$ BMDCs were equally capable of downregulating LY uptake after TLR stimulation. WT and *Ptpn22*$^{-/-}$ BMDCs were matured overnight using LPS. As expected,

LPS treatment reduced LY uptake, in comparison to immature BMDCs (Figure 4-1c), which is in agreement with previously published data[103]. However, WT and *Ptpn22*$^{-/-}$ BMDCs displayed a similar capacity to reduce LY internalisation after LPS treatment (Figure 4-1c-d).

Finally, expression of the autoimmune associated variant of PTPN22 was tested to see if it affected macropinocytosis of LY by BMDCs. Both *Ptpn22*^{R619} (WT) and *Ptpn22*^{R619W} BMDCs internalised LY to a similar extent over 30 minutes at 37°C (Figure 4-1e). In keeping with the findings from the Src and Syk inhibitor experiment (Figure 4-1a), these data confirmed that PTPN22 is not required for BMDC macropinocytosis.

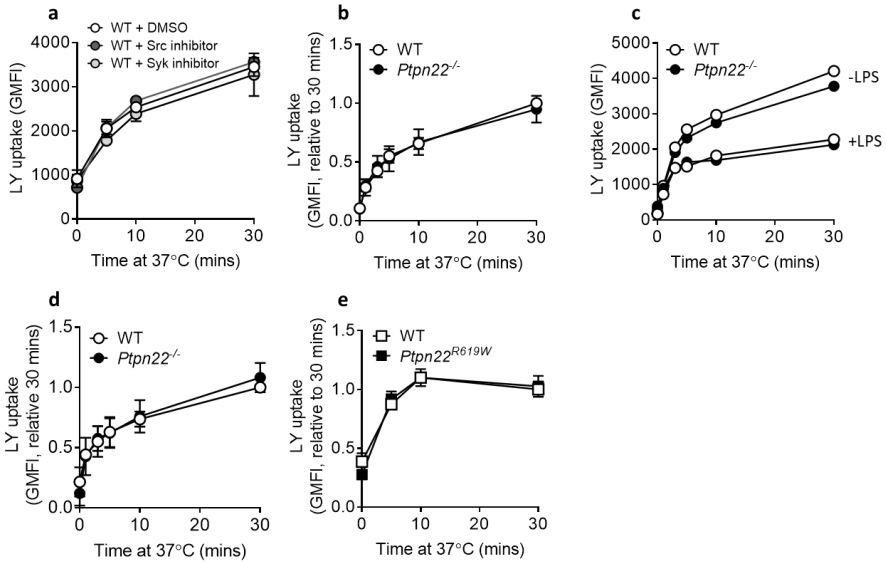

Figure 4-1: PTPN22 is dispensable for macropinocytosis of Lucifer yellow.

(a) WT BMDC Lucifer yellow (LY) uptake after pre-treatment with DMSO (vehicle control, white), Src inhibitor (dark grey) or Syk inhibitor (grey); n = 3 ± s.d. (b) LY uptake by WT (white) and Ptpn22$^{-/-}$ *(black) immature BMDCs. Data shown are geometric mean fluorescence intensity (GMFI) relative to maximal WT uptake at 30 minutes; n = 4 ± s.d. (c) LY uptake by immature (-LPS) or LPS matured (+LPS) WT (white) and Ptpn22*$^{-/-}$ *(black) BMDCs, showing representative LY GMFI of 3 independent experiments. (d) LY uptake by LPS matured WT (white) and Ptpn22*$^{-/-}$ *(black) BMDCs, showing GMFI relative to maximal WT uptake at 30 minutes; n = 3 ± s.d. (e) LY uptake by WT (white) and Ptpn22*^{R619W} *(black) immature BMDCs. Data shown are GMFI relative to maximal WT uptake at 30 minutes; n = 3 ± s.d. All data is gated on CD11c*$^{+}$ *live singlets.*

4.3.2 PTPN22 does not regulate antigen uptake via TLR2 or dectin-1

After determining that PTPN22 is dispensable for non-selective antigen uptake via macropinocytosis, I next investigated whether PTPN22 was required for receptor mediated endocytosis of specific antigens. DCs use a vast array of pattern recognition receptors (PRRs) to

recognise pattern associated molecular patterns (PAMPs) within microbial and mammalian antigens[266]. PRRs include TLRs, C-type lectin receptors (CLRs), nucleotide oligomerisation domain (NOD)-like receptors (NLRs) and retinoic acid inducible gene-I (RIG-I) like receptors (RLRs). Two PRR ligands were used to investigate whether PTPN22 may regulate receptor mediated endocytosis: *Listeria monocytogenes*, which is phagocytosed via TLR2 and *Candida albicans*, which is internalised by the CLR dectin-1.

The requirement for Src family kinases in TLR2 mediated endocytosis has been previously investigated. Src was found to be required for efficient internalisation of *Listeria monocytogenes* by the human epithelial Caco-2 cell line[267]. This paper also reported that Src family kinase inhibition using PP1 subtly reduced entry of *Listeria monocytogenes* into HEK293 cells. After ligand binding to TLR2, the tyrosine kinases Btk and Fyn (a Src family kinase) have been shown to phosphorylate tyrosine residues Y616 and Y761 within the TLR2 Toll/interleukin-1 receptor (TIR) domain. Phosphorylation of these residues is required for the recruitment of PI3K and Rac-1, and for NFκB activation[268], identifying a role of tyrosine phosphorylation in TLR2 signalling. The role of Syk in receptor mediated endocytosis via TLR2, on the other hand, has not been investigated. However, Syk has been shown to partially mediate LPS-dependent endocytosis of TLR4 and to play a role in downstream signalling in mouse BMDMs[269]. This was also shown in a more recent paper, where Syk inhibition led to a reduction in TLR4 endocytosis of *E. coli* by mouse BMDCs[270].

The requirement for Src and Syk family kinases in dectin-1 dependent phagocytosis appears to vary depending on the species and cell type under investigation. This is despite the fact that Src family kinases are responsible for the phosphorylation of the tyrosine within the hemi-ITAM motif in the cytoplasmic tail of dectin-1, which then recruits Syk, ultimately leading to downstream signalling. Syk has been found to be dispensable for dectin-1 dependent phagocytosis of fluorescent zymosan particles by RAW 264.7 macrophages, using the Syk inhibitor piceatannol, and by using *Syk*$^{-/-}$ mouse bone marrow macrophages[271]. A separate paper used piceatannol to inhibit Syk and showed a 50% reduction in zymosan uptake by RAW 264.7 macrophages[272]. The authors also inhibited Src family kinases using PP2 and showed a dramatic reduction in zymosan uptake by RAW 264.7 macrophages[272]. A more recent study found that Syk, but not Src was required for phagocytosis of fluorescent zymosan by primary human monocytes, using small molecule inhibitors[273]. In a separate report using WT and *Syk*$^{-/-}$ mouse BMDCs, Syk was again found to be required for internalisation of fluorescent zymosan[274].

As a role of Src and Syk family kinases in TLR2 mediated endocytosis has not been proven definitively, I first wanted to determine whether they were required for BMDC TLR2-mediated

ligand internalisation. A heat killed preparation of *Listeria monocytogenes* (HKLM) was stained with a fluorescent viability dye, in which all HKLM would be stained, and incubated with WT BMDCs, after pre-treatment with Src and Syk family inhibitors. The proportion of internalised HKLM increased with increasing time at 37°C, but the pre-treatment with either inhibitor had no effect, indicating that these kinases are not required for HKLM uptake by BMDCs (Figure 4-2a).

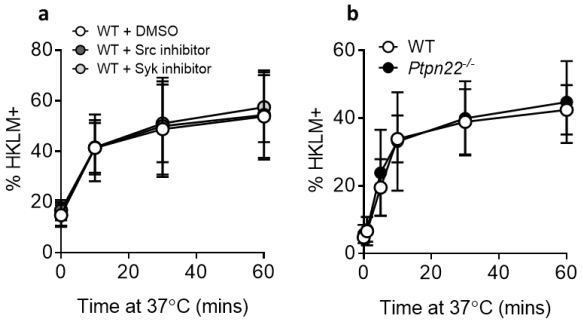

Figure 4-2: PTPN22 is dispensable for heat killed Listeria monocytogenes (HKLM) uptake.

(a) WT BMDCs were pre-treated with DMSO (vehicle control, white), Src inhibitor (dark grey) or Syk inhibitor (grey), before being incubated with HKLM (1 DC:30 HKLM) for 0-60 minutes at 37°C. Data shows HKLM uptake (gated on CD11c$^+$ singlets). n = 5 ± s.d. (b) WT (white) and Ptpn22$^{-/-}$ (black) BMDCs were incubated with HKLM (1 DC:30 HKLM) for 0-60 minutes at 37°C. Data shows HKLM uptake (gated on CD11c$^+$ singlets). n = 4 ± s.d.

To identify a role of PTPN22 in endocytosis via TLR2 and dectin-1, HKLM and heat killed *Candida albicans* (HKCA) were stained with a fluorescent dye and incubated with WT and *Ptpn22*$^{-/-}$ BMDCs for 0-60 minutes at 37°C (see Materials and Methods Figure 2-14 for experimental setup). Internalisation of both HKLM and HKCA increased over time at 37°C, but no difference in uptake was observed depending on the BMDC genotype (Figures 4-2b and 4-3a). To ensure that the HKCA was being internalised via dectin-1, WT BMDCs were pre-incubated with a dectin-1 blocking antibody, prior to incubation with HKCA. Uptake of HKCA was greatly reduced by the presence of the dectin-1 antibody, indicating that HKCA was internalised via this receptor (Figure 4-3a).

To determine whether expression of PTPN22^{R619W} would affect the ability of BMDCs to internalise HKCA, endocytosis assays were performed using *Ptpn22*^{R619} (WT) and *Ptpn22*^{R619W} BMDCs. As with *Ptpn22*$^{-/-}$ BMDCs, expression of PTPN22^{R619W} did not affect HKCA uptake (Figure 4-3b). Together these data indicate that despite evidence for a potential requirement for Src and Syk family kinases in TLR2 and dectin-1 dependent uptake, PTPN22 is not required for uptake of antigens via these receptors.

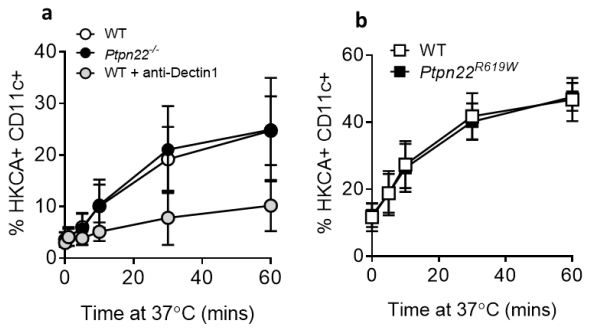

Figure 4-3: PTPN22 is dispensable for heat killed Candida albicans (HKCA) uptake.

(a*) Uptake of HKCA uptake by WT (white) and Ptpn22$^{-/-}$ (black) BMDCs or WT BMDCs pre-treated with anti-Dectin1 (grey) (1 DC:10 HKCA). n = 6 (WT and Ptpn22$^{-/-}$) or 3 (WT + anti-Dectin1) ± s.d. (b) Uptake of HKCA uptake by WT (white) and Ptpn22^{R619W} (black) BMDCs. (1 DC:10 HKCA). n = 4 ± s.d.*

4.3.3 PTPN22 does not regulate mannose receptor mediated antigen uptake

The mannose receptor (CD206) is a C-type lectin receptor which recognises mannose, fucose and N-acetylglucosamine present in glycans[275]. The requirement for the mannose receptor in soluble ovalbumin (ova) internalisation was demonstrated using BMDCs from *Mr*$^{-/-}$ mice (which lack expression of the mannose receptor), in which case, ova was not internalised, and ova specific CD8^{+} T cells were not activated[276]. The C-terminal intracellular domain does not contain specific signalling motifs[277], indicating that endocytosis via the mannose receptor may not require Src and Syk family kinases. However, Src family kinases are required for actin protrusions needed during early receptor mediated phagocytosis[267].

Before assessing whether PTPN22 was required for ova internalisation, I first ascertained the cell surface expression of the mannose receptor. This was found to be similar on WT and *Ptpn22*$^{-/-}$ BMDCs (Figure 4-4a) and *Ptpn22*^{R619} (WT) and *Ptpn22*^{R619W} BMDCs (Figure 4-4b).

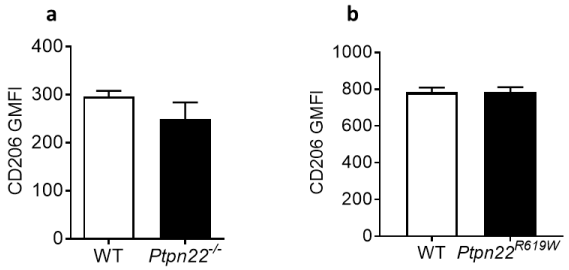

Figure 4-4: WT, Ptpn22$^{-/-}$ and Ptpn22^{R619W} BMDCs have similar cell surface expression of the mannose receptor.

(a-b) CD206 (mannose receptor) geometric mean fluorescence intensity (GMFI) on WT (white) and Ptpn22$^{-/-}$ (white) (a) and WT (white) and Ptpn22^{R619W} (black) (b) BMDCs (gated on CD11c^{+} live singlets). n = 5 ± s.d. (a), n = 3 ± s.d. (b).

To determine whether Src and Syk family kinases were required for ova uptake, WT BMDCs were pre-incubated with Src and Syk family kinases inhibitors, prior to incubation with fluorescent ova (ova-AF488) at 37°C for 0-60 minutes. Ova-AF488 uptake was measured by flow cytometry and although ova-AF488 internalisation at 37°C increased over time, it was not affected by Src and Syk family kinase inhibition, indicating that these kinases are not required for the process (Figure 4-5a).

I next assessed if PTPN22 was required for receptor mediated endocytosis of ova via the mannose receptor. WT, *Ptpn22$^{-/-}$*, *Ptpn22^{R619}* and *Ptpn22^{R619W}* BMDCs were incubated with ova-AF488 at 37°C for 0-60 minutes and uptake was monitored (see Materials and Methods Figure 2-15 for experimental setup). Over time, the proportion of ova-AF488^{+} BMDCs increased, but uptake at all time points by WT and *Ptpn22$^{-/-}$* BMDCs and by WT and *Ptpn22^{R619W}* BMDCs was quantitatively similar (Figure 4-5b-c). These data indicate that PTPN22 is not required for mannose receptor mediated endocytosis and demonstrates that WT and *Ptpn22$^{-/-}$* BMDCs used in the *in vitro* co-cultures (in Chapter 3), would have been capable of internalising similar amounts of ova, prior to culture with ova specific CD4^{+} T cells.

During maturation, the endocytic capacity of DCs is altered. As already discussed, this includes a dramatic reduction in macropinocytosis. However, DCs are still capable of receptor mediated endocytosis, albeit at a reduced rate[242]. To determine whether mature *Ptpn22$^{-/-}$* BMDCs endocytose ova via the mannose receptor at a similar rate to WT BMDCs, cells were matured with LPS and the ova uptake assay was performed. Although there was a slight reduction in the rate of ova internalisation after LPS treatment, uptake was similar by WT and *Ptpn22$^{-/-}$* BMDCs (Figure 4-5d).

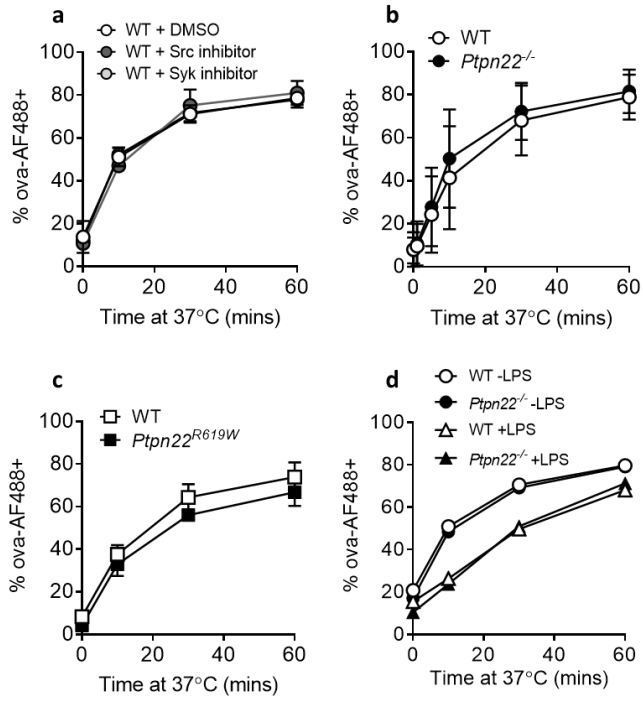

Figure 4-5: PTPN22 is not required for binding and internalisation of ova via mannose receptor mediated endocytosis and macropinocytosis.

(a) WT BMDC ova uptake after pre-treatment with DMSO (vehicle control, white), Src inhibitor (dark grey) or Syk inhibitor (grey). Graph shows % ova-AF488+ (gated on CD11c$^+$ live singlets). n = 3 ± s.d. (b) WT (white) and Ptpn22$^{-/-}$ (black) BMDCs were incubated with ovalbumin-AF488 for 0-60 minutes at 37°C. Graph shows % ova-AF488+ (gated on CD11c$^+$ live singlets). n = 5 ± s.d. (c) WT (white) and Ptpn22^{R619W} (black) BMDCs were incubated with ovalbumin-AF488 for 0-60 minutes at 37°C. Graph shows % ova-AF488+ (gated on CD11c$^+$ live singlets). n = 3 ± s.d. (d) WT (white) and Ptpn22$^{-/-}$ (black) immature (circle) and LPS matured (triangle) BMDCs were incubated with ovalbumin-AF488 for 0-60 minutes at 37°C. Graph shows % ova-AF488+ (gated on CD11c$^+$ live singlets). n = 3 (technical replicates) ± s.d.

As ova can be internalised via the mannose receptor and macropinocytosis, I carried out uptake assays in which the unbound ova-AF488 was removed by washing, prior to uptake at 37°C. In this case, ova uptake should be solely via the mannose receptor. As with the previous uptake assays, PTPN22 was not required for ova internalisation (Figure 4-6).

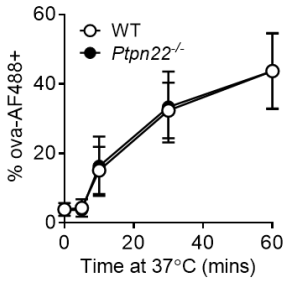

Figure 4-6: PTPN22 is not required for internalisation of ova via the mannose receptor.

WT (white) and Ptpn22$^{-/-}$ (black) BMDCs were incubated with ovalbumin-AF488 for 45 minutes on ice, after which unbound ova was removed by washing (such that uptake should be via the mannose receptor, and not via the mannose receptor and macropinocytosis). BMDCs were then incubated for 0-60 minutes at 37°C for uptake. Graph shows % ova-AF488+ (gated on CD11c^{+} live singlets). n = 8-11 ± s.d.

Finally, as GM-CSF BMDCs do not represent *in vivo* DC subsets, I carried out an ova uptake assay using WT and *Ptpn22*$^{-/-}$ Flt3L BMDCs. Again, PTPN22 was found to be dispensable for ova uptake (Figure 4-7).

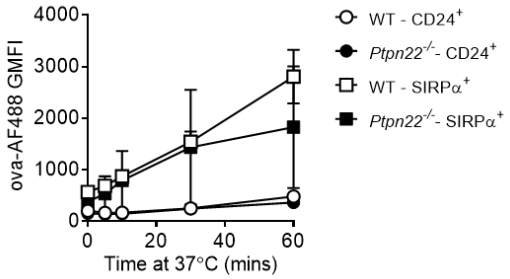

Figure 4-7: PTPN22 is dispensable for Flt3L BMDC ova internalisation.

WT (white) and Ptpn22$^{-/-}$ (black) Flt3L induced BMDCs were incubated with ovalbumin-AF488 for 45 minutes on ice, then incubated for 0-60 minutes at 37°C for uptake. Graph shows ova-AF488 GMFI (gated on CD11c^{+}, CD24^{+} (circle) or CD11c^{+}, SIRPα^{+} (square) live singlets). n = 2 ± s.d. (representative of 5 independent experiments).

4.3.4 Splenic conventional DC ovalbumin uptake does not require PTPN22

To determine whether PTPN22 may play a role in receptor mediated endocytosis of ova by *ex vivo* DCs, the spleens of WT, *Ptpn22*$^{-/-}$, *Ptpn22*^{R619} (WT) and *Ptpn22*^{R619W} mice were digested and red blood cells were lysed. Splenocytes were incubated with ova-AF647 for 45 minutes either on ice or at 37°C. Ova internalisation was monitored by flow cytometry, by gating on conventional (CD11c^{+} MHCII^{+}) splenic DCs (cDCs). WT, *Ptpn22*$^{-/-}$, *Ptpn22*^{R619} and *Ptpn22*^{R619W} splenic DCs internalised more ova-AF647 when incubated at 37°C compared to the

internalisation observed on ice, but the genotype of the DC did not affect ova-AF647 uptake (Figure 4-8a-c). This is in agreement with my data using BMDCs (Figure 4-5), and shows that PTPN22 is dispensable for mannose receptor mediated endocytosis of ova by DCs.

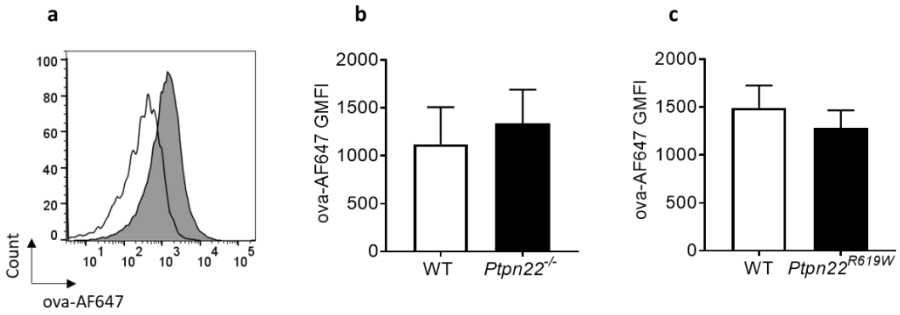

Figure 4-8: PTPN22 is dispensable for uptake of ova by splenic DCs.

(a*) Representative flow cytometry plot showing ova-AF647 uptake by CD11c$^+$ MHCII$^+$ splenic DCs incubated with ova-AF647 on ice (white) or at 37°C (grey) for 45 minutes. (b-c) WT (white) and Ptpn22$^{-/-}$ (black) (b) or WT (white) and Ptpn22^{R619W} (black) (c) splenocytes were incubated with ova-AF647 for 45 minutes at 37°C. Data shows ova-AF647 uptake by splenic DCs (GMFI, gated on lineage$^-$, CD11c$^+$, MHCII$^+$ live singlets). n = 4 ± s.d.*

4.3.5 FcγR-mediated binding and internalisation of immune complexes occurs independently of PTPN22

As ova IC pulsed *Ptpn22*$^{-/-}$ BMDCs caused enhanced ova specific CD4$^+$ T cell proliferation (Figures 3-18d and 3-19c), I next wanted to determine if PTPN22 regulated ova IC induced T cell proliferation by affecting FcγR dependent binding and uptake of ova ICs. To begin, the dependency on FcγRs was tested for ova IC uptake. WT BMDCs were pre-incubated with antibodies against FcγRI, FcγRII/III and FcγRIV before being incubated with ova-AF488:anti-ova ICs (ova-AF488 ICs). Pre-incubation with FcγR antibodies greatly reduced uptake of the fluorescent ova ICs, indicating that ova IC internalisation is FcγRs dependent (Figure 4-9a). The requirement for Src and Syk family kinases on uptake of ova-AF488 ICs was next tested. WT BMDCs were incubated with inhibitors of Src and Syk family kinases before being incubated with ova-AF488 ICs. This also led to a significant reduction in ova IC internalisation (Figure 4-9b), which is in agreement with previous published data demonstrating a role for Src and Syk family kinases in IC internalisation[121,122].

Having confirmed the requirement for Src and Syk family kinases in mediating ova-AF488 IC uptake, I next assessed if PTPN22 was required for ova-AF488 IC binding and internalisation. WT and *Ptpn22*$^{-/-}$ BMDCs were incubated with ova-AF488 ICs for 60 minutes on ice and cell surface

binding was assessed by flow cytometry (see Materials and Methods Figure 2-16 for experimental setup). A similar proportion of WT and *Ptpn22*$^{-/-}$ BMDCs had ova-AF488 ICs bound to their cell surface (Figure 4-9c). Next, ova-AF488 IC internalisation was assessed. The proportion of BMDCs that internalised ova-AF488 ICs increased over time at 37°C, but both WT and *Ptpn22*$^{-/-}$ BMDCs internalised similar amounts of ova-AF488 ICs (Figure 4-9d). This data shows that PTPN22 is dispensable for FcγR mediated binding and endocytosis of ova-AF488 ICs, therefore differences in these processes do not explain the enhanced T cell proliferation caused by ova IC pulsed *Ptpn22*$^{-/-}$ BMDCs (Figure 3-19c).

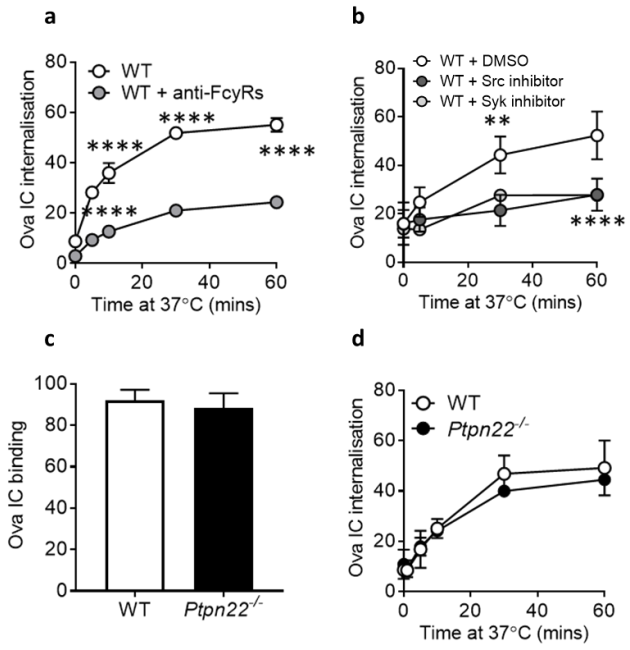

Figure 4-9: PTPN22 is dispensable for FcγR dependent immune complex binding and uptake.

(a*) WT BMDC ova-AF488 IC internalisation with (grey) or without (white) pre-incubation with anti-FcγRs (%, gated on CD11c*$^{+}$*, anti-rabbit*$^{-}$ *live singlets). n = 3 ± s.d.; ****p<0.0001 using 2-way ANOVA with Sidak's multiple comparisons test. (b) WT BMDC ova-AF488 IC internalisation after pre-treatment with DMSO (vehicle control, white), Src inhibitor (dark grey) or Syk inhibitor (grey) (%, gated on CD11c*$^{+}$*, anti-rabbit*$^{-}$ *live singlets). n = 7, 4, 3 ± s.d.; **p<0.01, ****p<0.0001 using 2-way ANOVA with Tukey's multiple comparisons test. (c) WT (white) and Ptpn22*$^{-/-}$ *(black) BMDCs were incubated with ova-AF488 ICs for 1 hour on ice. Cell surface ova-AF488 IC binding was determined (gated on CD11c*$^{+}$*, anti-rabbit*$^{+}$ *live singlets). n = 3-5 ± s.d. (d) Combined ova-AF488 IC internalisation by WT (white) and Ptpn22*$^{-/-}$ *(black) BMDCs was determined (gated on CD11c*$^{+}$*, anti-rabbit*$^{-}$ *live singlets). n = 3-5 ± s.d.*

4.3.6 Ova degradation occurs independently of PTPN22

Having established that PTPN22 was dispensable for immune complex binding and uptake, the next step to investigate was immune complex degradation. After antigens are internalised they

enter phagocytic endosomes which can fuse with acid rich lysosomes, allowing for antigen degradation. Once degraded into peptides, these can be presented in the context of MHCI and MHCII, as peptide-MHC complexes.

To assess antigen processing, BMDCs were incubated with ovalbumin-AF594 coated polystyrene beads for 0-5 hours at 37°C. Internalised beads were identified by staining with rabbit anti-ovalbumin followed by F(ab')2 goat anti-rabbit IgG-AF647, such that internalised beads could be identified as F(ab')2 goat anti-rabbit IgG-AF647^{-} (see Materials and Methods Figure 2-17 for experimental setup). To determine antigen degradation, loss of ovalbumin-AF594 fluorescence was assessed by flow cytometry on internalised beads[278]. In agreement with uptake of ovalbumin-AF488 (Figure 4-5b), both WT and *Ptpn22*$^{-/-}$ BMDCs were equally capable of internalising ovalbumin-AF594 coated beads (Figure 4-10b). Over time at 37°C, the intensity of ovalbumin-AF594 fluorescence on beads internalised by the BMDCs reduced (Figure 4-10c), indicative of antigen degradation. However, the amount of degradation (Figure 4-10c) and the proportion of internalised beads with degraded ova (Figure 4-10d) were similar for WT and *Ptpn22*$^{-/-}$ BMDCs, indicating that PTPN22 is dispensable for antigen processing, at least in this experimental system.

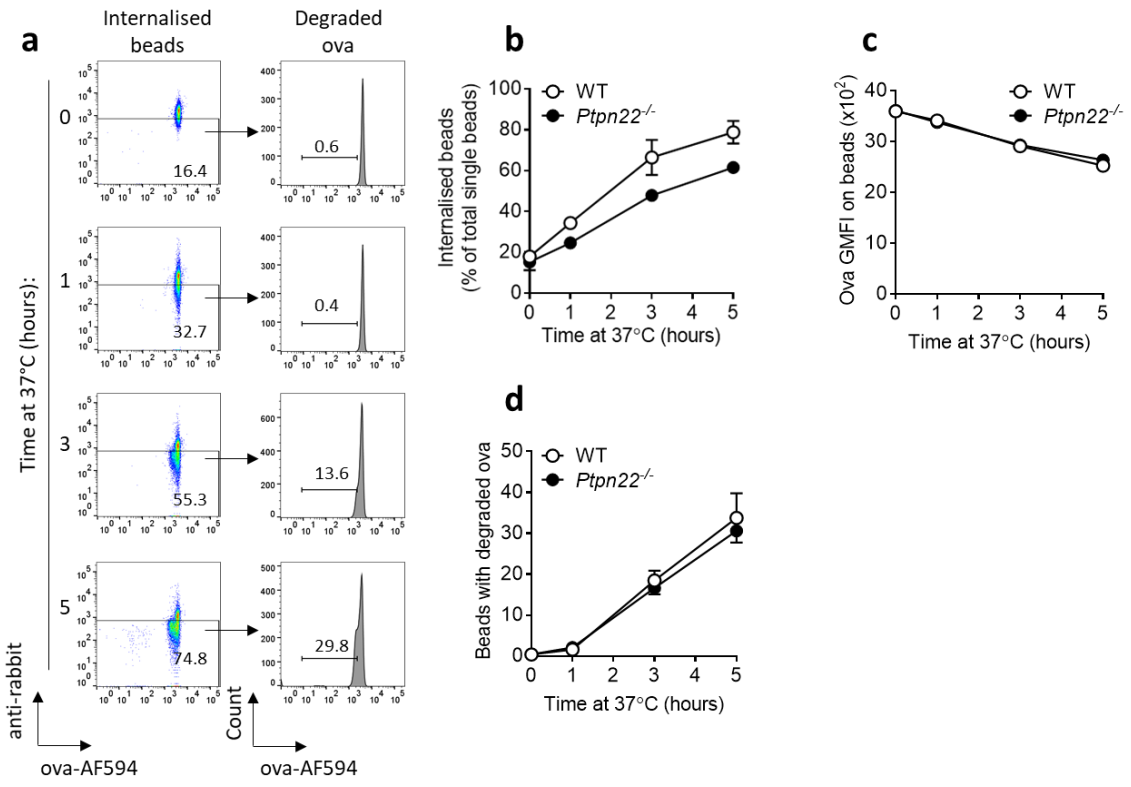

Figure 4-10: PTPN22 is not required for degradation of internalised ova.

(a-d) WT and Ptpn22$^{-/-}$ BMDCs were incubated with ova-AF594 coated beads for 0-5 hours at 37°C. (a) Representative flow cytometry plots showing ova-AF594 coated bead internalisation and ova degradation by BMDCs. (c-d) Graphs shows the proportion of ova-AF594 coated beads that were internalised (b), ova-AF594 geometric mean fluorescence intensity (GMFI) of internalised ova-AF594 coated beads (c), and the proportion of internalised ova-AF594 coated beads that have degraded ova-AF594 on them (d) by WT (white) and Ptpn22$^{-/-}$ (black) BMDCs (%, gated on single, anti-rabbit^{-} beads). n = 2 ± s.d. (representative of 7 independent experiments).

4.3.7 Immune complex degradation occurs independently of PTPN22

To determine whether PTPN22 may regulate degradation of immune complex derived antigens, WT and *Ptpn22*$^{-/-}$ BMDCs were incubated with ova-AF594:anti-ova coated polystyrene beads for 0-7 hours at 37°C, and antigen degradation was again measured on internalised beads by flow cytometry (see Materials and Methods Figure 2-18 for experimental setup). The rate of antigen degradation can affect the number of peptides which are available for MHCII presentation. PTPN22 is required for TRAF3 ubiquitination, which is needed for TLR induced production of type I interferons in myeloid cells[10], and FcγR ubiquitination aids internalisation and degradation of immune complexes[150]. Therefore, PTPN22 may be involved in immune complex internalisation and degradation.

The proportion of internalised ova-AF594:anti-ova coated beads was similar for WT and *Ptpn22*$^{-/-}$ BMDCs (Figure 4-11b). This agrees with previous experiments showing that PTPN22 is dispensable for ova IC uptake (Figure 4-9d). In addition, the proportions of internalised ova-AF594:anti-ova coated beads with degraded ova and the magnitude of ova degradation were similar by WT and *Ptpn22*$^{-/-}$ BMDCs (Figure 4-11c-d). This indicates that PTPN22 is not required for ova-AF594 degradation when coated to beads in the presence of anti-ova (to mimic an immune complex). Differences in immune complex processing are therefore unlikely to be the mechanism behind the enhanced immune complex induced T cell proliferation caused by *Ptpn22*$^{-/-}$ BMDCs.

To determine whether Src and Syk family kinases were required for internalisation of ova-AF594:anti-ova coated beads, WT BMDCs were pre-incubated with Src and Syk family inhibitors, prior to the degradation assay described above. Internalisation of ova-AF594:anti-ova coated beads was reduced after kinase inhibition, especially as a result of Syk kinase inhibition (Figure 4-11e). This indicates that Syk kinase is required for efficient phagocytosis of ova-AF594:anti-ova beads, despite the fact that PTPN22 was found to be dispensable (Figure 4-11b).

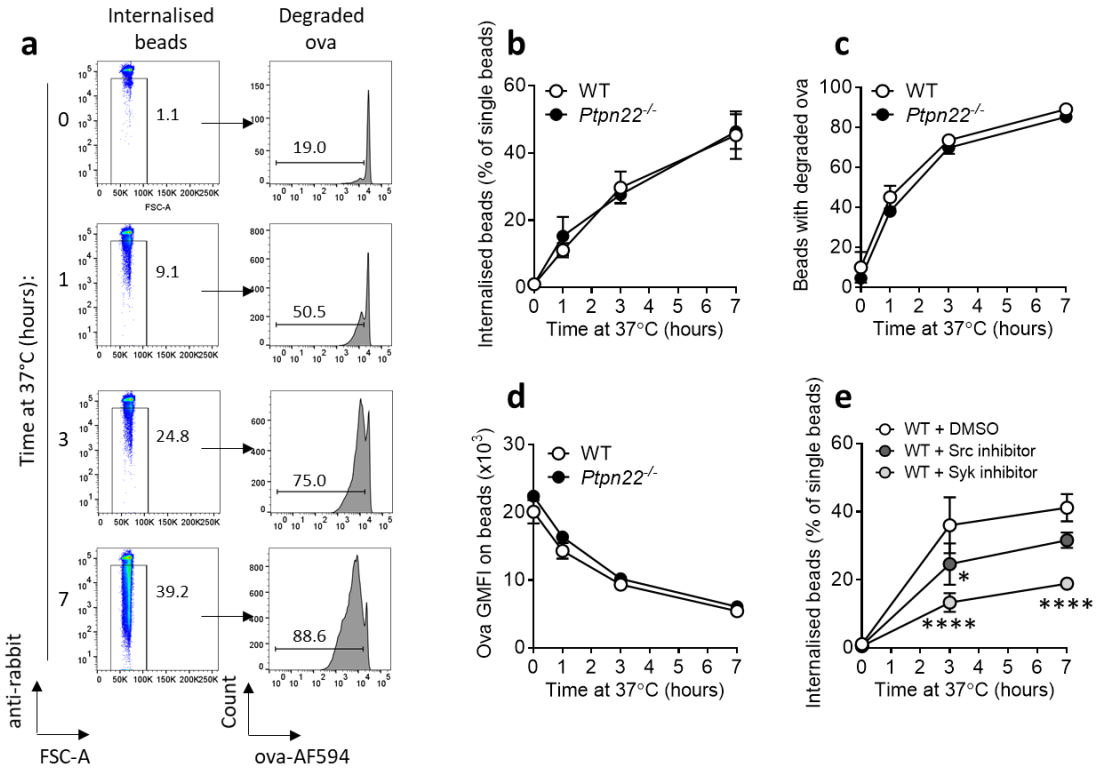

Figure 4-11: PTPN22 is not required for degradation of ova:anti-ova coated beads.

*(a-e) WT and Ptpn22$^{-/-}$ BMDCs were incubated with ova-AF594:anti-ova coated beads for 0-7 hours at 37°C. (a) Representative flow cytometry plots showing ova-AF594:anti-ova coated bead internalisation and ova degradation by BMDCs. (b-d) WT (white) and Ptpn22$^{-/-}$ (black) BMDC ova-AF594:anti-ova coated bead internalisation (b), proportion of internalised ova-AF594:anti-ova coated beads that have degraded ova-AF594 on them (c) and ova-AF594 GMFI of internalised ova-AF594:anti-ova coated beads (d) (%, gated on single, anti-rabbit^{-} beads). n = 3 ± s.d. (technical repeats, representative of 10 independent experiments). (e) WT BMDC ova-AF594:anti-ova coated bead internalisation after pre-treatment with DMSO (vehicle control, white), Src inhibitor (dark grey) or Syk inhibitor (grey), (%, gated on single, anti-rabbit^{-} beads). n = 3 ± s.d; *p<0.05, ****p<0.0001 using a 2-way ANOVA with Tukey's multiple comparisons test (comparisons shown are between WT + DMSO and WT + Src/Syk inhibitors).*

4.3.8 PTPN22 is dispensable for soluble antigen presentation, but negatively regulates presentation of immune complexed derived antigens

As antigen uptake and processing were found to occur independently of PTPN22 in BMDCs, I next assessed whether PTPN22 was required for presentation of peptides in MHCII. Firstly, WT and *Ptpn22$^{-/-}$* BMDCs were incubated for 18 hours at 37°C with GFP-Eα (or GFP as a negative control), a soluble fusion protein containing the Eα peptide epitope. Cell surface MHCII restricted presentation of Eα peptide was determined using a biotinylated antibody specific for the Eα$_{52\text{-}68}$-I-A^{b} peptide-MHCII complex, followed by streptavidin-APC[279] (see Materials and

Methods Figure 2-19 for experimental setup). Whilst more than 50% of the BMDCs expressed Eα$_{52-68}$ in MHCII on their cell surface after 18 hours, PTPN22 expression had no effect on the presentation of Eα peptides (Figure 4-12a-b).

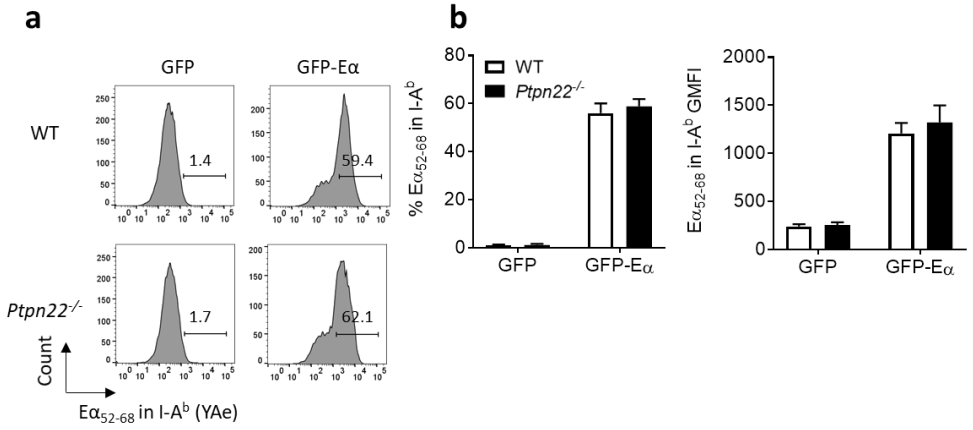

Figure 4-12: Ptpn22$^{-/-}$ BMDCs express similar levels of Eα derived peptides in MHCII on their cell surface.

(a) Representative flow cytometry plots of Eα$_{52-68}$ expression in I-A^b by WT (top) and Ptpn22$^{-/-}$ (bottom) BMDCs after 18 hour incubation with GFP (left) and GFP-Eα (right). (b) Combined proportion (left) and geometric mean fluorescence intensity (GMFI, right) of Eα$_{52-68}$ expression in I-A^b by WT (white) and Ptpn22$^{-/-}$ (black) BMDCs after 18 hour incubation with GFP and GFP-Eα (gated on CD11c$^+$ live singlets). n = 3 ± s.d.

I next wanted to determine whether PTPN22 may be required for the specific presentation of immune complex derived peptides, as PTPN22 was only found to regulate T cell proliferation after ova IC, and not ova pulsing of BMDCs. To address this, WT and *Ptpn22$^{-/-}$* BMDCs were incubated for 18 hours with GFP-Eα:anti-GFP immune complexes (or GFP:anti-GFP immune complexes as a negative control) and cell surface presentation of Eα$_{52-68}$ in I-A^b was again determined by flow cytometry. Similar proportions of WT and *Ptpn22$^{-/-}$* BMDCs expressed Eα$_{52-68}$ peptide-MHCII complexes (Figure 4-13a-b), however, *Ptpn22$^{-/-}$* BMDCs expressed higher levels of cell surface Eα$_{52-68}$ peptide (as demonstrated by increased GMFI, Figure 4-13b). To verify that this enhanced Eα$_{52-68}$ presentation was not due to differences in MHCII expression on WT and *Ptpn22$^{-/-}$* BMDCs, BMDCs that did not receive the Eα containing immune complexes were analysed for cell surface MHCII expression by flow cytometry. WT and *Ptpn22$^{-/-}$* BMDCs were found to express similar levels of MHCII on their cell surface (Figure 4-13c). Internalisation of the GFP-Eα:anti-GFP immune complexes could also be measured using GFP fluorescence. In agreement with previous endocytosis assays showing no role for PTPN22 in immune complex uptake, uptake of the GFP-Eα:anti-GFP immune complexes was comparable by WT and *Ptpn22$^{-/-}$* BMDCs (Figure 4-13d). Taken together, my data suggest that enhanced presentation of immune complex derived antigens could provide one potential mechanism for the increased T cell proliferation observed in Figure 3-19.

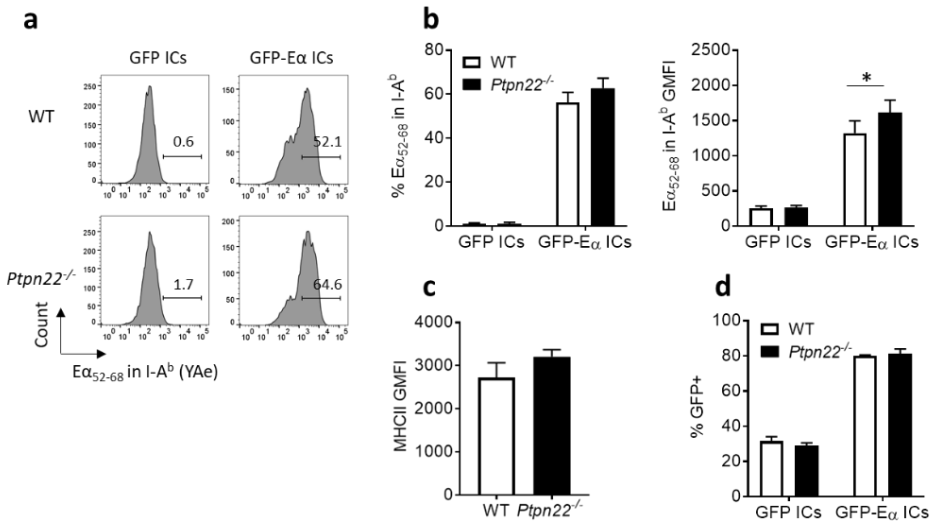

Figure 4-13: Ptpn22$^{-/-}$ BMDCs express more immune complex derived peptides in MHCII on their cell surface.

*(a) Representative flow cytometry plots of Eα$_{52-68}$ expression in I-A^b by WT (top) and Ptpn22$^{-/-}$ (bottom) BMDCs after 18 hour incubation with GFP/anti-GFP ICs (left) and GFP-Eα/anti-GFP ICs (right). (b) Combined proportion (left) and GMFI (right) of Eα$_{52-68}$ expression in I-A^b by WT (white) and Ptpn22$^{-/-}$ (black) BMDCs after 18 hour incubation with GFP:anti-GFP ICs and GFP-Eα:anti-GFP ICs (gated on CD11c$^+$ live singlets). n = 3 ± s.d; *p<0.05 using a 2-way ANOVA with Sidak's multiple comparisons test. (c) MHCII expression on WT (white) and Ptpn22$^{-/-}$ (black) BMDCs (GMFI, gated on CD11c$^+$ live singlets). n = 3 ± s.d. (d) GFP:anti-GFP IC and GFP-Eα:anti-GFP IC uptake after 18 hours by WT (white) and Ptpn22$^{-/-}$ (black) BMDCs (% GFP$^+$, gated on CD11c$^+$ live singlets). n = 3 ± s.d.*

4.3.9 PTPN22 is required for efficient immune complex induced conjugate formation, but is dispensable when using OVA$_{323-339}$ peptide or ova

For DCs to initiate T cell activation and proliferation, they must be capable of forming productive conjugates. First, I investigated whether PTPN22 was needed for conjugate formation between LPS matured, OVA$_{323-339}$ peptide pulsed or ova pulsed BMDCs and ova specific WT CD4$^+$ OT-II T cells. WT and *Ptpn22$^{-/-}$* BMDCs were pulsed with OVA$_{323-339}$ peptide or ova (or left unpulsed, as a negative control), and labelled with CellTrace Far Red (CTFR). CTFR labelled BMDCs were then incubated with CellTrace Violet (CTV) labelled WT CD4$^+$ OT-II T cells for 0-120 mins at 37°C. Conjugates were identified by flow cytometry as CTV$^+$ CTFR$^+$ events (see Materials and Methods Figure 2-9 for experimental setup). Neither unpulsed or ova pulsed WT and *Ptpn22$^{-/-}$* BMDCs produced a high number of conjugates with T cells (Figure 4-14a-c). LPS matured OVA$_{323-339}$ peptide pulsed BMDCs produced more conjugates, the proportion of which increased over time (Figure 4-14d). Despite this, conjugate formation was similar using both WT and *Ptpn22$^{-/-}$* OVA$_{323-339}$ peptide pulsed BMDCs (Figure 4-14d). This indicates that PTPN22 is dispensable for conjugate formation when BMDCs are unpulsed or pulsed with ova or OVA$_{323-339}$ peptide. These results

were not completely surprising as PTPN22 was not required for T cell proliferation when BMDCs were pulsed with $OVA_{323-339}$ peptide or ova (Figures 3-15d-e and 3-19b).

As *Ptpn22*$^{-/-}$ BMDCs were found to display enhanced immune complex derived cell surface peptide-MHCII presentation (Figure 4-13b), I next wanted to determine whether immune complex pulsed *Ptpn22*$^{-/-}$ BMDCs would be capable of forming more DC-T cell conjugates. WT and *Ptpn22*$^{-/-}$ BMDCs were pulsed overnight with ova ICs, labelled with CTFR and incubated with CTV labelled WT CD4^{+} OT-II T cells. Ova IC pulsed BMDCs formed conjugates with T cells, and the proportion of which increased over time (Figure 4-14e). In agreement with the ability of *Ptpn22*$^{-/-}$ BMDCs to express more immune complex derived antigens on their cell surface, ova IC pulsed *Ptpn22*$^{-/-}$ BMDCs had a significantly enhanced capability to form conjugates with WT CD4^{+} OT-II T cells than WT BMDCs (Figure 4-14e). This data, in addition to the enhanced immune complex derived antigen presentation, could explain the augmented immune complex induced T cell proliferation caused by *Ptpn22*$^{-/-}$ BMDCs.

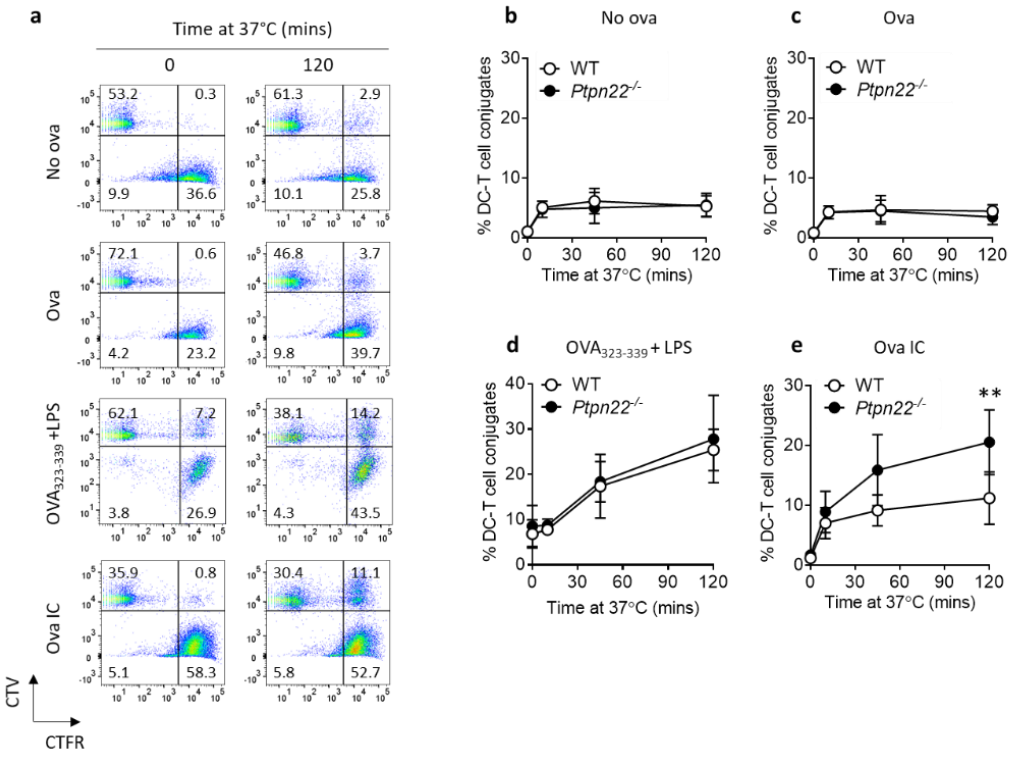

Figure 4-14: Ova IC pulsed Ptpn22$^{-/-}$ BMDCs form more conjugates with ova specific WT T cells.

*(a-e) Representative flow cytometry plots (a) and combined data (b-e) showing the proportion of WT OT-II T cells in conjugates with unpulsed (no ova) (b), 1 µM ova pulsed (c), 10 µM $OVA_{323-339}$ peptide and 100 ng/ml LPS pulsed (d), and 1 µM ova IC pulsed (e) WT (white) and Ptpn22$^{-/-}$ (black) BMDCs over time. Conjugates were identified as CTV^{+} CTFR^{+} events (%, gated on CTV^{+} total T cells). n = 4 ± s.d; **p<0.01 using a 2-way ANOVA with Sidak's multiple comparisons test.*

To further determine how PTPN22 may be regulating conjugate formation, WT BMDCs were pulsed overnight with ova ICs and treated with Src and Syk family kinase inhibitors, prior to the DC-T cell conjugate assay. Inhibition of Src and Syk family kinases led to a drastic reduction in conjugate formation (Figure 4-15a-b). This may indicate that PTPN22 is modulating conjugate formation by regulating the phosphorylation states of these kinases.

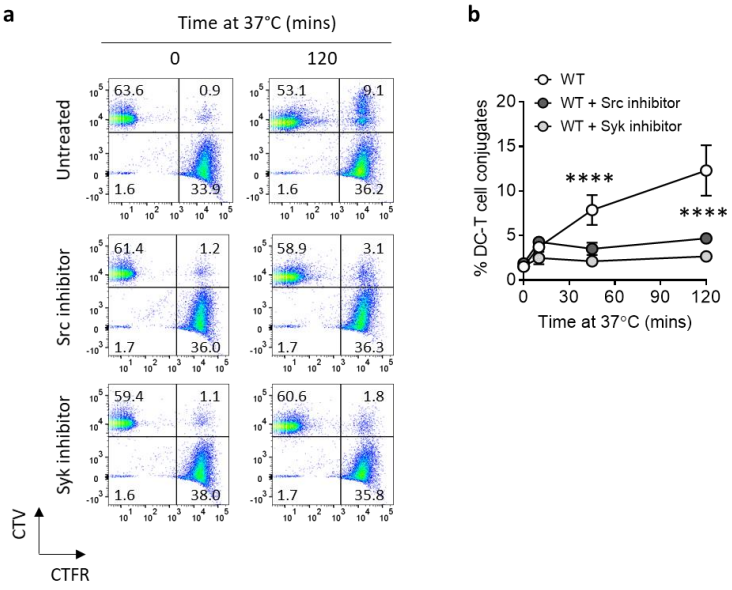

Figure 4-15: Src and Syk family kinases are required for efficient ova IC induced BMDC-T cell conjugate formation.

*(a-b) Representative flow cytometry plots (a) and combined data (b) for the proportion of WT OT-II T cells in conjugates with ova IC pulsed WT BMDCs, after pre-treatment with DMSO (vehicle control, white), Src inhibitor (dark grey) or Syk inhibitor (grey). Conjugates were identified as CTV^+ $CTFR^+$ events (%, gated on CTV^+ total T cells). n = 3 ± s.d.; ****p<0.0001 using a 2-way ANOVA with Tukey's multiple comparisons test.*

4.4 Overall findings

The main findings of this Chapter were:

1. PTPN22 is not required for BMDC internalisation of antigens via macropinocytosis or receptor mediated endocytosis via dectin-1, TLR2 or the mannose receptor.
2. PTPN22 is dispensable for FcγR dependent ova IC binding, internalisation and processing.
3. PTPN22 negatively regulates presentation of IC derived peptides in MHCII and ova IC dependent BMDC-T cell conjugate formation.

This data has been published in:

1. **Clarke F**, Jordan, CK, Gutierrez-Martinez E, Bibby JA, Sanchez-Blanco C, Cornish GH, Dai X, Rawlings DJ, Zamoyska R, Guermonprez P, Cope AP, Purvis HA. Protein Tyrosine Phosphatase PTPN22 is dispensable for DC antigen processing and promotion of T-cell activation by DCs. *PLoS ONE* **12** (2017).
2. **Clarke F**, Purvis HA, Sanchez-Blanco C, Gutiérrez-Martinez E, Cornish GH, Zamoyska R, Guermonprez P, Cope AP. The protein tyrosine phosphatase PTPN22 negatively regulates presentation of immune complex derived antigens. *Scientific Reports* **8** (2018).

4.5 Discussion

The aim of this Chapter was to identify a mechanism(s) behind the enhanced immune complex induced T cell proliferation by *Ptpn22*$^{-/-}$ BMDCs, described in Chapter 3. A systematic approach was taken to first determine whether PTPN22 was required for endocytosis via a variety of receptors, including FcγRs. PTPN22 was found to be dispensable for internalisation of Lucifer yellow, heat killed *Listeria monocytogenes*, heat killed *Candida albicans*, ova, ova ICs, ova coated beads, ova:anti-ova coated beads, GFP-Eα and GFP-Eα ICs. This is in contrast with previously published data showing that M1 polarised, LPS treated *Ptpn22*^{R619W} peritoneal macrophages were more efficient at phagocytosing heat killed fluorescent *E.coli* than WT macrophages[67]. This discrepancy may be due to using different antigens to measure phagocytosis, PTPN22 playing distinct roles in DCs compared to macrophages, and differences resulting from the expression of the autoimmune associated variant of PTPN22 compared to lacking expression of PTPN22 completely.

4.5.1 Receptor mediated endocytosis

Although ova is internalised by the mannose receptor, it can also enter cells via macropinocytosis[104]. This has been shown by the fact that the addition of excess mannan prior to incubation with ova only partially reduces ova uptake, indicating that it is also taken up by macropinocytosis[280]. During the ova uptake assay, excess, unbound ova was not washed off the BMDCs prior to being moved to the water bath for uptake, meaning that the ova may have been internalised by a combination of mannose receptor mediated endocytosis and macropinocytosis. I purposely did not wash off the unbound ova, as this would then model more

closely what is happening when BMDCs are pulsed overnight with ova, prior to the co-cultures. I did however also carry out endocytosis assays where unbound ova was washed off prior to uptake, such that the majority of the internalisation would be via the mannose receptor. In these experiments, PTPN22 was still found to be dispensable for ova internalisation. It has been shown, using mannose receptor knock out mice, that BMDCs utilise the mannose receptor to internalise ova destined to be presented as peptides in MHCI, for the activation of $CD8^+$ T cells, whereas they use macropinocytosis to internalise ova for MHCII presentation, and for the subsequent activation of $CD4^+$ T cells[104]. This indicates that ova uptake via macropinocytosis was more important for the $CD4^+$ T cell proliferation observed in the co-cultures. As PTPN22 was also found to be dispensable for uptake of Lucifer yellow by macropinocytosis, this is still consistent with the fact that PTPN22 was found to be dispensable for T cell proliferation after co-culture with ova pulsed BMDCs.

Although PTPN22 was found to be dispensable for dectin-1 dependent internalisation of heat killed *Candida albicans*, our lab has demonstrated that the phosphatase regulates signalling downstream of the receptor. *Ptpn22*$^{-/-}$ BMDCs pulsed with $OVA_{323-339}$ and the dectin-1 agonist curdlan caused enhanced OT-II T cell IL-17 secretion, which was found to be dependent on IL-1β secretion from the BMDCs. In addition, after dectin-1 stimulation, *Ptpn22*$^{-/-}$ BMDCs showed enhanced Syk and ERK phosphorylation[66]. This shows that PTPN22 is required to regulate specific facets of receptor signalling, which is similar to the regulation that PTPN22 appears to play in FcγR signalling, despite being dispensable for FcγR-dependent immune complex internalisation.

4.5.2 Antigen processing

As PTPN22 was found to be dispensable for endocytosis of antigens, the next step was to assess its role in antigen processing. For this, polystyrene beads were coated with ova or ova:anti-ova and the reduction of the ova fluorescence was assessed over time. Again, PTPN22 was found to be dispensable for this process. I did not investigate trafficking of internalised antigens in WT and *Ptpn22*$^{-/-}$ BMDCs, so it is possible that although PTPN22 was not required for their internalisation and processing, it may be required for intracellular vesicular trafficking of antigens, to allow for efficient presentation. A potential drawback of the bead processing assay is that it is based on the assumption that the reduction in ova-AF594 fluorescence is directly correlated with degradation of the ova or ova ICs. It is possible that the AF594 may be degraded at a different rate, or via a different pathway to the ova or ova ICs. To ensure that the loss of AF594 signal does correlate with antigen processing, it would be possible to repeat the assays

in the presence of an inhibitor of phagolysosomal degradation, for example chloroquine. Chloroquine prevents acidification of endosomes, inhibits lysosomal enzymes and prevents endosome-lysosome fusion, so if the loss of AF594 fluorescence was due to antigen degradation, then using this inhibitor should result in no loss of AF594 signal. It has been shown by the lab of Dr Pierre Guermonprez (King's College London) that during uptake of ova coated beads, ova-AF594 colocalises with LAMP-1^{+} vesicles and that with increasing time at 37°C, the AF594 is reduced (Appendix Figure 8-1). The BMDCs were only incubated with the ova or ova:anti-ova coated beads for a maximum of 7 hours at 37°C, after which point the AF594 signal was reduced, but still detectable. This indicates that complete antigen degradation had not occurred by this time point. In the future, it would be interesting to repeat the assays, but allowing the BMDCs longer to process the antigens. In addition, microscopy could have been utilised to visualise the location and degradation of the ova and ova ICs, including co-staining with antibodies for endosomal organelles, to see whether the ova and ova:anti-ova coated beads are being trafficked similarly in WT and *Ptpn22*$^{-/-}$ BMDCs.

The use of the F(ab')2 goat anti-rabbit IgG made it simple to distinguish between internalised and external ova ICs, ova coated beads or ova:anti-ova coated beads, as any cells that were F(ab')2 goat anti-rabbit IgG^{+} could be excluded as having external antigens. However, the disadvantage of this technique is that cells which had both internalised and external ova ICs were excluded. Therefore, only cells which had no external ova ICs were included in the analysis. An alternative technique could have been to conjugate the ova ICs with a pH sensitive dye, such as pHrodo, which would fluoresce differently depending on whether the ova ICs had been internalised into the more acidic endosomes/lysosomes, or whether they remained on the cell surface.

4.5.3 Antigen presentation

In order to induce T cell proliferation, internalised antigens need to be processed and presented on the cell surface. Using immune complexes containing the Eα protein, peptide presentation in MHCII was monitored. In this case, lacking expressing of PTPN22 led to a subtle, but significant increase in cell surface expression of $E\alpha_{52\text{-}68}$ expression in I-A^{b}. This may provide some explanation as to why immune complex pulsed *Ptpn22*$^{-/-}$ BMDCs caused enhanced T cell proliferation. I did not analyse intracellular levels of $E\alpha_{52\text{-}68}$ in MHCII, although this would have been interesting. From these experiments, it is therefore not possible to distinguish between a potential role of PTPN22 in $E\alpha_{52\text{-}68}$-MHCII formation and cell surface presentation. In the future,

microscopy experiments could be utilised to identify whether the peptide-MHC complexes were being formed and utilising similar pathways of vesicular trafficking in WT and *Ptpn22*$^{-/-}$ BMDCs.

A potential drawback of this antigen presentation assay is that I was not able to look directly at presentation of ova IC derived antigens in MHCII, as the reagents are not available, so the results from the GFP-Eα containing immune complex presentation assays have been extrapolated to the co-cultures. Alternatively, it would have been useful to be able to carry out the co-culture assays using the GFP-Eα containing immune complexes, to ensure that these still induced enhanced T cell proliferation, when presented by *Ptpn22*$^{-/-}$ BMDCs. However, there are not transgenic mice available whose T cell receptors are specific for peptides from Eα.

In addition, if PTPN22 is involved in trafficking and/or retention of peptide-MHCII complexes to the plasma membrane, then monitoring cell surface $E\alpha_{52\text{-}68}$ presentation in I-A^b over more time points could have been informative. It may be possible that PTPN22 is not required for initial peptide-MHCII complex formation and trafficking to the surface, but that it is required for cell surface retention. My data demonstrates that after 18 hours of incubation PTPN22 negatively regulates antigen presentation. This time point corresponds to the point when ova IC pulsed BMDCs are harvested for co-cultures with WT $CD4^+$ OT-II T cells, so this indicates that at this time point, *Ptpn22*$^{-/-}$ BMDCs are presenting more immune complex derived antigens to T cells, compared to WT BMDCs, resulting in enhanced T cell proliferation.

4.5.4 T cell:BMDC conjugate formation

Finally, the ability of WT and *Ptpn22*$^{-/-}$ BMDCs to form conjugates with T cells was assessed. Similar conjugate formation was found when BMDCs were left unpulsed, or pulsed with ova or $OVA_{323\text{-}339}$, however enhanced conjugate formation was observed when *Ptpn22*$^{-/-}$ BMDCs were pulsed with ova ICs; a process found to be dependent on Src and Syk family kinases. This observation provided a potential mechanism behind the enhanced immune complex induced T cell proliferation. How PTPN22 is regulating BMDC immune complex derived antigen presentation and conjugate formation is unclear but these data suggest that PTPN22 acts to negatively regulate FcγR induced immune responses, reducing the capability of DCs to activate T cells. One potential drawback of the conjugate assays is that they only model the first two hours of the interaction between BMDCs and T cells, so although in this timeframe *Ptpn22*$^{-/-}$ BMDCs pulsed with ova ICs were able to form more conjugates with ova specific WT $CD4^+$ T cells, the BMDCs and T cells were co-cultured for a lot longer, which ultimately led to enhanced T cell proliferation.

4.5.5 PTPN22 potential redundancy with other phosphatases

A potential reason why PTPN22 was found to be dispensable for ova IC uptake, may be due to the presence of other phosphatases which may compensate for the loss of PTPN22. Other phosphatases which are expressed in DCs, have been shown to regulate FcγR signalling in macrophages. For example, in the absence of the inositol 3-phosphatase PTEN, mouse peritoneal macrophages show an enhanced phagocytic ability[260]. The phosphatase SHIP-1 has also been shown to regulate FcγR dependent phagocytosis. Overexpression of SHIP-1 in RAW LR5 macrophages inhibited phagocytosis of IgG opsonised sheep red blood cells, whereas *Ship1*$^{-/-}$ mouse macrophages showed enhanced phagocytosis[281]. Similar results were found when investigating the role of SHIP-2 in FcγR dependent phagocytosis. Transient overexpression of SHIP-2 in RAW 264.7 macrophages reduced the ability of these cells to internalise IgG opsonised sheep red blood cells, whereas knock down of SHIP-2 led to enhanced phagocytosis[282]. The mechanism behind this regulation was shown to be by SHIP-2 suppressing the activation of Rac after FcγR crosslinking. Rac is required for actin polymerisation and cytoskeletal rearrangement, both of which are needed for phagocytosis. This data indicates that PTEN, SHIP-1 and SHIP-2 can negatively regulate FcγR dependent phagocytosis in macrophages, potentially explaining the lack of requirement for PTPN22 in immune complex uptake.

5. Results: Investigating the role of PTPN22 in a model of rheumatoid arthritis and in osteoclast differentiation and function

5.1 Introduction

To further understand the association of PTPN22^{R620W} in humans with an enhanced susceptibility to multiple autoimmune diseases such as RA, I used the K/BxN serum transfer model of arthritis[178]. This model allows the effector phase of arthritis to be examined, after autoantibodies have been produced, and so does not require T and B cells for its initiation. The transferred arthritogenic serum contains autoantibodies to the glycolytic enzyme glucose-6-phosphate isomerase (GPI) and allows arthritis to be studied in non-autoimmune prone strains of mice. Although T and B cells are dispensable for disease induction using this model, it has been shown that neutrophils[181] and macrophages[182,283] are required. In addition, the complement component C5[186], FcγRIII[187], IL-1[188] and LFA-1[189,190] have been shown to be necessary. Mice are injected with arthritogenic serum on days 0 and 2 and clinical signs of disease are visible within a few days. The disease is transient, usually peaking at 4-6 days and resolving by 10-12 days. Signs of disease are monitored daily, which involves assigning clinical scores to each paw, measuring paw swelling and weighing the mice. Although this model has been previously used in *Ptpn22*$^{-/-}$ mice by three independent groups, the results were contradictory, with two showing that PTPN22 was dispensable for disease development[10,59] and the other showing that PTPN22 exacerbated disease[63]. For this reason, I was interested to carry out the model not only using WT and *Ptpn22*^{R619W} mice, but also comparing WT with *Ptpn22*$^{-/-}$ mice.

Osteoclasts are multinucleated cells which differentiate from hematopoietic stem cells, usually in the presence of M-CSF and RANK-L. Osteoclasts function in concert with osteoblasts to allow for physiological bone remodelling, whereby osteoclasts erode bone and osteoblasts form new bone. However, in inflammatory diseases such as RA, the balance between the activity of osteoclasts and osteoblasts is dysregulated, leading to excessive bone erosion. Osteoclasts are the only cell type capable of eroding bone and are therefore responsible for the bone erosion seen in RA[284]. This has been demonstrated in mouse models of arthritis, whereby osteoclast deficient mice show no signs of joint destruction and are osteopetrotic[285]. There is evidence showing that kinases and phosphatases are essential for normal osteoclast differentiation and function. For example, if protein tyrosine phosphatase activity is inhibited, this prevents *in vitro*

differentiation of osteoclasts, and their subsequent ability to resorb bone[225]. In addition, tyrosine phosphorylation regulates signalling downstream of receptors required for osteoclast differentiation and function, including c-Fms[226] (the receptor for M-CSF), RANK (the receptor for RANK-L)[286,287] and integrins[288,289], which are required for adhesion of osteoclasts to cartilage and bone matrix. Finally, the PTPN22 family member, PTPN12, has been shown to be required for RANK-L dependent fusion of macrophages into osteoclasts[232]. For these reasons, this Chapter investigated whether PTPN22 may play a role in the differentiation and/or function of osteoclasts.

5.2 Aims

This Chapter aimed to determine whether PTPN22 plays a role in:

1. Disease development using the K/BxN serum transfer mouse model of rheumatoid arthritis.
2. Osteoclast differentiation and function *in vitro.*

5.3 Results

5.3.1 The absence of PTPN22 enhances disease severity using the K/BxN serum transfer model of arthritis

To begin to understand whether PTPN22 plays a role in arthritis development, the K/BxN mouse serum transfer model of arthritis was utilised. WT and *Ptpn22*$^{-/-}$ mice were injected with PBS or arthritogenic serum (diluted 1:1 with PBS) on days 0 and 2, and disease development was monitored daily for 9 days (see Materials and Methods Figure 2-20 for experimental setup). As expected, mice that received PBS did not display any signs of disease throughout the experiment (Figure 5-1a-c). However, mice that received the arthritogenic serum developed robust disease, shown by increasing clinical scores, which peaked at days 5-7 (Figure 5-1a). This was accompanied by a steady increase in paw thickness and in weight loss over time (Figure 5-1b-c). *Ptpn22*$^{-/-}$ mice developed more severe disease, as demonstrated by augmented clinical scores, paw swelling and weight loss in comparison to WT mice (Figure 5-1a-c). This indicates that PTPN22 plays a role in regulating inflammatory pathways implicated in arthritis development.

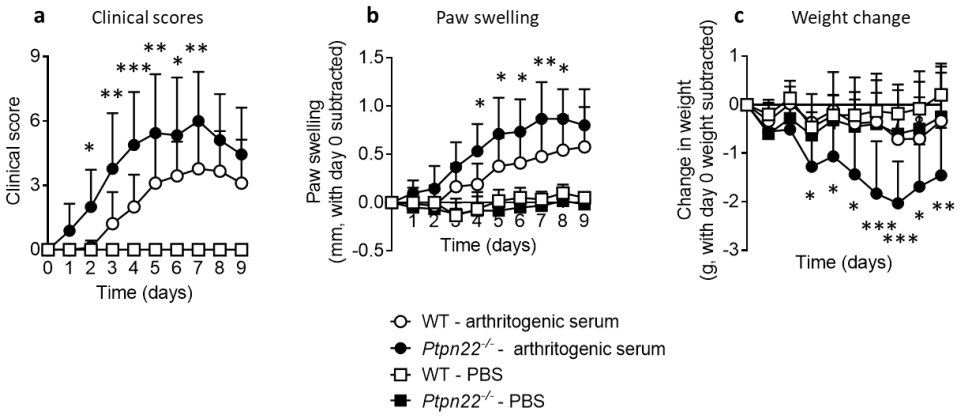

Figure 5-1: Ptpn22$^{-/-}$ mice develop more severe disease using the K/BxN serum transfer model of arthritis.

*(a-c) WT and Ptpn22$^{-/-}$ mice were injected (i.p.) with 150 µl PBS or arthritogenic serum (diluted 1:1 with PBS) on days 0 and 2. Clinical scores, paw swelling measurements and weight were collected daily for 9 days. Average clinical scores (a), paw swelling (left ankle shown as an example) (b) and weight change (c) are shown for WT (white) and Ptpn22$^{-/-}$ (black) mice injected with PBS (square) or arthritogenic serum (circle). n = 6 (PBS) and 9 (serum) ± s.d; ***p<0.005, **p<0.01, *p<0.05 using a 2-way ANOVA with Tukey's multiple comparisons test (shown for arthritogenic serum WT v Ptpn22$^{-/-}$ only).*

5.3.2 Expression of PTPN22^{R619W} is not sufficient to cause enhanced disease when using the K/BxN serum transfer model of arthritis

After revealing a role of PTPN22 in reducing disease severity using the K/BxN serum transfer model of arthritis, I next wanted to identify whether expression of the autoimmune associated variant of PTPN22 would also affect disease severity. *Ptpn22^{R619}* (WT) and *Ptpn22^{R619W}* mice were injected with PBS or arthritogenic serum (diluted 1:1 with PBS) on days 0 and 2, and disease progression was monitored daily for 10 days. Once again, clinical signs of disease were present in mice that had received arthritogenic serum. In these experiments, disease severity peaked at day 7 and plateaued until the end of the experiment on day 10 (Figure 5-2a-c). As expected, no disease was seen in mice that received PBS (Figure 5-2a-c). WT and *Ptpn22^{R619W}* mice developed similar levels of disease based on clinical scores, paw swelling measurements and weight loss (Figure 5-2a-c). This shows that expression of the autoimmune associated variant of PTPN22 is not sufficient to alter disease in the K/BxN serum transfer model of arthritis.

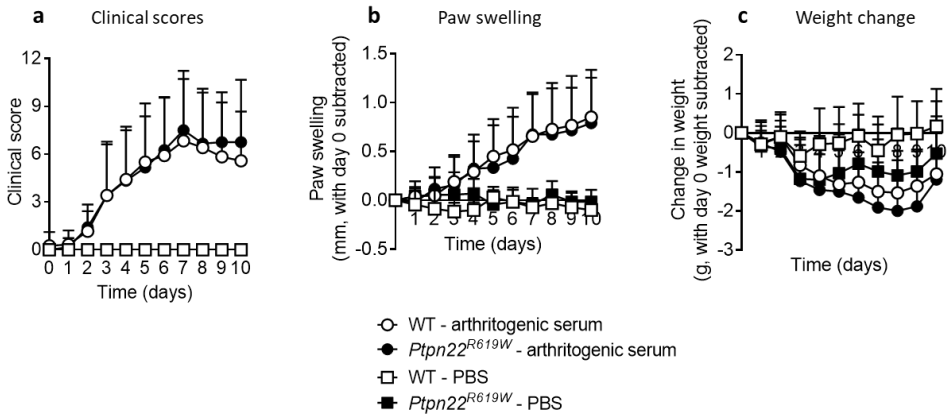

Figure 5-2: Expression of Ptpn22^{R619W} does not affect disease progression in the K/BxN serum transfer model of arthritis.

(a-c) Ptpn22^{R619} (WT) and Ptpn22^{R619W} mice were injected (i.p.) with 150 µl PBS or arthritogenic serum (diluted 1:1 with PBS) on days 0 and 2. Clinical scores, paw swelling measurements and weight were collected daily for 10 days. Average clinical scores (a), paw swelling (left ankle shown as an example) (b) and weight change (c) are shown for WT (white) and Ptpn22^{R619W} (black) mice injected with PBS (square) or arthritogenic serum (circle). n = 7 (PBS) and 12 (serum) ± s.d.

5.3.3 Serum cytokines and chemokines are similar in arthritic WT and *Ptpn22*$^{-/-}$ mice

To begin to understand the mechanism behind the enhanced disease seen in the absence of PTPN22, serum was harvested from WT and *Ptpn22*$^{-/-}$ mice by tail bleeds or cardiac punctures on days 1, 3, 5 and 9 of the model. Multiplex assays capable of identifying 13 analytes simultaneously were used to interrogate serum samples for a range of chemokines and cytokines. This included cytokines which are known to play a role in the pathogenesis of arthritis, including IL-1, IL-6, IL-17 and TNFα[290]. At day 1 and 3, mice that had received the arthritogenic serum had similar levels of cytokines in their serum as mice that had received PBS, except for IL-23, which was highest in healthy WT mice (Figure 5-3a-b). This difference was maintained at day 3 (Figure 5-3b), but IL-23 was not detected on days 5 and 9 (Figure 5-3c-d). On day 3, IL-27 and IFNβ expression was enhanced in the serum of *Ptpn22*$^{-/-}$ mice compared to WT mice, but this was found to be independent of the disease status (Figure 5-3b), indicating that this does not explain the enhanced disease seen in *Ptpn22*$^{-/-}$ mice. On day 5, IL-27 was also higher in the serum of arthritic *Ptpn22*$^{-/-}$ mice compared to WT mice (Figure 5-3c), but this difference was not maintained at day 9 of the model (Figure 5-3d).

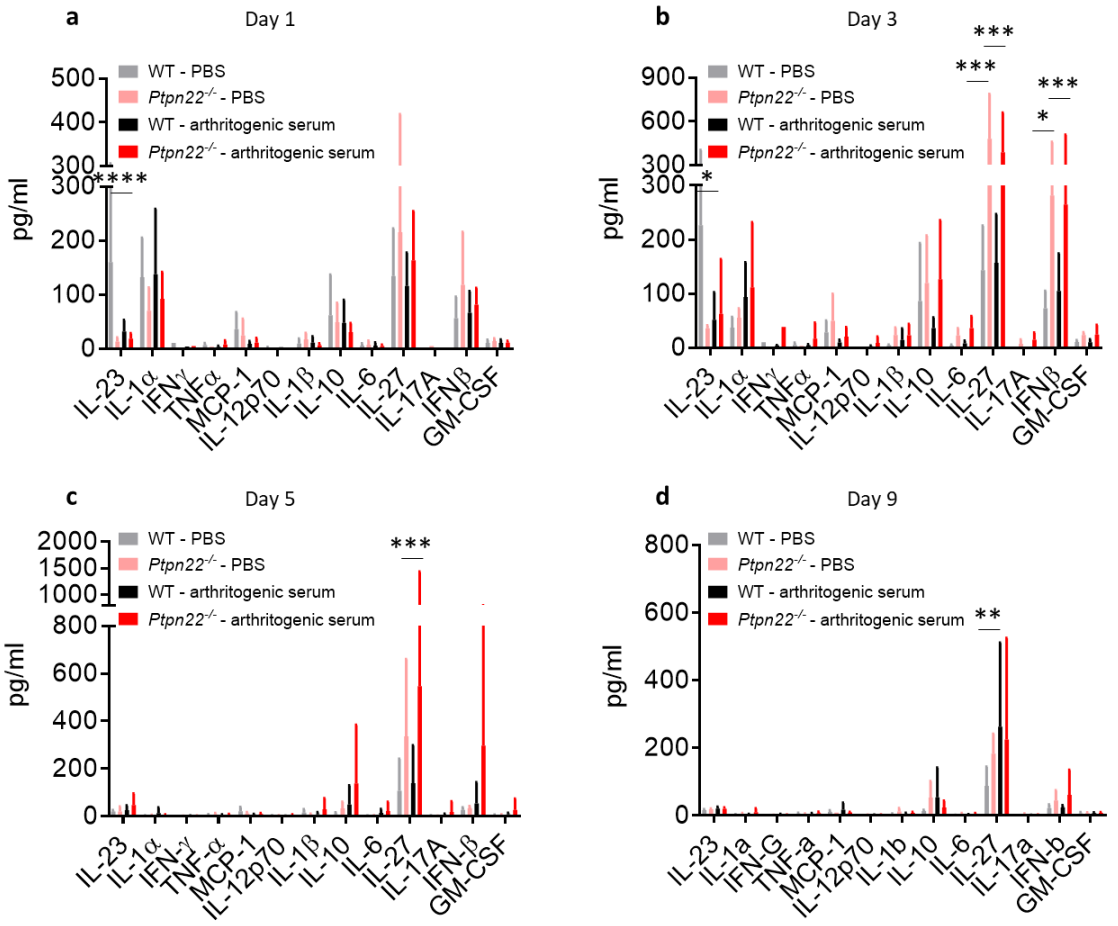

Figure 5-3: WT and Ptpn22$^{-/-}$ serum cytokines are similar at multiple time points of the K/BxN serum transfer model of arthritis.

*(a-d) WT and Ptpn22$^{-/-}$ mice were injected (i.p.) with 150 µl PBS or arthritogenic serum (diluted 1:1 with PBS) on days 0 and 2. Tail bleeds were carried out on days 1 (a) and 3 (b) and cardiac punctures were carried out on day 5 (c) and 9 (d). Serum cytokines were measured in from WT (grey and black) and Ptpn22$^{-/-}$ (pink and red) mice after injections with PBS (grey and pink) or arthritogenic serum (black and red) using a LEGENDplex inflammation panel. n = 3-4 (PBS) and 5-8 (arthritogenic serum) ± s.d; *p<0.05, **p<0.01, ***p<0.005 using a 2way ANOVA and Tukey's multiple comparisons test.*

Serum chemokines were analysed on days 5 and 9. Most of the analytes were undetectable, which may have been due to the late time points investigated, but those that were detectable, including Eotaxin and B lymphocyte chemoattractant (BLC, also known as CXCL13) were found at similar levels in the serum of both healthy and arthritic WT and *Ptpn22$^{-/-}$* mice (Figure 5-4a-b). Liposaccharide induced CXC chemokine (LIX, also known as CXCL5) was also detectable and found to be reduced in the serum of arthritic *Ptpn22$^{-/-}$* mice compared to arthritic WT mice on days 5 and 9 (Figure 5-4a-b). This analysis indicates that the enhanced disease seen in *Ptpn22$^{-/-}$* mice is not due to changes in expression of the chemokines and cytokines in the multiplex panels.

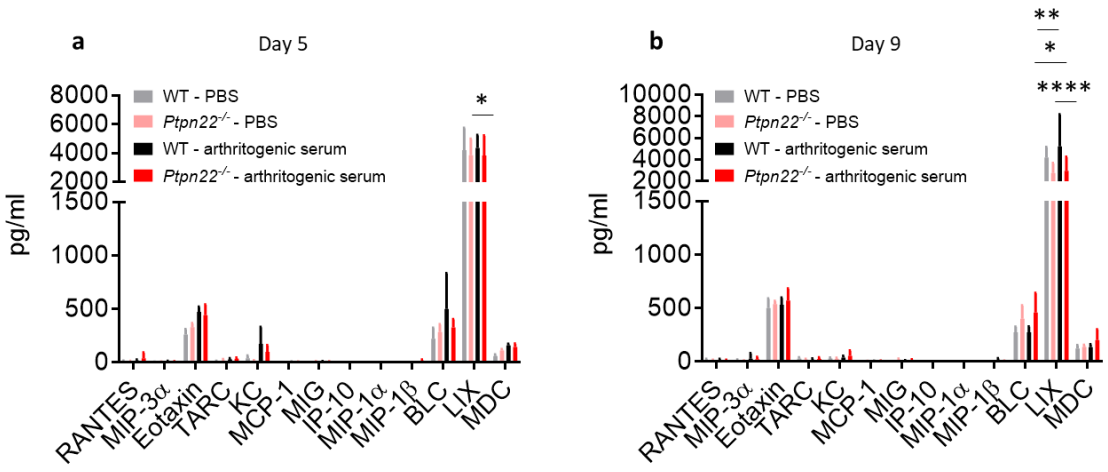

Figure 5-4: WT and Ptpn22$^{-/-}$ serum chemokines are similar at days 5 and 9 of the K/BxN serum transfer model of arthritis.

*(a-b) WT and Ptpn22$^{-/-}$ mice were injected (i.p.) with 150 µl PBS or arthritogenic serum (diluted 1:1 with PBS) on days 0 and 2. Cardiac punctures were carried out on days 5 (a) and 9 (b). Serum chemokines were measured in from WT (grey and black) and Ptpn22$^{-/-}$ (pink and red) mice after injections with PBS (grey and pink) or arthritogenic serum (black and red) using a LEGENDplex proinflammatory chemokine panel. n = 3 (PBS) and 5-6 (arthritogenic serum) ± s.d; *p<0.05, **p<0.01, ****p<0.0001 using a 2way ANOVA and Tukey's multiple comparisons test.*

5.3.4 Joint architecture is similar in WT, *Ptpn22*$^{-/-}$ and *Ptpn22*^{R619W} mice

To identify whether there were any microscopic differences between the arthritic joints of WT and *Ptpn22*$^{-/-}$ and WT and *Ptpn22*^{R619W} mice, ankle joints were removed at days 9 and 10 respectively, fixed, decalcified and stained using hematoxylin and eosin (H+E). H+E staining allows for the visualisation of the joint architecture and cell infiltration (see Figure 5-5b for examples). H+E stained joints were blindly scored by assigning a score of 0-3 for joint erosion and 0-3 for cell infiltration. Mice that received PBS did not show any signs of joint erosion or cell infiltration, as expected (Figure 5-5c-d). Mice that received the arthritogenic serum showed higher joint erosion and cell infiltration scores (Figure 5-5c-d). Despite the difference in external signs of disease between WT and *Ptpn22*$^{-/-}$ mice (Figure 5-5a), the joint erosion and cell infiltration scores were similar, although there was a trend towards enhanced cell infiltration in the ankles of *Ptpn22*$^{-/-}$ mice (Figure 5-5d).

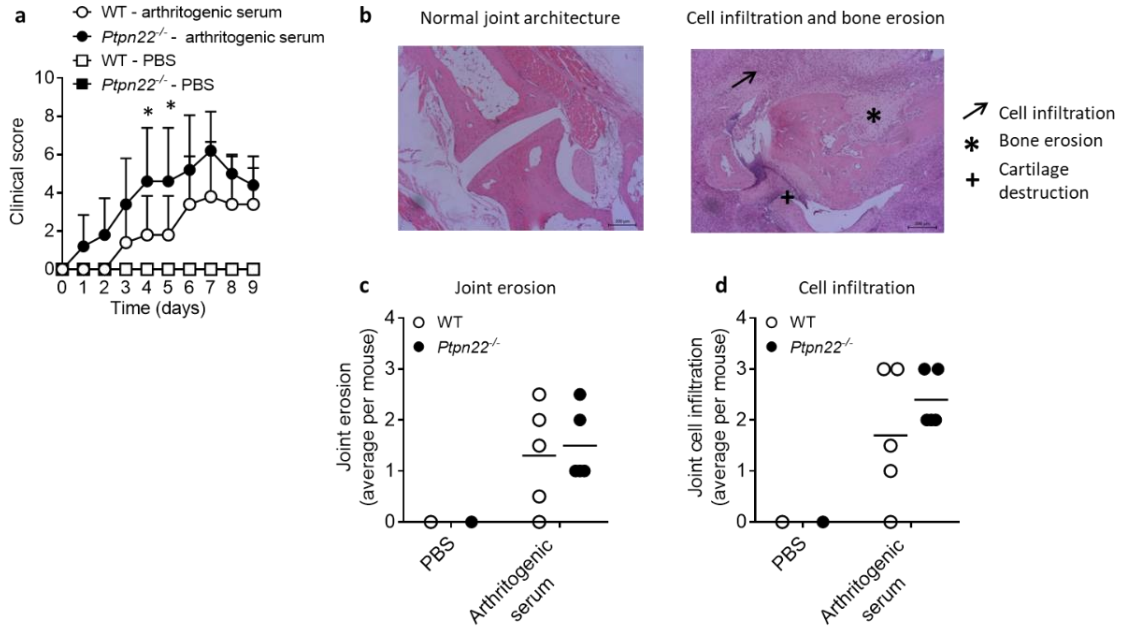

Figure 5-5: WT and Ptpn22$^{-/-}$ mice have similar ankle joint erosion and cell infiltration at day 9 of the K/BxN serum transfer model of arthritis.

*(a-d) WT and Ptpn22$^{-/-}$ mice were injected (i.p.) with 150 µl PBS or arthritogenic serum (diluted 1:1 with PBS) on days 0 and 2. On day 9, mice were culled and ankle joints were removed before being fixed, decalcified, embedded in paraffin, sectioned and stained with hematoxylin and eosin (H+E). (a) Average clinical scores are shown for WT (white) and Ptpn22$^{-/-}$ (black) mice injected with PBS (square) or arthritogenic serum (circle). n = 3 (PBS) and 5 (serum) ± s.d.; *p<0.05 using a 2-way ANOVA with Tukey's multiple comparisons test (shown for arthritogenic serum WT v Ptpn22$^{-/-}$ only). (b) Representative H+E stained healthy (left) and arthritic (right) ankle joints, showing cell infiltration (arrow), bone erosion (star) and cartilage destruction (cross). (c-d) WT (white) and Ptpn22$^{-/-}$ (black) ankle joint sections were scored from 0-3 for joint erosion (c) and cell infiltration (d). Scores shown are averages of 2 ankle joints per mouse. n = 1 (PBS) and 5 (arthritogenic serum), and were assigned blinded to clinical scores and genotypes.*

Similar levels of joint erosion and cell infiltration were seen in WT and *Ptpn22^{R619W}* mice on day 10 (Figure 5-6a-b). This was consistent with the macroscopic measurements taken during the course of the disease. This again indicates that the presence of the autoimmune associated variant of PTPN22 alone is not sufficient to enhance the susceptibility of mice to this model of arthritis.

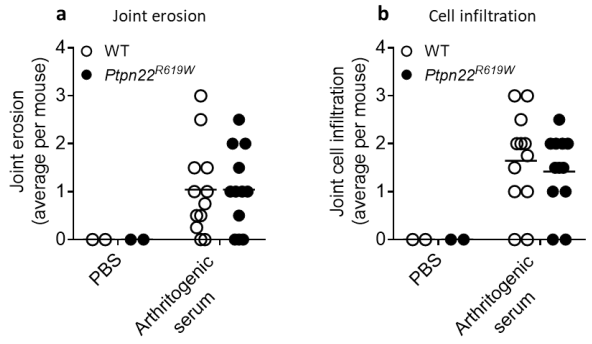

Figure 5-6: Ptpn22^{R619} (WT) and Ptpn22^{R619W} mice have similar ankle joint erosion and cell infiltration at day 10 of the K/BxN serum transfer model of arthritis.

(a-b) WT and Ptpn22^{R619} mice were injected (i.p.) with 150 µl PBS or arthritogenic serum (diluted 1:1 with PBS) on days 0 and 2. On day 10, mice were culled and ankle joints were removed before being fixed, decalcified, embedded in paraffin, sectioned and stained with Hematoxylin and Eosin. WT (white) and Ptpn22^{R619W} (black) ankle joint sections were scored from 0-3 for joint erosion (a) and cell infiltration (b). Scores shown are averages of 2 ankle joints per mouse. n = 2 (PBS) and 12 (arthritogenic serum), and were assigned blinded to clinical scores and genotypes.

5.3.5 Immune cell populations are similar in the spleens and joint draining LNs of WT and *Ptpn22*$^{-/-}$ mice

To identify whether changes in immune cell populations in the spleens or joint draining lymph nodes of WT and *Ptpn22*$^{-/-}$ arthritic mice could account for the observed differences in disease severity, mice were culled at the peak of disease and spleens and axial/brachial (wrist draining) and popliteal (ankle draining) lymph nodes were removed. Single cell suspensions were stained with antibodies to identify immune cell subsets including T cells, DCs, monocytes and neutrophils (see Materials and Methods Figure 2-23 for example gating). Similar numbers of T cells, monocytes and neutrophils were found in the wrist draining LNs and the spleens of WT and *Ptpn22*$^{-/-}$ mice, regardless of disease status (Figure 5-7b-c). *Ptpn22*$^{-/-}$ mice showed enhanced cDC and cDC2 populations in these organs, but this was also independent of disease status (Figure 5-7b-c). In contrast, enhanced numbers of T cells, monocytes, DCs and neutrophils were found in the ankle draining lymph nodes of arthritic compared to healthy mice (Figure 5-7d). Despite this, the numbers of these populations were not dependent on the genotype of the mice (Figure 5-7d). This shows that although disease state can be distinguished by the enhanced numbers of immune cells in the ankle draining lymph nodes, it does not provide an explanation for the enhanced disease seen in *Ptpn22*$^{-/-}$ mice (Figure 5-7a).

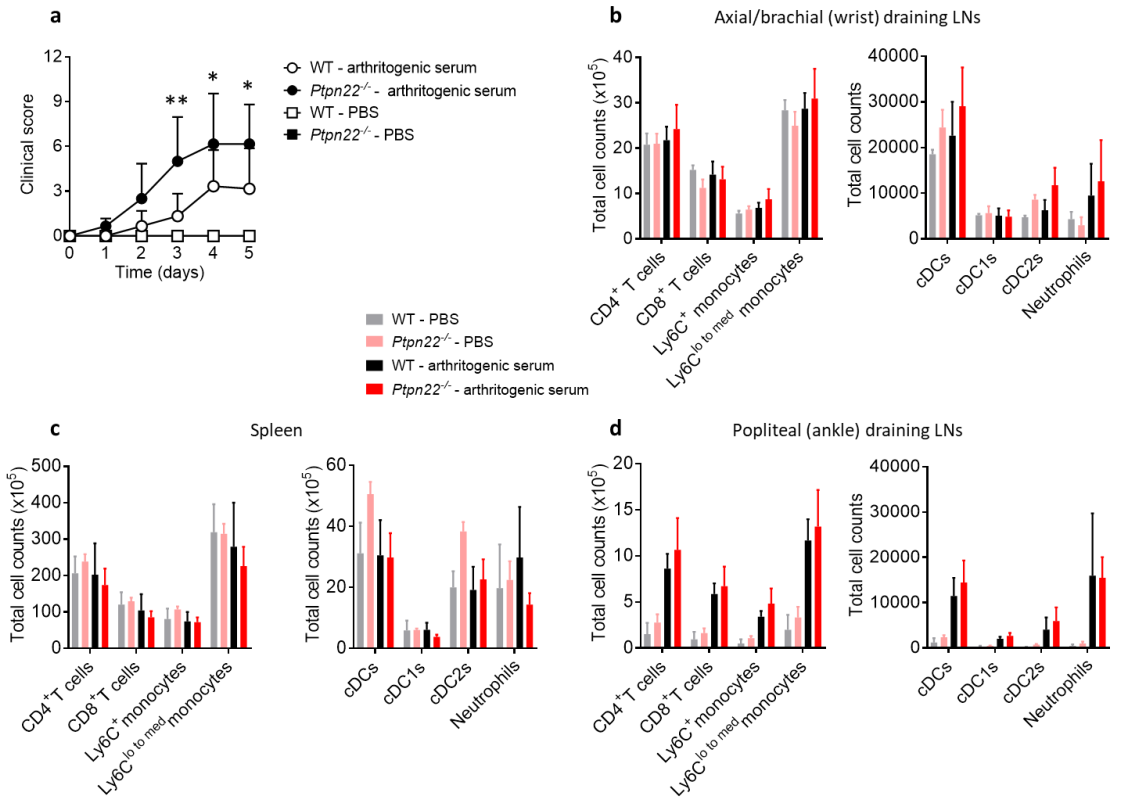

Figure 5-7: WT and Ptpn22$^{-/-}$ healthy and arthritic mice have equivalent numbers of immune cells in their draining lymph nodes and spleens on day 5 of the K/BxN serum transfer model of arthritis.

*(a-d) WT and Ptpn22$^{-/-}$ mice were injected (i.p.) with 150 µl PBS or arthritogenic serum (diluted 1:1 with PBS) on days 0 and 2. (a) Average clinical scores are shown for WT (white) and Ptpn22$^{-/-}$ (black) mice injected with PBS (square) or arthritogenic serum (circle). n= 3 (PBS) and 6 (arthritogenic serum) ± s.d; *p<0.05, **p<0.01 using a 2-way ANOVA with Tukey's multiple comparisons test (shown for arthritogenic serum WT v Ptpn22$^{-/-}$ only). (b-d) On day 5, mice were culled and joint draining lymph nodes and spleens were removed and stained for immune cell phenotyping by flow cytometry. Data shows total cell numbers for each population in the axial/brachial draining lymph nodes (b), spleens (c), and popliteal draining lymph nodes (d) of WT (grey and black) and Ptpn22$^{-/-}$ (pink and red) mice. n = 3 (PBS) and 6 (arthritogenic serum) ± s.d.*

5.3.6 There is a trend towards an enhanced neutrophil frequency in the ankle joints of *Ptpn22$^{-/-}$* arthritic mice

Since the immunophenotyping of spleens and LNs from healthy and arthritic mice did not show any striking differences between WT and *Ptpn22$^{-/-}$* mice, I next wanted to study the site of inflammation, by phenotyping the immune cells present in the joints of the mice. Only joints that were visually swollen were removed for analysis on day 5, because, based on the H+E staining, there is no cell infiltration in the joints of healthy mice (Figures 5-5d and 5-6b). Ankle joints and wrist joints were processed separately, but if a mouse had both ankle joints (or wrist

joints) that were swollen, then the cells from both joints were pooled. As different amounts of tissue were analysed for each mouse, absolute cell numbers for each immune population could not be calculated. Instead, the cell frequency of each subset within the total live cell population was calculated. $CD4^+$ T cells, monocytes and neutrophils could be detected in the joints, with the near complete absence of DCs and $CD8^+$ T cells (Figure 5-8a-b). Similar frequencies of $CD4^+$ T cells and monocytes were found in arthritic WT and *Ptpn22*$^{-/-}$ joints (Figure 5-8a-b). However, there was a trend towards an enhanced frequency of neutrophils in *Ptpn22*$^{-/-}$ ankle joints (Figure 5-8a). This observation was discovered in an independent experiment, but the number of mice analysed was low. If it is true that there are more neutrophils in the joints of *Ptpn22*$^{-/-}$ mice, this may provide an explanation for the enhanced disease observed.

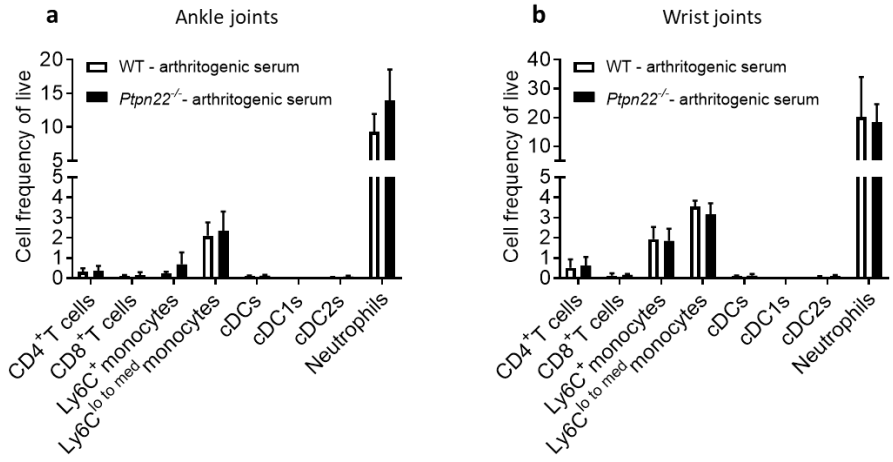

Figure 5-8: WT and Ptpn22$^{-/-}$ arthritic mice have equivalent numbers of immune cells in their joints on day 5 of the K/BxN serum transfer model of arthritis.

(a-b) WT and Ptpn22$^{-/-}$ mice were injected (i.p.) with 150 µl arthritogenic serum (diluted 1:1 with PBS) on days 0 and 2. On day 5, mice were culled and joints were removed and stained for immune cell phenotyping by flow cytometry. Data shows frequency of live for each population in the ankle joints (a) and wrist joints (b) of WT (white) and Ptpn22$^{-/-}$ (black) mice. n= 2 (WT ankle) or 3 (WT wrist) and 5 (Ptpn22$^{-/-}$) ± s.d.

5.3.7 Micro-CT analysis reveals an increase in bone volume and trabecular thickness in *Ptpn22*$^{-/-}$ arthritic mice

To identify whether there were differences in the structure of the bones in WT and *Ptpn22*$^{-/-}$ mice after the K/BxN serum transfer model of arthritis, ankle joints were removed from healthy and arthritic mice on day 10 after disease induction, and transferred to the lab of Dr Nicole Horwood (University of Oxford) for micro-CT analysis of the calcaneal bones. WT arthritic mice showed a reduction in bone volume and trabecular thickness compared to healthy WT mice

(who received PBS) (Figure 5-9b-c). This reduction was not observed between *Ptpn22*$^{-/-}$ healthy and arthritic mice (Figure 5-9b-c).

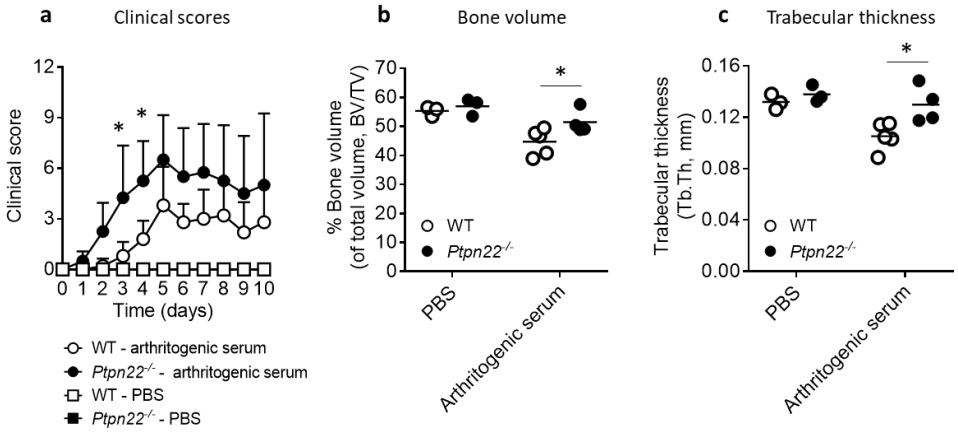

Figure 5-9: Micro-CT analysis of bones from WT and Ptpn22$^{-/-}$ healthy and arthritic mice.

*(a-c) WT and Ptpn22$^{-/-}$ mice were injected (i.p.) with 150 µl PBS or arthritogenic serum (diluted 1:1 with PBS) on days 0 and 2. Clinical scores were collected daily and bones were subjected to micro-CT scanning on day 10. (a) Average clinical scores are shown for WT (white) and Ptpn22$^{-/-}$ (black) mice injected with PBS (square) or arthritogenic serum (circle). n = 3 (PBS) and 4-5 (serum) ± s.d; *p<0.05 using a 2-way ANOVA with Tukey's multiple comparisons test (shown for arthritogenic serum WT v Ptpn22$^{-/-}$ only). (b-c) Micro-CT analysis of the calcaneal bone from WT (white) and Ptpn22$^{-/-}$ (black) mice on day 10, showing % bone volume of total volume (BV/TV) (b) and trabecular thickness (Tb.Th) (c). n = 3 (PBS) and 4-5 (serum), where each point is an individual mouse; *p<0.05 using a 2-way ANOVA with Sidak's multiple comparisons test. All micro-CT analysis was performed by the lab of Dr Nicole Horwood (University of Oxford).*

5.3.8 Using a novel PET radionuclide imaging tool to detect and quantify disease in whole animals

To visualise disease using the K/BxN transfer model of arthritis on the level of the whole organism, I utilised Positron Emission Tomography/Computed Tomography (PET/CT) imaging, a non-invasive imaging technique (see Materials and Methods Figure 2-24 for experimental setup). Using a trimeric RGD peptide chelated to a radioisotope ($^{68}Ga(HP_3\text{-}RGD_3)$), which binds to the integrin αvβ3, this technique allowed for the visualisation of areas of inflammation in an intact mouse. The integrin αvβ3 is expressed at low levels in healthy tissue, but is upregulated in sites of inflammation, on cells including angiogenic endothelium, osteoclasts and myeloid cells. PET/CT imaging was combined with biodistribution, which is invasive and terminal, but is more sensitive than PET imaging.

Initially, healthy and arthritic WT mice were imaged by PET, and uptake of $^{68}Ga(HP_3\text{-}RGD_3)$ was measured in different organs by biodistribution. Uptake was similar between healthy and arthritic mice in non-target organs including the blood, muscle, lung, spleen, pancreas, stomach, gut, liver and femur, although uptake in the kidney was higher in arthritic mice (Figure 5-10a). In the ankle and wrist joints, uptake was higher in the arthritic mice compared to the healthy mice (Figure 5-10a), and this was also apparent in the knees and the shoulders, which do not show obvious inflammation macroscopically. $^{68}Ga(HP_3\text{-}RGD_3)$ uptake in the hands and wrists, and feet and ankles was correlated with paw swelling (from the caliper measurements), to determine whether the use of this radiolabelled peptide was appropriate for monitoring disease severity. Both the hands and wrists, and the feet and ankles showed positive correlations between $^{68}Ga(HP_3\text{-}RGD_3)$ uptake and paw swelling (Figure 5-10b). In addition to analysing $^{68}Ga(HP_3\text{-}RGD_3)$ uptake by biodistribution, whole body PET/CT images were acquired. These showed non-specific uptake in the kidneys and bladder, due to normal excretion of the radiolabelled peptide, but there were also areas of RGD peptide uptake which were visible in the ankle and wrist joints of arthritic mice (Figure 5-10c), and this correlated with clinical scores.

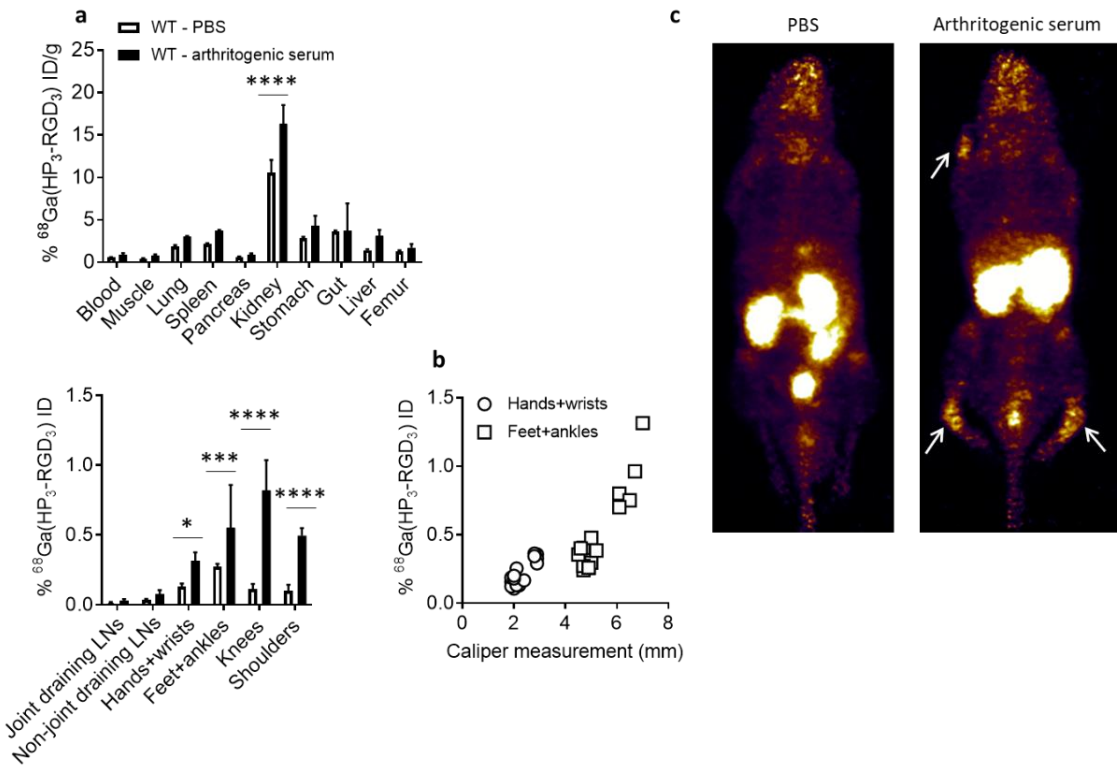

Figure 5-10: PET/CT imaging and biodistribution of WT mice.

*(a-c) WT mice were injected (i.p.) with 150 µl PBS or arthritogenic serum (diluted 1:1 with PBS) on days 0 and 2. Clinical scores were collected daily and mice were injected with $^{68}Ga(HP_3\text{-}RGD_3)$ (i.v.) on day 8. 1 hour post injection, mice were culled and subjected to PET/CT imaging and biodistribution. (a) % $^{68}Ga(HP_3\text{-}RGD_3)$ uptake in non-target organs (% of injected dose, ID, corrected for organ weight, in grams, top) and target organs (% of injected dose, ID, bottom) is shown for WT mice that received PBS (white) and WT mice that received arthritogenic serum (black). n = 3 ± s.d; *p<0.05,***p<0.005, ****p<0.0001 using a 2-way ANOVA with Tukey's multiple comparisons test. (b) Correlation showing % $^{68}Ga(HP_3\text{-}RGD_3)$ uptake in hands and wrists (circle) and feet and ankles (square) (% of injected dose, ID) with caliper measurements (for feet and ankles, the footpad and ankle measurements have been added together), from all mice, where each point represents an individual joint from a mouse; Pearson's r^2 = 0.762 (hands and wrists) and 0.8784 (feet and ankles). (c) Example PET images of a mouse that received PBS (left) and a mouse that received arthritogenic serum (right). Note the signal detected in the wrists and ankles of the arthritic mouse (indicated by arrows). All experiments were carried out with Dr Samantha Terry and Dr Michelle Ma (King's College London).*

To investigate whether this technique could be used to identify differences in disease in the absence and presence of PTPN22, similar experiments were carried out with WT and *Ptpn22*$^{-/-}$ mice. Uptake of $^{68}Ga(HP_3\text{-}RGD_3)$ in non-target organs was the same regardless of the genotype of the mice and the disease status (Figure 5-11a). In the joints, there was enhanced uptake in arthritic mice compared to healthy mice in the feet and ankles ($p<0.05$ for WT mice and $p<0.0001$ for *Ptpn22*$^{-/-}$ mice) (Figure 5-11a). In addition, there was enhanced uptake of $^{68}Ga(HP_3\text{-}RGD_3)$ in the hands and wrists, feet and ankles, and shoulders of *Ptpn22*$^{-/-}$ arthritic mice compared to WT arthritic mice (Figure 5-11a). This suggests that expression of αvβ3 is higher in

the joints of arthritic *Ptpn22*$^{-/-}$ mice compared to WT mice. Finally, uptake of the radiolabelled RGD peptide positively correlated with paw swelling measurements for both WT and *Ptpn22*$^{-/-}$ mice (Figure 5-11b). Enhanced ^{68}Ga(HP$_3$-RGD$_3$) uptake is due to higher integrin αvβ3 expression, and this could indicate that there are more osteoclasts present in the joints of arthritic *Ptpn22*$^{-/-}$ mice, which would then result in more bone erosion, thus correlating with the more severe arthritis that I have observed.

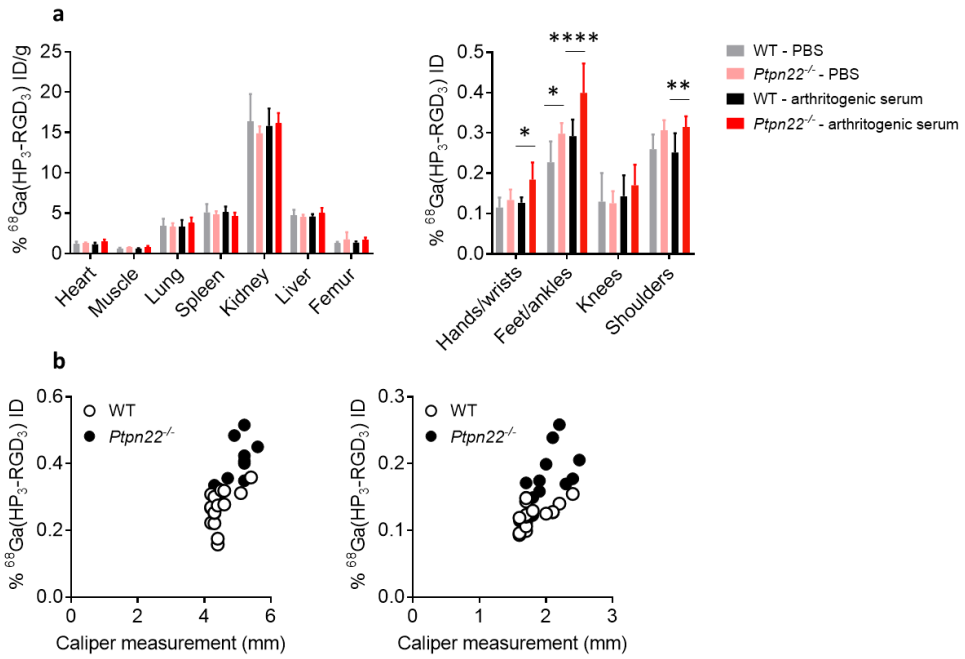

Figure 5-11: Biodistribution of WT and Ptpn22$^{-/-}$ healthy and arthritic mice after injection with ^{68}Ga(HP$_3$-RGD$_3$).

*(a-b) WT and Ptpn22$^{-/-}$ mice were injected (i.p.) with 150 µl PBS or arthritogenic serum (diluted 1:1 with PBS) on days 0 and 2. Clinical scores were collected daily and mice were injected with ^{68}Ga(HP$_3$-RGD$_3$) (i.v.) on day 6. 1 hour post injection, mice were culled and subjected to biodistribution. (a) % ^{68}Ga(HP$_3$-RGD$_3$) uptake in non-target organs (% of injected dose, ID, corrected for organ weight, in grams, left) and target organs (% of injected dose, ID, right) is shown for WT mice WT (grey and black) and Ptpn22$^{-/-}$ (pink and red) mice. n = 3 (PBS) and 5 (arthritogenic serum) ± s.d; *p<0.05,**p<0.01, ****p<0.0001 using a 2-way ANOVA with Tukey's multiple comparisons test (only WT v Ptpn22$^{-/-}$ comparisons for either PBS or arthritogenic serum are shown, for simplicity). (b) Correlation showing % ^{68}Ga(HP$_3$-RGD$_3$) uptake in feet and ankles (left) and hands and wrists (right) (% of injected dose, ID) with caliper measurements (for feet and ankles, the footpad and ankle measurements have been added together), from WT (white) and Ptpn22$^{-/-}$ (black) mice, where each point represents an individual joint from a mouse; Pearson's r^2 = 0.3713 (WT hands and wrists), 0.4679 (Ptpn22$^{-/-}$ hands and wrists), 0.2768 (WT feet and ankles) and 0.6452 (Ptpn22$^{-/-}$ feet and ankles). All experiments were carried out with Dr Samantha Terry and Dr Michelle Ma (King's College London).*

5.3.9 PTPN22 is dispensable for osteoclast differentiation *in vitro*

Osteoclasts are responsible for the bone erosion seen during arthritis, and as the enhanced uptake of $^{68}Ga(HP_3\text{-}RGD_3)$ in the joints of arthritic *Ptpn22*$^{-/-}$ mice suggests that there are more osteoclasts present in these mice, I next wanted to investigate whether PTPN22 played a role in their differentiation and/or function. WT and *Ptpn22*$^{-/-}$ bone marrow cells were differentiated *in vitro*, in the presence of M-CSF alone (as a negative control) and M-CSF and RANK-L (to differentiate osteoclasts). On day 10 of culture, a commercial kit was used to stain for the osteoclast specific enzyme tartrate-resistant acid phosphatase (TRAP). As osteoclasts are multinucleated cells, they are characterised as being TRAP positive, and having three of more nuclei. Quantification of the proportion of the cultures that were either TRAP$^-$, TRAP$^+$ with 1 or 2 nuclei, and TRAP$^+$ with three or more nuclei (osteoclasts), showed that the lack of PTPN22 expression did not affect osteoclast differentiation *in vitro* based on these readouts (Figure 5-12a-b).

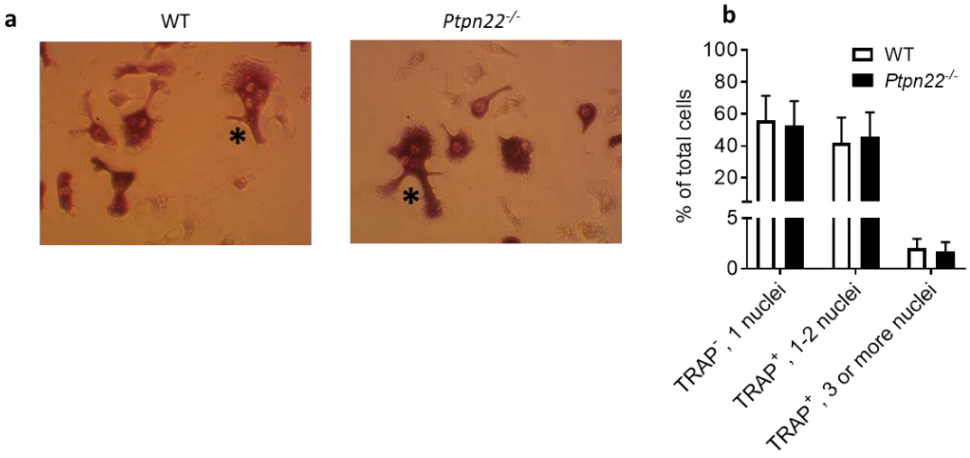

Figure 5-12: PTPN22 is dispensable for osteoclast differentiation in vitro.

(a-b) WT and Ptpn22$^{-/-}$ bone marrow progenitor cells were differentiated in the presence of M-CSF and RANK-L for 10 days. TRAP staining was carried out to visualise differentiated osteoclasts. (a) Example images of TRAP stained WT (left) and Ptpn22$^{-/-}$ (right) cultures, taken using a 40x objective. The stars indicate osteoclasts (TRAP$^+$, with 3 or more nuclei). (b) Combined quantification of TRAP stained WT (white) and Ptpn22$^{-/-}$ (black) TRAP stained cultures. n = 14 ± s.d.

In order to measure osteoclast differentiation in a more quantitative manner, RNA was extracted from osteoclast cultures at day 12 of culture and reverse transcribed into cDNA. Expression of *Ptpn22* was first analysed, to verify that WT osteoclasts expressed the gene and that *Ptpn22*$^{-/-}$ osteoclasts did not (Figure 5-13a). After this, qRT-PCR was carried out to look at the expression of osteoclast specific genes *Itgb3, Ctsk, Tnfrs11a* and *Mmp9*. cDNA from WT and

Ptpn22$^{-/-}$ bone marrow cells grown in the presence of M-CSF only were used as negative controls. Both WT and *Ptpn22*$^{-/-}$ bone marrow cells differentiated in the presence of M-CSF and RANK-L expressed higher levels of the osteoclast specific genes compared to M-CSF dependent macrophages, grown in the presence of M-CSF only (Figure 5-13b-e). Both WT and *Ptpn22*$^{-/-}$ cells expressed similar levels of these genes, indicating that PTPN22 is dispensable for osteoclast differentiation *in vitro*, which is consistent with the quantification of TRAP staining.

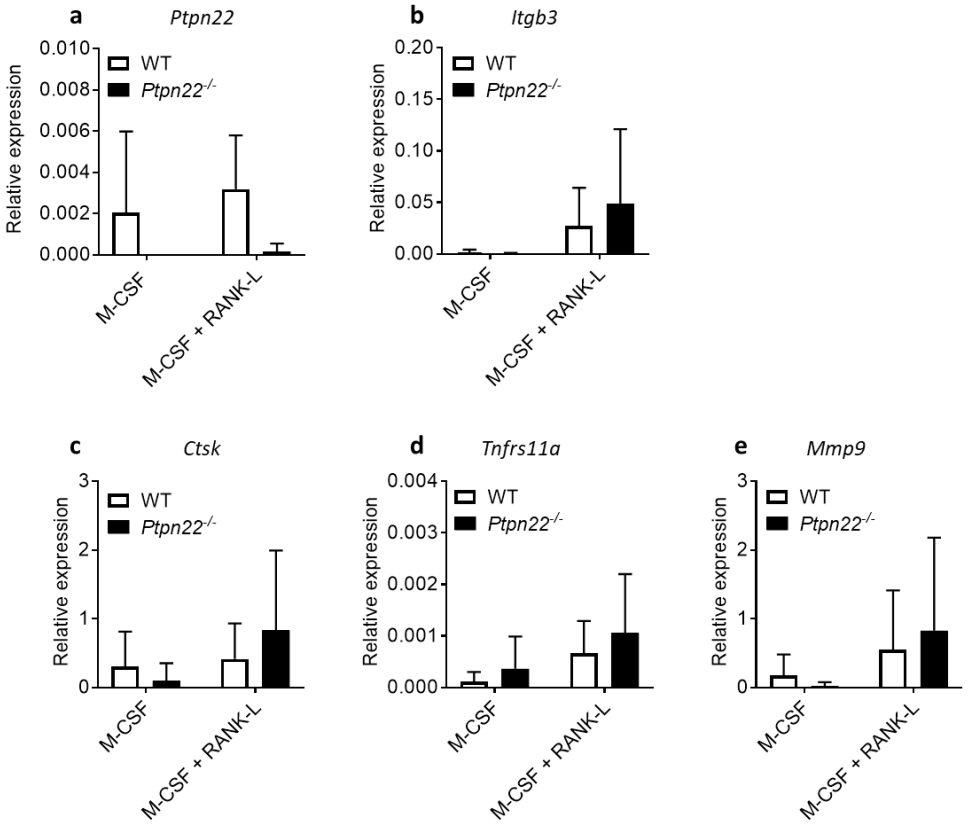

Figure 5-13: PTPN22 is dispensable for osteoclast differentiation in vitro.

(a-d) WT and Ptpn22$^{-/-}$ *bone marrow progenitor cells were differentiated in the presence of M-CSF alone or M-CSF and RANK-L for 12 days. Cells were lysed and mRNA was extracted and reverse transcribed into cDNA. qRT-PCR was carried out to look at expression of osteoclast specific genes. Expression was determined using* $2^{(-\Delta Ct)}$*, all relative to B2m. WT (white) and Ptpn22*$^{-/-}$ *(black) cell expression of Ptpn22 (a), Itgb3 (b), Ctsk (c), Tnfrs11a (d), and Mmp9 (e). n = 7* $\pm$ *s.d.*

5.3.10 PTPN22 is not required for osteoclast function *in vitro*

Although I have found that PTPN22 is not required for osteoclast differentiation *in vitro,* I wanted to investigate whether the phosphatase is required for their function. c-Src is needed for normal osteoclast structure and function, as osteoclasts from mice lacking c-Src expression are unable to form ruffled borders, have reduced cell migration and are unable to resorb bone[228].

To investigate a potential role of PTPN22 in osteoclast function, WT and *Ptpn22*$^{-/-}$ bone marrow cells were cultured in the presence of M-CSF or M-CSF and RANK-L in wells coated with Europium labelled collagen. As the cells differentiate, they will become capable of degrading the underlying collagen. This will cause the release of Europium labelled collagen fragments from the bottom of the wells, into the media. The released collagen fragments can be measured on a plate reader and used as a measure of osteoclast differentiation and degradation. Over the course of the culture, more collagen fragments were released from the bottom of the wells by the cells, and the level of collagen degradation was highest in the presence of M-CSF and RANK-L, compared to M-CSF alone (Figure 5-14). However, both WT and *Ptpn22*$^{-/-}$ cells released similar levels of collagen into the media, indicating that PTPN22 is not required for osteoclast function *in vitro* (Figure 5-14).

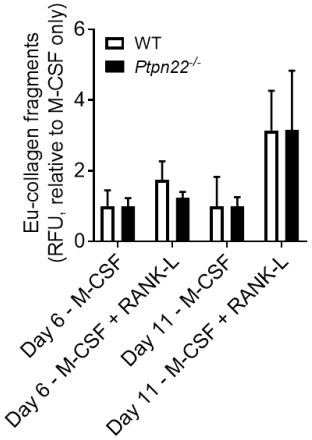

Figure 5-14: PTPN22 is dispensable for osteoclast dependent collagen degradation.

WT and Ptpn22$^{-/-}$ *bone marrow progenitor cells were differentiated in the presence of M-CSF alone or M-CSF and RANK-L for 11 days in wells coated with Europium labelled collagen. Cell-free supernatants were removed on days 6 and 11 and the amount of collagen fragments present in the media was determined using an OsteoLyse assay and measured using a plate reader. Collagen fragments detected in media from WT (white) and Ptpn22*$^{-/-}$ *(black) cells grown in the presence of M-CSF and RANK-L relative to cells grown in the presence of M-CSF alone. n = 3 ± s.d.*

5.4 Overall findings

The main findings of this Chapter were:

1. Lack of PTPN22 expression causes more severe disease using the K/BxN serum transfer model of arthritis.
2. This is not associated with detectable changes in serum cytokines, chemokines, joint damage or immune cell infiltration in the joints and joint draining lymph nodes.

3. PET imaging of a ^{68}Ga labelled RGD peptide can be used to image areas of inflammation in whole animals, and enhanced ^{68}Ga(HP_3-RGD_3) uptake was detected in the joints of arthritic *Ptpn22*$^{-/-}$ mice.
4. PTPN22 is dispensable for osteoclast differentiation and function *in vitro*.

Some of these data have been published in:

2. Imberti C, Terry SY, Cullinane C, **Clarke F**, Cornish GH, Ramakrishnan NK, Roselt P, Cope AP, Hicks RJ, Blower PJ, Ma MT. Enhancing PET Signal at Target Tissue in Vivo: Dendritic and Multimeric Tris(hydroxypyridinone) Conjugates for Molecular Imaging of $\alpha_v\beta_3$ Integrin Expression with Gallium-68. *Bioconjugate Chemistry* **28** (2017).

5.5 Discussion

This Chapter has investigated whether PTPN22 plays a role in a mouse model of rheumatoid arthritis and whether it is required for osteoclast differentiation and function. *Ptpn22*$^{-/-}$ mice were found to be more susceptible to the K/BxN serum transfer model of arthritis. As Chapters 3 and 4 demonstrated that PTPN22 is required to negatively regulate DC effector responses after immune complex engagement, and disease using this model is initiated by the transfer of autoantibodies, this suggests that dysregulated responses to autoantibodies/immune complexes in the absence of PTPN22 could account for the enhanced disease that I have observed.

My observation that *Ptpn22*$^{-/-}$ mice show enhanced disease using the K/BxN serum transfer model of arthritis is in contrast with published data showing that PTPN22 either augments[63] or has no effect on disease development[10,59]. There are multiple reasons for this discrepancy, including differences in the titre of the arthritogenic serum administered. It has been shown in $CD8^+$ T cells that PTPN22 negatively regulates TCR signalling by weak antigens, but has no effect on responses to strong antigens[291], so it may be possible that PTPN22 is regulating signalling downstream of FcγRs differently depending on the amount of autoantibodies/immune complexes present, which would be dependent on the titre of the serum used. In addition, it has been shown that the prevalence and severity of arthritis in the K/BxN model and the K/BxN serum transfer model of arthritis are regulated by the microbiota, such that after antibiotic treatment, arthritis severity is reduced[292,293]. The reduction in disease severity has been attributed to a deficiency of peripheral Th17 cells in the absence of the microbiota, especially

segmented filamentous bacteria[294]. Therefore, it is possible that differences in mouse housing between research groups could account for the disparity in results. In agreement with this, I have found that disease severity is drastically different between mice that have been bred in-house and C57Bl/6 mice that has been bought in from a commercial supplier. When I injected mice from our colony and C57Bl/6 mice from Charles River (age and sex matched) simultaneously, using the same batch of arthritogenic serum, the Charles River mice developed a more severe disease, with higher penetrance (unpublished observations).

Despite expression of PTPN22^{R620W} in humans being associated with an enhanced susceptibility to multiple autoimmune diseases, I did not find an increased incidence of arthritis in *Ptpn22^{R619W}* mice compared to WT mice. This result is not entirely unexpected, as although humans harbouring the PTPN22 variant have an increased risk of autoimmune disease, it is not considered to be a causative allele. There are more than 100 risk alleles which have been associated with RA[295,296], with the odds ratio of PTPN22^{R620W} for RA being 1.3-2.13[295]. In addition, environmental factors affect the likelihood of disease, and these are more varied in humans compared to inbred mice housed in a controlled environment. The K/BxN serum transfer model of arthritis has been previously reported using *Ptpn22^{R619W}* mice, where, in agreement with my data, they also displayed similar disease to WT mice[10].

Changes in serum cytokines and chemokines during the disease could not account for the difference in WT and *Ptpn22$^{-/-}$* disease. The difference in cytokine secretion between healthy and arthritic mice was not striking, which was surprising as it has been shown that enhanced expression of pro-inflammatory cytokines such as IL-17, IL-1 and TNFα in the joints can lead to tissue destruction[290]. However, as cytokines act locally, in a regulated manner, it would be beneficial in the future to look at cytokine secretion in the joints, as opposed to systemically. I did however find enhanced expression of IFNβ and IL-27 in the serum of *Ptpn22$^{-/-}$* mice on day 3, independent of disease status. Enhanced IL-27 has been found in the serum of RA patients, and this positively correlated with disease activity[297]. IL-27 is secreted by antigen presenting cells and can bind to its receptor on T cells and NK cells. In this way, IL-27 can promote the differentiation of naïve CD4$^+$ T cells into Th1 cells, thus inducing a pro-inflammatory response. It is therefore possible that by expressing enhanced IL-27 in the steady state, *Ptpn22$^{-/-}$* mice are more likely to show a more pro-inflammatory phenotype, as shown by enhanced disease after transfer of the arthritogenic serum. However, anti-inflammatory effects of IL-27 have also been documented. I did also detect reduced serum levels of LIX in arthritic *Ptpn22$^{-/-}$* mice compared to arthritic WT mice. LIX has been found to be elevated in the synovial fluid of RA patients compared to osteoarthritis patients[298]. It has also been shown to cause human neutrophil chemotaxis[299] and anti-LIX treatment reduced arthritis in mice[300]. This indicates that LIX is

involved in driving inflammation during arthritis, which is at odds with the fact that I found reduced serum levels of LIX in *Ptpn22*$^{-/-}$ mice, which showed enhanced clinical signs of disease compared to WT mice. This may be because I measured chemokine expression in the serum and not in the joints of the mice.

Histological analysis of the joints of healthy and arthritic mice demonstrated that joint cell infiltration and erosion were similar between WT and *Ptpn22*$^{-/-}$ mice. This may have been partly because in the experiment used for the histology, the *Ptpn22*$^{-/-}$ mice developed disease more rapidly and had begun to resolve by the end of the experiment. This meant that on day 9, the WT and *Ptpn22*$^{-/-}$ mice showed similar disease severity. There was however a slight trend towards enhanced cell infiltration in the ankle joints of *Ptpn22*$^{-/-}$ mice, but due to the low number of samples analysed, no conclusion could be made on this potential difference. By analysing more ankle joints in the future, it should be possible to draw more firm conclusions regarding a potential increase in joint cell infiltration in *Ptpn22*$^{-/-}$ mice. No difference in joint cell infiltration or joint erosion was observed between WT and *Ptpn22*^{R619W} mice, but this was not surprising, as there was no difference in disease severity.

Immune phenotyping of cells in the joints and joint draining lymph nodes revealed a trend towards an increased frequency of neutrophils in the ankle joints of arthritic *Ptpn22*$^{-/-}$ mice, but this was not significant, most likely due to the low number of samples. Neutrophils are pivotal in acute and chronic disease as they can release a variety of mediators which cause inflammation and tissue damage. This includes releasing pro-inflammatory cytokines, reactive oxygen species, secreting degradative enzymes (including MMP-8, MMP-9, cathepsin G, neutrophil elastase and proteinase 3) and releasing neutrophil extracellular traps (NETs)[301]. In addition, neutrophils have also been found to be indispensable for the K/BxN serum transfer model of arthritis[181].

In my experiments I found that the immune cell populations were greatly expanded in the ankle joint draining lymph nodes of arthritic mice compared to the healthy mice, although this was not the case in the wrist draining lymph nodes (except for neutrophils) or the spleens. The spleen is probably too systemic to see any changes. In the future, it would be interesting to look at these immune cell populations at different time points during the disease, as the different cell types do not enter the joints simultaneously. In addition, solely looking at changes in total cell numbers may not lead to a correlation with disease severity. Alternatively, it may be more revealing to do more in depth phenotyping, for example, to identify T cell subsets which are important in disease progression such as Th17 cells. It has been shown that blocking IL-17 in K/BxN mice causes reduced disease[294], mice lacking expression of IL-17 have reduced development of CIA[302] and that Th17 cells are elevated in the synovial fluid of RA patients compared to peripheral blood[303]. To further characterise the immune cells present in the joints

and joint draining lymph nodes, single cell suspensions could be stimulated *in vitro* with PMA and ionomycin such that expression of cytokines could be detected. In addition, specific cell populations could be isolated, and their function could be tested *in vitro.* It may be possible that PTPN22 regulates the function of immune cells present in the joints and/or draining lymph nodes, without affecting the cell frequencies or total cell numbers.

PET/CT imaging was found to be a useful technique to visualise areas of inflammation at the whole organism level using the K/BxN serum transfer model of arthritis. Uptake of $^{68}Ga(HP_3\text{-}RGD_3)$ by PET positively correlated with clinical scores, demonstrating that the technique provides a robust way of non-invasively monitoring disease in mice, especially those joints that are difficult to assess clinically (e.g. shoulders). In the future it would interesting to image mice at multiple time points, especially in very early disease, in order to identify whether the technique is sensitive enough to identify areas of inflammation before clinical signs are visible. It would also be beneficial to see whether the technique could be used to monitor resolution of disease and responses to therapies. If this was successful, then this technique could potentially be used to monitor patients to see whether a treatment was efficacious or not, thus potentially reducing the time before an alternative treatment could be administered.

By using biodistribution, uptake of the radiolabelled RGD peptide was found to be higher in the joints of *Ptpn22*$^{-/-}$ arthritic mice compared to WT arthritic mice. This indicates that expression of the integrin αvβ3 is higher in these mice. αvβ3 is expressed on a variety of cells in the arthritic joint including activated macrophages, activated endothelial cells and osteoclasts. It would be particularly interesting to evaluate the number of osteoclasts present in the joints, to see whether these may be responsible for the enhanced αvβ3 expression, and therefore could be responsible for the more severe disease seen in *Ptpn22*$^{-/-}$ mice. Visualisation of osteoclasts could be achieved by carrying out TRAP staining on joint sections.

As osteoclasts are the only bone resorbing cell type, the role of PTPN22 in their differentiation and function was assessed. Bone marrow cells lacking PTPN22 were found to differentiate normally into osteoclasts. In addition, *Ptpn22*$^{-/-}$ osteoclasts were equally capable of degrading collagen as WT osteoclasts. One of the reasons why PTPN22 may be dispensable for osteoclast differentiation, may be due to the presence of other protein tyrosine phosphatases of the PTP-PEST family, such as PTPN12. PTPN12 has been shown to be required for RANK-L dependent fusion of macrophages into osteoclasts[232]. One caveat of these *in vitro* cultures was that only a proportion of the bone marrow cells differentiated into osteoclasts, indicating that the culture conditions were not optimal. In the future, it would be interesting to test different osteoclast differentiation protocols, for example, differentiation using immune complexes[304,305]. In addition, the cells could have been differentiated for longer, to see whether this could increase

the proportion of osteoclasts in the cultures. Alternatively, the M-CSF and RANK-L concentrations could have been tested to see if a different concentration could have been more effective. Differentiating osteoclasts in tissue culture plates is not optimal as osteoclasts need to come into contact with bone in order to become fully functional osteoclasts, with a resorptive capacity. I could have instead cultured the progenitor cells on dentine slices, which more closely mimic differentiation of cells *in vivo*. The non-optimal culture conditions may provide a reason why the expression of osteoclast specific genes and the collagen degradation was not too dissimilar between cells cultured with M-CSF alone, or with M-CSF and RANK-L.

6. Discussion

6.1 New insights into the role of PTPN22 in mice, and potential implications for PTPN22^{R620W} expression in humans

When I started this research project, the majority of the published data reporting on the role of PTPN22 in regulating immune receptors in mice was focused on the TCR and BCR. More recently, its role in regulating myeloid cell receptor signalling has been investigated, and my studies have contributed to this knowledge. Table 6-1 lists the signalling pathways which have been investigated to date.

Signalling Pathway	Role of PTPN22 in regulating pathway	Likely substrates	Reference
TCR	Negative regulator	Lck, Fyn, ZAP-70	Hasegawa K, Science, 2004[55]
BCR	No affect/negative regulator	Lyn, Fyn, Blk, Syk	Hasegawa K, Science, 2004[55] and Dai X, JCI, 2013[13]
TLR	Positive regulator	TRAF3 (not via its enzymatic function)	Wang Y, Immunity, 2013[10]
Dectin-1	Negative regulator	Syk	Purvis HA, EJI, 2018[66]
LFA-1	Negative regulator	Lck, ZAP-70	Brownlie RJ, Science Signaling, 2012[58], Burn GL, Science Signaling, 2016[60] and Sanchez-Blanco C, Journal of Autoimmunity, 2018[61]
FcγR	Negative regulator	Src, Hck, Fgr, Lyn, Syk	Clarke F, Scientific Reports, 2018[306]

Table 6-1: Signalling pathways in mice in which the role of PTPN22 has been investigated.

Previous mouse and human data have provided multiple explanations as to why expression of PTPN22^{R620W} could increase the risk of autoimmunity. These include alterations in B cell development, leading to an increased frequency of autoreactive B cells[13,81], enhanced BCR signalling[13], which in turn activate autoreactive T cells, promoting the production of germinal centres[12] and subsequent autoantibody production by plasma cells[13], reduced BCR dependent B cell apoptosis[13], expansion of memory T cell populations[12,13,81] and altered T cell skewing[58], leading to a reduction in the ratio of T_{regs} to effector T cells[57], and changes in innate responses, such as reduced type I interferon production by myeloid cells after TLR stimulation[10].

My data compliments these findings by firstly showing that lacking PTPN22 expression, or expression of the autoimmune associated variant of PTPN22 does not regulate antigen endocytosis or processing by *in vitro* generated mouse BMDCs or *ex vivo* splenic DCs. This indicates that changes in antigen uptake and processing by DCs are unlikely to be responsible for promoting autoimmunity in humans harbouring the *PTPN22*^{R620W} risk allele. However, I have found that DC expression of PTPN22 negatively regulates immune complex induced T cell proliferation. If PTPN22^{R620W} acts as a loss-of-function mutation in the context of FcγR signalling, then a lack of regulation of immune complex signalling in DCs could cause enhanced T cell activation, potentially augmenting immune responses to self-antigens. In the future it would be beneficial to investigate FcγR dependent immune responses in DCs from humans expressing PTPN22^{R620W}, which would be especially important due to the presence of autoantibodies in most of the associated autoimmune diseases, such as SLE and RA.

Using the K/BxN serum transfer model of arthritis, mice expressing the orthologue of the human autoimmune associated variant did not develop more severe disease than WT mice. The fact that expression of PTPN22^{R619W} did not affect disease progression is not all together surprising, as although the human variant is associated with an enhanced susceptibility to arthritis, it is not a causative allele, and so not all people harbouring the variant develop arthritis. Other genetic and environmental factors play a role in disease development, which are not recapitulated in the experiments using *Ptpn22*^{R619W} mice. It is likely that investigating the role of the autoimmune associated variant of PTPN22, in both mouse and human cells may not provide a conclusive explanation for the enhanced disease susceptibility associated with PTPN22^{R620W} expression in humans. It may be more informative to investigate the role of this polymorphism in combination with additional risk alleles, for example those involved in TCR, BCR and co-stimulatory molecule signalling, which are also associated with an enhanced risk of autoimmune diseases[307,308].

I did however find that mice lacking expression of PTPN22 were more susceptible to arthritis using this model. This indicates that the impact of phosphatase deficiency is distinct to that associated with expression of the autoimmune associated variant of the phosphatase in this situation. This may be partly because the R619W/R620W mutation will affect the ability of PTPN22 to interact with other proteins but may not detrimentally affect its catalytic activity. In fact, it has been suggested that PTPN22^{R620W} has an increased catalytic activity compared to the WT protein[79]. This could indicate that PTPN22 may be affecting disease via its ability to dephosphorylate kinases, and not via its ability to interact with other proteins, which would explain why lacking the phosphatase affects disease severity whereas expression of the autoimmune associated variant does not.

It has been shown that human monocyte derived DCs which are differentiated in the presence of immune complexes express higher levels of CD40, CD83 and CD86 and that LPS treatment did not further enhance their expression. These DCs also showed low endocytic activity and were less able to induce T cell proliferation[309], indicating that immune complexes regulate DC differentiation and maturation. The phenotype of DCs grown in the presence of immune complexes was found to be similar to DCs from SLE patients. This suggests that in diseases that involve autoantibodies and immune complexes, such as those associated with *PTPN22*^{R620W} expression, altered responses of DCs and DC progenitors to FcγR engagement may play a role in the disease pathogenesis.

6.2 PTPN22 does not regulate antigen uptake or processing

Although Src and Syk family kinases are involved in multiple stages of antigen uptake and processing, I have found that PTPN22, which dephosphorylates these kinases, is dispensable for these processes. The role of PTPN22 in the internalisation of Lucifer yellow (via macropinocytosis) and HKLM, HKCA and ova (via receptor mediated endocytosis) by BMDCs was tested and PTPN22 was found not to be required. In addition, the expression of PTPN22^{R619W} was tested for its ability to affect BMDC internalisation of LY, HKCA and ova and again found not to play a role. This is in contrast with a published report that showed enhanced uptake of *Escherichia coli* (*E.coli*) by *Ptpn22*^{R619W} macrophages[67]. One likely explanation for this discrepancy may be the differences between macrophage and DC antigen uptake. Alternatively, PTPN22 may specifically regulate phagocytosis of *E. coli*, rather than regulating receptor mediated endocytosis more broadly.

6.3 PTPN22 is dispensable for OVA$_{323-339}$ peptide or ova induced T cell proliferation

When BMDCs were pulsed with OVA$_{323-339}$ peptide or ova, I found that PTPN22 was dispensable for WT CD4$^+$ T cell proliferation. PTPN22^{R619W} expression by BMDCs was also found to be dispensable for T cell proliferation after the BMDCs were pulsed with OVA$_{323-339}$ peptide. This is contrary to published reports, which showed that OVA$_{323-339}$ peptide or ova pulsed *Ptpn22*^{R619W} BMDCs induced enhanced T cell proliferation after 4 days[12], and that ova pulsed *Ptpn22*^{R619W} macrophages caused enhanced expression of CD69 on WT CD4$^+$ T cells after 18 hours of co-

culture and enhanced T cell proliferation after 5 days[67]. The reason for these observed differences in T cell activation between my experiments and these previous studies could be due to a variety of factors. One difference is the concentration of ova which has been used. I used 10 µg/ml ova, whereas the *Ptpn22*^{R619W} macrophages were pulsed with 10-100 µg/ml, with little difference in CD69 expression seen at 10 µg/ml and a greater difference being observed at 100 µg/ml[67]. For the ova pulsed *Ptpn22*^{R619W} BMDCs experiments, 100 µg/ml ova was used, and the ratio of T cells to DCs was also different, such that I used 1 DC:2 T cells, and the published report used 1 DC:4 T cells[12]. Finally, the length of the co-culture was not the same between the experiments, as I assessed T cell proliferation after 6 days of co-culture and the other groups used 4 or 5 days.

6.4 PTPN22 is required to regulate immune complex induced T cell proliferation

Investigating the role of PTPN22 in regulating FcγR dependent BMDC responses was a logical strategy because a major feature of the autoimmune diseases associated with *PTPN22*^{R620W} is the presence of autoantibodies. These autoantibodies bind to antigens to form immune complexes, the internalisation of which is mediated by FcRs, ultimately leading to the production of a T cell dependent immune response. Although my data have shown that PTPN22 is dispensable for immune complex binding, uptake and processing, I did however find that immune complex pulsed *Ptpn22*$^{-/-}$ BMDCs were more effective at inducing T cell proliferation. This was accompanied by an enhanced capacity to form BMDC-T cell conjugates, and to present immune complex derived antigens. The absence of PTPN22 may confer a subtle increase in FcγR dependent inflammatory signals that target immune complexed antigen for MHCII presentation. This increase could potentially be due to PTPN22 mediated changes to the balance of activating/inhibitory FcγR expression on the DC surface. This data shows that PTPN22 negatively regulates FcγR dependent T cell activation by BMDCs, and indicates that perturbations to PTPN22 in humans could affect immune complex induced DC effector responses.

The role of PTPN22 in the regulation of FcγR signalling has been previously addressed in neutrophils, where PTPN22 is required for optimal immune complex induced ROS production, adhesion and degranulation[63]. Contrary to this, I found no differences in BMDC effector functions after immune complex stimulation, including the upregulation of co-stimulatory molecules or cytokine secretion. This indicates that the requirement for PTPN22 in the context of FcγR signalling may differ depending on the cell type. Neutrophils are also capable of

mediating MHCII antigen presentation[310], and so in the future it would be interesting to test whether in neutrophils, where PTPN22 has been demonstrated to positively regulate multiple effector functions, FcγR mediated antigen presentation is positively or negatively regulated by PTPN22.

The role of Src and Syk family kinases in Fcγ receptor mediated endocytosis has been established[311]. Syk is essential for FcγR mediated uptake in macrophages[312], neutrophils[312] and DCs[245], and Src family kinases are not essential but are required for optimal uptake of IgG opsonised particles by macrophages[122]. By using small molecule inhibitors, I have also found that immune complex uptake via FcγRs requires Src and Syk family kinases. The discovery that PTPN22, which dephosphorylates these proteins, was dispensable for immune complex uptake may be due to the presence of other phosphatases such as SHP-1, SHP-2, SHIP-1 and SHIP-2 in *Ptpn22*$^{-/-}$ BMDCs. Alternatively, PTPN22 may regulate signalling downstream of FcγRs such that it specifically regulates MHCII antigen presentation, rather than broader BMDC effector functions. In the future, it would be useful to carry out pulldown assays which would allow me to determine whether PTPN22 was physically interacting with Src and Syk family kinases after FcγR crosslinking. If PTPN22 does not interact with its targets after FcγR engagement, then this would provide an explanation as to why PTPN22 is not required for FcγR mediated antigen internalisation and processing. It may then be possible to identify if different PTPN22 family members may instead be regulating FcγR signalling.

In order to identify whether PTPN22 was important in immune complex derived antigen presentation, I carried out assays using immune complexes containing GFP-Eα. I found that in the absence of PTPN22, BMDCs presented more $E\alpha_{52–68}$ peptide-MHCII complexes on their cell surface. However, these assays do not allow me to distinguish between PTPN22 playing a role in the formation of $E\alpha_{52–68}$ peptide-MHCII complexes, their trafficking to the cell surface, or presentation of these complexes on the cell surface. DCs use endolysosomal tubules to transport peptide-MHCII complexes to the cell surface for presentation to T cells[114]. Syk was shown to be required for efficient formation of peptide-MHCII complexes in a murine B cell line[313], and ITAM signalling is required to maintain peptide-MHCII complexes on the surface of DCs[140]. It is therefore possible that in the absence of PTPN22 mediated dephosphorylation, that Syk is more active and could therefore cause enhanced formation of peptide-MHCII complexes on the cell surface, explaining the enhanced immune complex derived antigen presentation that I have observed using *Ptpn22*$^{-/-}$ BMDCs. To look more closely at the formation and trafficking of peptide-MHCII complexes in WT and *Ptpn22*$^{-/-}$ BMDCs, it would be useful in the future to carry out experiments in which the localisation of GFP-Eα could be visualised in combination with antibodies against MHCII and organelle markers by confocal

microscopy; this would be straightforward due to the presence of the GFP tag. In addition, pulse-chase experiments could be used to shed light on peptide-MHCII complex presentation on the cell surface and recycling. It is possible that *Ptpn22*$^{-/-}$ BMDCs present more Eα_{52-68} peptide-MHCII complexes on their cell surface due to an increased rate of formation and/or trafficking, and/or a reduced rate of peptide-MHCII complex recycling. It is possible that by analysing the PTPN22 interactome in BMDCs, that this could provide some idea as to where in the presentation pathway PTPN22 is important.

As internalised immune complexes can also be presented on MHCI[243,253], via cross-presentation, it would be interesting to determine whether PTPN22 in DCs also reduces immune complex induced CD8$^+$ T cell responses. This pathway could be investigated using ova specific OT-I CD8$^+$ T cells. In addition, an antibody exists which detects the OVA peptide SIINFEKL when bound to MHCI (25-D1.16[314]), so this would allow for the role of PTPN22 in immune complex derived antigen cross-presentation to be investigated.

PTPN22 has also been shown to negatively regulate the fungal receptor dectin-1[66], although I have found that PTPN22 is not required for phagocytosis of *C. albicans* via dectin-1. It is possible that PTPN22 may regulate MHCII presentation of antigens derived from *C. albicans* and subsequent *C. albicans* specific T cell activation, but I have not tested this to date.

6.5 Potential redundancy of protein tyrosine phosphatase family members with PTPN22

As other PTP family members will be expressed in *Ptpn22*$^{-/-}$ mice, it is possible that redundancy of these phosphatases with PTPN22 could explain some of my data where PTPN22 has been found to be dispensable, despite the fact that Src and Syk family kinases have been implicated in the majority of the processes that I have investigated. PTP family members include PTPN2 (also known as T cell protein tyrosine phosphatase, TCPTP), PTPN6 (also known as SHP-1), PTPN11 (also known as SHP-2), PTPN12 (also known as PTP-PEST) and PTPN18 (also known as PTP-HSCF). Many of these phosphatases have been shown to play roles in processes that I have investigated. For example, PTPN6 has been shown to be important in negatively regulating signalling downstream of the C-type lectin receptor Siglec-G, leading to reduced expression of peptide-MHCI complexes on mouse CD8α^+ splenic DCs for cross-presentation[315]. In addition, PTPN6 has been shown to be required for phagosome acidification in mouse macrophages[316]. Like PTPN22, PTPN12 is also dispensable for BMDC ova protein induced T cell proliferation and

$OVA_{323-339}$ peptide induced DC-T cell conjugate formation, but is required for the induction of optimal IFNγ secretion by T cells[317]. These data indicate that members of the same phosphatase family can regulate specific and independent DC effector functions. Indeed, as *Ptpn22*$^{-/-}$ BMDCs will express PTPN12, this may also explain why IFNγ secretion was similar by T cells co-cultured with ova pulsed WT and *Ptpn22*$^{-/-}$ BMDCs. In addition, other non-PTP family member phosphatases will also be expressed in *Ptpn22*$^{-/-}$ BMDCs. These include phosphatases such as CD45 (PTPRC) and SHIP-1, which have been shown to regulate processes required for antigen uptake and processing[281,318].

As with my data investigating the role of PTPN22 in DCs, it may also be the case that PTPN22 is dispensable for osteoclast differentiation and function due to the presence of alternative phosphatases. For example, it has been shown that *Ship*$^{-/-}$ mice have increased numbers of osteoclast precursors and osteoclasts, due to enhanced signalling downstream of RANK and c-Fms (the receptors for RANK-L and M-CSF respectively). *Ship*$^{-/-}$ osteoclasts are more resorptive than WT osteoclasts and cause enhanced bone loss[319]. This shows that SHIP negatively regulates osteoclast development and function. In addition, *Shp-1*$^{-/-}$ mice have reduced bone density due to an increase in osteoclast numbers which have an increased resorptive ability[227], indicating that SHP-1 inhibits osteoclast differentiation and function. PTPN12 has also been shown to be required for IL-4 induced macrophage fusion into multinucleated giant cells and for RANK-L dependent fusion of RAW 264.7 macrophages into osteoclasts *in vitro*[232].

6.6 The drawbacks of using GM-CSF induced bone marrow derived DCs

Granulocyte-macrophage colony-stimulating factor (GM-CSF) and fms-like tyrosine kinases 3 ligand (Flt3L) have been shown to be capable of inducing DC expansion *in vivo*[320,321], which is why these cytokines have been used as part of a simple protocol to generate BMDCs *in vitro*. GM-CSF and Flt3L play different roles in DC development, as mice that lack GM-CSF have normal DC numbers in lymphoid tissues[322], but these cells are not capable of activating B and T cells[323]. Whereas, mice that lack Flt3L expression have a reduced number of DCs in the spleen, lymph nodes and thymus[92].

Signalling downstream of the GM-CSF receptor involves the phosphorylation of the tyrosine kinase janus kinase 2 (JAK2) and Src family kinases including Lyn, Fyn and Hck[324]. Downstream signalling involves the JAK/STAT, Ras/Raf/MEK/ERK and the PI3K/Akt pathways, all of which induce cell survival and proliferation[325]. Flt3L binding to Flt3 causes the receptor to dimerise,

which in turn causes receptor phosphorylation, potentially leading to the recruitment of Src family kinases[326,327]. Downstream signalling is mainly via the PI3K/Akt and JAK/STAT pathways, and signalling is negatively regulated by SHIP and SHP-2[328]. This indicates that PTPN22 may play a role in regulating signalling downstream of the GM-CSF receptor and Flt3. However, despite the presence of potential PTPN22 targets downstream of these receptors, I did not identify a role of PTPN22 in DC differentiation in response to either GM-CSF of Flt3L.

GM-CSF induced BMDCs have been used as a model of DCs for decades. They provide an abundant source of cells for experiments, and allow for experiments to be carried out which could not otherwise be performed using *ex vivo* isolated DCs. More recently, their suitability as a model of *in* vivo DCs, and inferring results from BMDCs to *in vitro* DCs has come under increasing scrutiny. It has become apparent that although the cultures are composed of $CD11c^+$ $MHCII^+$ cells, which broadly characterise DCs, they are a heterogenous population including both DC-like and macrophage-like cells[234]. It has also been shown that the concentration of GM-CSF affects the proportion of DC-like and macrophage-like cells in the cultures, such that with increased GM-CSF the proportion of DC-like cells decreases and macrophage-like cells increases[329]. As I kept the concentration of GM-CSF unchanged throughout my experiments, my cultures should have contained a consistent composition of both cell types. GM-CSF bone marrow cultures have been also found to contain basophils, eosinophils and monocytes[329]. This means that extrapolations between GM-CSF derived DCs and *in vivo* DC populations should be interpreted with caution. The functions of these DC-like and macrophage-like cells were tested and macrophage-like cells were found to have an enhanced phagocytic capability and to produce more pro-inflammatory cytokines in response to TLR stimulation, whereas DC-like cells induced enhanced T cell proliferation[329]. This affects the interpretation of my data, such that PTPN22 may not play a role in antigen uptake, which in these cultures is preferentially being carried out by macrophage-like cells, but may play a role in T cell proliferation, primarily induced by DC-like cells within the cultures. It is possible that PTPN22 is required for specific aspects of DC function, but that the presence of macrophage-like cells also in the cultures could mask this (if PTPN22 was dispensable for the same function in macrophage-like cells).

An alternative to using GM-CSF to differentiate DCs *in vitro*, is to use Flt3L instead. Flt3L induced BMDCs have been shown to produce cells which are more similar to *in vivo* DC subsets, as both $CD8\alpha^+$ ($CD24^+$, DC1-like cells) and $CD11b^+$ ($SIRP\alpha^+$, DC2-like cells) DCs are present in the cultures[246]. I carried out initial experiments with these cultures, but found once again that PTPN22 was dispensable for *in vitro* DC differentiation, ova uptake and immune complex induced co-stimulatory molecule upregulation. In the future it would be interesting to use Flt3L induced BMDCs in more assays, and to distinguish between the role of PTPN22 in both DC

subsets present within the cultures. This could be achieved by sorting the CD8α$^+$ and CD11b$^+$ DCs prior to the assays. DC1s and DC2s have different functions, for example, it is known that DC2s are more proficient at presenting internalised antigens to CD4$^+$ T cells, whereas DC1s are more effective at inducing CD8$^+$ T cell proliferation. This was found to correlate with an increased expression of proteins required for MHCI and MHCII processing in DC1s v DC2s respectively. In addition, by using antigens targeted to the specific DC subsets, DC2s were found to present more peptide-MHCII complexes on their cell surface compared to DC1s[330]. I found that ova uptake was much higher by CD11b$^+$ DCs within the cultures, despite the fact that it has been previously shown that DC1 and DC2-like cells from Flt3L cultures or splenic DC1s and DC2s are equally capable of binding and internalising biotin conjugated ova[331]. A separate report showed that out of the splenic DC populations, only CD8α$^+$ DCs expressed the mannose receptor[104]; however this may not be the case with *in vitro* differentiated DCs. Additional experiments using Flt3L BMDCs would be needed to explore this further.

One difference between the GM-CSF and Flt3L induced BMDC cultures was the way in which the cells were harvested. The GM-CSF BMDCs were harvested by pipetting, whereas Trypsin-EDTA was used for the Flt3L BMDCs. The use of Trypsin-EDTA may have affected the cell surface expression of receptors, including the receptors used for phenotyping the cultures, FcγRs, and the mannose receptor. If the mannose receptor was not expressed at high levels on the surface of the Flt3L BMDCs, then the observed ova-AF488 uptake may have been mainly via macropinocytosis and not receptor mediated endocytosis. In the future, it would be beneficial to rest the harvested Flt3L induced BMDCs after harvesting, and prior to use in an assay, so that the expression of cell surface receptors would have time to recover.

6.7 The role of PTPN22 *in vivo*

Although I found that PTPN22 was required for immune complex induced T cell proliferation *in vitro*, I was unable to replicate these findings *in vivo*. There are multiple potential reasons for this difference. For example, there are other antigen presenting cells *in vivo* that would be capable of presenting immune complex derived antigens to the T cells. The *in vitro* co-cultures demonstrated a reductionist approach in which only BMDCs and T cells were present.

A potential drawback of the FITC painting experiment, was that I used CD11c and MHCII expression to distinguish between resident and migratory DCs, such that migratory DCs express more MHCII and lower levels of CD11c. Although this gating is appropriate in the steady state, it

is less straight forward during inflammation. This is because resident DCs will also become activated and will therefore increase their MHCII expression[332]. However, as I applied the FITC in irritant locally, and only waited 24 hours before analysing FITC uptake by DCs, it is possible that I may still be able to use this gating strategy to distinguish between the migratory and resident DCs present in the draining LNs.

6.8 Lack of PTPN22 expression leads to an enhanced disease using the K/BxN serum transfer model of arthritis

I found that *Ptpn22*$^{-/-}$ mice develop more severe disease using the K/BxN serum transfer model of arthritis. Through my investigations, I was not able to determine a mechanism behind this, although there was a trend towards increased neutrophil infiltration in the ankle joints of *Ptpn22*$^{-/-}$ arthritic mice compared to WT mice. If this is true, the infiltrating neutrophils may be responsible for the enhanced disease seen, and therefore it would be important in the future to investigate how PTPN22 was regulating neutrophil function and/or migration. For example, PTPN22 may reduce their migration, such that in its absence there is an enhanced neutrophil influx into sites of inflammation. Neutrophils require LFA-1 to adhere to endothelial cells (via ICAM-1 or ICAM-2), prior to diapedesis from the blood into tissues[333], and as PTPN22 has been shown to negatively regulate LFA-1 signalling[60], this could provide a potential mechanism behind this. However, an enhanced neutrophil influx into the joints in the absence of PTPN22 would contradict a published report which showed that there was a reduced neutrophil population in the joints of *Ptpn22*$^{-/-}$ mice; interestingly, this report also showed a reduced severity of disease in *Ptpn22*$^{-/-}$ mice[63]. Although this paper demonstrated that PTPN22 positively regulates neutrophil effector functions in mice, a separate report has shown that expression of PTPN22^{R620W} in human neutrophils enhances cell migration, calcium flux and ROS production, indicating that in this context, enhanced neutrophil responses may contribute to the joint damage seen in RA patients expressing the variant[85]. My biodistribution data showed that there was an enhanced ^{68}Ga(HP_3-RGD_3) uptake in the wrists, ankles and shoulders of *Ptpn22*$^{-/-}$ arthritic mice, which correlates with the trend towards enhanced neutrophil frequencies found in the ankles of *Ptpn22*$^{-/-}$ arthritic mice by flow cytometry.

Although I did not observe any differences in serum cytokine and chemokine levels between WT and *Ptpn22*$^{-/-}$ mice, this may have been in part because analysis of serum analytes might only detect evidence of systemic inflammation. It is possible that I may have observed differences if I had measured these analytes in the joints and joint draining lymph nodes of the mice. This

could be achieved by either using cell suspensions from digested joints, or by analysing mRNA levels of cytokines and chemokines from the joint tissue. I also found little differences between the levels of cytokines and chemokines in the serum of healthy compared to arthritic mice, which was surprising. Again, this indicates that it would be more beneficial in the future to look specifically in areas of inflammation.

Using PET/CT imaging allowed me to visualise areas of inflammation at a whole body level. The addition of biodistribution analysis complemented this, by allowing for the quantitative analysis of $^{68}Ga(HP_3\text{-}RGD_3)$ uptake in specific organs. Initial experiments using WT mice showed that this radiolabelled peptide could be used to accurately visualise areas of inflammation. Further experiments showed that uptake of the peptide was higher in the joints of *Ptpn22*$^{-/-}$ mice compared to WT mice, indicating that cell infiltration and/or angiogenesis was enhanced in these animals.

A study using a radionuclide labelled RGD peptide has recently been investigated in humans as part of the INIRA-1 study (led by Dr Toby Garrood and colleagues, King's College London). This used ^{99m}Technetium labelled NC100692 peptide (maricliclatide), originally developed for detecting cancer cell metastases, and single-photon emission computed tomography (SPECT) imaging to see if uptake could be detected in the joints of patients with RA. Whole body and hands and feet SPECT/CT images were acquired from 5 RA patients and uptake of the ^{99m}Technetium labelled peptide was seen in all joints. Uptake positively correlated with disease activity scores for 28 joints (DAS28). Example SPECT images are shown in the Appendix (Figure 8-2). This indicates that the use of radiolabelled RGD peptides to visualise areas of inflammation is a promising technique to monitor patients in a non-invasive manner, in order to monitor response to treatment and disease status. This data also indicates that further analysis of radiolabelled RGD peptide uptake in mouse models could have merit, including measuring tracer uptake at early stages during disease development.

6.9 PTPN22 is dispensable for osteoclast differentiation and function *in vitro*

As osteoclasts are responsible for the bone erosion seen during human RA, but also during mouse models of RA, I wanted to determine whether PTPN22 may have a role in their differentiation and function. As osteoblasts do not develop from hematopoietic progenitors, they will not express PTPN22, and so any PTPN22 dependent changes in bone turnover will be due to PTPN22 expression in osteoclast precursors and osteoclasts. PTPN22 targets Src and Syk family kinases are involved in osteoclast development and function, including downstream of c-

Fms and RANK, so it is possible that PTPN22 may regulate these kinases. In addition, the F-BAR-proline-serine-threonine phosphatase interacting proteins 1 and 2 (PSTPIP1/2) have been shown to interact with PTPN22 and that they are required for the disassembly and assembly of podosomes in osteoclasts[334]. This may indicate that PTPN22 may play a role in osteoclast function via an indirect mechanism. I have not to date tested a potential direct or indirect role of PTPN22 in the formation of a podosome-rich sealing zone in osteoclasts. The sealing zone is essential for osteoclasts to release hydrogen ions and degradative enzymes, so this structure is essential for their bone resorbing capacity. This could be achieved in the future using microscopy and staining with phalloidin, to identify filamentous actin. It has been shown previously that RAW 264.7 macrophages differentiated into osteoclasts and when PTPN22 was silenced using siRNA these cells were incapable of forming sealing zones and were subsequently unable to resorb calcium phosphate[334]. These data suggested that PTPN22 may play a role in osteoclast function. Finally, I did not investigate a role of PTPN22 in regulating αvβ3 signalling. The integrin αvβ3 is required for adhesion of osteoclasts to bone, and is vital to allow for full osteoclast differentiation and their subsequent degradative capacity. There is precedent for PTPN22 in regulating integrin signalling, as in the context of LFA-1 in T cells, PTPN22 has been shown to negatively regulate signalling[60,61]. The increased radiolabelled RGD tracer uptake I observed in the joints of arthritic *Ptpn22*$^{-/-}$ mice also raised the possibility of a role of PTPN22 in osteoclasts.

Despite these potential associations between PTPN22 and osteoclasts, my *in vitro* experiments indicate that PTPN22 is not required for their differentiation or function. However, there are some caveats associated with these experiments. For example, full osteoclast differentiation only occurs when multinucleated osteoclasts are in contact with bone, so this would account for the fact that only a small proportion of my *in vitro* cultures differentiated into TRAP^{+} cells with three or more nuclei. In addition, I used M-CSF and RANK-L to induce osteoclast differentiation, however it has been shown that the presence of TGFβ can increase the number of TRAP^{+} cells[335,336], so this is something that would be interesting to investigate. An alternative differentiation pathway involves the differentiation of osteoclasts from osteoclast precursors in the presence of autoantibodies to citrullinated vimentin[304], so this method would be worthwhile investigating. I have found that PTPN22 regulates signalling downstream of FcγRs in BMDCs, and it has been published that PTPN22 is important for immune complex induced effector functions in neutrophils[63], so it is possible that PTPN22 may regulate osteoclast differentiation after autoantibody or immune complex stimulation. It has previously been shown that osteoclast precursors and osteoclasts express peptidylarginine deiminases (PADs) which citrullinate proteins. They also express vimentin and citrullinated vimentin, the expression of which

increases with osteoclast differentiation. Furthermore, autoantibodies against citrullinated vimentin (ACPAs) can directly stimulate osteoclastogenesis *in vitro* and *in vivo*[304].

7. Conclusion

In this thesis I have provided new evidence identifying the hematopoietic phosphatase PTPN22 as a negative regulator of FcγR dependent effector functions in mouse DCs. In the absence of PTPN22, this resulted in enhanced immune complex induced T cell proliferation, accompanied by augmented presentation of immune complex derived peptides in MHCII and DC-T cell conjugate formation. In addition, I have found that PTPN22 reduces disease severity using a mouse model of arthritis. This data has added to our knowledge of the function of PTPN22 in mice, and could have implications for people harbouring the *PTPN22*^{R620W} autoimmune associated variant.

8. Appendix

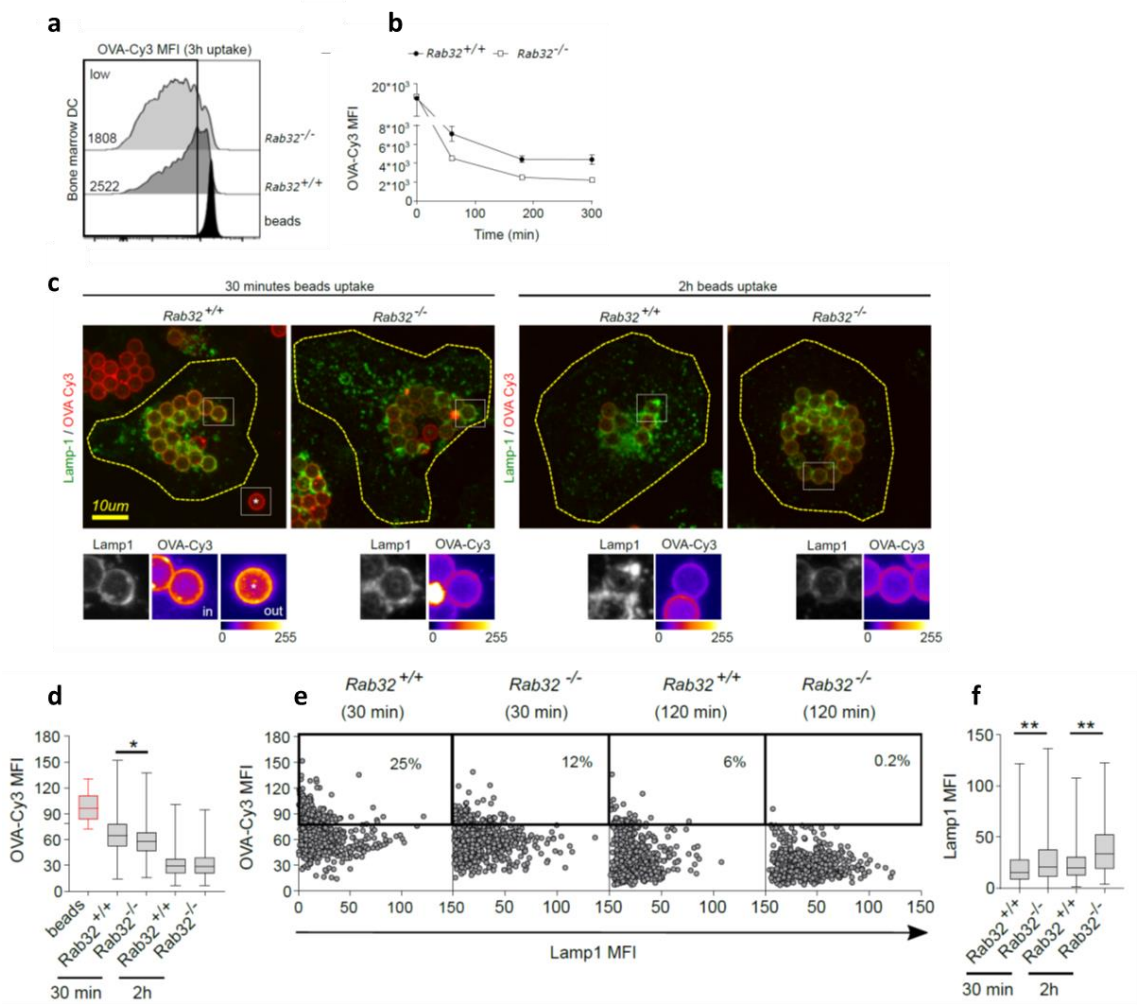

Figure 8-1: Internalised ova-AF568 coated beads co-localise with LAMP-1 and ova-AF568 fluorescence reduces over time, with a concomitant increase in LAMP-1 fluorescence.

*(a) Flow cytometry analysing the remaining ova-AF568 fluorescence intensity on phagocytosed beads after 3 hours at 37°C, isolated from Rab32$^{+/+}$ (WT) and Rab32$^{-/-}$ BMDCs. b) Mean fluorescence intensity of ova-AF568 in isolated beads after different times of phagocytosis by WT (white) and Rab32$^{-/-}$ (black) BMDCs. The initial time point represents the values of undegraded ova, the different times after phagocytosis show the values of the remaining ova in the degraded fraction. (c-f) WT and Rab32$^{-/-}$ BMDCs were pulsed for 30 minutes with ova-AF568 coated beads. At 30 minutes and 2 hours after the pulse, BMDCs were fixed and stained with anti-LAMP1 and analysed by confocal microscopy. (c) Example images of ova-AF568 and LAMP-1. An non-internalised bead is shown (star). (d) Ova-AF568 intensities in individual phagosomes. (e) Correlation between ova-AF568 and LAMP-1 fluorescence in individual phagosomes. (f) LAMP-1 intensities in individual phagosomes. Data is from one representative experiment in which a least 470 individual phagosomes in 10 different cells per condition were analysed (c-f). All data was created by Dr Enrique Gutiérrez-Martinez (undertaken in the Guermonprez laboratory, King's College London), and are presented with consent. **p<0.05 using an unpaired one-way ANOVA with Turkey's multiple comparison test.*

Figure 8-2: Single-photon emission computed tomography (SPECT) images of RA patients.

Example SPECT images of the hands of 5 RA patients after injection with ^{99m}Technetium labelled NC100692 peptide (mariciclatide), which contains the RGD peptide. Darker areas indicate areas of uptake. These were produced as part of the INIRA study, run by Toby Garrood and colleagues, King's College London, and are presented with consent.

9. Publications

1. **Clarke F**, Purvis HA, Sanchez-Blanco C, Gutiérrez-Martinez E, Cornish GH, Zamoyska R, Guermonprez P, Cope AP. The protein tyrosine phosphatase PTPN22 negatively regulates presentation of immune complex derived antigens. *Scientific Reports* **8** (2018).
2. Sanchez-Blanco C, **Clarke F**, Cornish GH, Depoil D, Thompson SJ, Dai X, Rawlings DJ, Dustin ML, Zamoyska R, Cope AP, Purvis HA. Protein tyrosine phosphatase PTPN22 regulates LFA-1 dependent Th1 responses. *Journal of Autoimmunity* **94** (2018).
3. **Clarke F**, Jordan, CK, Gutierrez-Martinez E, Bibby JA, Sanchez-Blanco C, Cornish GH, Dai X, Rawlings DJ, Zamoyska R, Guermonprez P, Cope AP, Purvis HA. Protein Tyrosine Phosphatase PTPN22 is dispensable for DC antigen processing and promotion of T-cell activation by DCs. *PLoS ONE* **12** (2017).
4. Purvis HA, **Clarke F**, Sanchez-Blanco C, Cornish GH, Rawlings DJ, Zamoyska R, Cope AP. Protein Tyrosine Phosphatase PTPN22 regulates IL-1β dependent Th17 responses by modulating dectin-1 signaling in mice. *European Journal of Immunology* **48** (2017).
5. Imberti C, Terry SY, Cullinane C, **Clarke F**, Cornish GH, Ramakrishnan NK, Roselt P, Cope AP, Hicks RJ, Blower PJ, Ma MT. Enhancing PET Signal at Target Tissue in Vivo: Dendritic and Multimeric Tris(hydroxypyridinone) Conjugates for Molecular Imaging of $\alpha_v\beta_3$ Integrin Expression with Gallium-68. *Bioconjugate Chemistry* **28** (2017).
6. Burn GA, Cornish GH, Potrzebowska K, Samuelsson M, Griffié J, Minoughan S, Yates M, Ashdown G, Pernodet N, Morrison VL, Sanchez-Blanco C, Purvis H, **Clarke F**, Brownlie RJ, Vyse TJ, Zamoyska R, Owen DM, Svensson LM, Cope AP. Superresolution imaging of the cytoplasmic phosphatase PTPN22 links integrin-mediated T cell adhesion with autoimmunity. *Science Signaling* **9** (2016).

10. References

1. Minton, K. Unravelling the motheaten phenotype. *Nat. Rev. Immunol.* **13,** 307–307 (2013).

2. Kozlowski, M. *et al.* Expression and catalytic activity of the tyrosine phosphatase PTP1C is severely impaired in motheaten and viable motheaten mice. *J. Exp. Med.* **178,** 2157–63 (1993).

3. Östman, A., Hellberg, C. & Böhmer, F. D. Protein-tyrosine phosphatases and cancer. *Nat. Rev. Cancer* **6,** 307–320 (2006).

4. Arimura, Y. & Yagi, J. Comprehensive Expression Profiles of Genes for Protein Tyrosine Phosphatases in Immune Cells. *Sci. Signal.* **3,** 1–11 (2010).

5. Matthews, R. J., Bowne, D. B., Flores, E. & Thomas, M. L. Characterization of hematopoietic intracellular protein tyrosine phosphatases: description of a phosphatase containing an SH2 domain and another enriched in proline-, glutamic acid-, serine-, and threonine-rich sequences. *Mol. Cell. Biol.* **12,** 2396–405 (1992).

6. Cohen, S., Dadi, H., Shaoul, E., Sharfe, N. & Roifman, C. M. Cloning and Characterization of a Lymphoid-Specific, Inducible Human Protein Tyrosine Phosphatase, Lyp. *Blood* **6,** 2013–2024 (1999).

7. Wang, S. *et al.* Identification of a variant form of tyrosine phosphatase LYP. *BMC Mol. Biol.* **11,** 78 (2010).

8. Bottini, N. *et al.* A functional variant of lymphoid tyrosine phosphatase is associated with type I diabetes. *Nat. Genet.* **36,** 337–338 (2004).

9. Wu, J. *et al.* Identification of substrates of human protein-tyrosine phosphatase PTPN22. *J. Biol. Chem.* **281,** 11002–10 (2006).

10. Wang, Y. *et al.* The Autoimmunity-Associated Gene PTPN22 Potentiates Toll-like Receptor-Driven, Type 1 Interferon-Dependent Immunity. *Immunity* **39,** 111–122 (2013).

11. Hill, R. J. *et al.* The lymphoid protein tyrosine phosphatase Lyp interacts with the adaptor molecule Grb2 and functions as a negative regulator of T-cell activation. *Exp. Hematol.* **30,** 237–244 (2002).

12. Zhang, J. *et al.* The autoimmune disease–associated PTPN22 variant promotes calpain-mediated Lyp/Pep degradation associated with lymphocyte and DC hyperresponsiveness. *Nat. Genet.* **43,** 902–907 (2011).

13. Dai, X. *et al.* A disease-associated PTPN22 variant promotes systemic autoimmunity in murine models. *J. Clin. Invest.* **123,** 2024–2036 (2013).

14. Gomez, L. M. *et al.* PTPN22 C1858T polymorphism in Colombian patients with autoimmune diseases. *Genes Immun.* **6,** 628–31 (2005).

15. Douroudis, K. *et al.* Protein tyrosine phosphatase non-receptor type 22 gene variants at position 1858 are associated with type 1 and type 2 diabetes in Estonian population. *Tissue Antigens* **72,** 425–30 (2008).

16. Fedetz, M. *et al.* The 1858T PTPN22 gene variant contributes to a genetic risk of type 1 diabetes in a Ukrainian population. *Tissue Antigens* **67,** 430–433 (2006).

17. Smyth, D. *et al.* Replication of an Association Between the Lymphoid General

Autoimmunity Locus. *Diabetes* **53,** 10–13 (2004).

18. Bottini, N. *et al.* A functional variant of lymphoid tyrosine phosphatase is associated with type I diabetes. *Nat. Genet.* **36,** 337–8 (2004).

19. Zhernakova, a *et al.* Differential association of the PTPN22 coding variant with autoimmune diseases in a Dutch population. *Genes Immun.* **6,** 459–61 (2005).

20. Zheng, W. & She, J.-X. Genetic Association Between a Lymphoid Tyrosine Phosphatase (PTPN22) and Type 1 Diabetes. *Diabetes* **54,** 906–908 (2005).

21. Kahles, H. *et al.* Sex-specific association of PTPN22 1858T with type 1 diabetes but not with Hashimoto's thyroiditis or Addison's disease in the German population. *Eur. J. Endocrinol.* **153,** 895–899 (2005).

22. Simkins, H. M. A. *et al.* Association of the PTPN22 locus with rheumatoid arthritis in a New Zealand Caucasian cohort. *Arthritis Rheum.* **52,** 2222–2225 (2005).

23. Hinks, A. *et al.* Association between the PTPN22 gene and rheumatoid arthritis and juvenile idiopathic arthritis in a UK population: Further support that PTPN22 is an autoimmunity gene. *Arthritis Rheum.* **52,** 1694–1699 (2005).

24. Plenge, R. M. *et al.* Replication of Putative Candidate-Gene Associations with Rheumatoid Arthritis in 14,000 Samples from North America and Sweden: Association of Susceptibility with PTPN22, CTLA4, and PADI4. *Am. J. Hum. Genet* **77,** 1044–1060 (2005).

25. Seldin, M. F. *et al.* Finnish case-control and family studies support PTPN22 R620W polymorphism as a risk factor in rheumatoid arthritis, but suggest only minimal or no effect in juvenile idiopathic arthritis. *Genes Immun.* **6,** 720–2 (2005).

26. Begovich, A. B. *et al.* A missense single-nucleotide polymorphism in a gene encoding a protein tyrosine phosphatase (PTPN22) is associated with rheumatoid arthritis. *Am J Hum Genet* **75,** 330–337 (2004).

27. Wesoly, J. *et al.* Association of the PTPN22 C1858T single-nucleotide polymorphism with rheumatoid arthritis phenotypes in an inception cohort. *Arthritis Rheum.* **52,** 2948–2950 (2005).

28. Kyogoku, C. *et al.* Genetic association of the R620W polymorphism of protein tyrosine phosphatase PTPN22 with human SLE. *Am. J. Hum. Genet.* **75,** 504–7 (2004).

29. Orozco, G. *et al.* Association of a functional single-nucleotide polymorphism of PTPN22 , encoding lymphoid protein phosphatase, with rheumatoid arthritis and systemic lupus erythematosus. *Arthritis Rheum.* **52,** 219–224 (2005).

30. Velaga, M. R. *et al.* The Codon 620 Tryptophan Allele of the Lymphoid Tyrosine Phosphatase (LYP) Gene Is a Major Determinant of Graves' Disease. *J. Clin. Endocrinol. Metab.* **89,** 5862–5865 (2004).

31. Skorka, A., Bednarczuk, T., Bar-Andziak, E., Nauman, J. & Ploski, R. Lymphoid tyrosine phosphatase (PTPN22/LYP) variant and Graves' disease in a Polish population: association and gene dose-dependent correlation with age of onset. *Clin. Endocrinol. (Oxf).* **62,** 679–682 (2005).

32. Zhebrun, D. *et al.* Association of PTPN22 1858T/T genotype with type 1 diabetes, Graves' disease but not with rheumatoid arthritis in Russian population. *Aging (Albany. NY).* **3,** 368–73 (2011).

33. Roycroft, M. *et al.* The tryptophan 620 allele of the lymphoid tyrosine phosphatase

(PTPN22) gene predisposes to autoimmune Addison's disease. *Clin. Endocrinol. (Oxf).* **70,** 358–362 (2009).

34. Skinningsrud, B. *et al.* Mutation screening of PTPN22: association of the 1858T-allele with Addison's disease. *Eur. J. Hum. Genet.* **16,** 977–982 (2008).

35. Begovich, A. B. *et al.* The R620W polymorphism of the protein tyrosine phosphatase PTPN22 is not associated with multiple sclerosis. *Am. J. Hum. Genet.* **76,** 184–7 (2005).

36. Matesanz, F. *et al.* Protein tyrosine phosphatase gene (PTPN22) polymorphism in multiple sclerosis. *J Neurol* **252,** 994–995 (2005).

37. Hedjoudje, A. *et al.* rs2476601 polymorphism in PTPN22 is associated with Crohn's disease but not with ulcerative colitis: a meta-analysis of 16,838 cases and 13,356 controls. *Ann. Gastroenterol.* **30,** 197–208 (2017).

38. Lamsyah, H. *et al.* Association of PTPN22 gene functional variants with development of pulmonary tuberculosis in Moroccan population. *Tissue Antigens* **74,** 228–232 (2009).

39. Gomez, L. M., Anaya, J.-M. & Martin, J. Genetic Influence of PTPN22 R620W Polymorphism in Tuberculosis. *Hum. Immunol.* **66,** 1242–1247 (2005).

40. Chapman, S. J. *et al.* PTPN22 and invasive bacterial disease. *Nat. Genet.* **38,** 499–500 (2006).

41. Montes-Cano, M. A. *et al.* PTPN22 C1858T Polymorphism and the Outcome of Hepatitis C Virus Infection. *Viral Immunol.* **21,** 491–494 (2008).

42. Chen, Z. *et al.* Association of PTPN22 gene (rs2488457) polymorphism with ulcerative colitis and high levels of PTPN22 mRNA in ulcerative colitis. *Int. J. Colorectal Dis.* **28,** 1351–1358 (2013).

43. El-Kafoury, A. A., Haroun, M., Embaby, A. M. & Dawoods, A. S. The association of polymorphic sites in some genes with type 1 diabetes mellitus in a sample of Egyptian children. *Egypt. J. Med. Hum. Genet.* **15,** 265–272 (2014).

44. Kawasaki, E. *et al.* Systematic search for single nucleotide polymorphisms in a lymphoid tyrosine phosphatase gene (PTPN22): Association between a promoter polymorphism and type 1 diabetes in Asian populations. *Am. J. Med. Genet. Part A* **140A,** 586–593 (2006).

45. Fan, Z.-D. *et al.* STAT4 rs7574865 G/T and PTPN22 rs2488457 G/C polymorphisms influence the risk of developing juvenile idiopathic arthritis in Han Chinese patients. *PLoS One* **10,** e0117389 (2015).

46. Feng, X. *et al.* Association of the PTPN22 gene (-1123G > C) polymorphism with rheumatoid arthritis in Chinese patients. *Tissue Antigens* **76,** 297–300 (2010).

47. Huang, J.-J. *et al.* A PTPN22 promoter polymorphism −1123G>C is associated with RA pathogenesis in Chinese. *Rheumatol. Int.* **32,** 767–771 (2012).

48. Zoledziewska, M. *et al.* Further evidence of a primary, causal association of the PTPN22 620W variant with type 1 diabetes. *Diabetes* **57,** 229–34 (2008).

49. Dieudé, P. *et al.* Testing for linkage and association with rheumatoid arthritis a ptpn22 promoter polymorphism reported to be associated and linked with type 1 diabetes in the Caucasian population. *Ann. Rheum. Dis.* **67,** 900–1 (2008).

50. Remuzgo-Martínez, S. *et al.* Protein tyrosine phosphatase non-receptor 22 and C-Src tyrosine kinase genes are down-regulated in patients with rheumatoid arthritis. *Sci.*

Rep. **7,** (2017).

51. Orrú, V. *et al.* A loss-of-function variant of PTPN22 is associated with reduced risk of systemic lupus erythematosus. *Hum. Mol. Genet.* **18,** 569–79 (2009).

52. López-Cano, D. J. *et al.* The PTPN22 R263Q polymorphism confers protection against systemic lupus erythematosus and rheumatoid arthritis, while PTPN22 R620W confers susceptibility to Graves' disease in a Mexican population. *Inflamm. Res.* **66,** 775–781 (2017).

53. Rodríguez-Rodríguez, L. *et al.* The PTPN22 R263Q polymorphism is a risk factor for rheumatoid arthritis in Caucasian case-control samples. *Arthritis Rheum.* **63,** 365–372 (2010).

54. Diaz-Gallo, L.-M. *et al.* Differential association of two PTPN22 coding variants with Crohn's disease and ulcerative colitis. *Inflamm. Bowel Dis.* **17,** 2287–2294 (2011).

55. Hasegawa, K. *et al.* PEST Domain–Enriched Tyrosine Phosphatase (PEP) Regulation of Effector/Memory T Cells. *Science (80-.).* **303,** 685–689 (2004).

56. Stanford, S. M., Rapini, N. & Bottini, N. Regulation of TCR signalling by tyrosine phosphatases: from immune homeostasis to autoimmunity. *Immunology* **137,** 1–19 (2012).

57. Maine, C. J. *et al.* PTPN22 Alters the Development of Regulatory T Cells in the Thymus. *J. Immunol.* **188,** 5267–5275 (2012).

58. Brownlie, R. J. *et al.* Lack of the Phosphatase PTPN22 Increases Adhesion of Murine Regulatory T Cells to Improve Their Immunosuppressive Function. *Sci. Signal.* **5,** ra87-ra87 (2012).

59. Maine, C. J., Marquardt, K., Cheung, J. & Sherman, L. A. PTPN22 controls the germinal center by influencing the numbers and activity of T follicular helper cells. *J. Immunol.* **192,** 1415–24 (2014).

60. Burn, G. L. *et al.* Superresolution imaging of the cytoplasmic phosphatase PTPN22 links integrin-mediated T cell adhesion with autoimmunity. *Sci. Signal.* **9,** (2016).

61. Sanchez-Blanco, C. *et al.* Protein tyrosine phosphatase PTPN22 regulates LFA-1 dependent Th1 responses. *J. Autoimmun.* (2018). doi:10.1016/J.JAUT.2018.07.008

62. Schickel, J.-N. *et al.* PTPN22 inhibition resets defective human central B cell tolerance. *Sci. Immunol.* **1,** (2016).

63. Vermeren, S. *et al.* PTPN22 Is a Critical Regulator of Fcγ Receptor–Mediated Neutrophil Activation. *J. Immunol.* **197,** 4771–4779 (2016).

64. Wang, Y. *et al.* PTPN22 Variant R620W Is Associated With Reduced Toll-like Receptor 7-Induced Type I Interferon in Systemic Lupus Erythematosus. *Arthritis Rheumatol.* **67,** 2403–2414 (2015).

65. Holmes, D. A. *et al.* Autoimmunity-associated protein tyrosine phosphatase PEP negatively regulates IFN-alpha receptor signaling. *J Exp Med* **212,** 1081–1093 (2015).

66. Purvis, H. A. *et al.* Protein tyrosine phosphatase PTPN22 regulates IL-1β dependent Th17 responses by modulating dectin-1 signaling in mice. *Eur. J. Immunol.* **48,** 306–315 (2018).

67. Li, M. *et al.* The common, autoimmunity-predisposing 620Arg > Trp variant of PTPN22 modulates macrophage function and morphology. *J. Autoimmun.* **79,** 74–83

(2017).

68. Zikherman, J. *et al.* PTPN22 deficiency cooperates with the CD45 E613R allele to break tolerance on a non-autoimmune background. *J. Immunol.* **182,** 4093–106 (2009).

69. Zheng, P. & Kissler, S. PTPN22 Silencing in the NOD Model Indicates the Type 1 Diabetes-Associated Allele Is Not a Loss-of-Function Variant. *Diabetes* **62,** 896–904 (2013).

70. Yeh, L.-T. *et al.* Different Modulation of Ptpn22 in Effector and Regulatory T Cells Leads to Attenuation of Autoimmune Diabetes in Transgenic Nonobese Diabetic Mice. *J. Immunol.* **191,** 594–607 (2013).

71. Lin, X. *et al.* CRISPR-Cas9-Mediated Modification of the NOD Mouse Genome With Ptpn22R619W Mutation Increases Autoimmune Diabetes. *Diabetes* **65,** 2134–8 (2016).

72. Fousteri, G. *et al.* PTPN22 controls virally-induced autoimmune diabetes by modulating cytotoxic T lymphocyte responses in an epitope-specific manner. *Clin. Immunol.* **156,** 98–108 (2015).

73. Sood, S. *et al.* Autoimmune Arthritis in SKG Mice PTPN22 Reduces Mannan-Induced Loss of the Protein Tyrosine Phosphatase. *J. Immunol.* (2016). doi:10.4049/jimmunol.1502656

74. Wu, D. J. *et al.* Autoimmunity-Associated LYP-W620 Does Not Impair Thymic Negative Selection of Autoreactive T Cells. *PLoS One* **9,** e86677 (2014).

75. Jofra, T. *et al.* Protein tyrosine phosphatase PTPN22 has dual roles in promoting pathogen versus homeostatic-driven CD8 T-cell responses. *Immunol. Cell Biol.* **95,** 121–128 (2017).

76. Jofra, T. *et al.* Extrinsic Protein Tyrosine Phosphatase Non-Receptor 22 Signals Contribute to CD8 T Cell Exhaustion and Promote Persistence of Chronic Lymphocytic Choriomeningitis Virus Infection. *Front. Immunol.* **8,** 811 (2017).

77. Maine, C. J., Teijaro, J. R., Marquardt, K. & Sherman, L. A. PTPN22 contributes to exhaustion of T lymphocytes during chronic viral infection. *Proc. Natl. Acad. Sci. U. S. A.* **113,** E7231–E7239 (2016).

78. Vang, T. *et al.* The autoimmune-predisposing variant of lymphoid tyrosine phosphatase favors T helper 1 responses. *Hum. Immunol.* **74,** 574–585 (2013).

79. Vang, T. *et al.* Autoimmune-associated lymphoid tyrosine phosphatase is a gain-of-function variant. *Nat. Genet.* **37,** 1317–1319 (2005).

80. Aarnisalo, J. *et al.* Reduced CD4+T cell activation in children with type 1 diabetes carrying the PTPN22/Lyp 620Trp variant. *J. Autoimmun.* **31,** 13–21 (2008).

81. Rieck, M. *et al.* Genetic variation in PTPN22 corresponds to altered function of T and B lymphocytes. *J. Immunol.* **179,** 4704–10 (2007).

82. Habib, T. *et al.* Altered B cell homeostasis is associated with type I diabetes and carriers of the PTPN22 allelic variant. *J. Immunol.* **188,** 487–96 (2012).

83. Menard, L. *et al.* The PTPN22 allele encoding an R620W variant interferes with the removal of developing autoreactive B cells in humans. *J. Clin. Invest.* **121,** 3635 (2011).

84. Metzler, G. *et al.* The Autoimmune Risk Variant PTPN22 C1858T Alters B Cell Tolerance at Discrete Checkpoints and Differentially Shapes the Naive Repertoire. *J. Immunol.* **199,** 2249–2260 (2017).

85. Bayley, R. *et al.* The autoimmune-associated genetic variant PTPN22 R620W enhances neutrophil activation and function in patients with rheumatoid arthritis and healthy individuals. *Ann. Rheum. Dis.* **74,** 1588–1595 (2015).

86. Douroudis, K., Shcherbakova, A., Everaus, H. & Aints, A. PTPN22 gene regulates natural killer cell proliferation during in vitro expansion. *Tissue Antigens* **76,** 315–318 (2010).

87. Vang, T., Nielsen, J. & Burn, G. L. A switch-variant model integrates the functions of an autoimmune variant of the phosphatase PTPN22. *Sci. Signal.* **11,** eaat0936 (2018).

88. Steinman, R. M. & Cohn, Z. A. Identification of a novel cell type in peripheral lymphoid organs of mice. I. Morphology, quantitation, tissue distribution. *J. Exp. Med.* **137,** 1142–62 (1973).

89. Swiecki, M. & Colonna, M. The multifaceted biology of plasmacytoid DCs. *Nat. Rev. Immunol.* **15,** 471–485 (2015).

90. Cisse, B. *et al.* Transcription Factor E2-2 Is an Essential and Specific Regulator of Plasmacytoid DC Development. *Cell* **135,** 37–48 (2008).

91. Ghosh, H. S., Cisse, B., Bunin, A., Lewis, K. L. & Reizis, B. Continuous Expression of the Transcription Factor E2-2 Maintains the Cell Fate of Mature Plasmacytoid DCs. *Immunity* **33,** 905–916 (2010).

92. McKenna, H. J. *et al.* Mice lacking flt3 ligand have deficient hematopoiesis affecting hematopoietic progenitor cells, DCs, and natural killer cells. *Blood* **95,** (2000).

93. Hildner, K. *et al.* Batf3 Deficiency Reveals a Critical Role for CD8alpha+ DCs in Cytotoxic T Cell Immunity. *Science (80-.).* **322,** 1097–1100 (2008).

94. Gurka, S., Hartung, E., Becker, M. & Kroczek, R. A. Mouse Conventional DCs Can be Universally Classified Based on the Mutually Exclusive Expression of XCR1 and SIRPα. *Front. Immunol.* **6,** 35 (2015).

95. Caton, M. L., Smith-Raska, M. R. & Reizis, B. Notch-RBP-J signaling controls the homeostasis of CD8- DCs in the spleen. *J. Exp. Med.* **204,** 1653–64 (2007).

96. Lewis, K. L. *et al.* Notch2 receptor signaling controls functional differentiation of DCs in the spleen and intestine. *Immunity* **35,** 780–91 (2011).

97. Xu, Y., Zhan, Y., Lew, A. M., Naik, S. H. & Kershaw, M. H. Differential development of murine DCs by GM-CSF versus Flt3 ligand has implications for inflammation and trafficking. *J. Immunol.* **179,** 7577–84 (2007).

98. Förster, R. *et al.* CCR7 Coordinates the Primary Immune Response by Establishing Functional Microenvironments in Secondary Lymphoid Organs. *Cell* **99,** 23–33 (1999).

99. Ohnmacht, C. *et al.* Constitutive ablation of DCs breaks self-tolerance of CD4 T cells and results in spontaneous fatal autoimmunity. *J. Exp. Med.* **206,** 549–59 (2009).

100. Racoosin, E. L. & Swanson, J. A. Macrophage colony-stimulating factor (rM-CSF) stimulates pinocytosis in bone marrow-derived macrophages. *J. Exp. Med.* **170,** 1635–48 (1989).

101. Araki, N., Johnson, M. T. & Swanson, J. A. A role for phosphoinositide 3-kinase in the completion of macropinocytosis and phagocytosis by macrophages. *J. Cell Biol.* **135,** 1249–60 (1996).

102. West, M. A., Prescott, A. R., Eskelinen, E.-L., Ridley, A. J. & Watts, C. Rac is required for constitutive macropinocytosis by DCs but does not control its downregulation. *Curr.*

Biol. **10,** 839–848 (2000).

103. Sallusto, F., Cella, M., Danieli, C. & Lanzavecchia, A. DCs Use Macropinocytosis and the Mannose Receptor to Concentrate Macromolecules in the Major Histocompatibility Complex Class 1I Compartment: Downregulation by Cytokines and Bacterial Products. doi:10.1084/jem.182.2.389

104. Burgdorf, S., Kautz, A., Böhnert, V., Knolle, P. A. & Kurts, C. Distinct pathways of antigen uptake and intracellular routing in CD4 and CD8 T cell activation. *Science* **316,** 612–6 (2007).

105. Norbury, C. C., Chambers, B. J., Prescott, A. R., Ljunggren, H. G. & Watts, C. Constitutive macropinocytosis allows TAP-dependent major histocompatibility compex class I presentation of exogenous soluble antigen by bone marrow-derived DCs. *Eur. J. Immunol.* **27,** 280–288 (1997).

106. Drutman, S. B. & Trombetta, E. S. DCs continue to capture and present antigens after maturation in vivo. *J. Immunol.* **185,** 2140–6 (2010).

107. Kloetzel, P.-M. Antigen processing by the proteasome. *Nat. Rev. Mol. Cell Biol.* **2,** 179–188 (2001).

108. ten Broeke, T., Wubbolts, R. & Stoorvogel, W. MHC class II antigen presentation by DCs regulated through endosomal sorting. *Cold Spring Harb. Perspect. Biol.* **5,** a016873 (2013).

109. Anderson, M. S. & Miller, J. Invariant chain can function as a chaperone protein for class II major histocompatibility complex molecules. *Proc. Natl. Acad. Sci. U. S. A.* **89,** 2282–6 (1992).

110. Marks, M. S., Germain, R. N. & Bonifacino, J. S. Transient aggregation of major histocompatibility complex class II chains during assembly in normal spleen cells. *J. Biol. Chem.* **270,** 10475–81 (1995).

111. Bonifacino, J. S. & Traub, L. M. Signals for Sorting of Transmembrane Proteins to Endosomes and Lysosomes. *Annu. Rev. Biochem.* **72,** 395–447 (2003).

112. Hofmann, M. W. *et al.* The leucine-based sorting motifs in the cytoplasmic domain of the invariant chain are recognized by the clathrin adaptors AP1 and AP2 and their medium chains. *J. Biol. Chem.* **274,** 36153–8 (1999).

113. Blum, J. S., Wearsch, P. A. & Cresswell, P. Pathways of Antigen Processing. *Annu. Rev. Immunol.* **31,** 443–473 (2013).

114. Vyas JM, Kim YM, Artavanis-Tsakonas K, Love JC, V. der V. A. and P. H. Tubulation of class II MHC compartments is microtubule dependent and involves multiple endolysosomal membrane proteins in primary DCs. *J Immunol* **178,** 7199–7210 (2007).

115. Furuta, K., Walseng, E. & Roche, P. A. Internalizing MHC class II-peptide complexes are ubiquitinated in early endosomes and targeted for lysosomal degradation. *Proc. Natl. Acad. Sci. U. S. A.* **110,** 20188–93 (2013).

116. Walseng, E. *et al.* Ubiquitination regulates MHC class II-peptide complex retention and degradation in DCs. *Proc. Natl. Acad. Sci. U. S. A.* **107,** 20465–70 (2010).

117. Delamarre, L., Pack, M., Chang, H., Mellman, I. & Trombetta, E. S. Differential Lysosomal Proteolysis in Antigen-Presenting Cells Determines Antigen Fate. *Science (80-.).* **307,** 1630–1634 (2005).

118. Lowell, C. A. Src-family and Syk kinases in activating and inhibitory pathways in innate

immune cells: signaling cross talk. *Cold Spring Harb. Perspect. Biol.* **3,** (2011).

119. Matsubara, S. *et al.* Syk Activation in DCs Is Essential for Airway Hyperresponsiveness and Inflammation. *Am. J. Respir. Cell Mol. Biol.* **34,** 426–433 (2006).

120. Nakashima, K. *et al.* A novel Syk kinase-selective inhibitor blocks antigen presentation of immune complexes in DCs. *Eur. J. Pharmacol.* **505,** 223–228 (2004).

121. Crowley, M. T. *et al.* A Critical Role for Syk in Signal Transduction and Phagocytosis Mediated by Fcγ Receptors on Macrophages. *J. Exp. Med.* **186,** 1027–1039 (1997).

122. Fitzer-Attas, C. J. *et al.* Fcgamma receptor-mediated phagocytosis in macrophages lacking the Src family tyrosine kinases Hck, Fgr, and Lyn. *J. Exp. Med.* **191,** 669–82 (2000).

123. Fousteri, G., Liossis, S. C. & Battaglia, M. Roles of the protein tyrosine phosphatase PTPN22 in immunity and autoimmunity. *Clin. Immunol.* **149,** 556–565 (2013).

124. Schroeder, H. W., Cavacini, L. & Cavacini, L. Structure and function of immunoglobulins. *J. Allergy Clin. Immunol.* **125,** S41-52 (2010).

125. Nimmerjahn, F. & Ravetch, J. V. Fcγ receptors as regulators of immune responses. *Nat. Immunol.* **8,** 34–47 (2008).

126. Bruhns, P. Properties of mouse and human IgG receptors and their contribution to disease models. *Blood* **119,** 5640–5650 (2012).

127. Guilliams, M., Bruhns, P., Saeys, Y., Hammad, H. & Lambrecht, B. N. The function of Fcγ receptors in DCs and macrophages. *Nat. Rev. Immunol.* **14,** 94–108 (2014).

128. Vidarsson, G., Dekkers, G. & Rispens, T. IgG Subclasses and Allotypes: From Structure to Effector Functions. *Front. Immunol.* **5,** 520 (2014).

129. Daëron, M. *et al.* The same tyrosine-based inhibition motif, in the intra-cytoplasmic domain of FcγRIIB, regulates negatively BCR-, TCR-, and FcR-dependent cell activation. *Immunity* **3,** 635–646 (1995).

130. Amigorena, S., Salamero, J., Davoust, J., Fridman, W. H. & Bonnerot, C. Tyrosine-containing motif that transduces cell activation signals also determines internalization and antigen presentation via type III receptors for IgG. *Nature* **358,** 337–341 (1992).

131. Miettinen, H. M., Rose, J. K. & Mellman, I. Fc receptor isoforms exhibit distinct abilities for coated pit localization as a result of cytoplasmic domain heterogeneity. *Cell* **58,** 317–327 (1989).

132. Daëron, M. Fc receptor biology. *Annu. Rev. Immunol.* **15,** 203–234 (1997).

133. Bergtold, A., Desai, D. D., Gavhane, A. & Clynes, R. Cell Surface Recycling of Internalized Antigen Permits DC Priming of B Cells. *Immunity* **23,** 503–514 (2005).

134. Qiao, S.-W. *et al.* Dependence of antibody-mediated presentation of antigen on FcRn. *Proc. Natl. Acad. Sci. U. S. A.* **105,** 9337–42 (2008).

135. Baker, K. *et al.* Neonatal Fc receptor for IgG (FcRn) regulates cross-presentation of IgG immune complexes by CD8-CD11b+ DCs. *Proc. Natl. Acad. Sci.* **108,** 9927–9932 (2011).

136. McEwan, W. A. *et al.* Intracellular antibody-bound pathogens stimulate immune signaling via the Fc receptor TRIM21. *Nat. Immunol.* **14,** 327–36 (2013).

137. Mallery, D. L. *et al.* Antibodies mediate intracellular immunity through tripartite motif-containing 21 (TRIM21). *Proc. Natl. Acad. Sci. U. S. A.* **107,** 19985–90 (2010).

138. de Haij, S. *et al.* In vivo Cytotoxicity of Type I CD20 Antibodies Critically Depends on Fc Receptor ITAM Signaling. *Cancer Res.* **70,** 3209–3217 (2010).

139. Boross, P. *et al.* FcR -Chain ITAM Signaling Is Critically Required for Cross-Presentation of Soluble Antibody-Antigen Complexes by DCs. *J. Immunol.* **193,** 5506–5514 (2014).

140. Graham, D. B. *et al.* ITAM signaling in DCs controls T helper cell priming by regulating MHC class II recycling. *Blood* **116,** 3208–18 (2010).

141. Takai, T. Roles of Fc receptors in autoimmunity. *Nat. Rev. Immunol.* **2,** 580–592 (2002).

142. D'Ambrosio, D. *et al.* Recruitment and activation of PTP1C in negative regulation of antigen receptor signaling by Fc gamma RIIB1. *Science* **268,** 293–7 (1995).

143. Ono, M., Bolland, S., Tempst, P. & Ravetch, J. V. Role of the inositol phosphatase SHIP in negative regulation of the immune system by the receptor FeγRIIB. *Nature* **383,** 263–266 (1996).

144. Ono, M. *et al.* Deletion of SHIP or SHP-1 reveals two distinct pathways for inhibitory signaling. *Cell* **90,** 293–301 (1997).

145. Schmidt, R. E. & Gessner, J. E. Fc receptors and their interaction with complement in autoimmunity. *Immunol. Lett.* **100,** 56–67 (2005).

146. Radeke, H. H. *et al.* Opposite regulation of type II and III receptors for immunoglobulin G in mouse glomerular mesangial cells and in the induction of anti-glomerular basement membrane (GBM) nephritis. *J. Biol. Chem.* **277,** 27535–44 (2002).

147. Tridandapani, S. *et al.* Regulated expression and inhibitory function of Fcgamma RIIb in human monocytic cells. *J. Biol. Chem.* **277,** 5082–9 (2002).

148. Blank, U., Launay, P., Benhamou, M. & Monteiro, R. C. Inhibitory ITAMs as novel regulators of immunity. *Immunol. Rev.* **232,** 59–71 (2009).

149. Getahun, A. & Cambier, J. C. Of ITIMs, ITAMs, and ITAMis: revisiting immunoglobulin Fc receptor signaling. *Immunol. Rev.* **268,** 66–73 (2015).

150. Molfetta, R. *et al.* Regulation of Fc receptor endocytic trafficking by ubiquitination. *Front. Immunol.* **5,** 1–9 (2014).

151. Skokowa, J. *et al.* Macrophages induce the inflammatory response in the pulmonary Arthus reaction through G alpha i2 activation that controls C5aR and Fc receptor cooperation. *J. Immunol.* **174,** 3041–50 (2005).

152. Shushakova, N. *et al.* C5a anaphylatoxin is a major regulator of activating versus inhibitory FcgammaRs in immune complex-induced lung disease. *J. Clin. Invest.* **110,** 1823–30 (2002).

153. Seligman, V. A. *et al.* The Fcgamma receptor IIIA-158F allele is a major risk factor for the development of lupus nephritis among Caucasians but not non-Caucasians. *Arthritis Rheum.* **44,** 618–625 (2001).

154. Nieto, A. *et al.* Involvement of Fcγ receptor IIIA genotypes in susceptibility to rheumatoid arthritis. *Arthritis Rheum.* **43,** 735 (2000).

155. Kastbom, A., Ahmadi, A., Söderkvist, P. & Skogh, T. The 158V polymorphism of Fc gamma receptor type IIIA in early rheumatoid arthritis: increased susceptibility and severity in male patients (the Swedish TIRA project). *Rheumatology* **44,** 1294–1298 (2005).

156. Kyogoku, C. *et al.* Fcgamma receptor gene polymorphisms in Japanese patients with

systemic lupus erythematosus: Contribution of FCGR2B to genetic susceptibility. *Arthritis Rheum.* **46,** 1242–1254 (2002).

157. Wu, J. *et al.* A novel polymorphism of FcgammaRIIIa (CD16) alters receptor function and predisposes to autoimmune disease. *J. Clin. Invest.* **100,** 1059–70 (1997).

158. Clynes, R. *et al.* Modulation of immune complex-induced inflammation in vivo by the coordinate expression of activation and inhibitory Fc receptors. *J. Exp. Med.* **189,** 179–85 (1999).

159. Watanabe, N. *et al.* Mast cells induce autoantibody-mediated vasculitis syndrome through tumor necrosis factor production upon triggering Fcgamma receptors. *Blood* **94,** 3855–63 (1999).

160. Kleinau, S., Martinsson, P. & Heyman, B. Induction and Suppression of Collagen-Induced Arthritis Is Dependent on Distinct Fcγ Receptors. *J. Exp. Med.* **191,** 1611–1616 (2000).

161. Maglione, P. J., Xu, J., Casadevall, A. & Chan, J. Fc Receptors Regulate Immune Activation and Susceptibility during Mycobacterium tuberculosis Infection. *J. Immunol.* **180,** 3329–3338 (2008).

162. van Lent, P. *et al.* The inhibitory receptor FcgammaRII reduces joint inflammation and destruction in experimental immune complex-mediated arthritides not only by inhibition of FcgammaRI/III but also by efficient clearance and endocytosis of immune complexes. *Am. J. Pathol.* **163,** 1839–48 (2003).

163. Yuasa, T. *et al.* Deletion of fcgamma receptor IIB renders H-2(b) mice susceptible to collagen-induced arthritis. *J. Exp. Med.* **189,** 187–94 (1999).

164. Bolland, S. & Ravetch, J. V. Spontaneous Autoimmune Disease in FcγRIIB-Deficient Mice Results from Strain-Specific Epistasis. *Immunity* **13,** 277–285 (2000).

165. Clatworthy, M. R. & Smith, K. G. C. FcgammaRIIb balances efficient pathogen clearance and the cytokine-mediated consequences of sepsis. *J. Exp. Med.* **199,** 717–23 (2004).

166. van Montfoort, N. *et al.* Fc Receptor IIb Strongly Regulates Fc Receptor-Facilitated T Cell Activation by DCs. *J. Immunol.* **189,** 92–101 (2012).

167. Goronzy, J. J. & Weyand, C. M. Developments in the scientific understanding of rheumatoid arthritis. *Arthritis Res. Ther.* **11,** 249 (2009).

168. Ling, S., Cline, E. N., Haug, T. S., Fox, D. A. & Holoshitz, J. Citrullinated calreticulin potentiates rheumatoid arthritis shared epitope signaling. *Arthritis Rheum.* **65,** 618–626 (2013).

169. MacGregor, A. J. *et al.* Characterizing the quantitative genetic contribution to rheumatoid arthritis using data from twins. *Arthritis Rheum.* **43,** 30–37 (2000).

170. Catrina, A. I., Joshua, V., Klareskog, L. & Malmström, V. Mechanisms involved in triggering rheumatoid arthritis. *Immunol. Rev.* **269,** 162–174 (2016).

171. Makrygiannakis, D. *et al.* Smoking increases peptidylarginine deiminase 2 enzyme expression in human lungs and increases citrullination in BAL cells. *Ann. Rheum. Dis.* **67,** 1488–1492 (2008).

172. McInnes, I. B. & Schett, G. The Pathogenesis of Rheumatoid Arthritis. *N. Engl. J. Med.* **365,** 2205–2219 (2011).

173. Scher, J. U. & Abramson, S. B. The microbiome and rheumatoid arthritis. *Nat. Rev. Rheumatol.* **7,** 569–578 (2011).

174. Trentham, D. E., Townes, A. S. & Kang, A. H. Autoimmunity to type II collagen an experimental model of arthritis. *J. Exp. Med.* **146,** 857–68 (1977).

175. Stuart, J. M. & Dixon, F. J. Serum transfer of collagen-induced arthritis in mice. *J. Exp. Med.* **158,** 378–92 (1983).

176. Holmdahl, R., Rubin, K., Klareskog, L., Larsson, E. & Wigzell, H. Characterization of the antibody response in mice with type II collagen–induced arthritis, using monoclonal anti–type II collagen antibodies. *Arthritis Rheum.* **29,** 400–410 (1986).

177. Keystone, E. C., Schorlemmer, H. U., Pope, C. & Allison, A. C. Zymosan—Induced Arthritis. *Arthritis Rheum.* **20,** 1396–1401 (1977).

178. Kouskoff, V. *et al.* Organ-specific autoimmune disease provoked by systemic autoimmunity. *Cell* **87,** 811–822 (1996).

179. Matsumoto, I. *et al.* How antibodies to a ubiquitous cytoplasmic enzyme may provoke joint-specific autoimmune disease. *Nat. Immunol.* **3,** 360–365 (2002).

180. Schaller, M., Burton, D. R. & Ditzel, H. J. Autoantibodies to GPI in rheumatoid arthritis: linkage between an animal model and human disease. *Nat. Immunol.* **2,** 746–753 (2001).

181. Wipke, B. T. & Allen, P. M. Essential role of neutrophils in the initiation and progression of a murine model of rheumatoid arthritis. *J. Immunol.* **167,** 1601–8 (2001).

182. Solomon, S., Rajasekaran, N., Jeisy-Walder, E., Snapper, S. B. & Illges, H. A crucial role for macrophages in the pathology of K/B × N serum-induced arthritis. *Eur. J. Immunol.* **35,** 3064–3073 (2005).

183. Misharin, A. V. *et al.* Nonclassical Ly6C- monocytes drive the development of inflammatory arthritis in mice. *Cell Rep.* **9,** 591–604 (2014).

184. Lee, D. M. *et al.* Mast cells: a cellular link between autoantibodies and inflammatory arthritis. *Science* **297,** 1689–92 (2002).

185. Elliott, E. R. *et al.* Deletion of Syk in Neutrophils Prevents Immune Complex Arthritis. *J. Immunol.* **187,** 4319–4330 (2011).

186. Ji, H. *et al.* Arthritis Critically Dependent on Innate Immune System Players. *Immunity* **16,** 157–168 (2002).

187. Corr, M. & Crain, B. The role of FcgammaR signaling in the K/B x N serum transfer model of arthritis. *J. Immunol.* **169,** 6604–6609 (2002).

188. Ji, H. *et al.* Critical roles for interleukin 1 and tumor necrosis factor alpha in antibody-induced arthritis. *J. Exp. Med.* **196,** 77–85 (2002).

189. Watts, G. M. *et al.* Manifestations of inflammatory arthritis are critically dependent on LFA-1. *J. Immunol.* **174,** 3668–75 (2005).

190. Monach, P. A. *et al.* Neutrophils in a mouse model of autoantibody-mediated arthritis: Critical producers of Fc receptor γ, the receptor for C5a, and lymphocyte function−associated antigen 1. *Arthritis Rheum.* **62,** 753–764 (2010).

191. Kovács, M. *et al.* The Src family kinases Hck, Fgr, and Lyn are critical for the generation of the in vivo inflammatory environment without a direct role in leukocyte recruitment. *J. Exp. Med.* **211,** 1993–2011 (2014).

192. Brackertz, D., Mitchell, G. F. & Mackay, I. R. Antigen-induced arthritis in mice. *Arthritis Rheum.* **20,** 841–850 (1977).

193. Keffer, J. *et al.* Transgenic mice expressing human tumour necrosis factor: a predictive genetic model of arthritis. *EMBO J.* **10,** 4025–31 (1991).

194. Li, P. & Schwarz, E. M. The TNF-α transgenic mouse model of inflammatory arthritis. *Springer Semin Immunopathol* **25,** 19–33 (2003).

195. Kollias, G., Douni, E., Kassiotis, G. & Kontoyiannis, D. On the role of tumor necrosis factor and receptors in models of multiorgan failure, rheumatoid arthritis, multiple sclerosis and inflammatory bowel disease. *Immunol. Rev.* **169,** 175–194 (1999).

196. Brennan, F. M. & McInnes, I. B. Evidence that cytokines play a role in rheumatoid arthritis. *J. Clin. Invest.* **118,** 3537–45 (2008).

197. Sakaguchi, S., Takahashi, T., Hata, H., Nomura, T. & Sakaguchi, N. SKG mice, a new genetic model of rheumatoid arthritis. *Arthritis Res. Ther.* **5,** 10 (2003).

198. Sakaguchi, N. *et al.* Altered thymic T-cell selection due to a mutation of the ZAP-70 gene causes autoimmune arthritis in mice. *Nature* **426,** 454–460 (2003).

199. Chen, H., Niu, G., Wu, H. & Chen, X. Clinical Application of Radiolabeled RGD Peptides for PET Imaging of Integrin αvβ3. *Theranostics* **6,** 78–92 (2016).

200. Wilder, R. L. Integrin alpha V beta 3 as a target for treatment of rheumatoid arthritis and related rheumatic diseases. *Ann. Rheum. Dis.* **61 Suppl 2,** ii96-9 (2002).

201. Terry, S. Y. A. *et al.* Monitoring Therapy Response of Experimental Arthritis with Radiolabeled Tracers Targeting Fibroblasts, Macrophages, or Integrin αvβ3. *J. Nucl. Med.* **57,** 467–72 (2016).

202. Hadjidakis, D. J. & Androulakis, I. I. Bone remodeling. *Ann. N. Y. Acad. Sci.* **1092,** 385–396 (2006).

203. Schett, G. & Gravallese, E. Bone erosion in rheumatoid arthritis: mechanisms, diagnosis and treatment. *Nat. Rev. Rheumatol.* **8,** 656–64 (2012).

204. Pettit, A. R. *et al.* TRANCE/RANKL Knockout Mice Are Protected from Bone Erosion in a Serum Transfer Model of Arthritis. *Am. J. Pathol.* **159,** 1689–1699 (2001).

205. Pettit, A. R. *et al.* Osteoclasts are essential for TNF-α – mediated joint destruction. *Am. J. Pathol.* **159,** 1419–1427 (2002).

206. Georgess, D., Machuca-Gayet, I., Blangy, A. & Jurdic, P. Podosome organization drives osteoclast-mediated bone resorption. *Cell Adh. Migr.* **8,** 191–204 (2014).

207. Yoshida, H. *et al.* The murine mutation osteopetrosis is in the coding region of the macrophage colony stimulating factor gene. *Nature* **345,** 442–444 (1990).

208. Kong, Y.-Y. *et al.* OPGL is a key regulator of osteoclastogenesis, lymphocyte development and lymph-node organogenesis. *Nature* **397,** 315–323 (1999).

209. Bucay, N. *et al.* osteoprotegerin-deficient mice develop early onset osteoporosis and arterial calcification. *Genes Dev.* **12,** 1260–8 (1998).

210. Negishi-Koga, T. *et al.* Immune complexes regulate bone metabolism through FcRγ signalling. *Nat. Commun.* **6,** 6637 (2015).

211. Li, Y. *et al.* B cells and T cells are critical for the preservation of bone homeostasis and attainment of peak bone mass in vivo. *Blood* **109,** 3839–3848 (2007).

212. Hofbauer, L. C. & Schoppet, M. Clinical Implications of the Osteoprotegerin/RANKL/RANK System for Bone and Vascular Diseases. *JAMA* **292,** 490

(2004).

213. Boyce, B. F., Yao, Z. & Xing, L. Osteoclasts have multiple roles in bone in addition to bone resorption. *Crit. Rev. Eukaryot. Gene Expr.* **19,** 171–80 (2009).

214. Amarasekara, D. S. *et al.* Regulation of Osteoclast Differentiation by Cytokine Networks. *Immune Netw.* **18,** e8 (2018).

215. Kitaura, H. *et al.* Immunological Reaction in TNF- *α* -Mediated Osteoclast Formation and Bone Resorption *In Vitro* and *In Vivo*. *Clin. Dev. Immunol.* **2013,** 1–8 (2013).

216. Axmann, R. *et al.* Inhibition of interleukin-6 receptor directly blocks osteoclast formation in vitro and in vivo. *Arthritis Rheum.* **60,** 2747–2756 (2009).

217. Nakamura, I. *et al.* IL-1 regulates cytoskeletal organization in osteoclasts via TNF receptor-associated factor 6/c-Src complex. *J. Immunol.* **168,** 5103–9 (2002).

218. Schiff, M. H. Role of interleukin 1 and interleukin 1 receptor antagonist in the mediation of rheumatoid arthritis. *Ann. Rheum. Dis.* **59 Suppl 1,** i103-8 (2000).

219. Hwang, S.-Y. *et al.* IL-17 induces production of IL-6 and IL-8 in rheumatoid arthritis synovial fibroblasts via NF-kappaB- and PI3-kinase/Akt-dependent pathways. *Arthritis Res. Ther.* **6,** R120 (2004).

220. Jovanovic, D. V *et al.* IL-17 stimulates the production and expression of proinflammatory cytokines, IL-beta and TNF-alpha, by human macrophages. *J. Immunol.* **160,** 3513–21 (1998).

221. Lubberts, E. *et al.* IL-17 promotes bone erosion in murine collagen-induced arthritis through loss of the receptor activator of NF-kappa B ligand/osteoprotegerin balance. *J. Immunol.* **170,** 2655–62 (2003).

222. Moon, Y.-M. *et al.* IL-32 and IL-17 interact and have the potential to aggravate osteoclastogenesis in rheumatoid arthritis. *Arthritis Res. Ther.* **14,** R246 (2012).

223. Xiong, Q., Zhang, L., Ge, W. & Tang, P. The roles of interferons in osteoclasts and osteoclastogenesis. *Jt. Bone Spine* **83,** 276–281 (2016).

224. Takayanagi, H. *et al.* T-cell-mediated regulation of osteoclastogenesis by signalling cross-talk between RANKL and IFN-γ. *Nature* **408,** 600–605 (2000).

225. Schmidt, A. *et al.* Protein-tyrosine phosphatase activity regulates osteoclast formation and function: inhibition by alendronate. *Proc. Natl. Acad. Sci. U. S. A.* **93,** 3068–73 (1996).

226. Kikuta, J. & Ishii, M. Osteoclast migration, differentiation and function: novel therapeutic targets for rheumatic diseases. *Rheumatology* **52,** 226–234 (2013).

227. Umeda, S. *et al.* Deficiency of SHP-1 Protein-Tyrosine Phosphatase Activity Results in Heightened Osteoclast Function and Decreased Bone Density. *Am. J. Pathol.* **155,** 223–233 (1999).

228. Boyce, B. F., Yoneda, T., Lowe, C., Soriano, P. & Mundy, G. R. Requirement of pp60c-src expression for osteoclasts to form ruffled borders and resorb bone in mice. *J. Clin. Invest.* **90,** 1622–1627 (1992).

229. Vérollet, C. *et al.* Hck contributes to bone homeostasis by controlling the recruitment of osteoclast precursors. *FASEB J.* **27,** 3608–3618 (2013).

230. Kim, H.-J. *et al.* Fyn promotes proliferation, differentiation, survival and function of osteoclast lineage cells. *J. Cell. Biochem.* **111,** 1107–1113 (2010).

231. Kim, H.-J. *et al.* The Src family kinase, Lyn, suppresses osteoclastogenesis in vitro and in vivo. *Proc. Natl. Acad. Sci. U. S. A.* **106,** 2325–30 (2009).

232. Rhee, I., Davidson, D., Souza, C. M., Vacher, J. & Veillette, A. Macrophage Fusion Is Controlled by the Cytoplasmic Protein Tyrosine Phosphatase PTP-PEST/PTPN12. *Mol. Cell. Biol.* **33,** 2458–2469 (2013).

233. Inaba, K. *et al.* Generation of large numbers of DCs from mouse bone marrow cultures supplemented with granulocyte/macrophage colony-stimulating factor. *J. Exp. Med.* **176,** 1693–702 (1992).

234. Helft, J. *et al.* GM-CSF Mouse Bone Marrow Cultures Comprise a Heterogeneous Population of CD11c(+)MHCII(+) Macrophages and DCs. *Immunity* **42,** 1197–211 (2015).

235. Ellsworth, J. L. *et al.* Targeting immune complex-mediated hypersensitivity with recombinant soluble human FcgammaRIA (CD64A). *J. Immunol.* **180,** 580–9 (2008).

236. Dekkers, G. *et al.* Multi-level glyco-engineering techniques to generate IgG with defined Fc-glycans OPEN. *Nat. Publ. Gr.* (2016). doi:10.1038/srep36964

237. Bottini, N. & Peterson, E. J. Tyrosine Phosphatase PTPN22: Multifunctional Regulator of Immune Signaling, Development, and Disease. *Annu. Rev. Immunol.* **32,** 83–119 (2014).

238. Guermonprez, P., Valladeau, J., Zitvogel, L., Théry, C. & Amigorena, S. Antigen Presentation and T cells Stimulation by DCs. *Annu. Rev. Immunol.* **20,** 621–667 (2002).

239. Woelbing, F. *et al.* Uptake of *Leishmania major* by DCs is mediated by Fcγ receptors and facilitates acquisition of protective immunity. *J. Exp. Med.* **203,** 177–188 (2006).

240. Shields, R. L. *et al.* Lack of fucose on human IgG1 N-linked oligosaccharide improves binding to human Fcgamma RIII and antibody-dependent cellular toxicity. *J. Biol. Chem.* **277,** 26733–40 (2002).

241. Fites, J. S. *et al.* An unappreciated role for neutrophil-DC hybrids in immunity to invasive fungal infections. *PLOS Pathog.* **14,** e1007073 (2018).

242. Platt, C. D. *et al.* Mature DCs use endocytic receptors to capture and present antigens. *Proc. Natl. Acad. Sci.* **107,** 4287–4292 (2010).

243. Rafiq, K., Bergtold, A. & Clynes, R. Immune complex – mediated antigen presentation induces tumor immunity. *J. Clin. Invest.* **110,** 71–79 (2002).

244. Mildner, A. & Jung, S. Development and function of DC subsets. *Immunity* **40,** 642–56 (2014).

245. Sedlik, C. *et al.* A Critical Role for Syk Protein Tyrosine Kinase in Fc Receptor-Mediated Antigen Presentation and Induction of DC Maturation. *J. Immunol.* **170,** 846–852 (2003).

246. Brasel, K., De Smedt, T., Smith, J. L. & Maliszewski, C. R. Generation of murine DCs from flt3-ligand-supplemented bone marrow cultures. *Blood* **96,** 3029–3039 (2000).

247. Zhang, D. *et al.* The Protein Tyrosine Phosphatase MEG2 Regulates the Transport and Signal Transduction of Tropomyosin Receptor Kinase A *. *J. Biol. Chem.* **29,** 23895–23905 (2016).

248. Saito, K., Williams, S., Bulankina, A., Höning, S. & Mustelin, T. Association of protein-tyrosine phosphatase MEG2 via its Sec14p homology domain with vesicle-trafficking proteins. *J. Biol. Chem.* **282,** 15170–8 (2007).

249. Guy, C. S. *et al.* Distinct TCR signaling pathways drive proliferation and cytokine

production in T cells. *Nat. Immunol.* **14,** 262–270 (2013).

250. Laouar, Y. & Crispe, I. N. Functional flexibility in T cells: independent regulation of CD4+ T cell proliferation and effector function in vivo. *Immunity* **13,** 291–301 (2000).

251. Napolitani, G., Bortoletto, N., Racioppi, L., Lanzavecchia, A. & D'Oro, U. Activation of src-family tyrosine kinases by LPS regulates cytokine production in DCs by controlling AP-1 formation. *Eur. J. Immunol.* **33,** 2832–2841 (2003).

252. Rittirsch, D. *et al.* Cross-talk between TLR4 and FcgammaReceptorIII (CD16) pathways. *PLoS Pathog.* **5,** e1000464 (2009).

253. Regnault, A. *et al.* Fcgamma receptor-mediated induction of DC maturation and major histocompatibility complex class I-restricted antigen presentation after immune complex internalization. *J. Exp. Med.* **189,** 371–80 (1999).

254. Rhee, I. & Veillette, A. Protein tyrosine phosphatases in lymphocyte activation and autoimmunity. *Nat. Immunol.* **13,** 439–447 (2012).

255. Kaneko, T. *et al.* DC-specific ablation of the protein tyrosine phosphatase Shp1 promotes Th1 cell differentiation and induces autoimmunity. *J. Immunol.* **188,** 5397–407 (2012).

256. Huber, M. *et al.* The src homology 2-containing inositol phosphatase (SHIP) is the gatekeeper of mast cell degranulation. *Proc. Natl. Acad. Sci. U. S. A.* **95,** 11330–5 (1998).

257. Pengal, R. A. *et al.* SHIP-2 inositol phosphatase is inducibly expressed in human monocytes and serves to regulate Fcgamma receptor-mediated signaling. *J. Biol. Chem.* **278,** 22657–63 (2003).

258. Hoffmeyer, F., Witte, K., Gebhardt, U. & Schmidt, R. E. The low affinity Fc gamma RIIa and Fc gamma RIIIb on polymorphonuclear neutrophils are differentially regulated by CD45 phosphatase. *J. Immunol.* **155,** 4016–23 (1995).

259. Gao, H., Henderson, A., Flynn, D. C., Landreth, K. S. & Ericson, S. G. Effects of the protein tyrosine phosphatase CD45 on FcγRIIa signaling and neutrophil function. *Exp. Hematol.* **28,** 1062–1070 (2000).

260. Cao, X. *et al.* The inositol 3-phosphatase PTEN negatively regulates Fc gamma receptor signaling, but supports Toll-like receptor 4 signaling in murine peritoneal macrophages. *J. Immunol.* **172,** 4851–7 (2004).

261. Mellman, I. & Steinman, R. M. DCs: Specialized and Regulated Antigen Processing Machines. *Cell* **106,** 255–258 (2001).

262. Zhu, J., Yu, D., Zeng, X.-C., Zhou, K. & Zhan, X. Receptor-mediated endocytosis involves tyrosine phosphorylation of cortactin. *J. Biol. Chem.* **282,** 16086–94 (2007).

263. Lim, J. P. & Gleeson, P. A. Macropinocytosis: An endocytic pathway for internalising large gulps. *Immunol. Cell Biol.* **89,** 836–843 (2011).

264. Nichols, B. J. & Lippincott-Schwartz, J. Endocytosis without clathrin coats. *Trends Cell Biol.* **11,** 406–412 (2001).

265. West, M. A. *et al.* Enhanced DC antigen capture via toll-like receptor-induced actin remodeling. *Science* **305,** 1153–7 (2004).

266. Freeman, S. & Freeman, S. A. Phagocytosis : Receptors , signal integration , and the cytoskeleton integration , and the cytoskeleton. *Immunol. Rev.* 193–215 (2014). doi:10.1111/imr.12212

267. Sousa, S. *et al.* Src, cortactin and Arp2/3 complex are required for E-cadherin-mediated internalization of Listeria into cells. *Cell. Microbiol.* **9,** 2629–2643 (2007).

268. Arbibe, L. *et al.* Toll-like receptor 2–mediated NF-κB activation requires a Rac1-dependent pathway. *Nat. Immunol.* **1,** 533–540 (2000).

269. Lin, Y.-C., Huang, D.-Y., Chu, C.-L., Lin, Y.-L. & Lin, W.-W. The tyrosine kinase Syk differentially regulates Toll-like receptor signaling downstream of the adaptor molecules TRAF6 and TRAF3. *Sci. Signal.* **6,** ra71 (2013).

270. Wu, Y., Ren, D. & Chen, G.-Y. Siglec-E Negatively Regulates the Activation of TLR4 by Controlling Its Endocytosis. *J. Immunol.* **197,** 3336–3347 (2016).

271. Underhill, D. M., Rossnagle, E., Lowell, C. A. & Simmons, R. M. Dectin-1 activates Syk tyrosine kinase in a dynamic subset of macrophages for reactive oxygen production. *Blood* **106,** 2543–50 (2005).

272. Herre, J. *et al.* Dectin-1 uses novel mechanisms for yeast phagocytosis in macrophages. (2004). doi:10.1182/blood-2004-03-1140

273. Elsori, D. H. *et al.* Protein kinase C is a critical component of Dectin-1 signaling in primary human monocytes. *J. Leukoc. Biol.* **90,** 599–611 (2011).

274. Rogers, N. C. *et al.* Syk-Dependent Cytokine Induction by Dectin-1 Reveals a Novel Pattern Recognition Pathway for C Type Lectins. *Immunity* **22,** 507–517 (2005).

275. Azad, A. K., Rajaram, M. V. S. & Schlesinger, L. S. Exploitation of the Macrophage Mannose Receptor (CD206) in Infectious Disease Diagnostics and Therapeutics. *J. Cytol. Mol. Biol.* **1,** (2014).

276. Burgdorf, S., Lukacs-Kornek, V. & Kurts, C. The Mannose Receptor Mediates Uptake of Soluble but Not of Cell-Associated Antigen for Cross-Presentation. *J. Immunol.* **176,** 6770–6776 (2006).

277. Taylor, P. R., Gordon, S. & Martinez-Pomares, L. The mannose receptor: linking homeostasis and immunity through sugar recognition. doi:10.1016/j.it.2004.12.001

278. Savina A., Vargas P., Guermonprez P., Lennon AM., A. S. *Measuring pH, ROS Production, Maturation, and Degradation in DC Phagosomes Using Cytofluorometry-Based Assays*. *Methods in Molecular Biology (methods and Protocols)* **595,** (2010).

279. Viret, C. & Janeway, C. A. Mice-Deficient α Related Self-Peptide(s) in I-E Structurally 68 − 52 α Presentation of E Functional and Phenotypic Evidence for. *J Immunol Ref.* **164,** 4627–4634 (2000).

280. Autenrieth, S. E. & Autenrieth, I. B. Variable antigen uptake due to different expression of the macrophage mannose receptor by DCs in various inbred mouse strains. *Immunology* **127,** 523–9 (2009).

281. Cox, D., Dale, B. M., Kashiwada, M., Helgason, C. D. & Greenberg, S. A regulatory role for Src homology 2 domain-containing inositol 5'-phosphatase (SHIP) in phagocytosis mediated by Fc gamma receptors and complement receptor 3 (alpha(M)beta(2); CD11b/CD18). *J. Exp. Med.* **193,** 61–71 (2001).

282. Ai, J. *et al.* The inositol phosphatase SHIP-2 down-regulates FcgammaR-mediated phagocytosis in murine macrophages independently of SHIP-1. *Blood* **107,** 813–20 (2006).

283. Misharin, A. V. *et al.* Nonclassical Ly6C− Monocytes Drive the Development of Inflammatory Arthritis in Mice. *Cell Rep.* **9,** 591–604 (2014).

284. Goldring, S. R. *et al.* Bone remodelling in inflammatory arthritis. *Ann. Rheum. Dis.* **72 Suppl 2,** ii52-5 (2013).

285. Redlich, K. *et al.* Osteoclasts are essential for TNF-α–mediated joint destruction. *J. Clin. Invest.* **110,** 1419–1427 (2002).

286. Soriano, P., Montgomery, C., Geske, R. & Bradley, A. Targeted disruption of the c-src proto-oncogene leads to osteopetrosis in mice. *Cell* **64,** 693–702 (1991).

287. Park, J. H., Lee, N. K. & Lee, S. Y. Current Understanding of RANK Signaling in Osteoclast Differentiation and Maturation. *Mol. Cells* **40,** 706–713 (2017).

288. Miyazaki, T. *et al.* Src kinase activity is essential for osteoclast function. *J. Biol. Chem.* **279,** 17660–6 (2004).

289. Koga, S. *et al.* Physical and functional association of c-Src and adhesion and degranulation promoting adaptor protein (ADAP) in osteoclastogenesis in vitro. *J. Biol. Chem.* **280,** 31564–71 (2005).

290. McInnes, I. B. & Schett, G. Cytokines in the pathogenesis of rheumatoid arthritis. *Nat. Rev. Immunol.* **7,** 429–442 (2007).

291. Salmond, R. J., Brownlie, R. J., Morrison, V. L. & Zamoyska, R. The tyrosine phosphatase PTPN22 discriminates weak self peptides from strong agonist TCR signals. *Nat. Immunol.* **15,** 875–883 (2014).

292. Block, K. E., Zheng, Z., Dent, A. L., Kee, B. L. & Huang, H. Gut Microbiota Regulates K/BxN Autoimmune Arthritis through Follicular Helper T but Not Th17 Cells. *J. Immunol.* **196,** 1550–7 (2016).

293. Lee, H. *et al.* Gut-residing Microbes Alter the Host Susceptibility to Autoantibody-mediated Arthritis. *Immune Netw.* **14,** 38–44 (2014).

294. Wu, H. *et al.* Gut-Residing Segmented Filamentous Bacteria Drive Autoimmune Arthritis via T Helper 17 Cells. *Immunity* **32,** 815–827 (2010).

295. Burn, G. L., Svensson, L., Sanchez-Blanco, C., Saini, M. & Cope, A. P. Why is PTPN22 a good candidate susceptibility gene for autoimmune disease? *FEBS Lett.* **585,** 3689–3698 (2011).

296. Saad, M. N., Mabrouk, M. S., Eldeib, A. M. & Shaker, O. G. Identification of rheumatoid arthritis biomarkers based on single nucleotide polymorphisms and haplotype blocks: A systematic review and meta-analysis Production and hosting by Elsevier. *J. Adv. Res.* **7,** 1–16 (2016).

297. Lai, X. *et al.* Circulating IL-27 Is Elevated in Rheumatoid Arthritis Patients. *Molecules* **21,** 1565 (2016).

298. Koch, A. E. *et al.* Epithelial neutrophil activating peptide-78: a novel chemotactic cytokine for neutrophils in arthritis. *J. Clin. Invest.* **94,** 1012–8 (1994).

299. Walz, A. *et al.* Structure and neutrophil-activating properties of a novel inflammatory peptide (ENA-78) with homology to interleukin 8. *J. Exp. Med.* **174,** 1355–62 (1991).

300. Pickens, S. R. *et al.* Anti-CXCL5 therapy ameliorates IL-17-induced arthritis by decreasing joint vascularization. *Angiogenesis* **14,** 443–55 (2011).

301. Wright, H. L., Moots, R. J. & Edwards, S. W. The multifactorial role of neutrophils in rheumatoid arthritis. *Nat. Rev. Rheumatol.* **10,** 593–601 (2014).

302. Nakae, S., Nambu, A., Sudo, K. & Iwakura, Y. Suppression of Immune Induction of

Collagen-Induced Arthritis in IL-17-Deficient Mice. *J. Immunol.* **171,** 6173–6177 (2003).

303. Church, L. D. *et al.* Rheumatoid synovial fluid interleukin-17-producing CD4 T cells have abundant tumor necrosis factor-alpha co-expression, but little interleukin-22 and interleukin-23R expression. *Arthritis Res. Ther.* **12,** R184 (2010).

304. Harre, U. *et al.* Induction of osteoclastogenesis and bone loss by human autoantibodies against citrullinated vimentin. *J. Clin. Invest.* **122,** 1791–802 (2012).

305. Seeling, M. *et al.* Inflammatory monocytes and Fcγ receptor IV on osteoclasts are critical for bone destruction during inflammatory arthritis in mice. *Proc. Natl. Acad. Sci. U. S. A.* **110,** 10729–34 (2013).

306. Clarke, F. *et al.* The protein tyrosine phosphatase PTPN22 negatively regulates presentation of immune complex derived antigens. *Sci. Rep.* **8,** 12692 (2018).

307. Sakaguchi, S., Benham, H., Cope, A. P. & Thomas, R. T-cell receptor signaling and the pathogenesis of autoimmune arthritis: insights from mouse and man. *Immunol. Cell Biol.* **90,** 277–287 (2012).

308. Rawlings, D. J., Metzler, G., Wray-Dutra, M. & Jackson, S. W. Altered B cell signalling in autoimmunity. *Nat. Rev. Immunol.* **17,** 421–436 (2017).

309. Laborde, E. A. *et al.* Immune Complexes Inhibit Differentiation, Maturation, and Function of Human Monocyte-Derived DCs. *J. Immunol.* **179,** 673–681 (2007).

310. Culshaw, S., Millington, O. R., Brewer, J. M. & McInnes, I. B. Murine neutrophils present Class II restricted antigen. *Immunol. Lett.* **118,** 49–54 (2008).

311. Strzelecka, A., Kwiatkowska, K. & Sobota, A. Tyrosine phosphorylation and Fcγ receptor-mediated phagocytosis. *FEBS Lett.* **400,** 11–14 (1997).

312. Kiefer, F. *et al.* The Syk protein tyrosine kinase is essential for Fcgamma receptor signaling in macrophages and neutrophils. *Mol. Cell. Biol.* **18,** 4209–20 (1998).

313. Le Roux, D. *et al.* Syk-dependent actin dynamics regulate endocytic trafficking and processing of antigens internalized through the B-cell receptor. *Mol. Biol. Cell* **18,** 3451–62 (2007).

314. Porgador, A., Yewdell, J. W., Deng, Y., Bennink, J. R. & Germain, R. N. Localization, quantitation, and in situ detection of specific peptide-MHC class I complexes using a monoclonal antibody. *Immunity* **6,** 715–26 (1997).

315. Ding, Y. *et al.* The lectin Siglec-G inhibits DC cross-presentation by impairing MHC class I–peptide complex formation. *Nat. Immunol.* **17,** 1167–1175 (2016).

316. Gómez, C. P., Tiemi Shio, M., Duplay, P., Olivier, M. & Descoteaux, A. The Protein Tyrosine Phosphatase SHP-1 Regulates Phagolysosome Biogenesis. *J. Immunol.* **189,** (2012).

317. Rhee, I., Zhong, M.-C., Reizis, B., Cheong, C. & Veillette, A. Control of DC Migration, T Cell-Dependent Immunity, and Autoimmunity by Protein Tyrosine Phosphatase PTPN12 Expressed in DCs. *Mol. Cell. Biol.* **34,** 888–899 (2014).

318. Goodridge, H. S. *et al.* Activation of the innate immune receptor Dectin-1 upon formation of a 'phagocytic synapse'. *Nature* **472,** 471–5 (2011).

319. Takeshita, S. *et al.* SHIP-deficient mice are severely osteoporotic due to increased numbers of hyper-resorptive osteoclasts. *Nat. Med.* **8,** 943–949 (2002).

320. Hanada, K., Tsunoda, R. & Hamada, H. GM-CSF-induced in vivo expansion of splenic DCs

and their strong costimulation activity. *J. Leukoc. Biol.* **60,** 181–190 (1996).

321. Maraskovsky, E. *et al.* Dramatic increase in the numbers of functionally mature DCs in Flt3 ligand-treated mice: multiple DC subpopulations identified. *J. Exp. Med.* **184,** 1953–62 (1996).

322. Vremec, D. *et al.* The influence of granulocyte/macrophage colony-stimulating factor on DC levels in mouse lymphoid organs. *Eur. J. Immunol.* **27,** 40–44 (1997).

323. Wada, H., Noguchi, Y., Marino, M. W., Dunn, A. R. & Old, L. J. T cell functions in granulocyte/macrophage colony-stimulating factor deficient mice. *Proc. Natl. Acad. Sci. U. S. A.* **94,** 12557–61 (1997).

324. Dahl, M. E., Arai, K. & Watanabe, S. Association of Lyn tyrosine kinase to the GM-CSF and IL-3 receptor common betac subunit and role of Src tyrosine kinases in DNA synthesis and anti-apoptosis. *Genes to Cells* **5,** 143–153 (2000).

325. Hercus, T. R. *et al.* The GM-CSF receptor family: Mechanism of activation and implications for disease. *Growth Factors* **30,** 63–75 (2012).

326. Heiss, E. *et al.* Identification of Y589 and Y599 in the juxtamembrane domain of Flt3 as ligand-induced autophosphorylation sites involved in binding of Src family kinases and the protein tyrosine phosphatase SHP2. *Blood* **108,** 1542–1550 (2006).

327. Dosil, M., Wang, S. & Lemischka, I. R. Mitogenic signalling and substrate specificity of the Flk2/Flt3 receptor tyrosine kinase in fibroblasts and interleukin 3-dependent hematopoietic cells. *Mol. Cell. Biol.* **13,** 6572–85 (1993).

328. Meshinchi, S. & Appelbaum, F. R. Structural and Functional Alterations of FLT3 in Acute Myeloid Leukemia. *Clin. Cancer Res.* **15,** 4263–4269 (2009).

329. Na, Y. R., Jung, D., Gu, G. J. & Seok, S. H. GM-CSF Grown Bone Marrow Derived Cells Are Composed of Phenotypically Different DCs and Macrophages. *Mol. Cells* **39,** 734–741 (2016).

330. Dudziak, D. *et al.* Differential antigen processing by DC subsets in vivo. *Science* **315,** 107–11 (2007).

331. Kamphorst, A. O., Guermonprez, P., Dudziak, D. & Nussenzweig, M. C. Route of antigen uptake differentially impacts presentation by DCs and activated monocytes. *J. Immunol.* **185,** 3426–35 (2010).

332. Merad, M., Sathe, P., Helft, J., Miller, J. & Mortha, A. The DC lineage: ontogeny and function of DCs and their subsets in the steady state and the inflamed setting. *Annu. Rev. Immunol.* **31,** 563–604 (2013).

333. Filippi, M.-D. Mechanism of Diapedesis: Importance of the Transcellular Route. *Adv. Immunol.* **129,** 25–53 (2016).

334. Sztacho, M. *et al.* BAR Proteins PSTPIP1/2 Regulate Podosome Dynamics and the Resorption Activity of Osteoclasts. *PLoS One* **11,** e0164829 (2016).

335. Quinn, J. M. W. *et al.* Transforming Growth Factor β Affects Osteoclast Differentiation via Direct and Indirect Actions. *J. Bone Miner. Res.* **16,** 1787–1794 (2001).

336. Sells Galvin, R. J., Gatlin, C. L., Horn, J. W. & Fuson, T. R. TGF-β Enhances Osteoclast Differentiation in Hematopoietic Cell Cultures Stimulated with RANKL and M-CSF. *Biochem. Biophys. Res. Commun.* **265,** 233–239 (1999).